National Aeronautics and Space Administration

Biennial Research and Technology Development Report

Johnson Space Center

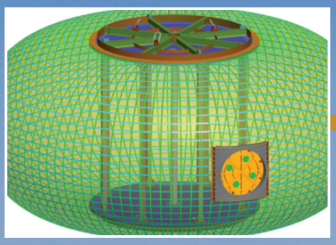

Johnson Space Center
External Relations Office
University Research and Affairs Office

Helen Lane, Ph.D.
Kamlesh Lulla, Ph.D.
Editors

TM-2009-214795/December 2009

Biennial Research and Technology Development Report

Johnson Space Center

Human Health and Medicine

Environmental Technologies

Materials Development and Testing

Flammability and Explosives Technologies

Power, Batteries, and Propulsion

Robotics, Autonomous Systems, and Software

Technologies for Extravehicular Activity and Protection from Harsh Environments

Space and Ground Operations

Planetary Sciences

Johnson Space Center
External Relations Office
University Research and Affairs Office

Helen Lane, Ph.D.
Kamlesh Lulla, Ph.D.
Editors

TM-2009-214795/December 2009

Contents

Foreword xi
An Introduction to the Biennial Research and Technology Development Report 2009 xii
Guide to Icons Used in This Document xiii
The Innovation Partnerships Office xiv
Overview of Exploration Program xvi
Acronyms and Abbreviations xx

Guide to Icons Used in This Document

Our experienced staff has made an attempt to identify an application or a use for each report employing a unique icon:

Commercial	Reports with near-term commercial applications
Low-Earth Orbit	Reports with use in low-Earth orbit operations
Long Duration	Reports with application for long-duration space flight
Exploration	Reports with technologies relevant to Exploration Program
Orion/CEV	Reports with technologies relevant to Orion/ Crew Exploration Vehicle (CEV) components
Moon	Reports relevant for missions to, operations on, or exploration of the moon

Human Health and Medicine

Space Life Sciences Innovation and Integration Successes 3
Space Medicine: Past, Present, and Future Issues 5
Human Adaptation to Space: Space Physiology and Countermeasures 7
Development and Clinical Evaluation of Intranasal Scopolamine Gel Formulation 9
Media Ion Composition Controls Regulatory and Virulence Response of *Salmonella* in Space Flight 10
Varicella-zoster Virus in the Saliva of Patients with Herpes Zoster 12
Innovative Treatments for Dental Emergencies During Lunar and Exploration Missions 13

Adaptation of the Skeletal System During Long-duration Space Flight 15

Recovery of Space-flight-induced Bone Loss: Bone Mineral Density After Long-duration Missions as Fitted with an Exponential Function 17

The Flight Analogs Project as a Test Platform for the Skeletal Effects of Space Flight 19

Vitamin D Studies: From the Antarctic to the International Space Station 22

Novel Skeletal Muscle Models for Space Exploration and Medical Applications 23

Gender Differences in Blood Pressure Control During 90-day Bedrest 25

Countermeasures to Space-flight-induced Orthostatic Hypotension 27

Environmental Technologies

Leadership in Energy and Environmental Design at Johnson Space Center 33

Exploration Life Support Air Revitalization System Technology Development for Human Test Subjects 36

Spacecraft Water Monitoring: Adapting to an Era of Emerging Scientific Challenges 39

Cascade Distillation Subsystem Development 41

Rotating Reverse Osmosis for Water Recovery on Long-term Space Missions 43

Urine Pretreatment Development 45

Air Quality Monitoring: Risk-based Choices 46

Design and Development of Airlock Contamination Detection Kits for the Space Shuttle and International Space Station 48

Space Radiation Protection Status and Challenges 50

Measuring Ionospheric Electric Field Gradients with the International Space Station Floating Potential Probe 53

Lunar In-situ Resource Utilization 55

Propellant Specification and Manual Development to Enable Testing 60

Using Lasers to Capture the Speed of a Hypervelocity Projectile 62

Lunar Dust and Lunar Dust Simulant Activation and Monitoring 64

Cleaning to Achieve Sterility: An Evaluation of State-of-the-art Cleaning Techniques to Remove Particles of Biological Origin 66

Materials Development and Testing

New Developments in Nondestructive Evaluation for Composite Pressure Vessel Testing 71

Acoustic Emission and Microscopic Characterization for Improved Composite Overwrapped Pressure Vessel Health Monitoring 73

Orion Composite Overwrapped Pressure Vessel Safety Testing 75

Thermal Radiation Impacts Protection System 77

Type-specific Single-wall Carbon Nanotube Growth and Separation 79

Improving the Process: Assessing Reactivity of Nonmetals in Aerospace Fluids 81

Lunar Inflatable Habitat Development 84

Computed Tomography Scanning and Analysis of the Stardust Heat Shield 86

Flammability and Explosives Technologies

Changing the Standards for Promoted Combustion Pass/Fail Criteria 91

Long-term Testing of Oxygen Compressors 93

Design and Verification of a Robust Filter for Oxygen Service 95

Understanding Ignition of Oxygen System Components by Particle Impact 98

Oxygen Compatibility Assessment Database Web Application 100

New Methodology: Hazard Assessment Protocol for Aerospace Hydrogen Systems 102

Evaluation of Spacecraft Materials Flammability for the Constellation Program 105

Determining the Time for Oxygen-exposed Materials to Return to Reduced Flammability 107

Redesign of Promoted Combustion Test System: Inductance Canceling Feedthrough for Pressurized Systems 110

Innovative Thermal Measurement Techniques for Y-shaped Primer Chamber Assembly Pyrotechnic Valves 112

Analysis of a Pyrovalve Firing: Estimating Pyrotechnic Reactions 115

Power, Batteries, and Propulsion

NASA Engineering and Safety Center-supported Battery Study 121

Advanced Battery Technology Programs 123

Advanced Fuel Cells for Space Exploration Applications 126

Orbiter Auxiliary Power Unit Hydrazine Fuel Line Vacuum Test 129

Improved Method: Short-term Determination of Low Corrosion Rates in Hydrazines 131

High-sensitivity Measurement for Hypergol Permeation of Personal Protective Equipment Materials 132

Robotics, Autonomous Systems, and Software

Robonaut/Centaur 137

Lunar Rover Development 140

Improving Robotic Operator Performance
Using Augmented Reality 142

The Performance of the Orbiter Wing
Leading Edge Impact Detection System
During Space Shuttle Ascent. 144

Anomaly Monitoring Inductive
Software System 146

Integrated Docking Simulation with
Six-degree-of-freedom Dynamic Test System 148

Autonomous Landing and Hazard
Avoidance Technology. 150

Using the Orbiter Wing Leading Edge Impact
Detection System for Micrometeoroid
and Orbital Debris Impact Monitoring. 153

Natural Feature Image Recognition
Enables Docking. 155

Fiber-optic Micrometeoroid Impact Sensor
for Future Lunar Exploration Missions 157

Technologies for Extravehicular Activity and Protection from Harsh Environments

Extravehicular Activity Technology
Development – Thermal Subsystem 161

Extravehicular Activity Technology
Development – Oxygen Subsystem 163

Extravehicular Activity Technology
Development – Ventilation Subsystem 165

Extravehicular Activity Technology
Development – Portable Life Support
System Packaging 167

First-generation Suit Port
Development and Testing 169

Electrical Shock Hazards during Extravehicular
Activity on the International Space Station. 171

Water Egress and Survival. 172

Space and Ground Operations

The Mobile Information System: A Hands-free Procedures System 177

Crew Exploration Vehicle Parachute Assembly System. 179

International Space Station Operations 182

Automating International Space Station File Management Using Agent-based Systems Integration 184

Planning and Monitoring International Space Station Solar Array Operations 186

Search and Relationship-mining of Heterogeneous Flight Control Documents 189

Trajectory Guidance for Lunar Descent and Landing 192

Targeting for Trans-Earth Injection Maneuvers 194

Low-impact Docking System. 196

Planetary Sciences

Astromaterials Research and Exploration Science Overview 201

Discovery of a New Mineral from a Cometary Particle. 203

Constraining Planetary Melting and Differentiation with Experimentation at High Pressure and Temperature 205

Celebrating Thirty Seasons of Antarctic Meteorites: Johnson Space Center Antarctic Meteorite Laboratory. 207

New Perspectives on Geomorphic Processes: Megafans in Terrestrial and Planetary Environments. 209

Searching for Antimatter and Dark Matter 211

Image Science Support for Exploration Program 214

Improving Access to Astronaut Photography through Google Earth 216

Object-based Image Analysis of Astronaut Photography 218

Foreword

NASA is in the midst of ushering in a "new age of exploration" with the fundamental goal "to advance U.S. scientific, educational, and economic interests through a robust space exploration program." Johnson Space Center is destined to play a vital role in our nation's human space exploration endeavors.

We are renewing our emphasis on enhancing the nation's science, technology, engineering, and mathematics education in our schools. We are also establishing partnerships with universities to help develop our technical workforce.

NASA has taken an active role in spurring the commercial aerospace industry to meet the challenges and exploit the opportunities in low-Earth operations. We are also making vigorous efforts to invest in technology development and encouraging innovation at our center.

This Biennial Research and Technology Development Report is a valuable compilation of the many exciting research initiatives accomplished by our remarkably talented and smart minds at Johnson Space Center. It is intended to give you insight into and technical information about important areas of investigations in support of human space exploration. These are exciting times to be in the space exploration business, and to be part of the team that is conducting groundbreaking research to enable us to achieve the next milestone in our pursuit of human space exploration.

I am positive that the information provided in this report will enable us to engage in dialogue with the science and engineering research community in universities, other federal agencies, industries, and nonprofit research institutions. Our goal is to build strong and lasting research partnerships as we continue our journey to the stars!

Michael L. Coats

Center Director

An Introduction to the Biennial Research and Technology Development Report 2009

The Johnson Space Center's (JSC's) core mission is human space flight and human space exploration. Center personnel have focused on human space flight for the past 5 decades, making great strides in engineering, science, and technology innovations and developments. Currently, JSC supports three major human space flight programs: the Space Shuttle, International Space Station (ISS), and Constellation Programs. To implement its assigned technical missions, JSC supports active engineering, mission operations, space and life sciences, and planetary science research in support of human space flight. JSC's talented scientists and engineers bridge the gap between conceptual laboratory research and technology development and real-life space flight applications. These research and technology developments have matured and evolved over the years. Each year the center's engineers and scientists innovate, collaborate, and share knowledge with cohorts in the U.S. government, international partners, aerospace companies, universities, industry, and various institutes to meet the new opportunities and challenges that are always occurring.

This Biennial Research and Technology Development Report highlights the diverse technical, scientific, and engineering research and technology development under way at JSC.

We want to engage the commercial, public, and academic sectors through our research and technology development, leading to collaborations of mutual interest with both commercial and academic groups. As all indicators point to a burgeoning commercial aerospace industry, we would like members of the commercial aerospace enterprise to look through the pages of this report and contact us concerning potential collaborative efforts in technologies of mutual interest.

To make this report user-friendly, we have organized the contents into the following nine broad categories:

Human health and medicine: Addresses topics from decision-making to practicing medicine in hostile/extreme environments, and analog medical research such as medical issues in Antarctica to new, cutting-edge medical technologies.

Environmental technologies: Covers resource recycling and recovery technologies, air quality monitoring, and radiation protection research.

Materials development and testing: Includes new developments in nondestructive evaluation tests and acoustic characterization of pressure vessels, single-wall carbon nanotube growth, and inflatable materials development.

Flammability and explosion testing, including protection and testing standards: Deals with the many NASA-pioneered testing methodologies in this arena as well as with the standards NASA helped to develop for use in industry.

Power, battery, and propulsion technologies: Encompasses NASA fuel cell and battery development efforts and high-sensitivity measurements for permeation of materials such as hypergol.

Robotics and automation technologies: Focuses on engineering and software developments for robotic systems, including human-assisted robotic devices for space and surface operations.

Technologies for harsh environments, including EVA [extravehicular activity] technologies: Contains reports on technologies such as ventilation systems, a potable life support system, and a water egress and survival training system.

Space and ground operations: Consists of software developments for ISS operations, data mining, and a low-impact docking system.

Planetary sciences: Concentrates on reports of new discoveries of cometary particle and results from planetary and rover research, educational, and outreach initiatives using Earth Observation imagery from ISS.

NASA's rigorous engineering and scientific demands to accomplish its mission lead either to the creation of new technologies or improvement and customization of those already available. Once proven, these technologies can potentially be used in a multitude of commercial products and markets.

Collaborating with Johnson Space Center

NASA and JSC have a long history of working with colleges and universities, industry, federal laboratories, and other research and technology development organizations. Means are in place to accomplish collaboration and partnership objectives. Both reimbursable and non-reimbursable collaborative agreements can be used to provide mutual leverage of government, university, and industry resources in the cooperative pursuit of joint-interest research and technology development efforts.

We look forward to working with both the commercial and the academic groups interested in partnering with JSC.

Helen Lane and Kamlesh Lulla
External Relations Office

John James
Advanced Planning Office

Al Conde
Constellation Program Office

Guide to Icons Used in This Document

Our experienced staff has made an attempt to identify an application or a use for each report employing a unique icon:

Commercial	Reports with near-term commercial applications
Low-Earth Orbit	Reports with use in low-Earth orbit operations
Long Duration	Reports with application for long-duration space flight
Exploration	Reports with technologies relevant to Exploration Program
Orion/CEV	Reports with technologies relevant to Orion/ Crew Exploration Vehicle (CEV) components
Moon	Reports relevant for missions to, operations on, or exploration of the moon

The Innovation Partnerships Office

Michelle Brekke, *Johnson Space Center*
Donna Anderson, *Johnson Space Center*
Jack James, *Johnson Space Center*

The Innovation Partnerships Office (IPO) at Johnson Space Center (JSC) uses partnerships to drive the infusion of technology, creative partnerships to develop technology, and traditional business partnerships to license and to transfer NASA-developed technology to the U.S. marketplace. Traditionally known as the Technology Transfer Office, the office changed its name to better reflect its expanding role and capabilities at the center.

For 50 years, NASA developed technologies to orbit the Earth, land on the moon, and explore the stars and galaxies. This human need to explore and its attendant curiosity created new ideas and innovations that benefit everyone here on Earth through spinoffs. Spinoffs are resulting commercial products that originate with NASA funding, research, licensing, facilities, or assistance. The founders of the space program, through the Space Act of 1958, require NASA to transfer its technologies to the marketplace so that the U.S. taxpayer can benefit from the advancements.

For decades, the space agency has triggered U.S. innovations and inventions, while nurturing partnerships to facilitate the transfer of NASA-developed technologies to the private marketplace through inclusive programs for both small and big businesses. NASA ingenuity, coupled with technology transfer initiatives, has garnered more than 1,600 documented commercial applications of NASA technology.

Areas of technology research and development at JSC focus on the center's technology core competencies of Environmental Control and Life Support, Extravehicular Activity, Lunar In-situ Resource Utilization, Lunar Operations, Thermal Management, Exploration Crew Health Capabilities, Space Human Factors and Food Systems, Space Radiation, and Sensors for Autonomous Systems and can be seen in the areas funded for development by IPO programs.

The IPO is now working on innovative partnership models to enhance and initiate technology research and development for infusion into the agency. It is also spinning NASA technologies out into the marketplace through private industry and investment.

JSC IPO launched a technology research and development program in 2008 for focused investment groups (FIGs) in which JSC Directorates presented their needs for technology development and their needs funding based on mission requirements and the ability to advance the technology to a readiness level to meet future space flight needs. Technologies being funded in the FIGs are Human System, Habitat Systems, Surface Mobility Systems, Mission Operations, and Mission Enabling Science. Each FIG was funded at levels that in many cases allowed for the leveraging of the Partnerships Office funds to gain outside additional supportive funding sources and partnerships to advance the development of the technology.

NASA also uses more traditional avenues to develop technology for infusion and spinout; these are the Small Business Innovative Research (SBIR) and Small Business Technology Transfer (STTR) programs. JSC's IPO has managed $69.7M for the SBIR program initiatives and $8M in STTR initiatives in the five most recent program years.

The SBIR/STTR programs, established by law, exist to stimulate technological innovation in the private sector by increasing participation by small business in federal research and technology development. A competitive proposal process is launched annually via a solicitation of proposals with the focus of meeting NASA technology program needs, coupled with the potential for commercialization. For more information on the SBIR/STTR programs, visit http://sbir.nasa.gov.

Investment Seed funding is also available through the Innovative Partnership Program at NASA; this program is administered by the IPO at JSC. The Seed Fund works to meet mission technology goals specifically to address barriers with joint-technology partnerships providing leveraged funding, resources, and expertise. It is sourced from NASA headquarters, managed through each of the centers, and requires coordination with NASA mission directorates who identify specific technology development needs.

A current partnership between JSC and Caterpillar Inc. (Peoria, Ill.) resulted from an IPP Seed Fund Award. JSC

needs to develop the capability to build bases and habitats – all of which requires heavy construction – for NASA's return to the moon. Caterpillar is known for its ability in mining and construction equipment designed to move earth. The partnership was formed with Caterpillar because of its potential to advance key technologies to meet critical NASA needs for the future, and Caterpillar has similar interests in advancing autonomous operations in a mining application. For more information about this partnership, visit http://technology.jsc.nasa.gov/. For more information the Seed Fund, email jsc-techtran@mail.nasa.gov.

The methods and tools used by IPO to infuse technology, spin out technology, and partner with business and universities include Space Act Agreements and Patent Licensing Agreements. Space Act Agreements are used primarily to collaborate with entities other than NASA for everything from lending personnel and expertise to equipment and other facilities and resources. Patent Licensing Agreements are used to license NASA technologies to businesses in the private sector to transfer the technology to the marketplace for further development and successful commercialization to benefit the U.S. taxpayer. For more information about JSC licensing opportunities, visit http://technology.jsc.nasa.gov/licensing.cfm.

Another NASA program is the Inventions and Contributions Board (ICB). Also established by the Space Act of 1958, the ICB Space Act Awards rewards and promotes outstanding scientific or technical contributions sponsored, adopted, supported, or used by NASA that are significant to aeronautics and space activities.

Over the past 50 years, the ICB issued more than 98,000 awards, equaling $44M, to NASA and its contractor employees as well as to other government, university, and industry personnel. The ICB award program also gave out 3,300 technical awards in 2008 totaling more than $2M. At JSC, the IPO administers the ICB Space Act Awards and presented $140,000 to 270 JSC innovators in 2008.

Overview of Exploration Program

Al Conde, *Johnson Space Center*

The Constellation Program is developing the flight systems and Earth-based ground infrastructure to establish an expanded human presence in the solar system. By building on the achievements of previous lunar exploration efforts and technological advancements made over the past 5 decades, and by conducting enhancing and enabling research and technology development, NASA will provide the foundation for the U.S. to continue to access the International Space Station (ISS), return humans to the moon, and enable human exploration of Mars and beyond.

The first step in this ambitious national undertaking is to formulate a safe, cost-effective, and sustainable strategy or architecture for lunar return. We must then design and develop the building blocks of the vehicles and systems necessary to accomplish this goal. Figure 1 illustrates the basic plan (reference mission) for the first human lunar landings.

The long-term objectives of U.S. space exploration continue to evolve. The near-term goals are well-established and under way: to develop the flight systems and ground infrastructure required to enable continued access to space and to enable future crewed missions to the ISS, the moon, and Mars.

The exploration vehicles we are developing to meet this goal include the Orion Crew Exploration Vehicle (CEV) spacecraft and two new launch vehicles – the Ares I and the Ares V. The Ares I launch vehicle will carry the Orion CEV to low-Earth orbit (LEO) where the CEV will dock with either the ISS or with a payload launched earlier on an Ares V launch vehicle for transit to the moon. For lunar missions, the Ares V launch vehicle will carry an Earth departure stage (EDS) and lunar payload (e.g., a lander) in a single launch. After the Orion CEV docks with the EDS/lunar payload in Earth orbit, the EDS engine will ignite and propel the lunar payload and the Orion CEV to the moon. Ares V launch vehicles will be used to launch the components needed to send and return a crew to Mars. This could include a Mars transfer vehicle, a lander, a surface habitat, and surface equipment. The Ares I and Orion CEV will also be used for crew transport to and from LEO for the Mars missions.

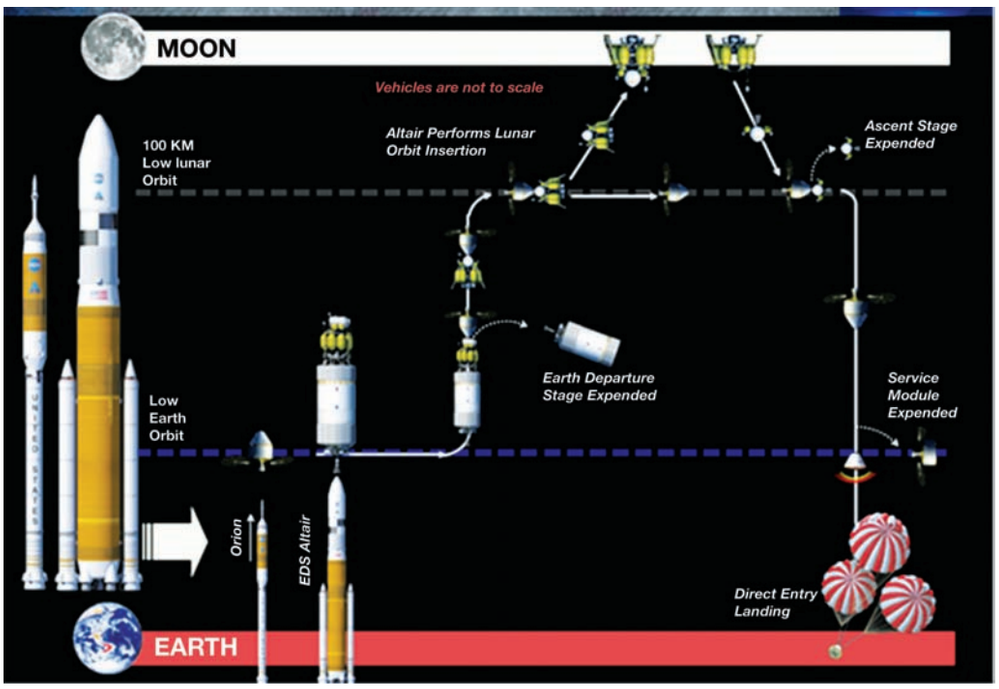

Fig. 1. *Typical lunar reference mission.*

The Constellation flight projects are as follows:

The Orion Crew exploration vehicle

The basic design of the Orion spacecraft consists of the crew module (CM), service module, spacecraft adapter, and Launch Abort System. The Orion spacecraft is approximately 5 m (16.4 ft) in diameter and 15.3 m (50.3 ft) in length with a mass of approximately 14,000 kg (31,000 lbs.). It provides crew habitation in space and docking

capability with other launched components and the ISS; and it performs Earth return, atmospheric entry, and landing. The Orion spacecraft can be configured to carry a crew of up to four to and from lunar orbit and up to six to and from the ISS.

Due to the physics associated with atmospheric entry, the overall shape of the CM is similar to that of the Apollo command module; however, the Orion CM is much larger, providing more than twice the usable interior volume and carrying double the crew size to the moon. The CM includes a pressurized crew transfer tunnel and docking device capable of mating with the ISS and the Altair lunar lander.

The CEV's technologies include: soft capture docking, a phase change material heat exchanger, optical navigation, and lightweight parachute material.

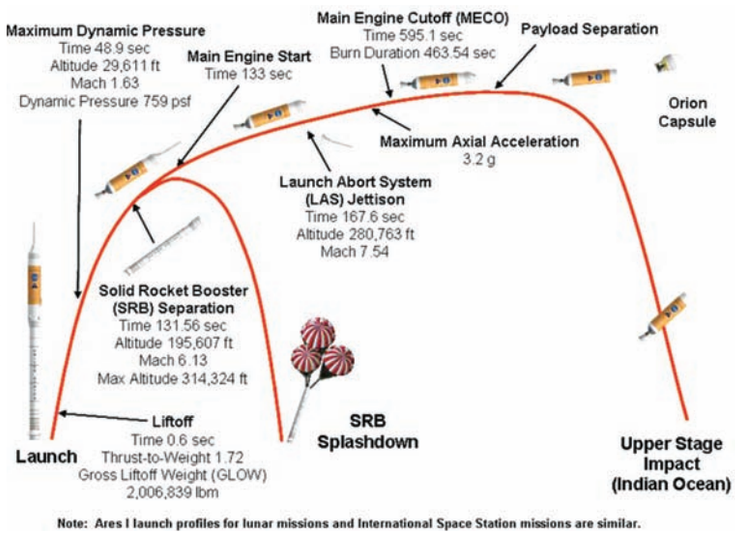

Fig. 2. *The Delta IV program.*

The Ares launch vehicles

The Ares I launch vehicle carries the Orion spacecraft to LEO where it can rendezvous and dock to the ISS or to the Altair lunar module previously launched by an Ares V heavy-lift rocket. We are developing the Ares I and Ares V concurrently with propulsion and structures hardware commonality, which results in significant design and manufacturing cost savings. Common elements being developed for the Ares I and Ares V launch vehicles include the solid rocket motors and the J-2X upper stage engine. Cost and risk reduction are also enhanced by using existing and proven hardware and systems whenever possible. This includes solid rocket booster technology from the Space Shuttle Program used as the basis for the Ares I first stage and Ares V booster rockets. The Ares I upper stage J-2X engine (and the EDS of the Ares V) is a generational upgrade of the J-2 engine used on Saturn V and Saturn IB launch vehicles during the Apollo Program. The RS-68 engines of the Ares V core stage were developed in the late 1990s and early 2000s for the U.S. Air Force's Evolved Expendable Launch Vehicle Program (Delta IV) (figure 2).

The Altair lunar lander

The Altair lunar lander (figure 3) will provide access to the lunar surface for astronaut crews and/or cargo via a descent stage, and will return the crew via an ascent stage to the Orion spacecraft in lunar orbit. A cargo-only version of the lunar lander will be able to transport cargo to the lunar surface; it may not include an ascent stage. Basic elements of the lunar lander will include the propellant tanks and engines associated with the ascent/descent stages, a living module for the crew (i.e., pressure vessel), a landing gear system, internal power supplies (e.g., rechargeable batteries) and provisions for crew access to the lunar surface. Propellants proposed for the lunar lander include liquid oxygen/liquid hydrogen for the descent stage and

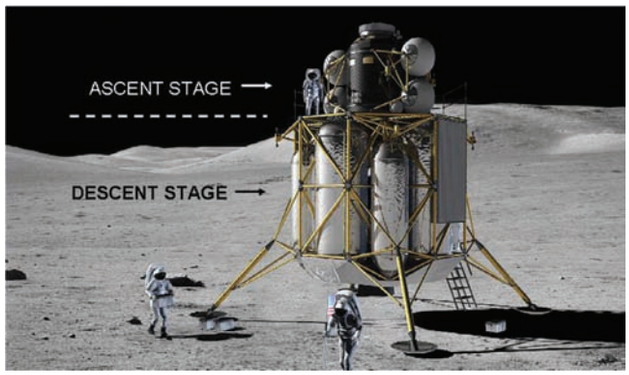

Fig. 3. *Concept design for the Altair lunar lander.*

liquid oxygen/methane for the ascent stage, although we have not made a final decision on propellants.

Altair lunar lander technologies include: autonomous landing and hazard avoidance technology, thermal control, and life support.

Extravehicular activity support equipment

The EVA [Extravehicular Activity] Systems Project provides the spacesuits and necessary tools for astronauts to work outside of the protective confines of a space vehicle. EVAs can be conducted in space or on the lunar surface, and are used for planned activities (e.g., research tasks or site exploration) as well as for contingency tasks (e.g., inspection or vehicle repair).

The EVA Systems Project will develop, certify, produce, and sustain the flight and training hardware systems necessary to support EVA and crew survival during all Constellation mission phases.

We are developing the following spacesuit capabilities:

- Crew protection and survival capability for launch and atmospheric entry, landing, and abort scenarios
- Contingency zero-gravity in-space EVA capability for the Orion spacecraft
- Surface EVA capability for exploration of the moon

The spacesuit – the extravehicular mobility unit, currently being used by the Space Shuttle Program and on the ISS – is not compatible with either the lunar or the martian environments because it was designed for zero-gravity operations in LEO. NASA is developing a new modular spacesuit system that will be used during launch, atmospheric entry, and abort as well as in zero-gravity and lunar environments. The spacesuit will support long-duration (180 days) missions, perform multiple EVAs, and function under conditions expected at lunar exploration sites. Figure 4 illustrates the two basic types of spacesuits being developed: the launch-entry-abort (LEA) suit and the lunar surface suit. These designs share many common elements, but the lunar surface suit provides additional micrometeoroid and dust protection and has an enhanced range of mobility to allow astronauts to work for extended periods of time in the lunar 1/6-g environment. Figure 5 shows engineers testing a prototype lunar surface suit in conjunction with a new lunar rover concept vehicle at the Johnson Space Center in early 2008.

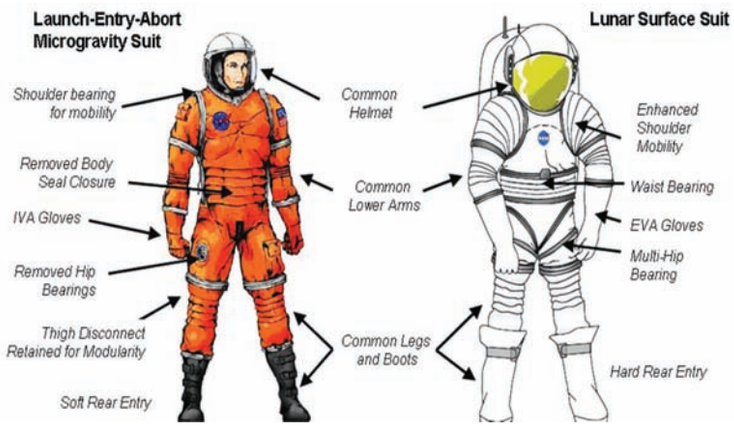

Fig. 4. *Early designs for the LEA suit and lunar surface suit.*

EVA support equipment technologies include: composite bearings, a modular helmet, a suit port, and abrasion-resistant suit material.

Lunar surface systems

Our primary goal in developing all of the launch capability and vehicle and suit infrastructure discussed above is to enable a sustained human presence on the moon. In June 2008, the Constellation Program completed the Lunar Capability Concept Review (LCCR). The LCCR was a major milestone and the result of over 9 months of various lunar exploration-related studies, including:

- Lunar surface infrastructure compatibility and maximum leverage with the Orion, Altair, and Ares vehicles already in development
- Lunar mission concept evaluations
- Habitat and logistics module concepts (hardside and inflatable)
- Lunar rovers and equipment mobility devices
- Construction equipment concepts for lunar soil excavation and movement
- Equipment and processes for oxygen extraction from lunar soil
- Lunar surface communications and navigation services
- Outpost evolution and growth (in both lunar equatorial and polar regions)
- Lunar infrastructure extensibility to Mars exploration

The Lunar Surface Systems Project is tasked with (1) continuing study and definition in all of these areas, and more, to refine an overall architecture for lunar surface operations; and (2) engaging the international community in preliminary discussions about long-term lunar outpost development.

Technologies for the lunar surface systems include: the Lunar Electric Rover gears, wheels, and mechanisms; robots for mobility; habitats; life support water recovery and air revitalization; in-suit resource utilization; habitability and human factors; and thermal control.

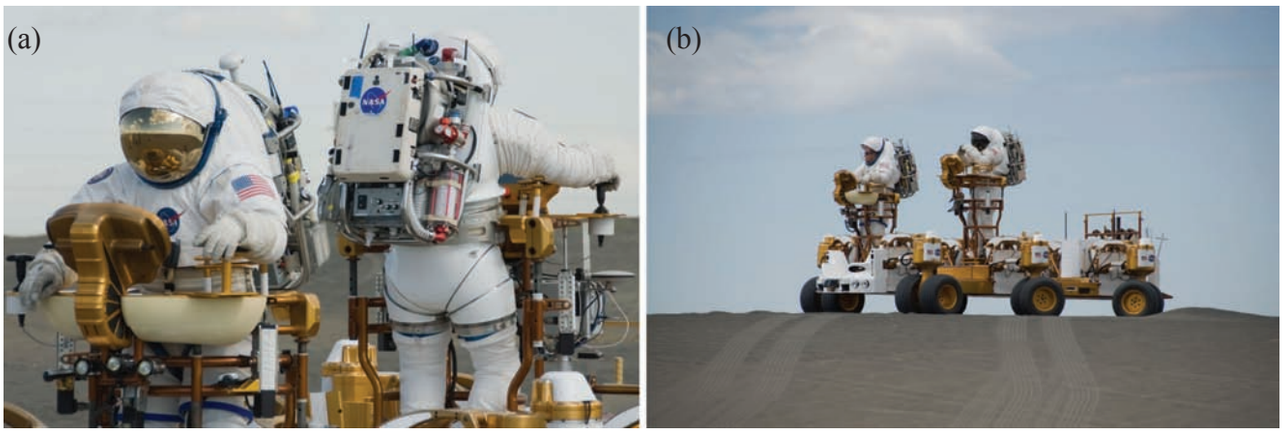

Fig. 5. *Engineers testing (a) prototype lunar surface suit, and (b) lunar rover concept vehicle.*

Acronyms and Abbreviations

ABR	antiorthostatic head-down bedrest
ACES	advanced crew escape suit
ACVS	AutoTRAC Computer Vision System
AGNC	autonomous guidance, navigation, and control
AGS	antigravity suit
AE	acoustic emission
AIAA	American Institute of Aeronautics and Astronautics
ALHAT	autonomous landing and hazard avoidance technology
ALS	advanced life support
AMISS	Anomaly Monitoring Inductive Software System
AMPEV	airlock manual pressure equalization valve
AMS	Aerospace Material Specification alpha magnetic spectrometer
ANITA	ammonia and nitrification analyzer
ANOVA	analysis of variance
ANSI	American National Standards Institute
ANSMET	Antarctic Search for Meteorites
APU	auxiliary propulsion unit
AR	augmented reality
AR&D	automated rendezvous and docking
ARC	NASA Ames Research Center
ARES	Astromaterials Research and Exploration Science
ASHRAE	American Society of Heating, Refrigeration, and Air-conditioning Engineers
ASME	American Society of Mechanical Engineers
ASTM	American Society for Testing and Materials
ATIC	advanced thin ionization calorimeter
ATV	automated transfer vehicle
AWRSDF	Advanced Water Recovery System Development Facility
BGA	beta gimbal assembly
BMD	bone mineral density
C/E	carbon fiber reinforced epoxy matrix
c.g.	center of gravity
C-SPE	colorimetric solid-phase extraction
CAMRAS	carbon dioxide and moisture removal amine swing-bed
CCSIT	CAMRAS/Constellation Suit Integrated Test
CDS	cascade distillation subsystem
CDT-2	Cluster Development Test 2
CDT-3	Cluster Development Test 3
CEV	Crew Exploration Vehicle
CFU	colony-forming unit
CH_4	methane
CID	current interrupt device
CLPA	camera, light, and pen/tilt unit assembly
CM	crew module
CMG	control moment gyroscope
CMI	cell-mediated immunity
CO	carbon monoxide
CO_2	carbon dioxide
COPV	composite overwrapped pressure vessel
COTS	commercial off-the-shelf
CPAS	CEV Parachute Assembly System
CPDS	charged particle directional spectrometer
CPOD	crew physiological observation device
CPSS	Critical Phase Software System
CR	Columbia Resin
CRV	Crew Return Vehicle
CSA-CP	compound specific analyzer-combustion products
CT	computed tomography
Cx	Constellation
CxP	Constellation Program
D	diameter
DA	digital astronaut
DACS	Data Acquisition and Control System
DEM	digital elevation map
DMC	Dartmouth-Hitchcock Medical Center
DNA	deoxyribonucleic acid
DOD	Department of Defense
DOE	Department of Energy
DOF	degree of freedom
DPD	deoxypyridinoline
DTED	Draeger®-Tube encapsulation device
DXA	dual-energy x-ray absorptiometry
EDS	Earth departure stage
EDU	engineering development unit

EDX	energy-dispersive x ray
EI	entry interface
EKG	electrocardiogram
ELS	Exploration Life Support
EM	engineering model
EMU	extravehicular mobility unit
EPR	electron paramagnetic resonance
EPS	Electrical Power System
ESEM	environmental scanning electron microscopy
ESMD	Exploration Systems Mission Directorate
ESR&T	Exploration Systems Research and Technology
ET	external tank
ETDP	exploration technology development program
EU	engineering unit
EUROPA	extensible universal remote operations planning architecture
EVA	extravehicular activity
FBC	forward bay cover
FCOVTB	fuel cell operational verification testbed
FCR	Flight Control Room
FCV	flow control valve
FDA	Food and Drug Administration
FeO	iron oxide
FIG	focused investment group
FOD	fiber optic displacement
FOMIS	fiber optic micrometeoroid impact sensor
FP	floating potential
FPMU	floating potential measurement unit
FRL	flight robotics laboratory
FY	fiscal year
Gen-1	Generation 1
GFE	government-furnished equipment
GN_2	gaseous nitrogen
GNC	guidance, navigation, and control
GRC	NASA Glenn Research Center
Grms	gravity, root mean square
H_2	hydrogen
H_2O	water vapor
HAZ	heat affected zone
HDA	hazard detection and avoidance
HEPA	high-efficiency particulate air
HHAP	Hydrogen Hazard Assessment Protocol
HITF	Hypervelocity Impact Technology Facility
HMD	head-mounted display
HNO_3	nitric acid
HRN	hazard relative navigation
HRP	Human Research Program
HSE	highly siderophile element
HSRB	Human System Risk Board
HST	Hubble Space Telescope
HVAC	heating, ventilation, and air conditioning
ICB	Inventions and Contributions Board
ICF	induction coil feedthrough
ICP-MS	inductively coupled plasma-mass spectrometry
IDR	Internal Design Review
IMA	International Mineralogical Association
IMS	Inductive Monitoring System
INSCOP	intranasal scopolamine
IPO	Innovation Partnerships Office
IR	infrared
ISRU	in-situ resource utilization
ISS	International Space Station
IV	intravehicular
JEOL	Japan Electron Optics Laboratory
JPL	NASA Jet Propulsion Laboratory
JSC	Johnson Space Center
K/E	Kevlar® fiber reinforced epoxy matrix
KCl	potassium chloride
KPH	kilometers per hour
LANCE	lunar attachment node for construction and excavation
LaRC	NASA Langley Research Center
LB	Lennox broth
LCCR	Lunar Capability Concept Review
LD_{50}	median lethal dose
LEA	launch-entry-abort
LEED	Leadership in Energy and Environmental Design
LEO	low-Earth orbit
LER	Lunar Electric Rover
LET	linear energy transfer
$Li(CF)_x$	lithium polycarbonmonofluoride
Li-ion	lithium-ion
Li-S	lithium-sulfur

LIDAR	light intensification detection and ranging
LiF	lithium fluoride
LIDAR	light intensification detection and ranging
LIDS	Low-impact Docking System
LIME	low-Fe, Mn-enriched
LM	Lockheed Martin Space Systems Company
LMA	Lockheed Martin Astronautics
LR	load ratio
LRES	lunar regolith environment simulator
LTER	Long Term Ecological Research
LVAD	low-velocity air drop
mAE	modal AE
MCA	major constituent analyzer
MCC	Mission Control Center
MDT-3	Main Development Test 3
MET	mission elapsed time
Metox	metal oxide
MIST	Mobile Information System
MIT	Massachusetts Institute of Technology
MMH	monomethylhydrazine
MMOD	micrometeoroid/orbital debris
MMSE	micrometeoroid and lunar secondary ejecta
MnSi	magnesium silicide
MOC	maximum oxygen concentration
MOD	Mission Operations Directorate
MOX	maximum oxygen concentration
MPH	monopropellant hydrazine
MPS	Main Propulsion System
MPSR	Multipurpose Support Room
MSFC	NASA Marshall Space Flight Center
MSL	Mars Science Laboratory
N_2H_4	hydrazine
NBL	Neutral Buoyancy Laboratory
NDE	nondestructive evaluation
NEEMO	NASA Extreme Environment Mission Operations
NESC	NASA Engineering Safety Center
NFIR	Natural Feature Image Recognition
NH_3	ammonia
NORCAT	Northern Centre for Advanced Technology Inc.
NPT	national pipe thread
NSF	National Science Foundation
NSI	NASA standard initiator
NSS	NASA Safety Standard
NTO	nitrogen tetroxide
NTX	N-telopeptide
O_2	oxygen
OCA	orbital communications adapter
OCAMS	OCA Mirroring System
OD	outside diameter
ORBITEC	Orbital Technologies Corporation
ORU	orbital replacement unit
OSP	orbital space plane
P-T	pressure and temperature
PA-1	Pad Abort-1
PAMELA	payload for antimatter exploration and light-nuclei astrophysics
PCTFE	polychlorotrifluoroethylene
Pd	palladium
PDI	powered descent initiation
PE	phenylephrine
PEMFC	proton exchange membrane fuel cell
PICA	phenolic impregnated carbon ablator
PILOT	precursor ISRU lunar oxygen test bed
PIM	Plasma Interaction Model
PK	pharmacokinetics
PLSS	Portable Life Support System
PLV	pulsed laser vaporization
PPE	personal protective equipment
ppm	parts per million
PRE	pre-reversal enhancement
PSI	Physical Sciences Inc.
PTC	positive temperature coefficient
PTV	parachute test vehicle
PVDF	polyvinylidene-fluoride
QCT	quantitative computed tomography
RCA	rapid cycle amine
RESOLVE	regolith and environment science and oxygen and lunar volatile extraction
RHTL	Remote Hypervelocity Test Laboratory
RNA	ribonucleic acid
RO	reverse osmosis
RRO	rotating reverse osmosis
SACE	Solar Array Constraint Engine
SARJ	solar alpha rotary joint

SBIR	Small Business Innovative Research
SBTT	Small Business Technology Transfer
SCM	soft capture mechanism
SD	standard deviation
SDTS	Six-DOF Dynamic Test System
SEH	Space Exposed Hardware
SLI	Space Launch Initiative
SLSD	Space Life Sciences Directorate
SM4	Servicing Mission 4
SMART-1	Small Missions for Advanced Research in Technology-1
SMS	space motion sickness
SNP	sodium nitroprusside
SPDM	special-purpose dexterous manipulator
SRB	solid rocket booster
SSC	space station computer
SSM	stepped stress method
STDEV	standard deviation
STEM	science, technology, engineering, and mathematics
STP	Sensor Technology Project
SU	sensor unit
SWCN	single-wall carbon nanotube
SWME	suit water membrane evaporator
2D	two-dimensional
3D	three-dimensional
TAMU	Texas A&M University
TC	thermocouple
TCM	trajectory correction maneuver
TEI	trans-Earth injection
TEM	transmission electron microscope
TEPC	tissue-equivalent proportional counter
TFIDF	term frequency inverse document frequency
THP	thermoelectric heat pump
TiO	titanium dioxide
TLD	thermoluminescent dosimetry
TOCA	total organic carbon analyzer
TPS	Thermal Protection System
TRIPS	Thermal Radiation Impact Protection System
TRL	technology readiness level
TRN	terrain relative navigation
UDMH	unsymmetrical dimethylhydrazine
UFORP	UDMH fuel/oxidizer reaction products
UT	ultrasound testing
UTS	ultimate tensile strength
UV	ultraviolet
UV-Vis-NIR	ultraviolet-visible-near infrared
VER	variable electronic regulator
VNS	visual navigation sensor
VO_2	oxygen uptake
VOA	volatile organic analyzer
VPU	video processing unit
VZV	varicella-zoster virus
WEST-P	Water Egress and Survival Trainer-Prototype
WLE	wing leading edge
WLEIDS	Wing Leading Edge Impact Detection System
WSTF	NASA White Sands Test Facility
Y-PCA	Y-shaped primer chamber assembly
YPR	yaw, pitch, and roll
ZPP	zirconium potassium perchlorate
ZrO_2	zirconium oxide

Human Health and Medicine

Space Life Sciences Innovation and Integration Successes

Jeffrey R. Davis, *Johnson Space Center and The University of Texas Medical Branch*

The Space Life Sciences Directorate (SLSD) at the Johnson Space Center (JSC) is implementing exciting, new changes in the integration and innovation of a complex technical body of work. The SLSD is comprised of professionals with a wide variety of degrees from MDs and PhDs in life sciences, engineering, and business. Many technical disciplines are required to provide services to all of our customers, as is experienced with project and program management. In addition to the three major space flight programs (i.e., the Space Shuttle, International Space Station (ISS), and Constellation Programs), SLSD also hosts the Human Research Program (HRP). SLSD truly functions as a team with members from multiple NASA centers, Wyle Integrated Science and Engineering (and several subcontractors), Baylor College of Medicine (as host to the National Space Biomedical Research Institute), and the Universities Space Research Association. The team is comprised of approximately 160 civil servants and 900 contractors.

Short- and especially long-duration human space flights challenge the human system, and we are responsible for maintaining the health and well-being of space travelers. Maintaining health and well-being requires not only medical services but also biomedical research to mitigate the hazards of space flight and technologies and to provide services for environmental monitoring, habitability, and human factors.

Integration

To address these challenges, SLSD recently took steps to better integrate all of these professional services for human space flight and to focus our efforts on the highest-priority human health and performance risks for various missions. Our first step was to view the human in space flight as a human system that must be optimally integrated with vehicle systems. While the definition of the human system will vary with organizations outside NASA, for our purposes it means: risks to the human from a medical, a physiological, a performance, an environmental (including radiation, fractional gravity, toxicology, and microbiology), a human factors, and a habitability standpoint. We have developed a comprehensive, standards-driven, risk-based system that focuses all our work on the highest-priority human health and performance risks during space flight.

Our next step was to form an integrated Human System Risk Board (HSRB) and forum. The JSC Chief Medical Officer chairs the HSRB; and HRP managers and managers from all SLSD divisions serve as active voting members on this decision-making board. The board structure permits the integration of medicine and research as well as all technical disciplines. As the HSRB focuses on the risks of human space flight, many disciplines (including expertise from medicine and research) can take part in comprehensive board discussions. Since the board was formed in April 2008, its members have made several timely decisions to rebalance the research portfolio, accepted a risk with operational mitigation, and agreed to new risks based on recent evidence. The HSRB is open through teleconferences and WebEx support to many who cannot attend it in person.

Innovation

The SLSD leadership team recognizes the need to accelerate and diversify innovative strategies to solve both short- and long-duration space flight problems. Accordingly, the team recently renewed its emphasis on flying commercially available hardware that can be adapted to space flight (e.g., flying this year a commercial automatic external defibrillator), and flew a commercial treadmill for astronaut use and a gas chromatograph/differential mobility spectrometer to monitor vehicle air quality.

The SLSD is also exploring techniques of open or distributed innovation. In April 2008, we collaborated with the Rice Business Alliance to form the Rice Business Plan Competition, offering the first-ever NASA Earth/Space Life Sciences prize. This prize is awarded for a technology that was developed for terrestrial uses, but that may also have application in space flight. Teams that participate in the Rice Business Plan Competition must demonstrate a solid technology and business plan. The initial team submissions are culled down to 36 team finalists, who compete in Houston each spring. HeartSounds, the winner of the 2008 NASA prize, came from the University of Illinois, Chicago. The HeartSounds technology, as its name suggests, is a wireless patch that can diagnose heart sounds and pressures and transmit the data to a small storage device for later downloading. The HeartSounds team visited JSC to collaborate with our medical doctors and scientists. In the April 2009 competition, the JSC Engineering

Space Life Sciences Innovation and Integration Successes

continued

Directorate joined with the SLSD to expand the prize offerings. The 2009 winner was Integrated Diagnostics, a team that designed the HemaScreen. The HemaScreen technology is a rapid clinical assay that uses integrated circuit technology to perform multiple immunoassay tests.

Another innovative technique that SLSD is exploring is an open source approach to further develop a computational physiological model of the human body – the digital astronaut (DA). The use of open source could accelerate the development of the DA in a cost-effective manner. It also allows for easier incorporation of previously developed sub-models from the broader national/international community of model developers, and facilitates participation of interested model developers from inside and outside the NASA community. This approach can potentially enrich the global knowledge base for computational physiological modeling. SLSD released the initial version of the DA in mid-2009.

Other initiatives in open or distributed innovation included sponsoring workshops on open innovation with professors and material from the Harvard Business School. As these workshops focused on community-based design, SLSD is now exploring various techniques to tap a larger community of expertise – perhaps by awarding national prizes.

These exciting changes in integration and innovation will truly position SLSD to be a valuable provider of services for the human system for the ISS as well as for future flights to the moon and Mars.

Websites

Space Life Sciences Website: http://slsd.jsc.nasa.gov

Rice Alliance Website: http://alliance.rice.edu

Space Medicine: Past, Present, and Future Issues

J. D. Polk, *Johnson Space Center*

Where do you start when your country wants you to go back to the moon and on to Mars? You start with where you have been and look at where you are now operationally. You must define the concept of operations and the levels of care. You also must understand the six tenets of flight medicine: mass, power, volume, time, money, and risk.

The mass you can carry is limited; launch cost is $10,000 to $20,000 per pound. The usable power and available volume are also limited. Crew member time is similarly limited, and so is the available money. The risks are very real, and we have to lower them. As we look at how to solve our medical innovation issues, we have to consider constraints and tradeoffs. (If you want your medical project to succeed, it should not increase more than two of these, and preferably should reduce at least one. – Polk's Law)

Originally we were not sure what would happen to people in space, and what we did learn, we did not easily share. Other countries were competitors, not partners. We selected crew members from a very specific type of individual, and their flights were very short – often lasting a few days. The average age for Apollo crew members, for example, was 36; the average age of members in today's Astronaut Corps is 46. We operated differently in the Apollo days.

While early crews consisted primarily of fighter pilots, today's crews now include scientists, educators, and people from many other backgrounds. The psychological makeup of these crews necessarily differs, too. Missions are longer, measured in weeks and months, and crew members can return to a planet that diverges socially from the one they left. For example, one cosmonaut left the USSR and, when he landed, his nation's form of government had changed.

Some key components of our current medical support system on orbit are: the ambulatory medical pack, containing mostly over-the-counter drugs and medical supplies; the advanced life support pack, which has more powerful drugs and supplies and can perform ultrasound; flight surgeon support (remotely, on console); and three exercise devices – the Cycle Ergometer with Vibration Isolation System; the Treadmill with Vibration Isolation System; and the advanced resistive exercise device.

NASA's overall flight medicine strategy is to practice offensive preventive medicine. This approach (and the bioastronautics research that supports it) massively reduces our risk, our cost, and the volume of what we have to fly. This overall strategy can be broken down into three primary preventive strategies.

Primary preventive strategy: *selection standards for crew*. We are extremely careful when choosing astronaut candidates.

Secondary preventive strategy: *fitness for duty and medical requirements*. We scan crews for long-duration issues (e.g., scans discovered a tumor in a crew member's pituitary gland that would have led to optic nerve problems). It is not cost-effective to discard astronauts once we have spent $1M to train them; at that point it is far easier to fix any problems they have.

Tertiary preventive strategy: *in-flight mitigation and treatment.* We fly therapies to treat the remaining risk.

Other factors that support this approach on the clinical side include quality and consistency, patient information dataflow, occupational health surveillance, and focused operational research and development. Because a lean Six Sigma practice has standardized guidelines of care, we focus on standardized electronic medical records (essential when crews train in Russia for a number of months), produced a SharePoint warehouse for mission data, maintain the Lifetime Surveillance of Astronaut Health, and created the Life Sciences Data Archive to preserve our lessons learned. NASA needs innovations and alliances in treatment processes and how we attack things on orbit, but the best thing we can do is to fly a healthy astronaut.

How does all this help space flight – and NASA's partners? Below are two examples.

Example 1: A closed-circuit ventilator with oxygen concentrator

This device was created as part of a partnership among NASA, the department of Defense (DOD), business, and academia. We focused on this problem for a number of reasons. If an ammonia release takes place on orbit and a crew member must be intubated for ventilation, that oxygen could leak into the cabin and

elevate the fire risk. The project created a closed-loop ventilator with net environmental oxygen change zero, in addition to saving the mass and volume of many bulky oxygen bottles. This device provided parallel benefits to DOD (i.e., to also not have to fly heavy, bulky oxygen bottles), and could potentially change care in small hospitals that have neither the time nor the space to support a more conventional solution.

Example 2: Crew physiological observation device

Fig. 1. *Crew physiological observation device.*

The NASA Ames Research Center developed a small (the size of a BlackBerry®) and light device for a belt carrier – the crew physiological observation device (CPOD) – that transmits ultrasound and EKG [electrocardiogram] data to the heads-up display (figure 1). We tested the CPOD and expect it to be available for use in private practice in about 10 years.

How do we start planning for the medical side of exploration?

To plan for the medical side of exploration, we must first answer the following questions:

What is the risk?

What are the medical diagnoses unique to space flight or astronaut populations?

What is the best mitigation strategy? Is it prevention, prophylactic surgery, genetic screening, flying a physician on the mission, or perhaps some combination of these?

Remember the six tenets of flight medicine and the constraints we have to work under. The higher the capabilities we fly, the lower the risk; but we cannot eliminate all risk, and we cannot fly all of the potential capabilities. Risk equals severity times probability, so we take the middle road of accepting some risk and fly capabilities and mitigations to reduce the remaining risks.

In the near future, NASA faces a number of unique aspects. The distance of Mars from Earth (20+ minutes communication time, 6+ months travel time) changes things. In-situ production of consumables and sustainability of power have never before been required on NASA missions. On future Exploration missions, crews will have to be relatively autonomous. We will also have to reverse the "life-limb-mission" paradigm. If a crew member in low-Earth orbit sustains an injury or becomes ill, it is possible to bring that crew member down for treatment of the injury or disease. On Exploration missions, it is a different story; we cannot fly all six crew members the several months back from Mars to treat one crew member's injury or disease. Triage thus becomes important.

The building blocks of Exploration clinical medicine will be modular; we will build on our hardware and our capabilities. We will fly equipment to the moon and leave it there, continuing to add to it. NASA is building toward 6-month lunar missions and 24-month Mars missions. But what levels of care are possible on these missions, and where do we have to stop? These are tough triage decisions. Common things occur regularly, and all space-flight-unique medical maladies as well as residuals are not necessarily screened out. What is possible is not always feasible, and is often limited by consumables.

NASA is leveraging experience from all of its past experiences, including Apollo, Skylab, shuttle, *Mir*, and the International Space Station (ISS). Flight analogs are Antarctic stations, submarines, and NEEMO [NASA Extreme Environment Mission Operations], an underwater center off the coast of Florida. We forecast, based on previous experience, our concept of operations, Delphi, flight tolerance, probability, and mitigation.

The concept of operations for Exploration medicine is clear. It takes 6 months to travel from Earth to Mars in microgravity. Six-month flights aboard ISS have allowed us to learn the issues there. The moon is at 1/6g; will our strategies and healing processes work in reduced gravity? The lunar missions will provide the necessary proof of concept to see whether those processes will work on the 3/8g of Mars.

Human Adaptation to Space: Space Physiology and Countermeasures

Jennifer Fogarty, *Johnson Space Center*

Humans engaged in space flight respond to more than just the microgravity environment. They also respond to acceleration impacts, living and working in confined spaces, remote deployment, restricted communication, limited privacy, demanding timelines, critical operations, and little or no availability of evacuation. All of this contributes to physiological, mental, and emotional stress. NASA flies sundry types of missions with a diverse corps of astronauts, each of whom responds differently to the stressors to which he or she is exposed. So in our planning, we must consider the likelihood and consequences of health and performance risks, alterations in acute health, performance, and long-term health in the context of mission objectives.

Astronauts adapt to microgravity within the first few days of exposure. The space adaptation process, common to both short- and long-duration missions, is less noticeable in the context of a long-duration mission because it takes up a much smaller portion of the overall mission time (~22% of short-duration and ~1.5% of long-duration missions). In light of this, how do we prioritize risks and risk factors to address differing mission lengths?

To make well-informed decisions, NASA invests in measuring and understanding a number of physiological systems. This is because it is at the level of these systems, and the risk factors manifested within them, that we can successfully intervene and perhaps minimize the likelihood and/or consequence of a risk. Conditions common to short-duration flight include: space motion sickness, headache, back pain, insomnia, nasal congestion, constipation, nosebleeds, urinary retention, and incontinence. These conditions, as a group, are known as space adaptation syndrome.

Space adaptation syndrome manifests early in space flight (within minutes or hours) and can last 72 hours or longer. A tremendous amount of individual variability exists with regard to the intensity and duration of its symptoms and conditions, however. We know, for example, that astronauts who flew on more than one mission experienced a different adaptation process for each mission. It is thus difficult to predict what an individual will experience in adapting to space. This inability to predict intensity and duration challenges us in terms of supplying appropriate therapies, including prophylaxis. Therefore, we need to cultivate an understanding of the mechanisms behind these responses to be better prepared with regard to resources, and to leverage terrestrial medicine and try different and perhaps more effective solutions without introducing new risks via side effects or contraindications.

The concern with crews engaged in long-duration missions is not just space adaptation, but continued degradation of physiological systems and manifestation of disease over time. To date, we regularly analyze data on 20 long-duration International Space Station (ISS) astronauts (through Expedition 16) who have spent an average of 4 to 6 months in space. But if a future Exploration mission lasted 9 or 12 months, would the documented trends continue in a linear fashion? Are the decrements reversible once an astronaut returns to Earth?

We currently collect data on bone mineral density, aerobic capacity, neurovestibular organs, and performance changes. We are also using a three-device countermeasure system on the ISS to address the physiological effects of space flight. Each of these is discussed below.

Space medicine practitioners measure bone mineral density to document bone loss conferred by space flight. The imaging methodology in use today provides a two-dimensional (2D) measurement of bone mineral density. Because we now know, based on results of a published research study, that the three-dimensional (3D) architecture of the bone is altered in space flight, we are unsure of the degree of alteration and the consequence to bone strength. We thus need to develop an in-flight imaging solution to help us understand the 3D structure of bone to assess alterations in bone strength; this tool would need to be small, light, and lean (figure 1).

In addition to bone mineral density, we also measure aerobic capacity pre-flight, in flight (every 30 days), and post-flight to provide an index of the detraining effect of microgravity. These measurements show that: in flight, a precipitous decline occurs in aerobic capacity immediately; a small recovery takes place during the second and third month and then plateaus; and a noticeable decrement occurs immediately post-flight, 4 to 7 days after landing. We hypothesize that loss of muscle mass, redistribution of fluids, and alterations in the sensorimotor capability

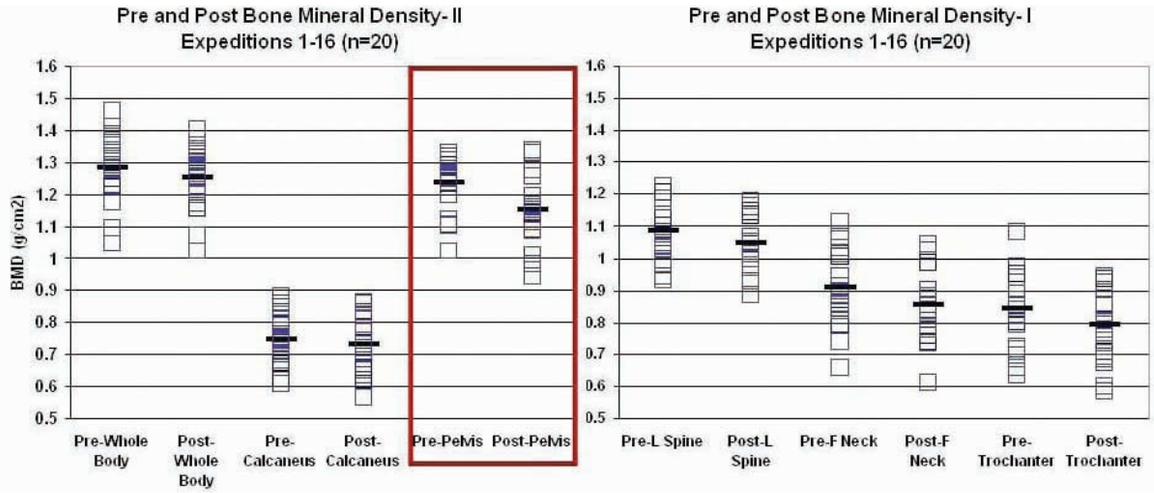

Fig. 1. *Pre and post bone mineral densities.*

lead, in concert, to reduced aerobic capacity post-flight. Fortunately, by 1 month after return, most astronauts have returned to their baseline or better. Yet although functional capacity is regained, it is unclear whether structural changes to the involved systems may persist (figure 2).

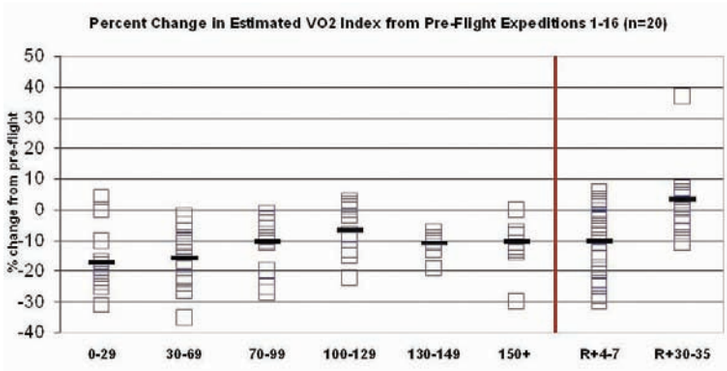

Fig. 2. *Percent change in estimated oxygen uptake (VO_2) index.*

Scientists have established that neurovestibular organs are affected by space flight, but it is often hard to determine the relative contribution of a cardiovascular effect and a neurological effect when a post-flight crew member is unable to remain upright. The sensorimotor test has proven effective for performing this assessment. We have therefore found that neurovestibular function returns post-flight, but not as quickly as cardiovascular function.

To assess performance impacts it is necessary to have specific information strength, flexibility, and core stability. Functional fitness data demonstrate that upper and lower body strength are diminished. A decrement is measured immediately post-flight. Fortunately, crew members do regain all functional fitness capabilities, often surpassing their pre-flight baseline.

A three-device countermeasure system (the resistive exercise device, treadmill, and cycle ergometer) is used on ISS to address the physiological effects of space flight. This integrated system supports crew capability for normal and contingency operations with limited redundancy and crossover. Ground crews, flight surgeons, and astronaut strength and conditioning specialists monitor crew data and adjust exercise programs accordingly. They also track the availability and reliability of the hardware to assess the equipment and determine whether it is meeting the needs of crew members, requires repair, and/or needs to be replaced.

To summarize, it is essential to use both current space flight missions and analog environments to study the effects of the stressors (e.g., acceleration, vibration, microgravity, fractional gravity) that we are placing on humans. Our ability to understand these effects at a fundamental and mechanistic level will allow us to better target countermeasure development, design selection criteria, and build medical kits to address conditions that we cannot prevent.

Development and Clinical Evaluation of Intranasal Scopolamine Gel Formulation

Lakshmi Putcha, *Johnson Space Center*

Jason L. Boyd, *Johnson Space Center*

The goal of this research is to develop a noninvasive, efficacious dosage form of scopolamine, the clear drug of choice for the treatment of space motion sickness (SMS). An alternative route of administration – intranasal to oral – aims at circumventing the gastrointestinal dysfunction caused by SMS, thereby enhancing the efficacy. Earlier reports indicate that intranasal dosing with scopolamine increases the absorption rate and bioavailability compared to an equivalent oral dose. Another advantage of intranasal administration of medications is the avoidance of first-pass metabolism by the liver to which certain drugs are subjected after oral administration. This new formulation design is based on the hypothesis that gel formulations are more suited than liquid dosage forms for prophylaxis and treatment of SMS.

Three FDA [Food and Drug Administration]-sponsored clinical trials were designed to characterize pharmacokinetics (PK) and pharmacodynamics, and to evaluate the safety and efficacy of intranasal scopolamine (INSCOP). The first of three trials of the relative bioavailability and PK of INSCOP, conducted at MDS Pharma Services, King of Prussia, Pa., entailed the administration of three doses of INSCOP to 12 subjects to establish the dose range for treatment. In figure 1, the area under the curve, a measure of bioavailability, increases linearly with dose while all other parameters are consistent for all three doses. These results confirm that the bioavailability and PK of scopolamine are linear at the dose range of this investigation.

The second clinical trial, conducted at the Dartmouth-Hitchcock Medical Center (DMC) in Lebanon, N.H., determined the efficacy of two doses of INSCOP for the treatment of motion-induced sickness that was simulated by an off-axis vertical rotation chair in 18 motion-sickness-susceptible subjects. Results suggest that INSCOP is equally efficacious at both low and high doses (0.2 and 0.4 mg), as indicated by the longer chair ride times of subjects who had been administered INSCOP than the times of those who had been administered a placebo.

The third and final clinical trial, conducted at MDS Pharma Services, examined changes in the bioavailability and PK of two doses of INSCOP in 12 subjects using a ground-based microgravity analog – an antiorthostatic head-down bedrest (ABR) model. Results indicate that: (1) the relative bioavailability of a higher dose (0.4 mg) and not a lower dose (0.2 mg) of INSCOP increased during ABR compared to that available during ambulation; and (2) gender-specific differences exist in the bioavailability and PK of INSCOP during ABR.

We conducted a follow-on collaborative study, funded by Naval Aerospace Medical Research Laboratory, Pensacola, Fla., to examine the relative efficacy of standard treatment regimes of motion sickness to that of INSCOP. Results from this study agreed with those from DMC and confirmed that a 0.4-mg dose of INSCOP was efficacious in suppressing motion sickness symptoms caused by the motion simulator dome, which is another paradigm for motion-induced sickness. Indeed, INSCOP significantly increased time in the dome in motion-susceptible subjects (figure 1). INSCOP was also used by a small number of crew members as needed for treatment of SMS during space flight. Anecdotal reports from crew members and flight surgeons indicate that the formulation was efficacious for the treatment of SMS. We expect to continue to work with the pharmaceutical industry and academia on these types of studies.

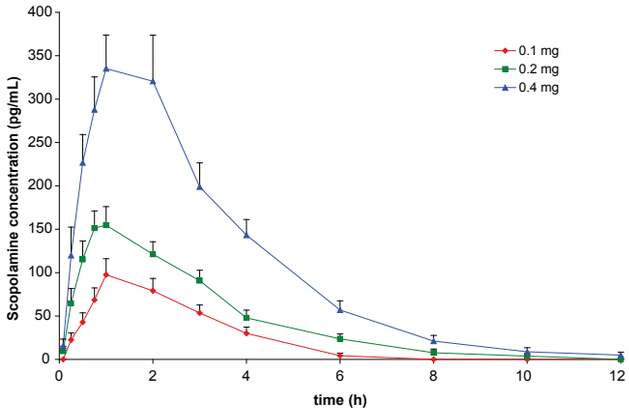

Fig. 1. *Plasma concentration-time profiles after INSCOP administration (n=12).*

Media Ion Composition Controls Regulatory and Virulence Response of *Salmonella* in Space Flight

C. Mark Ott, *Johnson Space Center*
James W. Wilson, *The Biodesign Institute, Center for Infectious Diseases and Vaccinology, Arizona State University; Department of Biology, Villanova University*
Duane L. Pierson, *Johnson Space Center*
Cheryl A. Nickerson, *The Biodesign Institute, Center for Infectious Diseases and Vaccinology, Arizona State University*

Microbial pathogens cultured during space flight appear to cause disease differently than those cultured using traditional methods. This difference offers a key insight into not only fundamental cellular and molecular response mechanisms but also the potential identification of previously undiscovered classes of genes and proteins that are important for the infectious disease process. Historically, the study of microbial responses in extreme environments (e.g., severe shifts in pH, osmotic concentration, or temperature) has provided tremendous insight into our understanding of how pathogens adapt and respond during the infection process in vivo. For pathogens, many of these conditions reflect the environment they encounter during the normal infection process. In this regard, the conditions that microorganisms encounter in the microgravity environment of space flight are relevant to the low-fluid-shear areas encountered by pathogens during infection of a human host, such as in areas of the intestinal tract. This latter environment holds importance for enteric pathogens such as *Salmonella typhimurium*.

In early NASA-supported studies by Cheryl A. Nickerson of Arizona State University, cultures of *S. typhimurium* grown in space-flight-analog bioreactors in rich Lennox broth (LB) media displayed increased virulence and global changes in gene expression, including a large number of genes encoding ion response pathways that were differentially regulated in response to this low-fluid-shear growth condition. The potential role for ion-mediated regulation of cellular responses to this environment was observed in additional flight-analog bioreactor experiments, which showed that in the low-nutrient, high-inorganic salt of M9 minimal media, *Salmonella* lag phase and generation time were shortened compared to the lag phase and generation time of controls. This effect was not observed in LB media under identical growth conditions. These analog observations led to flight experiments with *S. typhimurium* aboard space shuttle mission STS-115, which demonstrated that cultures grown in rich LB media in space flight display major alterations in global gene expression (including a large number of genes encoding ion response pathways) and increased virulence. A central role was also identified for the conserved small regulatory ribonucleic acid (RNA)-binding protein Hfq in regulating key aspects of the space flight microgravity responses.

Nickerson and her team wanted to further the understanding of the effect of space flight on bacterial virulence and to test the hypothesis that ion concentrations could be manipulated to prevent the enhanced *Salmonella* virulence imparted during flight. They performed additional analyses on STS-115 with *S. typhimurium* cultured in M9 minimal media, and then on a follow-up shuttle flight opportunity on STS-123 that allowed direct comparisons between *Salmonella* cultured in LB, M9, and LB-M9 salts supplemented with inorganic ions to the same levels as those found in M9 medium (LB-M9 salts). As with space flight growth in LB media, *S. typhimurium* growth in M9 media displayed differential expression of many genes, including those associated with either the regulation of, or regulation by, the Hfq protein and small regulatory RNAs – thus suggesting conserved regulatory mechanisms for

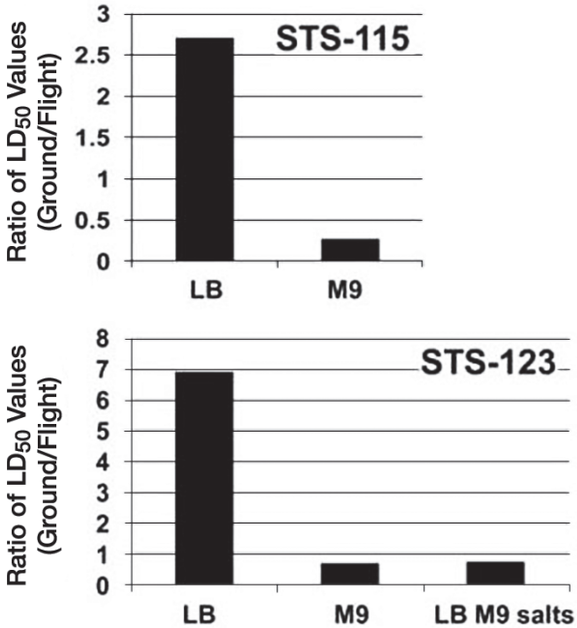

Fig. 1. S. typhimurium *virulence in LB, M9, and LB-M9 salts.*

cellular responses to space flight. *S. typhimurium* grown in various media demonstrated that ion concentrations had a direct effect on the virulence of the cultures – beyond what would be expected in normal ground controls. When *S. typhimurium* was grown in LB medium on board STS-123, an evaluation of the median lethal dose (LD_{50}) values and time to death using a murine model of infection confirmed a space-flight-associated increase in virulence (figure 1). However, when *S. typhimurium* was grown in M9 media on this same flight, no increase in virulence was observed. To determine whether key inorganic salts in the M9 media were responsible for virulence changes during flight, additional cultures of *S. typhimurium* were grown in LB medium supplemented with five salts/ions that were in high concentration in the M9 medium (LB-M9 salts). *S. typhimurium* grown in LB-M9 salts had LD_{50} and time-to-death values similar to those of cultures grown in M9 media, indicating no increase in virulence and suggesting that the ions played a key role in the space-flight-associated virulence effect. Subsequent space-flight-analog bioreactor studies indicate that higher concentrations of phosphate ions are a key in the mechanism for altering *S. typhimurium* responses to space flight.

This space flight experiment provides the first evidence of an environmental mechanism behind space-flight-associated virulence changes in *S. typhimurium*, imparts a breakthrough in our understanding of how NASA can mitigate infectious disease risk to a crew during space flight, and may be exploited to better understand microbial pathogenesis as well as to develop innovative therapeutics on Earth.

Varicella-zoster Virus in the Saliva of Patients with Herpes Zoster

Satish K. Mehta, *Johnson Space Center*
Stephen K. Tyring,
University of Texas Health Science Center
Donald H. Gilden,
University of Colorado Health Sciences Center
Randall J. Cohrs,
University of Colorado Health Science Center
Melanie J. Leal, *Johnson Space Center*
Victoria A. Castro, *Johnson Space Center*
Alan H. Feiveson, *Johnson Space Center*
C. Mark Ott, *Johnson Space Center*
Duane L Pierson, *Johnson Space Center*

Varicella-zoster virus (VZV) is the etiologic agent of two diseases, varicella (chickenpox) and zoster (shingles). Varicella typically results from the first exposure to VZV and most commonly is a disease in young children. After the chickenpox resolves, the virus becomes latent in ganglia along the entire neuraxis. Zoster is most commonly a disease of adults. As the cell-mediated immunity (CMI) to VZV declines, usually decades after initial exposure to VZV, the virus reactivates to produce shingles (figure 1). We completed a set of studies to evaluate CMI and viral reactivation in astronauts during flight.

Previous studies demonstrated declines in CMI as well as innate immunity in astronauts. Our initial study of astronauts examined their saliva to determine whether space-flight-associated factors decreased CMI enough to allow VZV reactivation and subsequent shedding in saliva. We used a polymerase chain reaction assay to detect VZV deoxyribonucleic acid (DNA). Astronauts on a shuttle mission reactivated VZV and shed the virus in saliva. No symptoms attributable to VZV reactivation occurred, but reactivation of the VZV and other latent viruses serves as a sensitive biomarker for decreased CMI.

Fig. 1. *Patient with varicella-zoster virus.*

This astronaut study led directly to a clinical study of zoster patients. The objective was to determine whether zoster patients shed VZV in saliva. Fifty-four patients with herpes zoster were treated with valacyclovir. On treatment days 1, 8, and 15, we scored pain and examined saliva for VZV DNA. We found VZV DNA in every patient the day treatment started; the virus later disappeared in 82% of the patients. This provided a positive correlation between the presence of VZV DNA and pain and between VZV DNA copy number and pain ($P<0.0005$). We found VZV DNA in one patient before rash and in four patients after pain resolved; it was not present in any of six subjects with chronic pain or in the 14 healthy subjects.

This was the first large study that demonstrated the presence of VZV in saliva of shingles patients. More importantly, it showed the presence and amount of VZV in saliva correlated with clinical disease; that is, as the symptoms (e.g., pain) dissipated and lesions healed, the VZV in the patients' saliva disappeared. It appears that VZV reactivates during periods of decreased immunity and is shed in saliva prior to rash formation. In one patient, pain preceded rash. After we detected VZV DNA in both a patient's saliva and plasma, that patient's physician treated her immediately with oral valacyclovir. This resulted in a significant decrease in pain coinciding with the disappearance of VZV DNA in her saliva and plasma.

An early clinical sign of impending shingles is pain in one or two dermatomes prior to the appearance of the zoster rash. Early indications are that VZV appears in saliva during this prodromal period. Detection of VZV allows for early diagnosis and rapid intervention therapy. Rapid treatment limits nerve damage.

This study led to the development of a rapid test for VZV in saliva that can be conducted in a physician's office in fewer than 30 minutes. In addition to shingles applications, the test is potentially useful in the diagnosis of neurological disease produced by VZV without rash. In this study, we demonstrated the practical application of NASA-developed technology to everyday life.

Patent application no. 61/087,04 was filed on August 8, 2009 under *Saliva assay for rapid identification of VZV.*

Innovative Treatments for Dental Emergencies During Lunar and Exploration Missions

Diane Byerly, *Johnson Space Center*
Dickey Arndt, *Johnson Space Center*
Marguerite Sognier, *Johnson Space Center*
Ivan Stangel, *BioMat Sciences*
John Dusl, *Johnson Space Center*
Phong Ngo, *Johnson Space Center*
Chau Phan, *Johnson Space Center*

The risk of astronaut dental problems occurring on extended Exploration missions represents a significant health and safety concern that can impact mission success. Despite pre-flight examination and treatment of astronauts, not all dental problems can be prevented. The longer the space flights, the higher the probability that dental problems will occur. As none of the current treatments is amenable to astronauts who are on extended-duration space missions, we developed alternative methods to treat dental caries (tooth decay).

The current treatment of caries requires: (1) the administration of a local anesthetic; (2) drilling to remove the decayed part of a tooth; and (3) tooth reconstruction using composites that are also needed to manage tooth fracture or failed fillings. Presently available composite materials and standard techniques for reconstructing teeth are less than optimal for space exploration missions. Procedures necessitate a variety of bulky equipment and can be very complicated. For example, root canal treatment for spontaneously occurring tooth pain requires considerable skill and the transportation of bulky equipment. The treatment includes drilling to access the canal deep in the tooth, locating canal orifices in the presence of internal tooth bleeding, using fine instruments to remove all of the cell contents, and shaping and filling the canal. Not only is considerable skill essential to achieve this, but local anesthetic is also needed, which entails another set of complex skills.

We developed a lightweight, miniaturized microwave system to enable emergency dental treatments by a non-dental expert (e.g., an astronaut). This handheld microwave system consists of a sharply focused antenna, a signal source, and a power amplifier (figure 1). The system is customized to effectively (1) eliminate bacteria that are involved in the formation of caries; (2) cure (solidify) proprietary composites for repair and reconstruction of teeth in a patient's mouth in real time; and (3) treat diseased pulpal tissue (root canal) without drilling (patents).

Our results show that microwave energy focused through use of the newly developed antenna system can successfully cure the proprietary composites supplied by

Fig. 1. *Microwave prototype device for dental treatments.*

BioMat Sciences for tooth repair and reconstruction. This will enable rapid tooth reconstruction (following trauma) and caries treatment in real time in the patient's mouth. This system is under development to automatically determine how much time is required for curing the composite, thereby obviating the need for skilled dental training.

These studies required the development of a number of unique bacteria and mammalian cell-based model test systems. Results produced through use of these unique testbeds show that more than 99% of the caries that cause bacteria are killed within a 20- to 30-second exposure to microwave energy while minimally affecting the healthy gum tissue simulant. The proprietary composite materials for tooth reconstruction can be cured within 30 seconds. Preliminary results involving the efficacy of pulpal disease treatment indicate that effective ablation of diseased tissue may be achieved within 60 seconds.

This new technology development supports the (1) NASA Policy Directive to provide dental care during all mission phases; and (2) Human Research Program, Exploration Science Mission Directorate, and Space Operations Mission Directorate goals. It will also have widespread commercial applications on Earth, enabling dental care to be simplified, less invasive, less expensive, and longer lasting. This technology will be of particular value in military battlefield situations and to populations who, because they are living in isolated areas (figure 2), have limited access to dental care.

Innovative Treatments for Dental Emergencies During Lunar and Exploration Missions

continued

Patents

Noninvasive Treatment of Diseased Pulpal Tissue Using Focused Microwave Energy

Dental Composite Curing Using Focused Microwave Energy

Noninvasive Treatment of Dental Caries Using Focused Microwave Energy

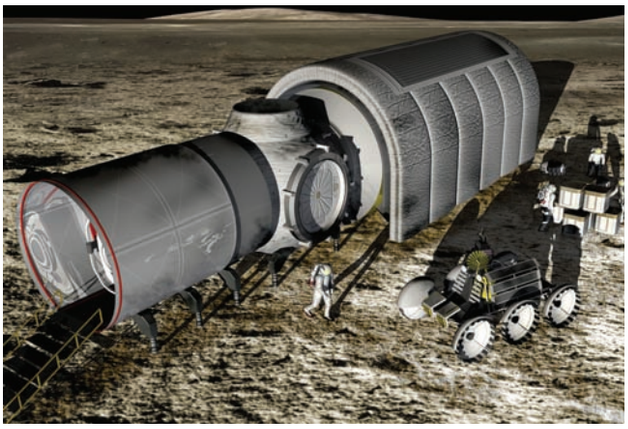

Fig. 2. *An example of an isolated area (lunar habitat).*

Adaptation of the Skeletal System During Long-duration Space Flight

Jean D. Sibonga, *Johnson Space Center*
Peter R. Cavanagh,
Lerner Research Institute, Cleveland Clinic
Thomas F. Lang, *University of California, San Francisco*
Adrian D. LeBlanc,
Universities Space Research Association
Victor S. Schneider, *NASA Headquarters*
Linda C. Shackelford, *Johnson Space Center*
Scott M. Smith, *Johnson Space Center*
Laurence Vico, *Jean Monnet University, France*

Evidence from crew members who flew on space missions longer than 90 days suggests that adaptations of the skeletal system to mechanical unloading may predispose these crew members to an accelerated onset of osteoporosis after they return to Earth. By definition, osteoporosis is a skeletal disorder that is characterized by low bone mineral density and structural deterioration. It reduces the ability of bones to resist fracture under the loading of normal daily activities. Age-related osteoporosis is readily recognized as a syndrome afflicting the elderly because the insipid and asymptomatic nature of bone loss does not typically manifest as fractures until after approximately age 60. This review draws parallels between the rapid and earlier bone loss in females that occurs with menopause and the rapid bone loss in middle-aged crew members that occurs with space flight unloading, and how the cumulative effects of space flight and aging could be detrimental, particularly if skeletal effects are totally or partially irreversible.

On Earth, the adult human skeleton renews and repairs itself with approximately one-tenth renewed annually. The putative osteocytic cells signal the skeleton to initiate remodeling in discrete packets. In a well-orchestrated manner, bone-resorbing cells (osteoclasts) remove bone tissue while bone-forming cells (osteoblasts) replace it. When remodeling is accelerated, as occurs with menopausal bone loss, the "birth rate" of bone remodeling units is high. This acceleration can be quantified by histomorphometry with the index of activation frequency, which has been shown to increase in the aging female. Histomorphometric analyses have further revealed how increased numbers of bone-remodeling units can perforate horizontal trabecular struts of cancellous bone microarchitecture and induce greater porosity in cortical bone. The loss of trabecular elements and of connectivity between trabeculae reduces the mechanical strength of the trabecular scaffold. The accelerated loss of bone with menopause targets the cancellous bone compartment (i.e., the trabecular or spongy bone) in which resorption preferentially occurs along the bone surfaces adjacent to bone marrow. This mechanism of bone loss leads to: (1) thinning of the cortical bone shell and the trabecular plates; (2) perforation of trabecular struts; and (3) loss of trabecular elements and connectivity. With menopause, there is a 20% to 30% reduction in cancellous bone compared to the 5% to 10% loss of cortical bone associated with the first decade after menopause. This bone loss accounts for a higher incidence of fractures in women (compared to men of the same age range) at skeletal sites predominantly composed of cancellous bone (i.e., wrist fractures and vertebral crush fractures). Increased remodeling can also be inferred by increased levels of biomarkers for bone formation and bone resorption.

The application of quantitative computed tomography [QCT] to a population study substantiated the earlier and persistent losses in cancellous bone occurring in both men and women (~33% and 50% of total lifetime loss, respectively). Likewise, substantial losses in cortical bone in women begin around midlife with menopause onset, while cortical bone loss in men does not accelerate until much later. Not only do women have smaller bones than men from the outset, the deficiency of estrogen with menopause is a major contributing factor to osteoporosis (and its associated fragility fractures) in women compared to men at the same age. The knowledge base underlying space-flight-induced bone loss is limited in comparison to what is known about either the pathophysiology of primary osteoporosis or the cellular mechanisms of secondary osteoporosis in terrestrial populations. Space flight missions do not typically provide controllable experimental conditions that permit the systematic collection of data; experiments are restricted by power, mass, and volume requirements; flight opportunities are few and far between; and subjects for testing or for longitudinal measures are too few to obtain definitive answers. Nevertheless, the limited data from space flight can be evaluated in the context of the extensive knowledge base for terrestrial osteoporosis.

We analyzed the perturbations in calcium homeostasis and bone remodeling detected with short-duration space flights (<90 days as defined herein, but typically <2 to 3 weeks based on mission durations) and the measurable decrements in bone mineral densities and bone structure in

"long-duration" crew members after space flight exposures of typically approximately 4 to 6 months (Tables 1 and 2).

Crew members exposed to the weightlessness of space for a typical long-duration (i.e., 4- to 6-month) mission on the Russian Space Station *Mir* or the International Space Station (ISS)

1) Display bone resorption that is aggressive, targets normally weight-bearing skeletal sites, is uncoupled to bone formation, and results in areal bone mineral density (BMD) deficits that can range between 6% and 20% of pre-flight BMD.

2) Exhibit compartment-specific declines in volumetric BMD in the proximal femur (a skeletal site of clinical interest) that significantly reduce its compressive and bending strength, and that may account for the loss in hip bone strength (i.e., force to failure).

3) Recover BMD over a post-flight time period that exceeds space flight exposure, but for which the restoration of whole bone strength remains an open issue and may involve structural alteration.

4) Present risk factors for bone loss – e.g., the negative calcium balance and down-regulated calcium-regulating hormones in response to bone atrophy – that can be compounded by the constraints of conducting mission operations (an inability to provide essential nutrients and vitamins).

Substantiating whether space flight increases the risk for accelerated osteoporosis ultimately centers on determining whether space-flight-induced skeletal changes are irreversible after a crew returns to Earth. If space-flight-induced bone loss is not restored and decrements in whole bone strength are not recovered in the post-flight period, crew members will experience the combined effects of space and aging on the skeleton, and will be predisposed to an earlier incidence of osteoporosis and fragility fractures. This risk will be even greater for female crew members, since bone loss with space flight will be compounded by bone loss with menopause.

What determines whether bone loss and whole bone strength are restored? Pre- and post-flight measurements of bone include bone size and geometry, volumetric BMD of bone compartments, bone microarchitecture, and mechanical strength testing by computer modeling and virtual loading, as developed with these expanded measurements. Longitudinal measures during the post-career lifetime of a crew member should also be conducted. Moreover, understanding the time course of bone turnover during space flight will improve our ability to evaluate the risk of longer exposures to skeletal integrity and its impact on recovery after a crew member returns to Earth. These additional indices will enhance the probabilistic risk assessments for crew members who are returning from long-duration space flight missions.

Variable	N	%/Month Change	SD
BMD Lumbar Spine	18	–1.06	0.63
BMD Femoral Neck	18	–1.15	0.84
BMD Trochanter	18	–1.56	0.99
BMD Total Body	17	–0.35	0.25
BMD Pelvis	17	–1.35	0.54
BMD Arm	17	–0.04	0.88
BMD Leg	16	–0.34	0.33

Table 1. *BMD and body composition after 4 to 14.4 months of space flight.*

Lumbar Spine (Integral)	–0.9±0.5
Lumbar Spine (Trabecular)	–1.7±0.6
Total Hip (Integral)	–1.4±0.8
Total Hip (Trabecular)	–2.3±0.8
Femoral Neck (Integral)	–1.2±0.7
Femoral neck (Trabecular)	–2.7±1.9

Table 2. *QCT changes in volumetric BMD in 14 ISS crew members (% per month + SD [standard deviation]).*

Recovery of Space-flight-induced Bone Loss: Bone Mineral Density After Long-duration Missions as Fitted with an Exponential Function

Jean D. Sibonga,
Universities Space Research Association
H. G. Sung, *Universities Space Research Association*
E. R. Spector, *Wyle Laboratories*
Thomas F. Lang, *University of California, San Francisco*
V. S. Oganov, *Russian Academy of Science*
A. V. Bakulin, *Russian Academy of Science*
Linda C. Shackelford, *Johnson Space Center*

Accelerated bone loss in crew members in space is a well-recognized effect of weightlessness on the skeletal system and a critical risk factor for the early onset of osteoporosis after return to Earth. Studies using calcium kinetics, site-specific bone densitometry, and bone turnover markers document atrophy in the gravitationally unloaded skeleton of crew members who had flown either on Skylab (28, 56, and 84 days) or on long-duration missions (>4 months) aboard the Russian Space Station *Mir* and the International Space Station (ISS). Although scientists have used calcium kinetics and bone biomarkers to characterize bone health during space flight, no reports have addressed the impact of space flight on long-term bone health after space flight; i.e., the recovery of skeletal integrity, its nature, and its time course.

Since the Skylab missions of the 1970s, scientists have used measurements of bone mineral and bone mineral density to evaluate the effects of space flight on the skeleton. More recently, researchers used quantitative computed tomography (QCT) scans of long-duration crew members to evaluate changes in volumetric bone mineral density and in hip structure after space flight. The report described herein expands on the QCT-measured changes in crew members (performed immediately and at 1 year after return from ISS mission) by evaluating the restoration of areal bone mineral density (BMD) in long-duration crew members who were periodically scanned by dual-energy x-ray absorptiometry (DXA) for almost as much as 5 years post-flight. We developed a method to analyze this repository of BMD data to describe the skeletal recovery of astronauts after their return to Earth. Through cooperative agreements with the Russian Space Agency, we obtained access to DXA data (pre- and post-flight BMD) of Russian cosmonauts who similarly served on long-duration missions to increase the value of this analysis. In our analysis, we attempted to provide an index that would reflect rate of BMD restoration after prolonged space habitation (typically between 4 and 6 months). This report is the first to characterize the recovery of space-flight-induced bone loss over multiple years on Earth in a crew member population of this size.

We applied an exponential mathematical function to a database of BMD measurements to describe the temporal, asymptotic recovery of BMD in crew members after return to Earth. The database contained BMD data from 45 different crew members serving over a total of 56 long-duration flights. From this mathematical fit of BMD changes during the post-flight period (representing both longitudinal and cross-sectional data), we assert that most crew members who flew on long-duration missions would return to a pre-flight BMD measure within 3 years – suggesting the period for recovery is greater than the duration of the mission. Our estimate of a longer recovery period is supported by similar, but limited, reports on recovery and is consistent with animal models of disuse. This estimation from our data is based on BMD changes in the trochanter, which is the skeletal site that consistently displays the greatest deficit in BMD in space flight and flight-analog studies and appears to take the longest (albeit, not statistically significant) time to recover. With our mathematical fit indicating an approximately 9-month 50% recovery time in the trochanter (figure 1), we estimate a substantial restoration (i.e., 15/16ths recovery at four times the half-life) to occur within 36 months of return. For each post-flight BMD scan, we plotted the percentage change between post- and pre-flight BMD against the number of days after landing when the scan was performed. The intercept of the fitted line represents the change in BMD as a direct consequence of space flight (at the time of landing). Dotted lines represent 95% confidence limits for the BMD data. Data points denoted by circles (vs. crosses) represent BMD changes measured in flyers who served on multiple long-duration missions. The intercept of the fitted line shows the space-flight-induced bone loss of 7.8% in the trochanter where 50% recovery time for loss would occur at 255 days, or about 8.5 months. We also generated similar plots and estimations from BMD scans of the femoral neck, lumbar spine, pelvis, and calcaneus (Table 1).

It is important, however, to note that skeletal recovery is highly variable among crew members. Some crew members recover within the first year after return while other crew members do not recover until much later. Factors

Recovery of Space-flight-induced Bone Loss: Bone Mineral Density After Long-duration Missions as Fitted with an Exponential Function

continued

that contribute to this variability in recovery are likely to include nutrition, skeletal muscle reconditioning, and genetics. Some of these factors may delay the ability and motivation of crew members to become ambulatory and, thus, mechanically load their skeletons. It is interesting to note three outliers for BMD loss in the femoral neck (>15% deficit, data not shown) for which two were older than the average age of, or in space longer than the average duration for, long-duration crew members. The missions corresponding to these outliers also represent the outliers' first long-duration flight. Risk factors contributing to bone loss in crew members should also be considered to evaluate their influence on recovery. Collectively, future studies will not only need to evaluate how bone metabolism responds to changes in mechanical loading (at the molecular, cellular, and tissue level) but how changes in skeletal mass and structure correlate with changes in muscle forces, with expression of skeletally relevant genes, and with nutrient uptake in this crew member population.

This investigation addresses a fundamental issue of how bone mass responds to changes in skeletal loading. These results would have an additional relevance to patient populations subjected to prolonged periods of immobilization and to the skeleton's capacity to recover.

Skeletal Site	Loss at landing (%)	50% Recovery Time (days)
Femoral Neck	6.8 (5.7, 7.9)	211 (129, 346)
Trochanter	7.8 (6.8, 8.8)	255 (173, 377)
Pelvis	7.7 (6.5, 8.9)	97 (56, 168)
Lumbar Spine	4.9 (3.8, 6.0)	151 (72, 315)
Calcaneus	2.9 (2.0, 3.8)	163 (67, 395)

Table 1. *Summary of fitted data per skeletal site.*

The percentage of pre-flight BMD loss (L0) at the time of landing and the "50% recovery time" are listed per skeletal site. The 50% recovery time represents the number of days after landing at which half of the bone mineral lost during space flight is restored. We determined the L0 and recovery times from BMD data fitted to a two-parameter exponential function for recovery of skeletal BMD after landing: Lt = L0 *exp[ln(0.5)*t/HL]. Confidence limits (95%) for the fitted values are provided in parentheses. The intercept for the fitted data (L0) (figure 1) represents BMD loss as a direct consequence of space flight.

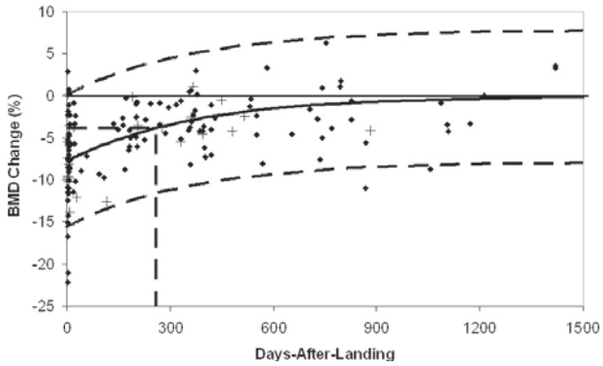

Fig. 1. *Changes in BMD at the trochanter after landing.*

The Flight Analogs Project as a Test Platform for the Skeletal Effects of Space Flight

Elisabeth R. Spector, *Johnson Space Center*
Scott M. Smith, *Johnson Space Center*
Jean D. Sibonga, *Johnson Space Center*

Early in the space program, scientists recognized bone atrophy with exposure to space flight as best documented by reduced bone mineral density of the heel and increased urinary and fecal excretion of calcium detected in the Skylab crews. Consistent with Wolff's Law, which asserts that the skeleton will remodel its structure in an adaptive response to its physiological and mechanical functions, densitometry data from long-duration space flight crew members substantiate a demineralization of the skeleton in those regions that experience the greatest reduction in strain; i.e., weight-bearing skeletal sites. It is the accelerated atrophy, and the potential deterioration of microarchitecture, that identifies "bone loss" as a primary risk factor for human health during the occupation and exploration of space. This space-flight-induced loss of bone mass may increase the risks of skeletal fractures and of renal stone formation, while the uncoupled response of bone cells during remodeling could impair fracture healing. These skeletal risks could influence the ability of space flight crew members to perform an emergency egress, or increase the risk of injury during egress. Moreover, incomplete recovery of bone mass and irreversible changes to geometry and microarchitecture may accelerate the onset of age-related osteoporosis in long-duration space flight crew members as they age back on Earth. Osteoporosis therapy on Earth focuses on prevention; thus, bone loss countermeasures that prevent or mitigate skeletal deconditioning may be required to maintain skeletal integrity and to meet the performance demands of space exploration missions. Critical to the development of these countermeasures is the ability to model the skeletal deconditioning observed in space to test countermeasure efficacy in a controlled experimental environment.

In this paper, we report changes in regional bone mineral density (BMD), along with serum and urinary biomarkers of bone turnover, measured in test subjects skeletally unloaded in a flight analog of prolonged bedrest. We compared bone measures, conducted at the Johnson Space Center Flight Analog Facility (long-duration head-down bedrest), located at the University of Texas Medical Branch in Galveston, to data from previously reported bedrest studies and to data from crew members after long-duration space flight.

Regional BMD measurements were obtained by dual-energy x-ray absorptiometry (DXA) using either a Hologic QDR 4500 (subjects 1–3) or a Hologic Discovery (subjects 4–13) whole body densitometer. We performed DXA scans once during the pre-bedrest period to provide a baseline assessment and again within 2 days after the end of the bedrest period. In addition, two subjects (12 and 13) participated in an extra DXA session at the intermediate time point of 60 days of bedrest. At each testing session, we performed a series of scans to include the whole body, lumbar spine, left and right hips, heel, and forearm. Subjects were multiply scanned to generate triplicate BMD measures of each region. (However, we performed duplicate rather than triplicate scans on subjects 8–11, who were scanned at bedrest days 42, 44, 49, or 52 (referred to here as ~47d) due to the urgency of the Hurricane Ike evacuation.) Left and right hip values for each subject were averaged to improve measurement precision of hip BMD as were triplicate (or duplicate) BMD values per region for each test session. A single operator performed and analyzed all DXA scans to reduce inter-operator variation. After completion of the bedrest study, we requested that subjects return for follow-up DXA scans (DXA series performed only once per follow-up) to evaluate bone recovery. Of the 13 subjects, 10 returned for follow-up testing at 6 months of reambulation (R+6mo), and six of those 10 returned also at 12 months (R+12mo). Follow-up heel scans were not obtained on the subjects scanned at the approximately 47d time point.

We assayed biomarkers for bone turnover in urine and serum specimens to provide a corroborating index, at the whole tissue level, by which to monitor the relative effects of bedrest on bone resorption and bone formation. We also assayed N-telopeptide (NTX) and deoxypyridinoline (DPD) from 24-hour urine collections as biomarkers of bone resorption. Levels of serum bone-specific alkaline phosphatase and osteocalcin served as markers of bone formation. Other bone-related assays included urinary calcium, serum calcium, pyridinium crosslinks, alkaline phosphatase, intact parathyroid hormone, 1,25 dihydroxyvitamin D, and 25-hydroxyvitamin D, using standard commercial techniques.

We calculated and expressed the difference between pre- and post-bedrest measurements of BMD as a percentage

of pre-bedrest BMD with regional BMD changes as group means ± SD for each time period of bedrest (i.e., ~47, 60, or 90d). Total BMD changes were also averaged over the total months of bedrest (% change per month) for comparison to calculated monthly BMD changes after space flight missions. To determine a significant effect of bedrest on BMD for each bedrest duration, we performed one-tailed, paired Student's t-tests on the absolute BMD data; significant effects were designated at $P < 0.05$. The one exception to this approach was for the forearm (two-tailed) because there was no a priori expectation of a change in BMD, based on previous bedrest and space flight studies. To maintain an approach consistent with the BMD data, we expressed the bone biomarker data as a percent change from pre-bedrest values; we used Student's t-tests (two-tailed, paired, based on the absolute BMD values) to determine statistical significance for the pre- vs. post-bedrest changes. BMD recovery after bedrest was concluded if increased BMD with re-ambulation exceeded the measurement error ("Least Significant Change") established for that skeletal site at the 95% confidence level.

Figure 1 shows the average BMD changes, per skeletal region, for the various durations of bedrest. The figure also provides the calculated *average* monthly rate of BMD changes for each region. We noted statistically significant changes from pre-bedrest BMD in the lumbar spine, hip, pelvis, and heel, although not for every duration of bedrest. Mean BMD values of the total hip, hip trochanter, and pelvis were significantly decreased at all durations of bedrest. We detected significant loss in the heel only at the approximately 47d bedrest time point, and loss in the lumbar spine only at 60d of bedrest. No significant changes were noted in the forearm (serving as an "internal" negative control) for any periods of bedrest. The team analyzed paired, longitudinal BMD measurements for the six subjects (subjects 4–7, 12, and 13) who had DXA scans both at 60d and 90d of bedrest (figure 2). Statistically significant differences between the 60d and 90d measurements for the lumbar spine and heel were recorded.

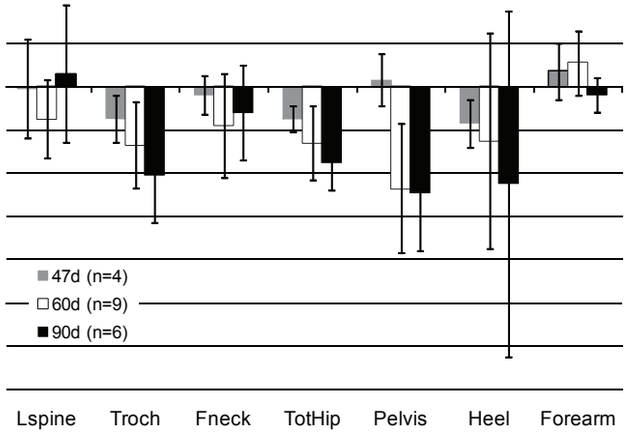

Fig. 1. *Percent change from pre-bedrest BMD.*

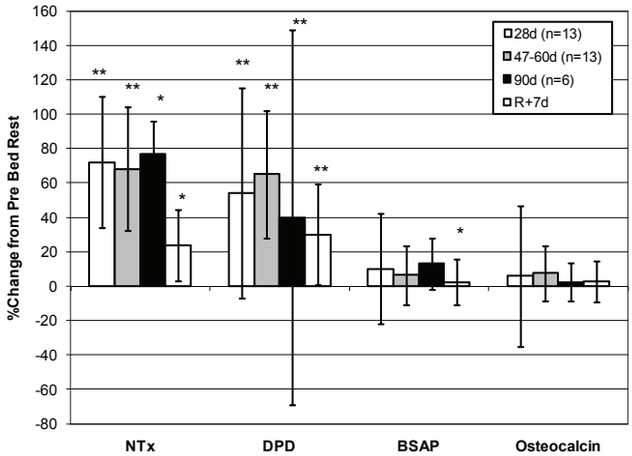

Fig. 2. *Percent change from pre-bedrest N-telopeptide, deoxypyridinoline, bone-specific alkaline phosphatase.*

Three of the 10 subjects who participated in follow-up DXA scans still had BMD deficits in at least one bone site after 6 months of re-ambulation (BR+6mo). Some bone regions in these individuals exhibited no significant increase in BMD from the immediate post-bedrest measurement; i.e., BR+0 values. Of the six subjects who had follow-up DXA scans at BR+12mo (three 60d subjects, two 90d subjects, one ~47d subject), two subjects still had BMD losses in at least one bone site that were greater than the least significant change value. Furthermore, these deficits were equal to or even greater than those documented at the BR+0 and BR+6mo time points, although we did not test these differences statistically. We examined the recovery data for group changes as well.

For the nine subjects who had recovery measurements at BR+6mo, t-tests indicated that mean BMD increases from BR+0 were statistically significant ($P < 0.01$) for the trochanter, total hip, pelvis, and heel. We noted no significant increase for the femoral neck or lumbar spine (the latter of which showed no measurable decrease from baseline at BR+0 and therefore would not be expected to show "recovery"). In the six subjects who had recovery measurements at both BR+6mo and BR+12mo, no statistically significant differences were noted for any bone region between the BR+6mo and BR+12mo time points.

Figure 3 outlines the changes in bone biomarkers during and after bedrest. Bone resorption markers (DPD, NTX) showed significant elevations above baseline at 28 days of bedrest, and these changes persisted through bedrest days 60 and 90 and into the first week of recovery. Bone formation markers were generally unchanged from pre-bedrest.

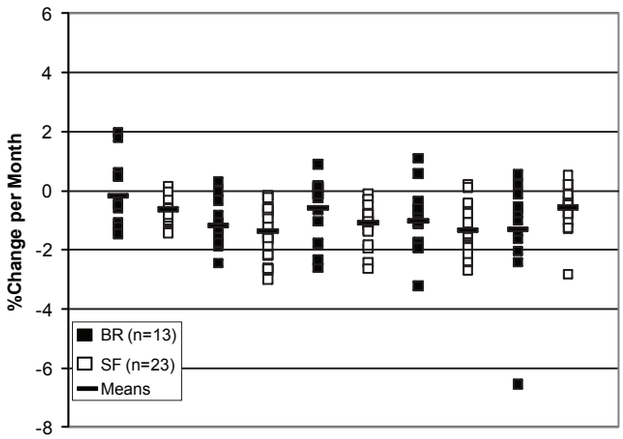

Fig. 3. *Percent change per month. Comparison of bedrest (BR) and space flight (SF) studies.*

DXA BMD changes measured in the 13 subjects reported here are consistent with BMD changes documented in earlier bedrest and space flight studies, with statistically significant losses occurring in the hip, pelvis, and heel. The lumbar spine results suggest the possibility that subject positioning in the axial direction and in-bed activity during bedrest might affect regional BMD results. Bone biomarker data are also consistent with previous space flight and bedrest findings, and demonstrate an increase in bone resorption with no significant change in formation. Finally, preliminary results regarding recovery of BMD following head-down tilt bedrest appear similar to observations of space flight BMD recovery, which include the considerable BMD variability between site-specific measurements within one individual and between several individuals, as well as the prolonged period of recovery relative to period of disuse. Based on bone measurements obtained from this first series of studies, the NASA Flight Analogs Project integrated bedrest protocol appears to be a valid testbed for skeletal disuse studies, and should provide a useful research platform for evaluating countermeasures to space-flight-induced bone loss.

Vitamin D Studies: From the Antarctic to the International Space Station

Sara R. Zwart, *Johnson Space Center*
Scott M. Smith, *Johnson Space Center*
James Locke, *Johnson Space Center*

Vitamin D is unique in that exposure to ultraviolet light allows the body to synthesize it from a precursor in the skin. Because the diet of most individuals includes few good natural sources of this vitamin, many people are dependent on sun exposure or supplements for most of their vitamin D requirement.

Vitamin D is critical for space travelers because they lack exposure to ultraviolet light and have an insufficient dietary supply of vitamin D. Despite the provision of vitamin D supplements to International Space Station crew members, the vitamin D status is consistently lower after flight than before and, in several crew members, decreased to levels considered clinically significant.

The most recognized role of vitamin D is its involvement in calcium metabolism. One of its major functions is to maintain normal blood levels of calcium and phosphorus. The typical gold-standard measurement for determining vitamin D status in the body is 25-hydroxyvitamin D, but 1,25-dihydroxyvitamin D is the active form of the vitamin in the body. The liver converts vitamin D to 25-hydroxyvitamin D, which is converted to 1,25-dihydroxyvitamin D in the kidney. From there, 1,25-dihydroxyvitamin D is transported by the circulatory system to target organs. Classic target organs include bone, intestine, and kidney.

Vitamin D has other functions besides those related to skeletal health. Functions that do not involve calcium metabolism include the role of 1,25-dihydroxyvitamin D as an important immune system regulator. In addition, vitamin D may inhibit development of autoimmune diseases including experimental inflammatory bowel disease, rheumatoid arthritis, multiple sclerosis, and type 1 diabetes.

We used Antarctica as a ground-based model for determining the optimal dose and metabolism of vitamin D because of the limited sunlight exposure there during the approximately 6-month winter period. The Antarctic science station model was successful as a ground-based analog for space flights in studies of behavior, immune response, and reactivation of latent viruses. Our studies in Antarctica showed that ground-based models of insufficient sun exposure are a valuable asset to clearly determine the optimal dose of vitamin D required to maintain circulating 25-hydroxyvitamin D at optimal levels.

We investigated the effectiveness of three different daily doses of vitamin D in maintaining serum 25-hydroxyvitamin D at 80 nmol/L with volunteers living in the Antarctic during the winter. While we found that 2,000 IU/d increased vitamin D status from baseline levels to about 70 nmol/L, we also found that compliance in taking the supplements was an issue. In the winter of 2009, we conducted a follow-up study at McMurdo Station in Antarctica to determine whether a weekly dose could be used as effectively as a daily dose. A secondary goal of this study was to investigate the effect of vitamin D status on immune system function. In collaboration with the Johnson Space Center (JSC) Microbiology Laboratory, we investigated latent virus reactivation in relation to the vitamin D status of individuals staying in Antarctica during the winter. Latent virus reactivation is also an established phenomenon in environments such as Antarctica and space flight.

In addition to studies being performed in Antarctica, we are completing an investigation at JSC to determine the kinetics of vitamin D metabolism in subjects taking different doses of a vitamin D supplement: 2,000 IU per day, 10,000 IU per week, or 50,000 IU per month. In collaboration with Dr. John Milner and his Nutritional Science Research Group in the Division of Cancer Prevention at the National Cancer Institute, Bethesda, Md., we are also testing how vitamin D affects gene expression, which may allow us to better understand the role of this vitamin in immune function.

Data from these ground-based experiments will enable us to provide space crews with evidence-based recommendations for vitamin D supplementation. The findings have implications not only for astronauts, but also for other persons with limited exposure to ultraviolet light, including polar workers and the elderly.

Novel Skeletal Muscle Models for Space Exploration and Medical Applications

Michele Marquette,
The University of Texas Medical Branch
Diane Byerly, *Johnson Space Center*

Marguerite Sognier,
Universities Space Research Association

Alleviating space-induced muscle atrophy in astronauts will greatly facilitate the success of future long-duration Exploration missions. Muscle atrophy, the progressive loss of muscle mass, results in diminished contraction strength and endurance. This can have deleterious affects on astronaut health and, consequently, mission success. Current countermeasures to address these effects include the performance of specific exercise protocols by astronauts in flight. These countermeasures reduce, but do not eliminate, muscle atrophy. By elucidating the alterations occurring at the cellular level in muscle under microgravity conditions, different countermeasures may be found. Studying muscle atrophy on a cellular basis is challenging due to the limited number of astronauts who have flown on long-duration space flights (e.g., International Space Station). Although human bedrest and rodent hind limb suspension models are used as equivalent models for muscle atrophy research, these models can be costly and time-consuming.

Cell-based models are a cost-effective, rapid method to study human disorders, yet tissue-equivalent skeletal muscle models are very difficult to generate due to the complex structure of the tissue. This is because skeletal muscle is unique among human body tissues in that it is composed of very long, multinucleated cells that must be aligned to simultaneously contract and exert maximum force. Immature muscle cells (myoblasts) must proliferate, align, fuse to form myotubes (elongated, multinucleated cells), and differentiate to enable muscle contraction. Duplicating these processes in the laboratory is difficult, time-consuming, and costly. Two steps are currently used to generate skeletal muscle models: (1) the introduction of various growth factors to induce fusion and differentiation; and (2) the use of complex micropatterned substrates that force myoblasts and subsequent myotubes into parallel alignment. Neither of these steps, either alone or in combination, produces the quantity of contracting muscle cells required for mechanistic studies.

To overcome these issues, we developed two new methodologies that produced novel skeletal muscle model testbeds. These methods are more tissue-equivalent; that is, capable of contraction. This work will facilitate the discovery of novel approaches to prevent and/or alleviate muscle atrophy, and will lead to an increased understanding of the complex processes necessary for skeletal muscle generation and repair.

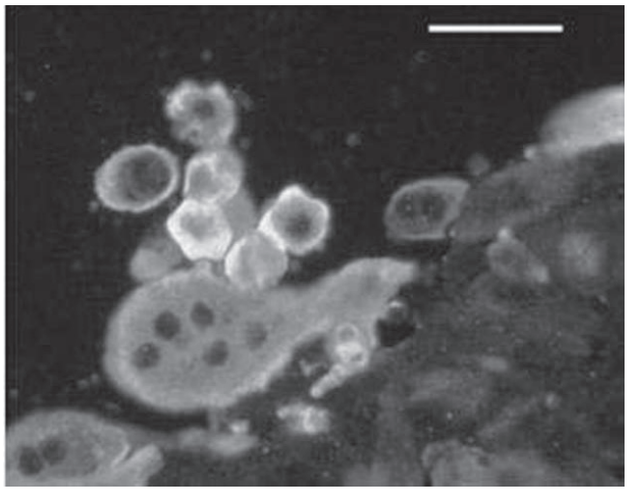

Fig. 1. *Thin section of 3D skeletal muscle aggregate.*

The first new methodology involves generating three-dimensional (3D) skeletal muscle models from C2C12 mouse myoblasts (figure 1). The C2C12 mouse cells are easily cultured, grow quickly (compared to human cell lines), are readily available, and perform a similar function (again compared to human cell lines) of restoration and repair of myoblasts. We cultured single-cell suspensions of myoblasts – without exogenous support structures/substrates and in the absence of differentiation factors – using the NASA-designed bioreactor, which is used to model some aspects of the microgravity environment. Within 12 hours, cell aggregation occurred. The myoblasts then fused and differentiated into 3D constructs without the use of serum alterations or other stimulants. Examination of thin sections of the aggregates revealed that a muscle differentiation marker, sarcomeric myosin heavy chain, was expressed in areas of synctia formation. Experiments with this model demonstrated that myoblasts could differentiate in modeled microgravity conditions. This model test system is particularly useful for investigating initial cell-binding events, myoblast fusion, and differentiation processes, which are required for muscle generation and repair. A better understanding of these processes will improve skeletal muscle tissue engineering approaches

(figure 2), current myoblast transplantation methodologies, regenerative medicine applications, and the development of cell-based countermeasures for muscle atrophy.

The second new methodology represents a major advance in tissue engineering in that, for the first time, precursor cells spontaneously fused and differentiated into masses of perfectly aligned, contracting myotubes. This cost-effective, multistep approach does not require the use of the serum alterations or micropatterned substrates thought to be essential to obtain similar constructs. Myoblasts are seeded in Petri dishes under very specific conditions (patent pending, Marquette and Sognier) that culminate in aligned, contracting myotubes as early as day 5 in culture. Numerous myotubes exhibit spontaneous contraction by the second week of culture. Additional time in culture results in sheets of aligned, synchronously contracting myotubes. This method enables (1) the construction of improved two-dimensional (monolayer) skeletal muscle testbeds; (2) the development of contracting 3D models; and (3) improved transplantable muscle tissue for biomedical and regenerative medicine applications. With adaptation, this method could be applied to produce other tissue types (i.e., bone and cardiac) from corresponding precursor cells.

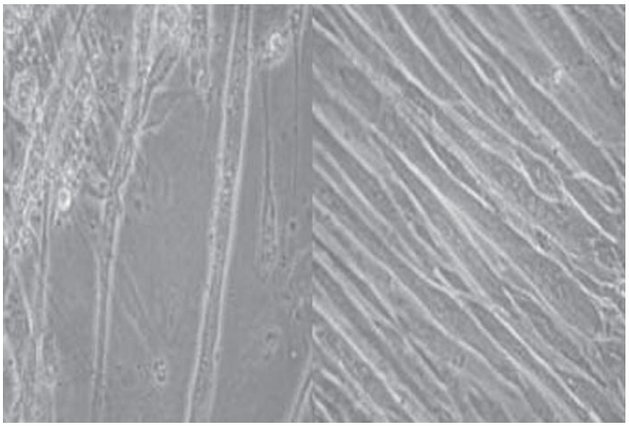

Fig. 2. *Comparison of skeletal muscle engineered using different methods.*

In summary, the two novel testbeds advance the current state-of-the art and are suitable for determining the cellular alterations involved in muscle atrophy. Such knowledge can be used to develop unique countermeasures. These models are valuable for elucidating the mechanisms of muscle diseases and atrophy associated with aging, immobilization, and denervation. Ultimately this elucidation is expected to culminate in the development of more effective therapies for use both in space and here on Earth.

Gender Differences in Blood Pressure Control During 90-day Bedrest

Natalia M. Arzeno, *Johnson Space Center*
Michael B. Stenger, *Johnson Space Center*
Stuart M. C. Lee, *Johnson Space Center*
Steven H. Platts, *Johnson Space Center*

Introduction

Space-flight-induced physiological changes increase the risk of orthostatic hypotension on return to Earth, particularly for women. Orthostatic hypotension, or low blood pressure when sitting upright or standing, could impair a crew member's ability to perform routine or mission-critical tasks. The physiological mechanisms responsible for increased orthostatic hypotension in female astronauts are unclear. Several contributing factors to lower tolerance in women after space flight have been postulated, including a lower center of mass, higher circulating estrogen levels, and smaller and stiffer left ventricles.

We are currently studying the effects of gender on baroreflex sensitivity and orthostatic tolerance after bedrest, a well-accepted model of space flight deconditioning. The overall aim of this project is to examine factors that contribute to arterial blood pressure control in men and women, and to determine how men and women are affected during 90 days of 6-deg head-down-tilt bedrest. After space flight and bedrest, the capacity of the human body to regulate heart rate to compensate for sudden changes in blood pressure is decreased. Previous studies concentrate on a single blood pressure perturbation, such as a tilt test, bolus drug injections, or rapid neck chamber decompressions. By contrast, in this study we infused drugs that manipulated systemic vasoconstriction and vasodilation to produce changes in blood pressure to determine how well heart rate is regulated to compensate for these changes across the duration of bedrest.

Methods

Twenty-three volunteers (15 males, eight females) were tested 1 day before bedrest and then during near-bedrest days 30, 60, and 90. Normal saline was infused for 10 minutes followed by three 10-minute infusions of phenylephrine (PE) (a vasoconstrictor) of increasing concentrations (0.4, 0.8, and 1.6 $\mu g \cdot kg^{-1} \cdot min^{-1}$). After 20 minutes of rest with no infusions, saline was infused again for 10 minutes, followed by three 10-minute infusions of sodium nitroprusside (SNP) (a vasodilator) of increasing concentrations (0.4, 0.8, and 1.2 $\mu g \cdot kg^{-1} \cdot min^{-1}$). Electrocardiogram and blood pressure were measured continuously to examine heart rate responses to changes in blood pressure. Spectral and cross-spectral blood pressure and heart rate variability algorithms were used to assess the indices of autonomic balance and baroreflex sensitivity.

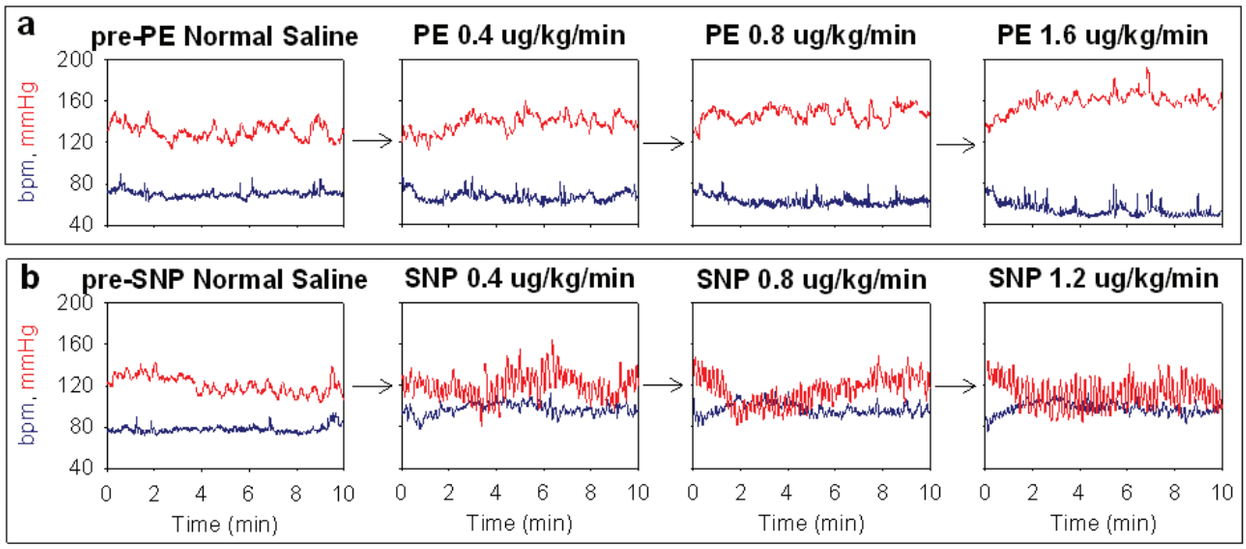

Fig. 1. *Heart rate (dark blue) and systolic blood pressure (red) response to drug infusions for one subject post-bedrest.*

Gender Differences in Blood Pressure Control During 90-day Bedrest

continued

Results

As expected, mean heart rate increased and mean resting blood pressure decreased with bedrest for all of the volunteers, and the women had lower blood pressure than the men. Cross-spectral phase changes indicated that women's heart rates responded slower than men's to both increases and decreases in blood pressure. During increasing concentrations of PE infusion, blood pressure increased and heart rate compensated by decreasing (figure 1a). During increasing concentrations of SNP infusions, blood pressure decreased and heart rate compensated by increasing (figure 1b). Spectral indices of heart rate variability indicate that heart rate control of blood pressure decreased throughout bedrest for both men and women, with a larger effect in women.

Conclusions

Post-space-flight orthostatic intolerance can be partially explained by the diminished capacity of heart rate to regulate changes in blood pressure. These preliminary results indicate that women experience a greater decrease in blood pressure control and a slower heart rate response during bedrest, both factors that would contribute to their higher incidence of orthostatic intolerance.

Countermeasures to Space-flight-induced Orthostatic Hypotension

L. Christine Ribeiro, *Johnson Space Center*
Stuart M. C. Lee, *Johnson Space Center*
Angela K. Brown, *Johnson Space Center*
Michael B. Stenger, *Johnson Space Center*
Steven H. Platts, *Johnson Space Center*

Introduction

Astronauts generally adapt well to the space flight environment, but this may bring about physiologic changes that can negatively impact their health and performance on entry into Earth gravity or the partial-gravity environments of the moon and Mars. The structure and function of the human cardiovascular system are particularly affected by space flight, which may lead to an astronaut's inability to appropriately regulate blood pressure and cerebral perfusion, resulting in a clinical condition called orthostatic intolerance. Orthostatic intolerance, in its more benign form, can be manifested as an elevated heart rate and/or decreased blood pressure when seated or standing; but, in more extreme cases, it may result in lightheadedness (presyncope) and fainting (syncope). Presyncopal symptoms or syncope during a 10-minute stand or an 80-deg head-up tilt affects approximately 30% of astronauts after short-duration missions (4–18 days), and approximately 80% of astronauts after long-duration missions (≥30 days). Orthostatic intolerance after space flight could impair an astronaut's ability to perform routine tasks, and is a significant concern for emergency egress scenarios. During future visits to the lunar surface and human flights to Mars, astronauts will be working in environments without ground support teams, so the occurrence of severe orthostatic intolerance could be disastrous. It is paramount that countermeasures to orthostatic intolerance be developed to protect astronaut health and mission success.

Midodrine

Pharmacological countermeasures to orthostatic intolerance are attractive because they require little storage space and few resources during long-duration missions. We recently studied midodrine, an α_1-adrenergic agonist used to treat clinical cases of orthostatic hypotension. For the initial testing, we administered midodrine to shuttle crew members within 2 hours following space shuttle landings, and determined its side effects 1 hour later under controlled conditions in the baseline data collection clinic. Astronauts who were previously not prone to presyncope on landing day experienced no negative side effects; and in the one astronaut who had a history of presyncope, the midodrine protected against orthostatic hypotension. The next study built on the success of this initial study by testing the efficacy of midodrine under operational conditions. Astronaut subjects ingested midodrine prior to the shuttle deorbit burn to protect against hypotension on landing. They then participated in a tilt test within 30 minutes of shuttle wheelstop on the crew transport vehicle. The five control astronaut subjects who did not ingest the midodrine participated in the same tilt test in the crew transport vehicle.

Unfortunately, one side effect of midodrine is that it may cause ventricular arrhythmias (i.e., torsades de pointes) in subjects who have a prolonged QT_c interval. While this is not an issue following short-duration space flight, we found that in long-duration space flight midodrine may cause a prolonged QT_c interval in some individuals. Because of this limitation and the potential for untoward interactions with other pharmaceutical agents, our laboratory is pursuing the development of non-pharmaceutical countermeasures.

Hypovolemia model of space-flight-induced orthostatic intolerance

Our laboratory developed a model of space-flight-induced orthostatic intolerance in normal ambulatory subjects. Using furosemide, an FDA [Food and Drug Administration]-approved diuretic, followed by a very-low-sodium diet, we create a condition of hypovolemia in which the plasma volume is reduced in subjects to a level similar to that experienced by astronauts during space flight. Consequently, test subjects experience symptoms that mimic those experienced by astronauts on landing day. The hemodynamic responses of six veteran astronauts to 80-deg head-up tilt during hypovolemia reproduced their responses to tilt testing on landing day after a previous space shuttle mission. This verified the model.

NASA and Russian antigravity suits

Using this model, we initiated a series of studies to examine the efficacy of mechanical compression garments applied to the lower body to prevent peripheral venous pooling and protect against orthostatic hypotension. In the first study, we compared the level of protection afforded by NASA's current antigravity suit (AGS) (figure 1), worn under the U.S. advanced crew escape suit (ACES) by crews returning on the space shuttle, to the Russian Kentavr

re-entry garment (figure 2), worn under the Russian Sokol suit by crews returning on the Soyuz capsule.

The AGS has five interconnected inflatable air bladders covering the abdomen, thighs, and calves. It can be inflated to pressures ranging from 0.5 psi (25.9 mmHg) to 2.5 psi (129.3 mmHg), but typically is inflated to 1.5 psi (77.7 mmHg) during shuttle re-entry and landing. The Kentavr is composed of shorts that extend from the waist to the knee and a pair of gaiters, made of an elastic fabric, that covers the calves. Each component of the Kentavr has lacings to allow an individualized fit. The nominal pressure provided by the Kentavr is 0.6 ± 0.1 psi (30 ± 5 mmHg).

We tested 35 subjects for orthostatic intolerance under hypovolemic conditions while wearing either the Kentavr (n=10), the AGS (n=9), or no countermeasure (n=16). All 19 subjects wearing either the Kentavr or the AGS were able to complete a 15-minute, 80-deg head-up tilt test. Only 44% (seven of 16) of the control subjects completed this tilt test. Both the Kentavr and the AGS provided protection against orthostatic intolerance under hypovolemic conditions, suggesting that the compression of the AGS applied in this study (~78 mmHg) might be in excess of that required (Kentavr = ~30 mmHg) to mitigate orthostatic hypotension.

Fig. 1. *NASA's AGS currently worn with the advanced crew escape suit post-bedrest.*

Fig. 2. *Russia's Kentavr suit worn by cosmonauts under the Sokol suit during re-entry and landing.*

JOBST® compression garments

In the second compression garments study, we compared clinically available JOBST® custom thigh-high compression garments (figure 3) to the AGS. JOBST® compression garments are custom-fit to each subject based on pre-test measurements of leg circumference to create a graduated pressure gradient spanning the length of the leg. The JOBST® compression pressure is highest at the ankle (~55 mmHg) and lowest at the thigh (~6 mmHg), with an average of 25 mmHg over the length of the garment. In this study, the AGS was inflated to

Fig. 3. JOBST® thigh-high compression garments.

0.5 psi (~25 mmHg), based on observations from our previous study and reports by astronauts that 1.5 psi is uncomfortable, especially on the abdomen, following the mandated fluid-loading regimen prior to re-entry. Initial results from this ongoing ground study suggest that both this style of JOBST® compression garment and the AGS at this level of inflation are protective, but perhaps not to the same degree as higher-pressure garments.

These JOBST® custom, thigh-high compression garments were recently tested on five astronauts on the landing day of a space shuttle mission. During re-entry and landing, these astronauts wore the standard AGS. After removing their ACES and AGS following shuttle egress, they donned JOBST® compression garments. All of the astronauts participated in a 10-minute, 80-deg head-up tilt at the baseline data collection facility within 4 hours of landing. We completed a comparison of the hemodynamic responses to tilt in these five astronauts to nine other astronauts who also participated in a tilt test without compression garments following space shuttle flights of a similar duration. During tilt, there were no incidences of orthostatic intolerance in astronauts wearing JOBST® compression garments. In contrast, three of the nine subjects in the control group experienced presyncope during tilt and were unable to complete the tilt test. Astronauts who wore the JOBST® thigh-high compression garments had higher systolic blood pressure, stroke volume, and cardiac output throughout tilt than those who did not wear the compression garments. Continued ground-based testing and future testing with more astronaut crews will be required to confirm the efficacy of these JOBST® thigh-high compression garments.

Conclusions

We will continue to investigate the most efficacious method to protect returning space crews against orthostatic intolerance. Although pharmacological interventions show promise, concerns with the unintended side effects of these medications may limit their use. Our results demonstrate that, in a ground-based model of space-flight-induced orthostatic hypotension, compression garments are effective, but the nominal application of compression of the NASA garment may be greater than is necessary. Current and future studies will focus on the required level and location of compression required to protect astronauts from orthostatic intolerance. For example, to determine whether additional compression of the splanchnic vasculature would be beneficial, we recently initiated testing with breast-high, custom JOBST® compression garments with an average compression of 25 mmHg over the length of the leg and of 12 mmHg over the gut. Additionally, we will later study knee-high garments that cover only the calves, the site of greatest fluid accumulation during standing, but will provide greater levels of compression (35 mmHg average over the length of the garment). These tests will be conducted using subjects who have induced hypovolemia. If those results are promising, further tests will be conducted on astronauts after space flight. The overall objective of this work is to determine the specifications of the compression garment that performs most effectively against orthostatic intolerance while still being comfortable for the astronaut.

Environmental Technologies

Leadership in Energy and Environmental Design at Johnson Space Center

Charles Noel, *Johnson Space Center*

The designs of all new construction and major renovation of facilities at the Johnson Space Center (JSC) meet the Leadership in Energy and Environmental Design (LEED) criteria. This criterion ensures energy and material efficiency and sustainability are inherent in all new construction.

To make certain JSC meets NASA Headquarters' minimal LEED Silver requirements, the architect-engineer firm performing the design, project manager, and project team performed an LEED design charette at the pre-design stage. This charette calls for an item-by-item review of the U.S. Green Building Council's LEED Project Scorecard to determine which LEED points are reasonable to accomplish within the scope of a project and which are open possibilities.

As a project progresses through its 30%, 60%, and 90% design review, we reexamine the scorecard to determine which points must be dropped out or might be added due to the latest engineering design data. At the 30% stage, we justify by a life cycle cost analysis the design concept proposed by the architect-engineer. This analysis is adjusted and refined as the project progresses to its final stage.

This process has enabled JSC to design and construct the following LEED buildings over the past 4 years:

LEED Certified

Building 27: The Astronaut Quarantine Facility

Designed to LEED Silver

Building 207A: Gilruth Recreation Center facility addition (construction complete, LEED certification pending)

Building 29: Constellation Avionics Integration Laboratory (under construction, total building refurbishment)

Building 265: Source Evaluation Board office additions (under construction, building addition)

Designed to LEED Gold

Building 2 North: Office of Communications and Public Affairs (under construction, total building refurbishment)

Building 26: The Center for Human Space Flight Performance and Research (under construction)

Building 12: Offices (in design, total building refurbishment)

Building 20: New Office Building (under construction)

The two most unusual LEED facilities are the Astronaut Quarantine Facility (Bldg. 27) and The New Office Building (Bldg. 20). We will describe these below.

Building 27: The Astronaut Quarantine Facility

Building description

JSC's single-story, 12,000-ft^2 Astronaut Quarantine Facility uses sustainable features; it earned the LEED Certified rating by the U.S. Green Building Council (figure 1). Prior to space flight, astronauts live in this facility to receive daylight and nightlight conditioning from high-output lights that modify their circadian rhythms to match the upcoming sleep/wake flight schedule. This circadian rhythm lighting consumes significant energy and produces a considerable heat load that the air-conditioning system must remove.

Fig. 1. *Building 27: The Astronaut Quarantine Facility.*

Features included in the project

Faced with the challenge of optimizing building energy performance, the design team oriented the Astronaut Quarantine Facility to maximize daylight harvesting and installed an ENERGY-STAR-compliant, highly reflective roof. The design includes high-efficiency, variable-speed

heating, ventilation, and air-conditioning (HVAC) equipment and the use of an energy recovery system with an enthalpy wheel and preconditioned outside air (figure 2).

Designers used energy-efficient windows and added insulation on the exterior walls (figure 3). Low-flow restroom fixtures, including waterless urinals, dual-flush valves, and flow restrictors on the faucets, were installed.

Native plants and adapted species (figure 4) are seeded around the facility to reduce maintenance and water use, and condensate water acts as the primary irrigation source.

As designed, the Astronaut Quarantine Facility is expected to reduce potable water consumption for landscape irrigation by 50%, be 55% more energy efficient then ASHRAE [American Society of Heating, Refrigeration, and Air-conditioning Engineers] 90.1 specifies, and divert greater then 50% of all construction waste from disposal.

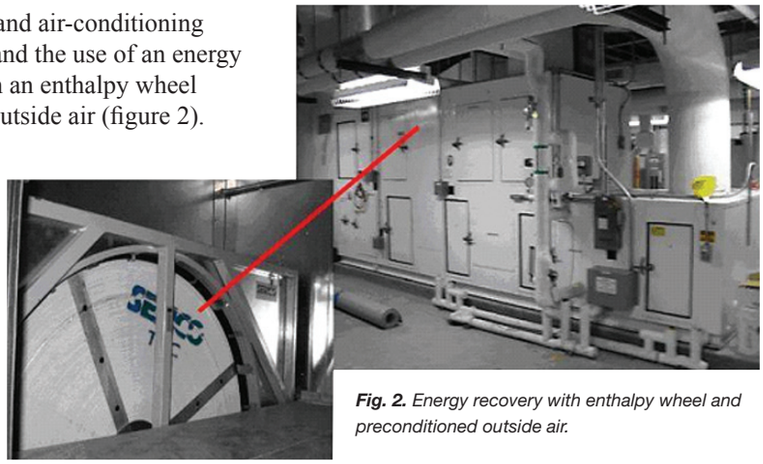

Fig. 2. *Energy recovery with enthalpy wheel and preconditioned outside air.*

Fig. 3. *Efficient building shell – minimum windows, added insulation, efficient windows.*

Fig. 4. *Native plants and adapted species.*

Building 20: The New Office Building

Building description

JSC's newest facility (figure 5), the New Office Building, is a three-story, 83,000-ft^2 office building employing numerous sustainable features. In the design JSC originally strove for an LEED Gold rating but, because of improvements and innovation during facility construction, the center hopes it will earn its first Platinum LEED rating by the U.S. Green Building Council. The New Office Building is presently being constructed to support JSC's multi-year building refurbishment program to provide "flex" space for employees temporarily relocated due to refurbishment of another building. The main design decisions for the building centered on creating a highly flexible space that could be altered quickly at minimum cost. Additionally, designers meant to create a highly sustainable facility using the "less-is-more strategy" (i.e., a very efficient building design reduces the programmed building area and the amount of finishes where applicable).

Fig. 5. *Building 20: The New Office Building.*

Features included in the project

As with Building 27, the design team oriented the New Office Building to maximize daylight harvesting and installed an ENERGY-STAR-compliant, highly reflective roof. Low-flow restroom fixtures, including waterless urinals, dual-flush valves, and flow restrictors on the faucets, will be installed. Native plants and adapted species are seeded around the facility to reduce maintenance and water use, and condensate water is used as the primary irrigation source.

Faced with the extra challenge of optimizing building energy performance for a facility anticipated to undergo significant change over the coming years, the design team installed a high-efficiency underfloor HVAC system for flexibility.

The project design team, in striving to win JSC's first LEED Platinum rating, included such extras as Solarban® 70 energy-efficient windows (figure 6), built-in solar shading barriers, solar hot water heating for the restrooms, ultraviolet lighting in air handlers to reduce microbial growth, and a detention pond and structural controls to manage and improve storm water runoff.

As designed, the New Office Building is expected to reduce potable water consumption for landscape irrigation by 54%, use 34% less water than a building that just meets baseline fixture performance requirements of the Energy Policy Act of 1992, be 55% more energy efficient then ASHRAE 90.1 specifies, and divert greater then 90% of all construction waste from disposal.

Facility occupants will benefit from a building designed to provide natural daylight to all office spaces.

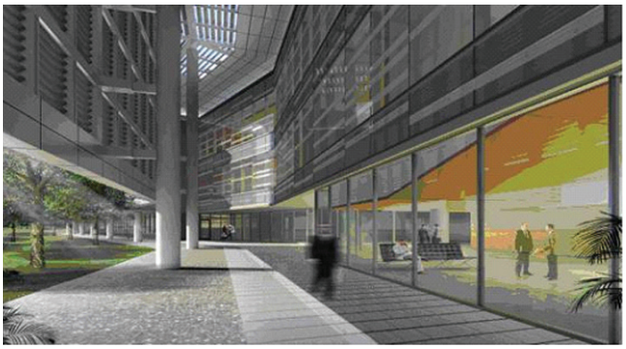

Fig. 6. *High-efficiency glazing and solar shading reduces energy use by 54% compared to typical office.*

Natural light in the stairwells, bicycle racks, and showers was included to encourage employee health and fitness. Project construction is scheduled so that occupancy should begin in the winter of 2009/2010.

Exploration Life Support Air Revitalization System Technology Development for Human Test Subjects

Jeff Sweterlitsch, *Johnson Space Center*

The baselined Crew Exploration Vehicle (Orion) Environmental Control and Life Support System (ECLSS) technology for controlling metabolically produced carbon dioxide (CO_2) and water vapor (H_2O) is a pressure-swing adsorption bed that uses a regenerable amine-based sorbent. The sorbent selectively scrubs H_2O and CO_2 gases from the cabin environment and vents them to the vacuum of space. Carbon dioxide and moisture removal amine swing-bed (CAMRAS) technology (developed by Hamilton Sundstrand, Windsor Locks, Conn.) has undergone extensive test and evaluation activities.

The CAMRAS technology uses a pair of packed beds of amine-based sorbent, which have an affinity for gaseous CO_2 and H_2O. Cabin air is forced through one of the beds, and the CO_2 and H_2O in the air adsorbs onto the sorbent media. Concurrently, the other bed is isolated from the cabin environment and exposed to space vacuum. The change in partial pressure of the CO_2 and H_2O due to space vacuum causes these gases to desorb from the sorbent media and vent to space, thereby regenerating the sorbent media. A spool valve on the CAMRAS hardware translates from one position to the opposite position, and the process is reversed: the bed exposed to vacuum is now exposed to the cabin environment, and the bed exposed to the cabin environment is now being regenerated. The packed beds are interleaved and thermally linked in the CAMRAS hardware. The adsorption process is exothermic and the desorption is endothermic. Heat is thus transferred from the bed that is adsorbing CO_2 and H_2O is transferred to the bed that is undergoing desorption. This arrangement provides a compact design, low-pressure drop, and relatively isothermal performance. Figure 1 presents a visualization of the CAMRAS hardware. The spool valve is located on top of the hardware, and the lower section contains the interwoven beds of sorbent media.

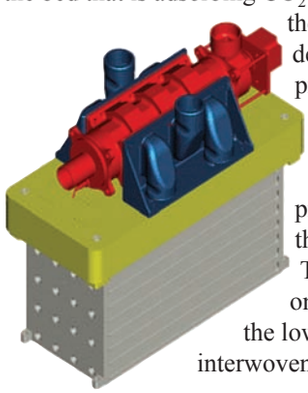

Fig. 1. *Carbon dioxide and moisture removal amine swing-bed.*

Following more than 2 years of crewless testing on the CAMRAS hardware using simulated metabolic loads, a three-part CAMRAS/Constellation Suit Integrated Test (CCSIT) series was developed where different technologies and hardware components will be integrated and tested as a subsystem rather than as individual components.

The initial CCSIT with the CAMRAS hardware in a relevant environment with humans occurred in 2008. Most tests involved either four or six test subjects at a time in a sealed-up test chamber configured for a volume similar to that of Orion. Test subjects were asked to perform activities at metabolic loads, including nominal activities, exercise, and sleeping. The test team maintained test chamber pressure at 14.7 psia, and introduced oxygen (O_2) into the chamber so as to maintain 21% O_2 levels throughout the length of the tests. Two CAMRAS units were used in parallel. Oxygen, CO_2, and H_2O levels in the air were continuously monitored. Figure 2 is a picture of the ECLSS hardware that was installed in the test chamber.

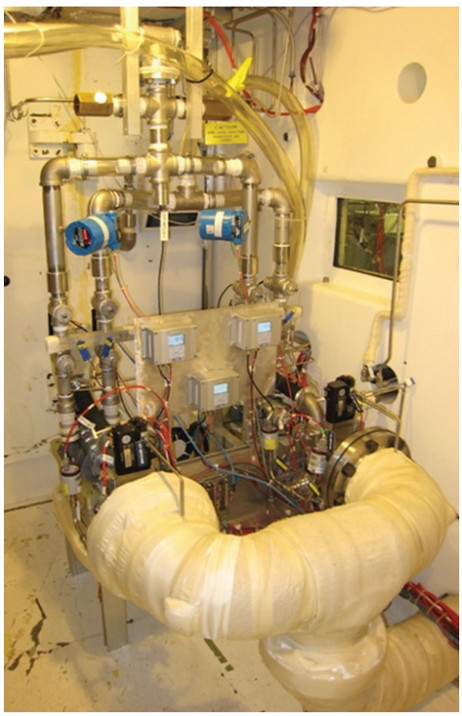

Fig. 2. *CAMRAS hardware in the test chamber.*

Nominal activities generally comprised either four or six test subjects sitting, standing, stretching, moving about, working on their computers, eating, and using the toilet. Subjects provided regular feedback to the test team on how the environment felt while inside the chamber. Tests lasted 6 to 10 hours, depending on how long it took to achieve steady-state levels of CO_2 and H_2O inside the chamber. The test team adjusted flow rate and cycle time of the CAMRAS valve during the test to target dew points between 35°F and 45°F. Results indicate that CO_2 levels were comparable to the crewless simulated tests, but that humidity levels were lower than expected. Because of this, the flow rates required to achieve the target dew points were lower than modeling and crewless tests had suggested.

Exercise activities were conducted for many of the tests, where either one test subject would exercise for 30 minutes while the other three test subjects performed nominal activities or the test subjects would take turns exercising for 30 minutes each, with 15-minute breaks between test subjects. Test subjects who were exercising would wear a heart-rate monitor to verify they achieved a target exercise rate of 75% VO_2 max. The test team monitored power output, a measure of how much work the test subject was doing while exercising on the stationary bicycle, during the exercise period. When only one test subject exercised for a given test day, the team evaluated how long it took for the chamber air to return to pre-exercise CO_2 and moisture levels, including drying time for sweat-drenched clothing, and compared this with human-systems integration requirements values for H_2O generation rates. When test subjects exercised in series, the test team evaluated how high the dew point would get with the CAMRAS units operating at full capacity (50 cfm airflow through each CAMRAS unit, 3-minute cycle time for rapid regeneration). Condensation could occur if the atmospheric dew point exceeded the coldest inside surface of the habitable portion of the Orion crew module. Results indicated that for single-exerciser cases, maximum dew points varied from 42°F to 49°F and 60 to 75 minutes later the dew point returned to pre-exercise levels. For the multiple-exercisers cases, maximum dew points range from 51°F to 56°F and also took 60 to 75 minutes to recover to pre-exercise levels. The humidity and CO_2 levels for both the single-exerciser cases and the multiple-exerciser cases trended similarly with simulated exercise loads. Figure 3 shows one of the test subjects exercising on the bicycle.

Fig. 3. *Test subject exercising in the test chamber.*

Sleep scenario cases involved four test subjects entering the test chamber 2 hours prior followed by an 8-hour sleep period. One hour after waking, one test subject exercised for 30 minutes on the exercise bicycle to induce a significant change in humidity and CO_2 levels in a short amount of time and to determine how well the CAMRAS hardware could catch up with the dramatic change. Results indicate that humidity levels were erratic throughout the night, and a steady-state level was never achieved, although the CO_2 concentration achieved steady-state levels 2 hours after the test subjects went to sleep.

Exploration Life Support Air Revitalization System Technology Development for Human Test Subjects

continued

Additional tests involved test subjects on respirators that were specially designed to be plumbed directly to the ECLSS cabin process air loop plumbing. This was to simulate an emergency scenario where crew members would breathe directly off the ECLSS hardware if a toxic event occurred inside the cabin. One, four, and six test subjects donned and doffed respirators at different intervals. The objectives were to determine how dry the air would get if the only source of humidity is from respiration (vs. respiration, perspiration, and evaporation) and what pressure/flow effects occur when the fixed volume shrinks from approximately 570 ft^3 to approximately 6 ft^3. Results indicate that the dew point could get as low as –4°F (the relative humidity was less than 5%) in the case of only one test subject; the dew point was as high as 10°F for more test subjects. Pressure effects were also dramatic. The expandable respirator hoses changed shape during the test each time the test subjects inhaled or exhaled. This effect was especially pronounced when six test subjects were directed to inhale and exhale at the same time (figure 4). A second set of CCSIT operation uses CAMRAS hardware, prototype Constellation umbilicals, and spacesuit volume-simulator tanks. These crewless tests are performed in a vacuum chamber at simulated spacesuit operational conditions of 100% O_2 at a reduced pressure of 4.3 psia. CAMRAS performance and pressure drop/flow characteristics of the umbilicals are evaluated for different operation parameters.

Fig. 4. *Test subjects during in-line respirator tests.*

Phase 2 is also the first time that the CAMRAS hardware is tested in these extreme environmental conditions.

For the third phase of CCSIT operation, the CAMRAS hardware, spacesuit umbilicals, and pressure suits use an integrated hardware over the full range of mission scenarios. Tests include human test subjects in shirtsleeve cabin environments during sleep, nominal, and exercise metabolic loads; at various cabin pressures and O_2 concentrations; and in pressure-suit environments. All tests must be completed prior to the Orion Critical Design Review.

Spacecraft Water Monitoring: Adapting to an Era of Emerging Scientific Challenges

J. Torin McCoy, *Johnson Space Center*

The International Space Station (ISS) obtains water from a variety of sources. Ground-supplied water is launched reliably to station on Russian Progress vehicles, via the European automated transfer vehicle, and by means of the Japanese H-II transfer vehicle. Another key source is potable water transferred from the shuttle; this high-quality water is generated as a by-product of the shuttle fuel cells. The ISS has the capability to use recycled humidity condensate and even urine reclamation to "recycle" water. The NASA publication "Spacecraft Water Exposure Guidelines" http://hefd.jsc.nasa.gov/toxeg.htm#sweg provides chemical-specific environmental challenges and health-based guidelines for the shuttle and the station. These limits are used to develop water-quality-monitoring technologies (Table 1).

The ISS is a closed-loop environment, so water quality controls are essential. Bladder/tank materials, added biocides, pollutants in source water, and unintended contributions from processors can negatively impact a spacecraft water supply that has no appropriate protections. Scientists discovered a variety of anomalies from water samples returned from the shuttle, Russian Space Station *Mir*, and ISS. Monitoring and anomaly mitigation from a remote environment is clearly a challenge. This report focuses on these challenges.

Water data are currently acquired through archive sampling or various real-time techniques. The ISS has 300-ml or 1-L bags for on-orbit collection. These bags are returned to the ground by Russian Soyuz or shuttle flights for testing, which allows for full microbial and chemical characterization. The weakness in this procedure is that it requires crew time, upmass for bags and adapters, and downmass for sample return, and it does not allow for in-flight decision-making.

ISS has a total organic carbon analyzer (TOCA) that works in conjunction with the water recovery systems on both the shuttle and the station. The TOCA provides information by taking compounds in the water, oxidizing them to carbon dioxide (CO_2), and reading the CO_2 level. It then provides screening indicators for water safety. The returned archive samples are analyzed to fully determine what compounds are associated with that organic carbon level.

Water-inoculated agar plates provide in-flight microbial analysis to determine the total bacterial count, and the archives allow for interpretation of microbes that are present. Water-inoculated agar plates provide in-flight microbial analysis to determine the total bacterial count, and the archives allow for interpretation of microbes that are present. The ISS also carries coliform bags that change colors in the presence of certain indicator organisms.

With the imminent retirement of the shuttle, downmass is more limited than upmass because of the reliance that will be placed on the Russian Soyuz capsule. As water can be relatively heavy to return, the new six-person crew is adding pressure for upmass and downmass to support systems on the ISS and to allow for troubleshooting. Ground control must be able to check out and provide data to all stakeholders on the function of these new systems. NASA therefore needs new hardware that is rugged, noncomplex, and less dependent on archives and resupply.

A number of potential technology needs exist at this time, including the need for a total alcohol detector since alcohol is a priority for environmental control. A front-end unit for water monitoring that is compatible with in-flight air monitoring systems (i.e., one piece of equipment that monitors both air and water) is also needed, as is a chemical-specific colorimetric test strip that would provide an indication of water contamination. To complicate this technology development, air-water interfaces in microgravity differ from those on Earth. For example, water bubbles in space do not escape the same way as they do on Earth. Simply put, small things can cause big complications, false results, and equipment failures.

A number of vital questions address the suitability of a technology to the unique conditions of Exploration missions. These are as follows:

Can the technology meet the required analytical detection limits?

Does the technology require resupply of consumables?

Does the technology use chemicals or reagents that can pose a crew health concern in a closed-loop spacecraft environment?

Spacecraft Water Monitoring: Adapting to an Era of Emerging Scientific Challenges

continued

Does the technology have the specificity to handle mixtures of pollutants without affecting the reliability of individual results?

Can the technology be adapted to the uniqueness of a microgravity environment?

Is the technology rugged enough to perform in a microgravity environment?

Does the technology minimize critical crew time/interactions?

Are weight and power needs within practical limits?

Colorimetric Solid-phase Extraction

Colorimetric solid-phase extraction (C-SPE) uses solid-phase extraction membranes impregnated with analyte-specific colorimetric reagents to rapidly and selectively measure low levels of key water quality indicators. The extractor, with water introduction, produces a color change in about 2 minutes.

A spectrometer then reads the color change and translates it into a concentration. C-SPE is used for iodine and silver, but can be adapted to other compounds as well.

The development of C-SPE is a success story because of a partnership that was formed among NASA, business, and academia. Iowa State University, Ames, scientists were developing a novel technology that could concentrate water analytes on a membrane and produce a measurable color change across a broad concentration range. Because they had to read that color change, they partnered with BYK-Gardner, Columbia, Md., who created the commercial technology used in "paint color matching." This commercially produced spectrophotometer was adapted to allow the translation of color change to analyte concentration. Through partnership with Iowa State University and BYK-Gardner, NASA thus developed a promising technology for space flight. Technical successes that arose from this three-way partnership include: small size, mass, and power needs; simplicity and adaptability; and in-flight data that can be used operationally.

ISS U.S. Laboratory condensate	Shuttle-generated fuel cell water	Ground-supplied Russian "Rodnik" water (Progress launched)
Benzyl achohol	Nickel[2]	Chloroform
Ethanol	Ethanol[1]	Manganese
Methanol	Iodine[1]	Silver[1]
Acetate	Free gas	
Formate	Cadmium[2]	
Proprionate	Lead	
Zinc[2]	Caprolactam[3]	
Nickel[2]		
Formaldehyde		
Ethylene glycol		
Propylene glycol		

[1] Related to biocide addition
[2] Generally resulting from releases from metallic heat-exchanger coatings, or dispenser parts
[3] Resulting from leaching for bladder material

Table.1. *Comparison of contaminants of concern for different potable waters.*

Cascade Distillation Subsystem Development

Karen Pickering, *Johnson Space Center*

Recovery of potable water from wastewater is essential for the success of long-term human missions to the moon and Mars. Honeywell International, Morristown, N.J., and the Johnson Space Center (JSC) Crew and Thermal Systems Division are developing a wastewater processing subsystem based on centrifugal vacuum distillation. This wastewater processing cascade distillation subsystem (CDS) uses an efficient multistage thermodynamic process to produce purified water. The rotary centrifugal design of the system also provides gas/liquid phase separation and liquid transport under microgravity conditions. We built, delivered, and integrated a five-stage prototype of the subsystem into the JSC Advanced Water Recovery Systems Development Facility (AWRSDF) for development testing. The system, currently being tested at JSC, has been challenged with a variety of ersatz and human-generated waste streams representative of lunar outpost and transit mission wastewater.

A simplified schematic of the CDS is shown in figure 1. In general, operation of the CDS involves evaporation and

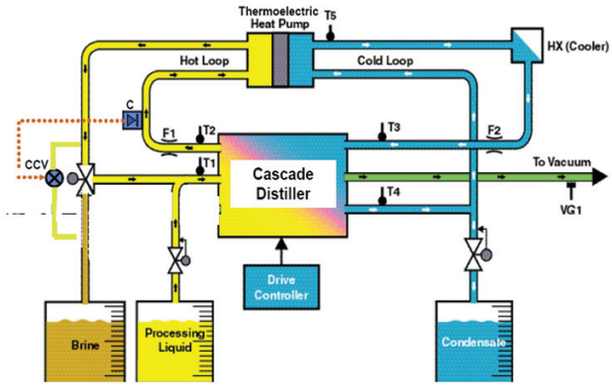

Fig. 1. *CDS block diagram.*

condensation of wastewater and brine within a rotating drum apparatus. The drum is divided into five distillation compartments by means of specially designed baffles. Influent feed and recycled brine solutions are fed into the rotating drum at various stages within the distillation process. The vapor formed within each distillation chamber is condensed on the surface of the partition opposite the next evaporation stage. Each of the five distillation compartments is maintained at successively lower operating pressure, allowing the heat of vaporization to be recovered four times. To enhance the liquid evaporation process, we employed an external thermoelectric heat pump (THP) to provide heat energy to the hot side of the liquid recirculation loop. The THP also provides cooling energy to the cold recirculation loop used to remove the heat of vaporization not recuperated from the process. A trimming heat exchanger provides additional cooling energy to balance the thermal inefficiencies common to the THP technology. By operating at reduced pressure and recovering the latent heat of vaporization, we conserved the energy requirements of the CDS. In addition, the centrifugal forces produced during rotation of the drum assembly support the transport of all liquids within the system and the operation of the distiller at reduced gravity.

The CDS test stand, as integrated into the JSC AWRSDF, is shown in figure 2. We began performance testing of the CDS in September 6, 2007 and ended it July 29, 2008. Over the course of this testing, we processed in excess of 1,180 liters of influent feed solution through

Fig. 2. *AWRSDF CDS test system.*

the CDS in more than 120 batch runs. Logged hours in the laboratory exceeded 830, including over 400 hours of distiller operation. In total, we tested more than

Cascade Distillation Subsystem Development

continued

10 influent feed streams, including deionized water, sodium chloride solutions, human- and ersatz-generated pretreated urine, human- and ersatz-generated humidity condensate, and mixed waste streams comprising solutions of a transit mission ersatz and solutions containing human-generated urine mixed with both human- and ersatz-generated humidity condensate.

The average water recovery over the course of testing was 82% ± 8%. We demonstrated recoveries as high as 91.2% ± 0.7% for specific test points on mixed waste streams. The performance of the CDS was highly consistent and within acceptable limits for all test phases and test solution types. Based on these results, the system is now in development to support an Exploration Life Support (ELS) Project distillation comparison test begun in 2009. One of the project objectives was to reconfigure the system in support of the ELS comparison tests. We challenged the CDS, along with two other candidate distillation technologies, using a series of human-generated waste streams representative of those anticipated for a lunar outpost.

Rotating Reverse Osmosis for Water Recovery on Long-term Space Missions

Karen Pickering, *Johnson Space Center*

Water is essential to sustain human life. The large quantities necessary for consumption and hygiene make the supply of this resource on space missions costly. Although periodic resupply is feasible for short-term missions, water recovery from wastewater will be essential to operate a lunar base or to carry out missions to Mars.

A number of physical-chemical technologies are candidates for use on a lunar outpost. Northwestern University, Evanston, Ill., via a NASA Research Announcement grant, developed one of these technologies – rotating reverse osmosis (RRO). To understand how RRO works, we must first understand the process of reverse osmosis (RO).

RO is a separation process by which, through applying a pressure in excess of the osmotic pressure, water is forced across a semipermeable membrane from a solution of high concentration to a solution of low concentration. This water passes through the membrane at a much higher rate than that of the solutes, which leads to separation of the water and the solutes.

The small size of the system and its low energy cost compared to thermal systems make RO a good candidate water purification method for space flight. NASA is also considering the technology for its advantages in recovering potable water from hygiene water. However, there are issues with the use of RO. Because the feed solution is concentrated as water passes through the membrane, solutes build up on the membrane over time in a phenomenon known as fouling. To reduce fouling, RO systems are typically operated at low recovery rates and in a crossflow configuration in which the fluid is run parallel to the surface of the membrane. This combination increases shear force across the membrane surface and effectively washes away the concentrated solutes, extending the life of the membrane.

We designed the RRO system to minimize fouling to allow for increased recovery rates. In this system, an inner cylinder supporting the RO membrane is rotated within a fixed outer cylinder. This configuration alters the flow characteristics of the fluid within the annulus, which further increases shear across the membrane and reduces the buildup of solutes on the membrane surface.

Scientists delivered a second-generation RRO prototype to the Johnson Space Center Advanced Water Recovery Systems Development Facility for evaluation (figure 1). A number of analyses were subsequently performed on the system to answer three key questions: (1) Does a rotating RO configuration reduce membrane fouling? (2) Can an RRO system successfully remove a surfactant from an influent stream? and (3) Can an RRO system successfully recover water from a mixed stream of early lunar base wastewater?

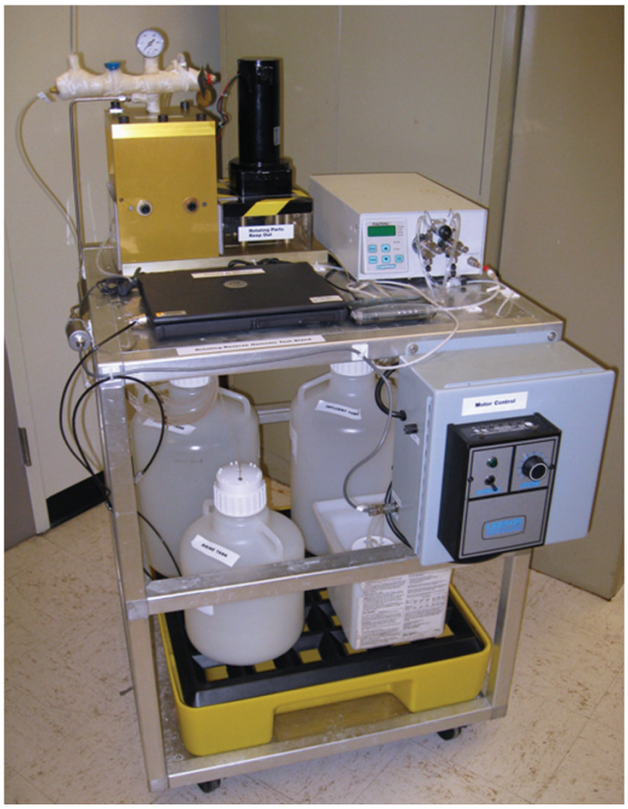

Fig. 1. *Second-generation RRO system.*

Results of various feasibility tests demonstrated that the flux, or fluid flow across a membrane area, of the RRO was affected by the rotating configuration. The rotating test points had a higher flux at 500 psig than the non-

rotating test points. This suggests that the RRO does reduce membrane fouling; however, the flux declined within the first 12 hours of operation, after which the rotation no longer provided an advantage (figure 2). While the recovery showed similar trends, it was highly dependent on the flow rate of the brine, which varied during each test point.

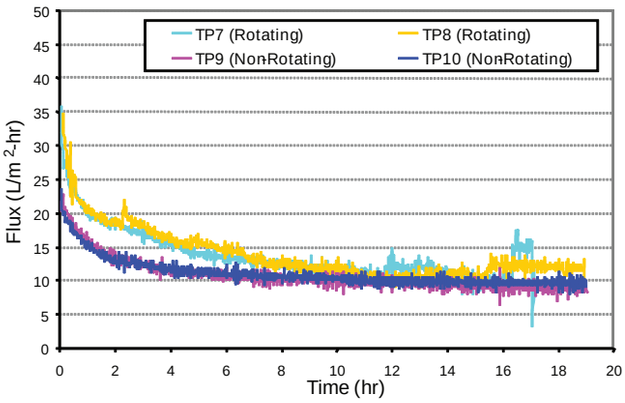

Fig. 2. *Flux over time for two rotating and two non-rotating mixed waste stream test points.*

The RRO was capable of excluding a number of contaminants, including surfactants, but did not appear to provide an advantage over a non-rotating RO system in product water quality.

Further RRO development will need to address several mechanical issues. For example, because of the rotating nature of the system and the membrane geometry, a number of components are susceptible to failure. More importantly, the rotating and non-rotating seals need to be redesigned to reduce leakage and to facilitate membrane replacement. The integrity of the membrane also requires improvement to reduce failures at its seams.

In summary, although the RRO system has several advantages compared to operation of a static RO system, additional development work is needed before this technology can be baselined as part of a water recovery system for Exploration missions.

Urine Pretreatment Development

Karen Pickering, *Johnson Space Center*

Recovery of potable water from wastewater is a critical requirement for long-duration space missions. For many hardware systems used to recover potable water from wastewater, the most efficient operation requires wastewater that is stabilized to prevent deterioration of the contaminants. This is referred to as "pretreatment" of wastewater, since a chemical is typically added to the wastewater prior to storage.

The current pretreatment method used on space shuttle adds potassium peroxymonosulfate (Oxone®, DuPont), an acidic oxidizing biocide that must be replaced daily by crew. Potassium peroxymonosulfate is a highly reactive compound that is hazardous to human health. Our exploration life support team is working to develop alternate pretreatment techniques that have a lower toxicity than the current space shuttle urine pretreatment method.

Our urine pretreatment efforts focused on identifying and testing low-toxicity chemicals to stabilize urine and prevent the biological and chemical changes that cause precipitates and fouling of plumbing surfaces. We also experimentally determined the lowest effective concentration of the chemicals.

The team conducted a series of laboratory experiments to test urine pretreatment chemicals that are less toxic than potassium peroxymonosulfate. The Crew Exploration Vehicle is expected to require urine pretreatment to prevent microbial contamination and the formation of alkaline precipitates that interfere with urine dumps to space vacuum. We performed this investigation to identify biocide pretreatment chemicals that are less toxic than potassium peroxymonosulfate and to suppress and prevent microbial contamination that aids in preventing the subsequent production of alkaline precipitates during urine storage. Team members examined a number of low-toxicity chemical compounds commonly used to stabilize personal hygiene products for their effectiveness at preventing microorganism contamination and growth in wastewater.

We based urine pretreatment development on 13 experiments assessing the effectiveness of low-toxicity urine pretreatment chemicals to stabilize urine during storage. In the first set of three experiments, maleic and malonic acid were shown to prevent urea hydrolysis in urine for 3 weeks even with the addition of urease-producing bacteria. In the second group of five experiments, 13 different, low-toxicity biocides were tested. The team determined the required mass concentration of these alternative biocides to stabilize urine. In the final set of five experiments, we tested 20 combinations of biocides and organic acids. We conducted toxicological hazard assessments on the biocides that were effective at killing bacteria and preventing precipitates in stored urine, and identified two effective, nonoxidizing pretreatment liquid pretreatment alternatives to potassium peroxymonosulfate. One low-solubility dry chemical was an effective biocide at 1 gram per liter urine. These formulations have some advantages over potassium peroxymonosulfate in that they are less toxic, add less dissolved solids to urine, and do not produce toxic volatile organics compounds. Development of an in-tank delivery system is in work to study methods of delivering the dry chemical pellets by slow release within the wastewater tank.

Air Quality Monitoring: Risk-based Choices

John T. James, *Johnson Space Center*

When monitoring spacecraft air quality, we first focus on controlling the risk of toxic exposure. We are also careful to learn from adverse events. For example, we use nontoxic chemicals wherever we can and limit access to those chemicals that are toxic; the use of ethylene glycol on the Russian Space Station *Mir* taught us this lesson. This chemical leaked episodically on *Mir* and caused crew symptoms; therefore, it was replaced in the International Space Station (ISS) systems by a much less toxic fluid consisting of glycerol and water (triol). It is also important that materials do not off-gas significantly. Toxicants (such as in batteries) are contained in payloads according to their risk, and we use nontoxic utility compounds.

We provide both a robust air-scrubbing capability and personal protective equipment for the crew to don if needed, as well as the ability to abandon the spacecraft if needed.

When adverse events occur, we intentionally learn from them. Toxic propellants, fires, pyrolysis events, thermal control system leaks, excess carbon dioxide (CO_2), formaldehyde accumulation, and dust have all proven (predictably) to be issues in past space flights. Crew members may be particularly sensitive to CO_2 in the closed environment of space because of fluid shifts.

The following adverse events are a few of those from which we have learned vital lessons:

> In 1975 during the Apollo-Soyuz Program, the Apollo capsule was contaminated with nitrogen tetroxide in the course of repressurization. One crew member was unconscious at landing, and the other two crew members had delayed pulmonary issues that were later resolved. The lesson we learned from this was to keep the pressurization equalization port as far from the thrusters as possible.
>
> In 1997 the solid fuel oxygen generator fire aboard *Mir*, from a toxicology perspective, was a minor fire. Few toxic contaminants were released into the air. The "beauty" of this fire was that it was a hot fire and, because it was an oxygen generator, carbon monoxide (CO) became CO_2.
>
> Also in 1997, a small fire in the trace contaminant purification system on board *Mir* generated a puff of smoke. At 10 hours post-event, the crew reported nausea and headache, consistent with a serious CO exposure. From this we learned that the physiological effects of exposure are delayed until the carboxyhemoglobin builds up in the human system.
>
> Ethylene glycol leaks were also very common on *Mir* in the 1990s. Levels were measured with Draeger-Tubes®. The leaks occurred in the Kvant module, and the contaminant was not distributed evenly through the space. Our lesson learned from this was that the ethylene glycol was seeking cold surfaces, condensing, and then slowly revolatizing again until it reached equilibrium.

While these types of events could have been anticipated, other events have proven more unpredictable. For example, post-extravehicular activity (EVA) the crew of ISS Increment 7A re-entered the station and started to desorb the metal oxide (Metox) canisters used to purify suit air during EVAs. The Metox regeneration system (by design) desorbed pollutants into the vehicle, not into space. The system was particularly loud, however, and the crew turned it off during the process – leaving the canisters inside. Another crew came on board station several months later, performed an EVA, and prepared to desorb their own canisters. As they started the process, because of the old canisters, the environment became incredibly noxious, and they had to go into the Russian segment for 30 hours.

We are now in the process of transitioning to real-time, on-board analysis. Grab-sample canisters enable us to aspirate samples through a valve by vacuum in <5 seconds to later analyze by gas chromatography. The primary weakness of these instruments is that air particulates occasionally clog the valve, preventing it from seating properly. Formaldehyde badges are another cheap and effective solution to detecting air particulates. We fly them in pairs on station, and crew members can wear them on their suit or fix them to a wall that has a good cross flow of air. Badges, while effective on station, will prove less effective in long-duration missions to the moon to Mars because they still have to be returned for analysis.

Current ISS on-board analysis technologies

Compound specific analyzer-combustion products (CSA-CP): The CSA-CP is a handheld monitor, adapted from a commercial product, that can perform at low pressures. We have experienced some problems with its electrochemical sensors.

CO_2 monitor: This handheld commercial monitor is very rugged, using infrared spectrometry to measure CO_2 levels.

Drager chip measurement system: This unit, flown by our Russian partners, has a 2-year shelf life. It is very quick and reliable, but can only monitor one analyte at a time. The unit is not good at high humidity levels and not sensitive enough to follow nominal atmospheric pollutants.

Major constituent analyzer (MCA): The MCA is a large, one-of-a-kind instrument flown by Life Support engineers. It is used to monitor life support gases and also CO_2.

Volatile organic analyzer (VOA): The VOA is a large, one-of-a-kind instrument flown by the Johnson Space Center toxicology group. It is a double-channel gas chromatograph ion mobility spectrometer that measures many trace organic compounds. Although the VOA has the advantage of not requiring a lot of pumps, it has only worked about half the time.

The European Space Agency's ISS instrument is the ANITA [ammonia and nitrification analyzer], adapted from commercial technology to deconvolute the optical spectrum, but only one individual can interpret it, thus limiting its usability. Another instrument is the electronic nose, but it targets only a few compounds and lacks specificity. The air quality analyzer, a gas chromatograph differential mobility spectrometer, is unproven as it is about to fly.

Another key issue in air quality on current and future missions revolves around how monitors present data to the crew in the absence of ground support and interpretation. Crew members need to be fairly autonomous and able to solve their own problems, so we must present data to them in a clear and meaningful way.

We must weigh the pros and cons of commercial vs. one-of-a-kind instruments as we change our approach to environmental monitoring. Commercial items tend to be smaller and less expensive than one-of-a-kind versions; they also are likely to have experience history and established support that we cannot get for our own inventions. While one-of-a-kind units have the advantage of being built to requirements, commercial versions are generally adaptable to requirements and are much easier to sustain.

Finally, lunar dust will be a major future issue for environmental quality. It is tiny, is easily inhalable, is porous, and has great surface area. High iron content gives it magnetic properties, which may enable us to solve control problems with magnets. Mars is likely to have greater dust issues than the moon, which is problematic for both hardware and crew health. Mars has global dust storms and local dust devils that move the dust into everything on a massive scale.

In conclusion, air monitoring is secondary to maintaining rigid control of risks to air quality, and it requires us to target the credible residual risks. We must transition from archival to real-time, on-board monitoring, although the constraints we have on monitoring devices are severe. We must provide data to a crew in a way that allows that crew to interpret the findings. Finally, dust management and monitoring may be a major concern for Exploration-class missions to the moon and Mars.

Design and Development of Airlock Contamination Detection Kits for the Space Shuttle and International Space Station

Steven D. Hornung, *White Sands Test Facility*

NASA White Sands Test Facility (WSTF) has designed and developed toxic vapor detectors for flight applications. Three types of detectors are discussed in this paper: (1) a Draeger-Tube® encapsulation device (DTED) that detects parts per million (ppm) levels of ammonia (NH_3); (2) a detector using a gold salt (potassium tetrachloroaurate), which changes color from yellow to purple on exposure to hydrazines, that detects monomethylhydrazine (MMH) and unsymmetrical dimethylhydrazine (UDMH); and (3) a prototype detector for UDMH fuel/oxidizer reaction products (UFORP) that, after design and testing, is ready for flight qualification when needed. The first two vapor detectors are now included in airlock contamination detection kits on the International Space Station (ISS).

Extravehicular activity (EVA) operations sometimes require astronauts to move along translation paths near thrusters, thus placing them at risk of exposure to MMH or UDMH as a residual or from leaks in the thruster valves. Some ISS EVAs also require disconnecting and connecting NH_3 coolant lines, and leaking NH_3 can contaminate EVA suit materials. All of these compounds are toxic and must be under spacecraft maximum allowable concentration limits within the habitable areas of the shuttle or ISS. In a case of suspected contamination, the sampling protocol at the end of an EVA requires astronauts to enter the airlock, repressurize it to 5 psia, and then check for residual compounds using the contamination detection kit. MMH and UDMH require a 10-minite sample, and ammonia requires 3.5 minutes at the 5-psia hold pressure.

Draeger-Tube® Encapsulation Device

Draeger-Tubes® are sealed glass tubes containing a color change reagent that changes color when exposed to the chemical of interest. The length of the color change can be used to determine the concentration of the chemical. Normally, the tube is opened on each end using a tool that scores and breaks off the tips, thus producing small sharp pieces of glass from the broken ends. To eliminate problems of handling and floating orbit debris, WSTF devised a DTED fixture (figure 1). The DTED incorporates anodized aluminum end caps to hold the Draeger-Tube® within a clear Lexan® sleeve. A flow restrictor is installed at the outlet end to limit the nominal flow to 50 sccm and provide for a distinct color front in the tube. Viton® O-rings inserted into a groove in each end cap seal the Draeger-Tube® in place. Tether rings, mounted on the end caps, open the flow path for sampling when broken off. The DTED is assembled under an inert nitrogen atmosphere to prevent moisture and air from degrading the color change reagent over time.

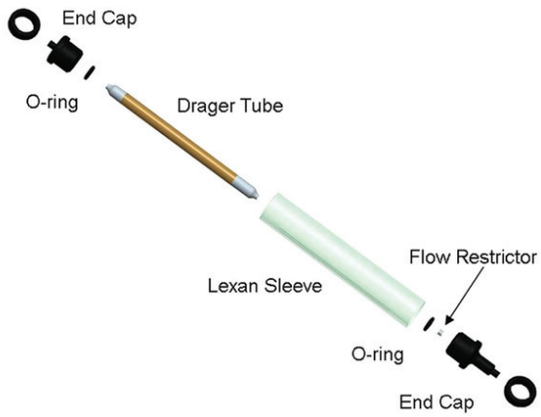

Fig. 1. *Exploded view of the Draeger-Tube® encapsulation device (DTED).*

The ISS airlock contamination kits are supplied with prepared DTEDs. After the airlock has been repressurized at 5 psia for 10 minutes, an adaptor is placed over the airlock manual pressure equalization valve (AMPEV) and the opened detector is inserted in the adapter. The AMPEV is then opened and air is drawn through the detector and out to an external vent. Figure 2 provides a

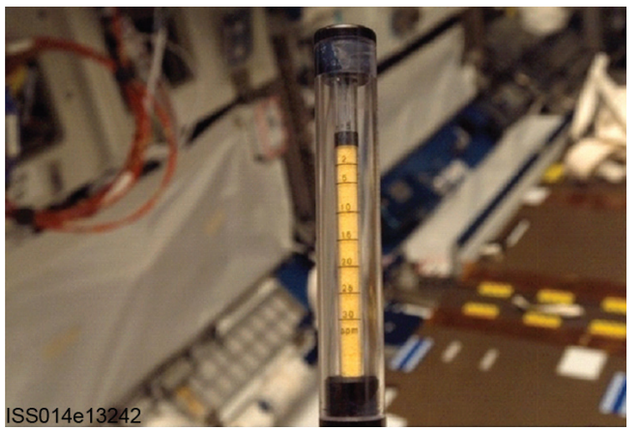

Fig. 2. *A used DTED floating in the ISS airlock.*

photograph of a used DTED floating in the ISS airlock after sampling (photo by Astronaut M. Lopez-Alegria).

Gold salt detector

WSTF developed a detector for the colorimetric determination of trace hydrazine, MMH, and UDMH vapors. In this application, a filter treated with potassium tetrachloroaurate is reduced to elemental gold by the hydrazine fuels, resulting in a purple or grey coloration on the pad. The intensity of the color change is proportional to the concentration of hydrazine, MMH, or UDMH, and users determine this concentration by comparison to a color reference chart. The flight-certified gold salt detector for the ISS consists of the treated filter pad with a porous backing, a pad holder with tether holes, and a retaining cap (figure 3). NASA includes gold salt detectors and the color reference chart in ISS airlock contamination detection kits. For use, the detector is removed from its protective wrapper and placed in the AMPEV adapter, and a sample is pulled through the detector for 10 minutes. The user compares the resulting color with the color reference chart to determine whether the concentration is above or below a critical concentration.

Fig. 3. Gold salt detector showing parts of the assembly, packaged for flight, and the color card.

UFORP detector

This protoype detector combines two commercial off-the-shelf technologies: a U.S. Department of Justice-approved presumptive forensic field test method for methamphetamine, and a nitrite test strip for water quality. The prototype detector indicates dramatic color changes in the presence of the two components of UFORP, dimethylamine and nitrite, both of which are toxic in an airlock environment. The methamphetamine test kit is a durable plastic pouch containing reagent ampoules that, when broken and mixed, change color in the presence of a secondary amine (although it is a much smaller molecule, dimethylamine, like methamphetamine, is a secondary amine). The user removes a clip to open the pouch, adds the UFORP material, and closes and clips shut the pouch. Nitrite concentration is first determined from the nitrite test strip color change; the reagent ampoules are then broken in sequence and agitated, and the resultant color due to the presence of dimethylamine is observed.

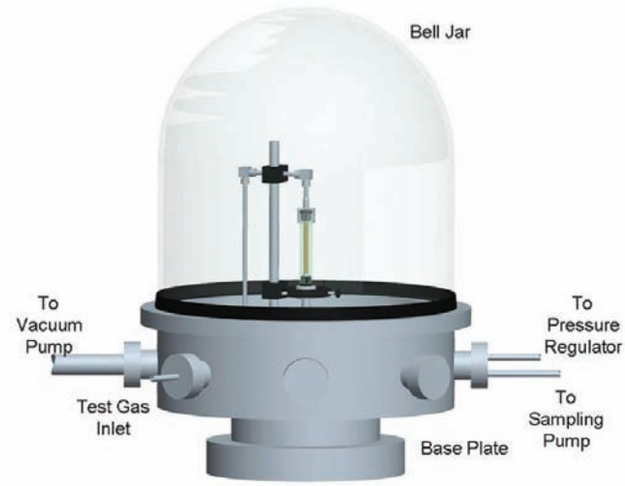

Fig. 4. Reduced pressure exposure system.

Qualification testing

We tested and qualified for flight the ammonia DTED and the gold salt detector using a reduced-pressure exposure test system (figure 4) that maintained a simulated 5-psia airlock pressure. We passed the target gas standard through a flow meter, into the chamber, and terminated it in the sampling cup placed over the inlet of the detector. We then attached the sampling end of the detector to feed through a mass flow meter and a sampling vacuum pump, thereby simulating the vacuum produced by the AMPEV in the airlock and providing the necessary airflow for sampling.

Space Radiation Protection Status and Challenges

Neal Zapp, *Johnson Space Center*

The radiation environment in space has virtually nothing to do with the radiation environment on the ground. Three main factors create the space radiation environment: (1) the galactic cosmic background, a slowly varying omnidirectional field that is as many as 60 ions of the periodic table in measurable abundances at over 12 orders of energy magnitude; (2) solar particle radiation, the transient or event source; and (3) objects trapped in the geomagnetosphere, mainly protons and electrons.

NASA organizes its space radiation protection activities into three main areas: (1) fundamental human-related research in radiation and radiobiology; (2) space medicine radiation health recordkeeping (translating "physicist" to "physician") and working in risk estimation and crew selection (how NASA conducts itself related to human health: what is wrong, and how do we fix it); and (3) the space radiation analysis that provides radiological console support, extravehicular activity (EVA) crew exposure projections, comprehensive crew exposure modeling capability, and radiation characterization of the environment inside and outside of the vehicle.

Vehicle location, as opposed to the environmental state, is the primary driver for radiation in low-Earth orbit (LEO). This is counterintuitive, and results from the protection provided to LEO missions by the Earth's magnetic field. In considering operational issues, vehicle phase and ground track are essential concerns. As we consider Constellation and other long-term missions, the question of "how long until they phase in" is eliminated; the answer is always "right now."

Our radiation approach in low-Earth orbit

The point of greatest vulnerability for our crew occurs during EVA activity, so we select the right people and preplan EVA very carefully. If an event does occur based on situational awareness, we can "manipulate the timeline" to appropriately minimize the mission impact.

The primary limitations of this approach include our limited descriptions of the geomagnetic field, a highly dynamic and nonlinear system. The best tools available today are static in nature. We want to preplan activities, so we have to project tomorrow's exposure, not just account for yesterday's exposure. We are also limited by the models of trapped particles in the Earth's magnetic field.

Current passive crew and area monitoring tools include thermoluminescent dosimetry(TLD)100, 300, 600-700, and CR-39® (Columbia Resin) to measure bulk dose. Number designations here denote materials changes that produce slightly differing sensitivities. TLD 100 is the overall industry standard of lithium fluoride (LiF), which gives a relatively high efficiency for low-linear energy transfer (LET) radiation fields (i.e., photons, beta/electron sources). TLD 300 is calcium fluoride doped with thulium; it represents a measurement from which semiquantitative information can be extracted with respect to contributions of low- vs. high-LET sources. TLD 600 or 700 material is again LiF, in which abundances of fluorine isotopes are weighted to either Li_6 or Li_7 respectively. Li_6 has a very high absorption cross section for thermal neutrons, while Li_7 has a correspondingly very low cross section. As a pair then, information can be extracted concerning the contribution to total measured radiation dose resulting from thermal neutron exposure. CR-39® is a moniker for the use of allyl diglycol carbonate plastic, commonly used in the production of eyeglass lenses as a measurement device. Ionizing radiation with LET values greater than approximately 10 keV/μm cause molecular deformations in the plastic polymer. These deformations are then exacerbated with a chemical etch and individually scored. Each visible track is evaluated, geometrically relating the size and shape of the visible track to the LET of the producing particle through careful calibration. In this way we obtain a passive measurement of LET spectrum for derivation of personal regulatory quantities of interest. We will continue with passive monitoring because this form of monitoring is absolutely reliable and "unkillable," and is relatively low cost because of its low mass and volume.

Our active monitoring practices are shaped by two essential technologies leading our approach to autonomous exploration of the moon and Mars. The tissue-equivalent proportional counter (TEPC) gives real-time dose information and radiation field quality. These data are provided 24 hours a day in 1-minute cadences. The charged particle directional spectrometer (CPDS) is a stack of silicon wafers. As ionizing

radiation passes through the CPDS, the signature left on the wafer indicates the nature of the radiation.

We are starting to build next-generation hardware for the International Space Station (ISS), and are involved with the exploration Constellation Program. The next-generation TEPC is approximately the size of a deck of playing cards and weighs less than 2 lbs. The next-generation CPDS, a product of a NASA-industry-academia collaboration, is already in place for the Mars 09 mission.

Constellation: The future

In designing the next generation of U.S. space vehicles, we are driven by the inherently mass-contained nature of the physics of a lunar mission. Therefore, management of radiation exposure is achieved through vehicle reconfigurations rather than with parasitic shielding. Experience gained through the Space Shuttle and ISS Programs permits us to focus on providing multifunctional spacecraft components, allowing us to minimize crew risk at a concurrent minimum risk of vehicle additional mass and overall system impact. Minimization is particularly important in this case, as the magnitude of possible exposures outside the confines of LEO increases dramatically.

First gap: Orion from a radiation perspective

In figure 1, the parts of Orion (i.e., the crew compartment for ISS and the moon) that are blue are cool/good; the red parts are hot/bad. We have taken inventory of the items already on the vehicle and reconfigured them and the crew geometrically to increase the radiation protection by a factor of 3 without adding anything to the vehicle. The same kind of approach is being investigated with respect to notional habitat and rover designs. The price paid for this is computational power – a gap where we would like to see improvement.

Second gap: Program planning and probability

The biggest problem we have is that we cannot predict what will happen next. When dealing with most environmental concerns, one is interested in environments that were brought with the crew on the vehicle – that is to say, that have engineering solutions. The natural radiation environment is, of course, not under control, and no vehicle can be designed to simply exclude it as one would approach an air contaminant. The three normal tenets of radiation protection (time, in which you minimize a person's exposure to the source; distance, in which you get the person farther away from the source of exposure;

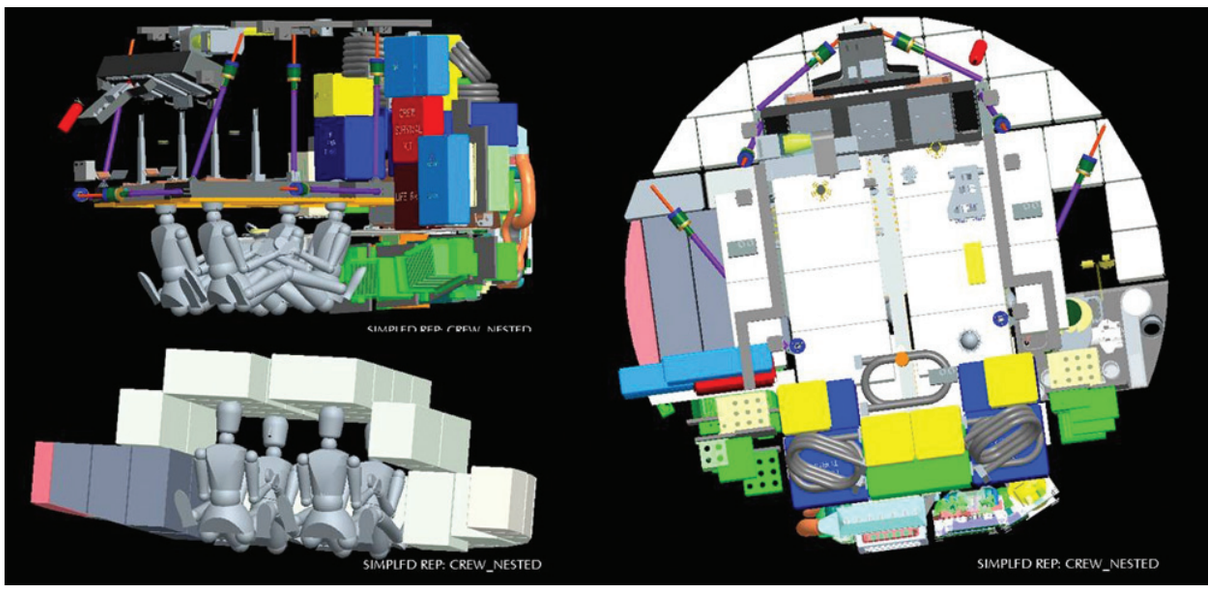

Fig. 1. *Orion from a radiation perspective.*

and shielding, in which you put something between the person and the exposure) are not effective for dealing with the space flight problem. The question is not whether radiation will impact an Exploration mission; the question is when, and what the available mitigations will be.

Third gap: Space weather monitoring

How are we going to get there? As we embark on Exploration missions, our radiation monitoring requirements must necessarily expand. We therefore need alternative data sources to those in place today. We must work together to develop accurate forecasting tools that will give us anywhere from 30 minutes to 24 hours of lead time for events. We are often asked: "How much time is needed?" The answer is: "As much as is possible." There are very real applications for a 2-hour look-ahead, as there are in a longer time frame.

Fourth gap: Transition from research to operations

It is difficult to turn fundamental scientific research into operations, but we must have the perspective to work together.

Radiation represents a significant risk to humans venturing beyond the confines of LEO that we do not yet know how to solve. There is a driving uncertainty in the environment; we simply cannot predict the future behavior of the sun as a physical system. Additionally, there is a driving uncertainty in radiobiology: understanding what it means when you are exposed. Operationally, we are working with three primary mitigations: vehicle design, crew selection, and situational awareness – all of which play a major role in space radiation protection for our crews (figure 2).

Fig. 2. *Concept for individual shielding during predicted solar event.*

Measuring Ionospheric Electric Field Gradients with the International Space Station Floating Potential Probe

Steve Koontz, *Johnson Space Center*
John Alred, *Johnson Space Center*
Leonard Kramer, *The Boeing Company*
Drew Hartman, *The Boeing Company*
Ron Mikatarian, *The Boeing Company*
Kendall Smith, *The Boeing Company*

The International Space Station (ISS) operates in the Earth's ionosphere – an electrically conductive ionized gas or plasma. The station's electrical power systems and metallic structures interact with the ionospheric plasma and with Earth's magnetic field to produce an electric charge on the structure that changes as the vehicle orbits the Earth. This charge is measured by the floating potential measurement unit (FPMU) instruments now attached to ISS. One of these instruments is a floating potential probe comprised of a high-impedance voltmeter that measures the difference in voltage between the ISS structure and its surrounding electrically conductive plasma environment.

We are interested in the ISS floating potential because of its impact both on crew safety and possibly on vehicle performance. Figure 1 shows measurements from the FPMU. The floating potential in the upper panel illustrates variation in the vehicle's voltage, measured with respect to the surrounding ionospheric plasma, as the station orbits the Earth.

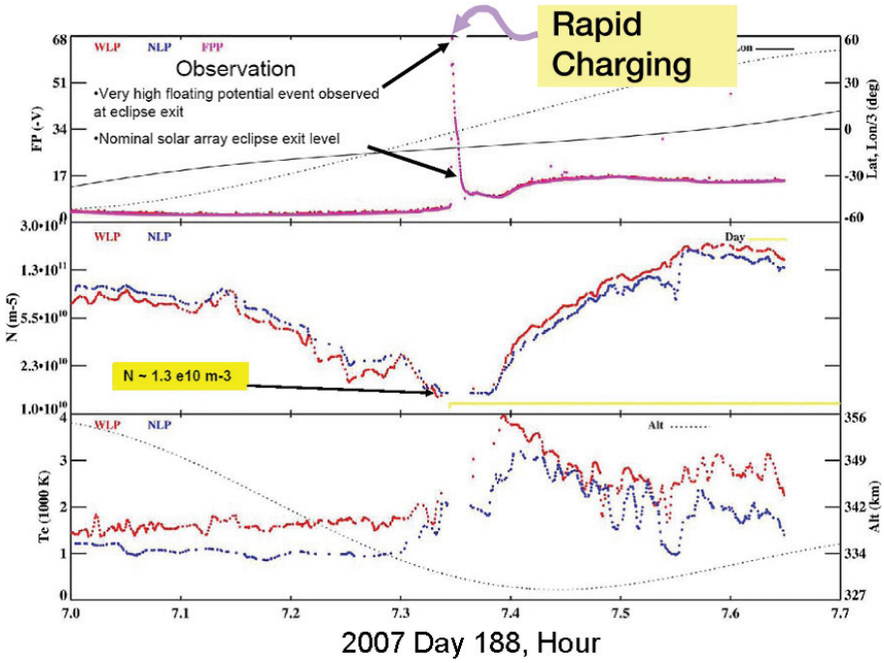

Fig. 2. *Rapid charging observed at low latitude.*

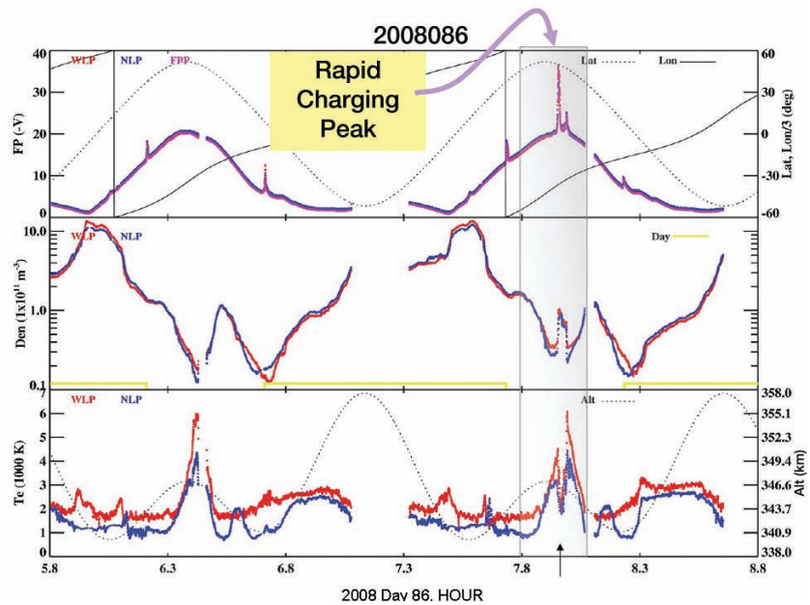

Fig. 1. *FPMU measurements of plasma floating potential, density, and temperature in the ISS environment.*

The charge on ISS is controlled naturally by electron collection at positively charged surfaces and by ion flux removal of electrons at negatively charged surfaces. These physical principals are used in a numerical model, the Plasma Interaction Model (PIM), developed by NASA and The Boeing Company, Chicago, Ill., to predict and control, through use of artificial plasma sources, the ISS floating potential.

Many features of the floating potential (e.g., its broad increase and decrease during each orbit) are well understood

and were accurately predicted by PIM. However, within the past couple of years, analysis of data from the FPMU has revealed rapid and anomalous vehicle charging peaks not captured by PIM physics. One of these peaks is identified in figure 1 and another in figure 2. NASA and Boeing have now established that these anomalous charging peaks are related to voltage gradients in Earth's ionosphere along the ISS flight path as the station orbits the Earth rather than to changes in electron and ion collection by ISS electrical power systems or structural components. In fact, these anomalous rapid charging peaks are only observed in connection with the unusually low ionospheric plasma densities associated with the minimum of the 11-year solar cycle.

We have discovered through this study that the ionospheric reference potential is changing rapidly as the ISS transits geographic regions of high and low potential. As a result of the large size and unprecedented electrical capacitance of the vehicle, these geographic variations in potential appear as observed changes in vehicle floating potential measured with respect to the ionospheric plasma.

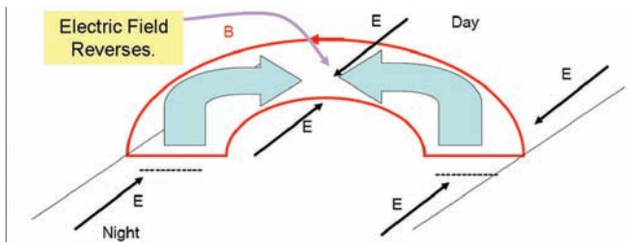

Fig. 3. *Diagram showing reversal of geophysical electric field, often occurring at low latitude when the ISS exits darkness and associated with anomalous rapid charging of the vehicle for several seconds.*

Our NASA/Boeing team identified two immediate sources of geographic variability. One appears at low latitude when the ISS exits darkness and the other appears at high latitude. At low latitude, a condition of reversed electric field often occurs in the natural ionosphere. Figure 3 illustrates this so-called pre-reversal enhancement (PRE). The PRE has long been recognized by the geophysical sciences, and has been observed on many science satellite missions.

The high-latitude, rapid-charging events are associated with geophysical mechanisms that provide a varying electric potential. However, for these high-latitude cases, the mechanism has more to do with solar-wind-driven electric fields that penetrate vertically from high altitudes in the polar zones and then turn horizontally.

These penetration electric fields are illustrated in figure 4. As the ISS transits regions of different electric field orientation, the potential can change rapidly and is responsible for the spike-like events seen in figure 1.

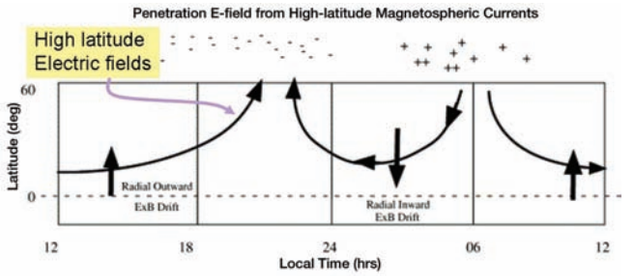

Fig. 4. *Diagram showing vertically oriented electric fields that occur at high latitude and contribute to rapid charging events.*

The electric potential difference for penetration fields is governed by solar wind processes occurring at very high altitude in the interplanetary medium. These processes involve solar wind speed and interplanetary magnetic field orientation, which affect the currents and fields in the Earth's polar and high-latitude regions.

NASA, with support from The Boeing Company, is identifying and managing charging risks on the ISS by monitoring the space environment through FPMU data, analyzing and interpreting FPMU data with the PIM, and innovatively applying well-known geophysical principles. In particular, we have now identified previously unsuspected spacecraft charging mechanisms with variable electric potential in the ionospheric environment that can be attributed to previously known geophysical processes. The subject charging processes can be readily observed only on a spacecraft as large as ISS.

Lunar In-situ Resource Utilization

Gerald B. Sanders, *Johnson Space Center*
Tom Simon, *Johnson Space Center*
William E. Larson, *Kennedy Space Center*
Jackie Quinn, *Kennedy Space Center*
Robert P. Mueller, *Kennedy Space Center*
Kurt R. Sacksteder, *Glenn Research Center*
John Caruso, *Glenn Research Center*

A robust project is under way to develop the capabilities needed to produce most of the consumables required to sustain a lunar outpost from resources found on the moon. A key to fulfilling the goal of sustained and affordable human and robotic exploration is the ability to use resources that are available at the site of exploration (to "live off the land"), known as in-situ resource utilization (ISRU). Traditionally, these resources are the elements found in the soil or the atmosphere. However, ISRU can also include waste products that are the result of human presence. For example, the descent stage of the Altair lander contains residual propellants that can be scavenged. The tanks containing the propellants can be removed from the lander to provide storage tanks on the surface. Plastics from the astronauts' food containers can provide an important source of carbon at locations, such as the moon, that are carbon poor. By producing propellants, life support and fuel cell power consumables, and other items from in-situ resources and eliminating the need to launch everything from Earth, long-term launch and mission costs can be reduced while potentially increasing science and exploration capabilities as well as mission safety. The ability to modify the lunar landscape for safer landing, transfer payloads from the lander to an outpost, mitigate dust generation, and place and build up infrastructure is also extremely important for long-term lunar operations.

As ISRU hardware and systems for human robotic systems, energy storage and power systems, thermal control for surface systems, exploration life support, extravehicular activity (EVA), dust mitigation, cryogenic fluid management, and nontoxic propulsion have never been demonstrated before, NASA is hesitant to add these capabilities into mission designs and plans and make lunar mission success contingent on them. However, once demonstrated, these ISRU capabilities could be inserted into the lunar architecture. With this in mind, the NASA ISRU Project initiated development and testing of hardware and systems in three main focus areas: (1) regolith excavation, handling, and material transportation; (2) oxygen (O_2) extraction from regolith; and (3) ISRU concept evaluations. To minimize cost and ensure that ISRU technologies, systems, and functions are integrated properly into the outpost, technology development efforts are being coordinated with other lunar exploration development areas such as: human robotic systems, energy storage and power systems, thermal control for surface systems, exploration life support, EVA, dust mitigation, cryogenic fluid management, and nontoxic propulsion as well as outside government agencies, industry, academia, and International Partners. The goal is to maximize our ability to leverage funding and increase commonality of hardware at the outpost. Lastly, laboratory and field system-level tests and demonstrations are being performed as often as possible to demonstrate improvements in capabilities (e.g., digging deeper), performance (e.g., lower power), and duration (e.g., more autonomy or robustness) as well as to form the affiliations with industry and International Partners that will be needed once actual outpost flight hardware development and deployment begins.

The first step in the manufacture of lunar O_2 is to excavate the lunar regolith for delivery to the O_2 production system. Depending on the ultimate O_2 extraction efficiency achieved, the production of 1 mt (1.1 tons) of O_2 would, at worst, require the excavation of an area the size of a U.S. football field to a depth of perhaps 1 cm (0.39 in.) over a period of 9 months to 1 year. If more efficient O_2-production technologies are perfected, the excavation area could shrink to the size of a basketball court. Since this excavation is primarily a granular flow and physics issue, work focuses on three primary tasks: (1) modeling the granular behavior and flow of irregular-shaped, varied-size, and multiple mineral and glass particles and regolith-excavation implement interactions; (2) performing a controlled laboratory test with prepared soil bins; and (3) building and testing concept excavation and material transport hardware. A recent and significant accomplishment was re-creating and performing controlled testing of the Surveyor 3 bucket to compare to lunar flight data (figures 1(a) and 1(b)). Although not performed in either vacuum or 1/6g, the tests still provided confidence that our laboratory tests and modeling efforts are anchored by actual lunar measurement. Tests with the Cratos excavation concept vehicle have demonstrated that a small

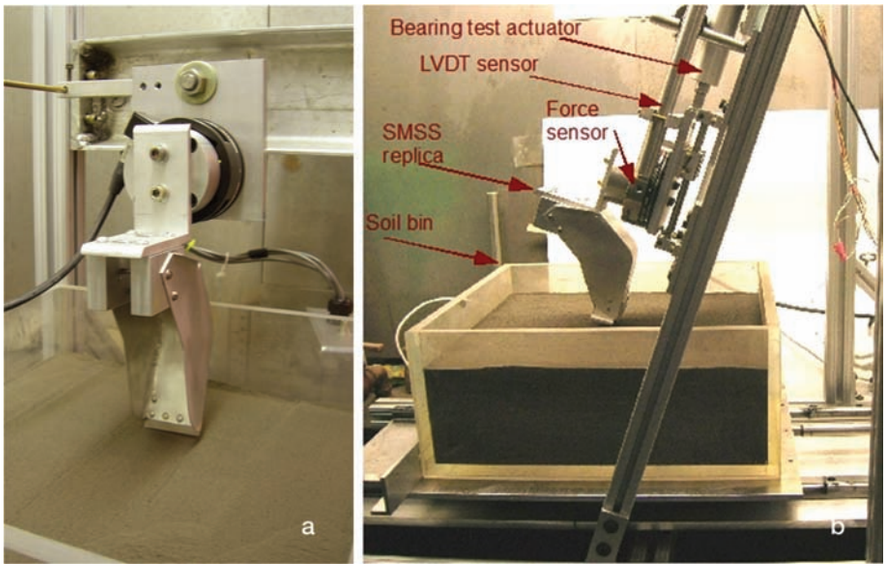

Fig. 1. *(a) Benchtop soil bin with blade. (b) Surveyor scoop replica tests.*

vehicle (~80 kg (176.4 lbs.)) can easily meet early O_2-extraction regolith delivery needs (figures 2(a) and 2(b)).

For O_2 production, we selected three processes that span the range of low risk/low yield to high risk/high yield. These processes under development are: hydrogen (H_2) reduction of regolith, carbothermal reduction from regolith, and molten electrolysis.

Hydrogen reduction is the simplest and least efficient of the three processes. When regolith is heated to around 1,000°C (1,832°F) and mixed with H_2 gas, iron-oxide (FeO)-bearing minerals and glasses in the lunar regolith (e.g., ilmenite ($FeO{\cdot}TiO_2$) are reduced to produce water vapor. This water vapor is condensed and electrolyzed to produce O_2 and to regenerate the reactant H_2 for subsequent processing. While this is not the most efficient process (the amount of FeO in lunar regolith is fairly low (5% to 15%)), it does have the advantage of lower temperatures that keep the lunar regolith in granular form, which greatly simplifies material handling. Both Lockheed Martin Astronautics (LMA, Denver, Colo.) and NASA are leading separate regolith processing reactor design efforts. LMA is designing and testing a rotating reactor with a single inlet/outlet port, and NASA is designing a fluidized bed with separate inlet/outlet ports. Both systems were fabricated, assembled, and tested (figures 3(a) and 3(b)). Before the full systems were built, subscale reactors were tested to determine temperature, H_2 flow rate, and reaction kinetic parameters.

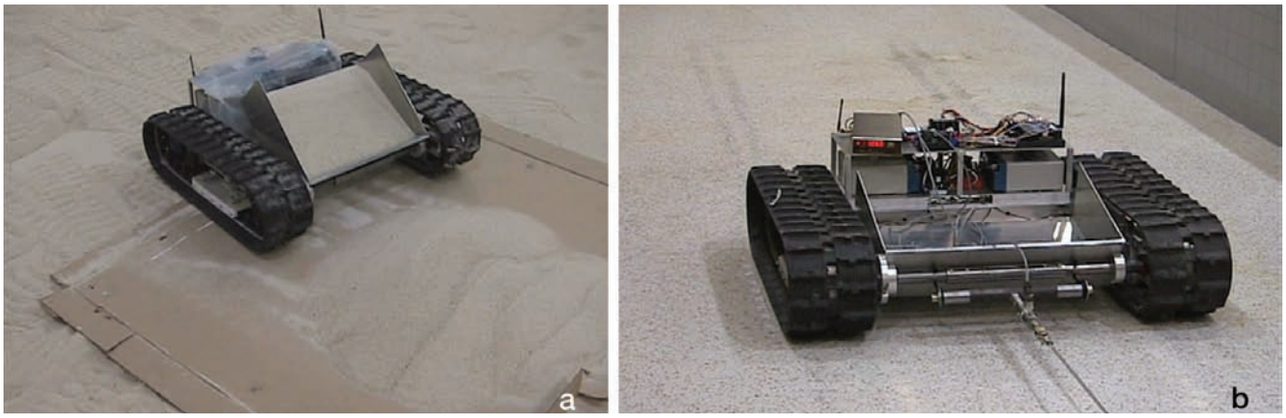

Fig. 2. *(a) Cratos excavation and delivery test. (b) Cratos drawbar pull and payload transit tests.*

Fig. 3. *(a) LMA PILOT system. (b) JSC ROxygen system.*

These first-generation systems thus verified performance and demonstrated operation feasibility at production rates scaled to outpost needs, so weight and volume were not minimized. The LMA precursor ISRU lunar oxygen test bed (PILOT) operated at one-fourth scale, and the NASA ROxygen system operated at two-third scale; both achieved the predicted 1% to 2% O_2 extraction (by mass).

The carbothermal reduction process is a more efficient O_2-production technique than the H_2-reduction process because not only will it reduce the FeO but also some of the silicates found abundantly in the lunar regolith. The process requires much higher temperatures (1,600°C (2,912°F)), however, so the regolith becomes molten. When methane (CH_4) is introduced into the melt chamber, it reacts with the molten regolith and carbon monoxide (CO) is produced. The CO is fed with H_2 into a methanation reactor where the CH_4 is regenerated and water is produced. The water is electrolyzed to recover the H_2 and produce O_2. This process can achieve efficiencies of 14% extraction of O_2 by mass or greater, but the main challenges of this approach are delivering the energy needed to form the melt and developing techniques to deal with molten materials. Orbital Technologies Corporation (ORBITEC), Madison, Wis., after performing successive tests of larger and larger melt/CH_4 reduction tests, designed and built a first-generation system. This system will combine with a solar concentrator system under development by Physical Sciences Inc. (PSI), Andover, Mass., through Small Business Innovative Research contracts (figures 4(a) and 4(b)) to produce O_2.

Through such cooperative development efforts, we plan to integrate ISRU technologies with lunar surface system architecture. In particular, the ability to produce and regenerate mission-critical consumables (e.g., O_2, water, and fuel for crew, power, and propulsion) can change surface element designs, technologies, and operations. Of course ISRU is only beneficial for exploration if other elements use the products and capabilities available. We coordinate with rovers, cryogenic oxygen storage, and thermal management to ensure that ISRU development is aligned with other lunar surface system development areas. The ISRU Project has also initiated

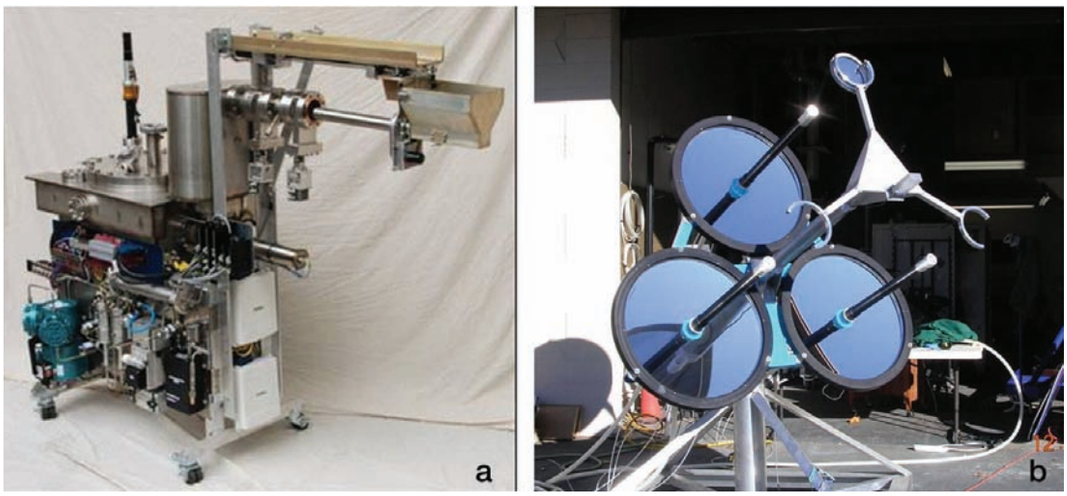

Fig. 4. *(a) ORBITEC carbothermal system. (b) PSI solar concentrator and fiber-optic cables.*

lunar analog field tests with other surface project areas using requirements and capabilities identified and defined in human lunar architecture studies.

Three capabilities of potential interest demonstrated in recent field tests are: (1) area clearing and berm building for landing and plume debris protection, (2) end-to-end O_2 extraction from regolith with excavation and O_2 storage, and (3) mobile resource characterization of permanently shadowed craters and subscale precursor O_2 extraction from regolith. The first capability was demonstrated both at the Johnson Space Center rockyard and at Moses Lake, Wash. The lunar attachment node for construction and excavation (LANCE), a blade for excavation, is 4.11 m (13.5 ft) wide by 0.52 m (1.7 ft) high and weighs about 143 kg (315 lbs.). This proof-of-concept composite blade was hard-mounted to the "Chariot" crew rover. In addition to clearing a large area, the LANCE-Chariot system also built a 1.2-m (3.94-ft) ramp berm (figure 5). The second and third tests occurred near the Mauna Kea, Hawaii, Visitor Center. To demonstrate the end-to-end hardware and operations associated with O_2 extraction of regolith, NASA built two separate and completely different systems.

Fig. 5. *LANCE blade on Chariot at Moses Lake, Wash.*

These systems had common requirements and common interfaces between the main units/modules for excavation, regolith processing, gas/water cleanup, water electrolysis, and O_2 storage such that the modules and excavators could be exchanged, if desired. The systems, based around the PILOT and ROxygen hydrogen reduction reactors (figures 6(a) and 6(b)), laid the cornerstone for creating a modular and expandable surface architecture. To demonstrate the mobile resource characterization applicable to a future lunar polar crater robotic precursor mission, NASA built the regolith and environment science and oxygen and lunar volatile extraction (RESOLVE) system. The RESOLVE system was mounted on the Carnegie Mellon University (Pittsburgh, Pa.) Scarab rover, with a NORCAT [Northern Centre for Advanced Technology Inc., Sudbury, Ontario Canada] drill and the Canadian Space Agency Neptec (Ottawa, Ontario Canada) TriDAR navigation vision system (figure 6(c)). All field tests verified that performance and operations as well as information will be used in future lunar surface system architecture studies.

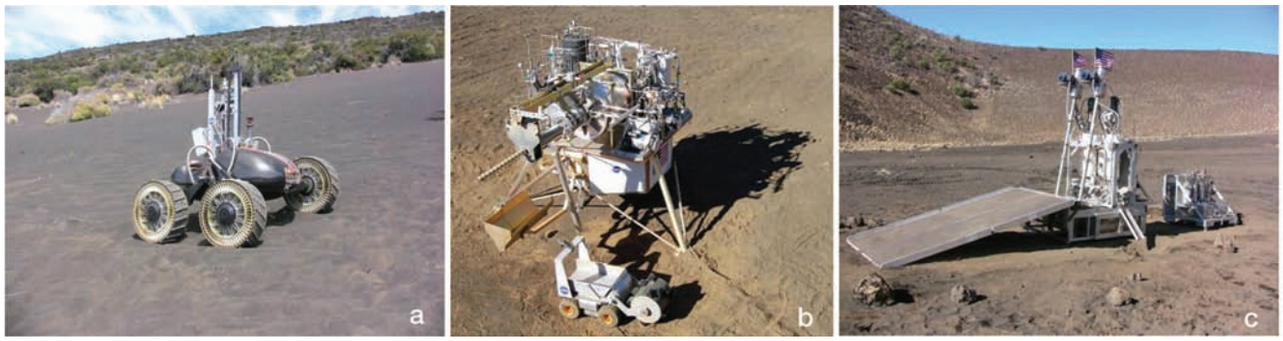

Fig. 6. *(a) NASA RESOLVE on Carnegie Mellon University Scarab rover. (b) LMA PILOT and Bucketdrum rover. (c) JSC ROxygen.*

Propellant Specification and Manual Development to Enable Testing

Benjamin Greene, *White Sands Test Facility*
Dion J. Mast, *White Sands Test Facility*
Mark B. McClure, *White Sands Test Facility*
Miguel J. Maes, *White Sands Test Facility*

New propellant initiatives require special quality, engineering, and safety considerations. NASA White Sands Test Facility (WSTF) is one of NASA's leading centers of excellence for the development of hypergolic propellant specifications and manuals to enable their safe use (figure 1). Specifications are explicit sets of requirements to be satisfied by the propellant; they contain information on sampling, analysis, and quality criteria for the different grades, as applicable. Manuals enable the user to assess the hazards of the fluids under a variety of conditions. Propellants are used to power crewed and crewless spacecraft, and their performance, quality, and reliability is of utmost importance to mission assurance and astronaut safety.

Fig. 1. *WSTF produces numerous manuals and handbooks.*

Not only must propellants meet the most stringent specifications, but because they are potentially quite hazardous, their fire, explosion, and safety hazards must be well understood and documented to enable safe handling and testing. WSTF has developed numerous manuals that cover the fire, explosion, and safety hazards of liquid propellants. These manuals, sometimes referred to as handbooks, consolidate valuable data and allow users to perform hazard assessments of the propellants under various conditions. These documents provide engineering information, lessons learned, and options to address technical issues; classification of similar items, materials, or processes; and interpretative direction and techniques. This type of guidance may help the government or its contractors in the design, construction, selection, management, support, or operation of systems, products, processes, or services. WSTF analyzes and tests the propellants according to their specifications, while the hazards manuals are extremely helpful to engineers, chemists, field personnel, test conductors, safety personnel, and industrial hygienists in existing test programs.

WSTF has been involved in the development of two new propellant specifications and corresponding manuals, in addition to the review and update of numerous other propellant specifications. In recent years, there has been ever-increasing interest in "green" space propellants that are environmentally less damaging and have reduced toxicity when compared to commonly used solid propellants (including ammonium perchlorate), liquid hypergols (including monomethylhydrazine/nitrogen tetroxide), and liquid monopropellants (including hydrazine). Ideally, green propellants are easier and safer to handle than conventional propellants, and are expected to drive down the costs associated with propellant transport and storage as well as spacecraft development, ground support, and operations. Hydrogen peroxide was regarded as a green propellant because of its relatively benign exhaust products and low vapor pressure when compared to propellant hydrazine fuels and nitrogen tetroxide oxidizers in bipropellant systems, and also when compared to hydrazine in monopropellant systems.

A resurgence in interest in hydrogen peroxide propellant led to the development of MIL-PRF-16005.F *Performance Specification Propellant, Hydrogen Peroxide*. Previous and related specifications were obsolete or inadequate to cover the requirements of this challenging and hazardous propellant, which has a rich history of periods of use and nonuse. This specification covers four types and two grades of hydrogen peroxide propellant intended for use as an oxidizer or monopropellant in rocket engines. WSTF propellant chemists were active in the development of this specification, and ensured that it was not only technically achievable but practical and cost-effective. Incorporated in the specification is a method for performing one of the

more time-consuming procedures in the previous military specification. This method is for the continuous, unattended decomposition of the propellant in a closed-loop system using a platinum wire enclosed in a loop of inert tubing. The previous method was performed using a manual, drop-wise method by the gradual addition of hydrogen peroxide to a platinum crucible that required continuous attendance.

Concurrent with the effort to develop the hydrogen peroxide specification, NASA initiated a program for WSTF to prepare a hydrogen peroxide hazards manual. WSTF scientists researched and coordinated the development of NASA/TM-2005-213151 *Fire, Explosion, Compatibility, and Safety Hazards of Hydrogen Peroxide* to provide data for hydrogen peroxide propellant users. Addressed in this manual are fire, explosion, compatibility hazards, and overall safety and environmental considerations in addition to physical and thermodynamic data and lessons learned.

More recently, liquid oxygen-liquid methane propellant was proposed for use in the Crew Exploration Vehicle propulsion system. While programmatic requirements are subject to change, the potential for methane as a viable propellant that could be synthesized in extraterrestrial environments using various in-situ propellant production techniques kept it on the forefront as a propellant candidate for space exploration to Mars and beyond. Stringent use requirements led to the development of a new specification for the propellant methane. WSTF chemists participated in the development of MIL-PRF-32207 *Performance Specification Propellant, Methane*. This participation ensured the ability of a laboratory to perform the required analyses. In addition, WSTF chemists developed a novel chamber in which to collect liquid methane samples for the nonvolatile residue determination and observation of visual appearance, which were requirements of the specification that could be done in the field. The chamber's use was validated at WSTF Test Stand 401, where liquid methane was used and tested (figure 2).

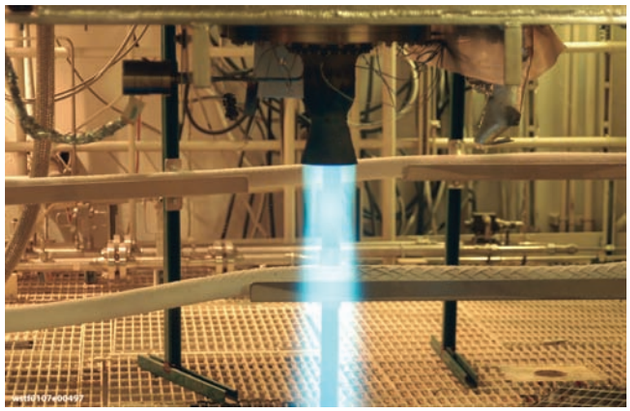

Fig. 2. *Liquid oxygen-methane engine firing.*

Along with the effort to develop the liquid methane specification, a program was initiated for WSTF to prepare a liquid methane hazards manual, which includes liquefied and gaseous natural gas and methane. The program's goal was to summarize the existing hazards of liquid methane and liquefied natural gas in one document. WSTF-RD-1056-001-07 *Fire, Explosion, Compatibility, and Safety Hazards of Liquid and Gaseous Methane and Natural Gas* was accordingly developed and relied on for engine testing at WSTF. The document included: fire and explosion, materials and reactivity, personnel and environmental hazards, chemical and physical properties, analytical spectroscopy, specifications, analytical methods, and summaries of accidents, close calls, and lessons learned.

The military specifications for hydrogen peroxide and liquid methane are available to the public; the WSTF hazards manuals are subject to export control and are available to other government agencies. WSTF previously authored *Fire, Explosion, Compatibility, and Safety Hazards of Hydrazine* (RD-WSTF-0002), *Fire, Explosion, Compatibility, and Safety Hazards of Monomethylhydrazine* (RD-WSTF-0003), and *Fire, Explosion, Compatibility, and Safety Hazards of Nitrogen Tetroxide* (RD-WSTF-0017).

Using Lasers to Capture the Speed of a Hypervelocity Projectile

Darin M. Franzoni, *White Sands Test Facility*

Millions of human-made debris particles and naturally occurring meteoroids are found in the near-Earth space environment. These objects travel through space at any velocity with a magnitude over 3 km/s, or hypervelocity. This near-Earth region of space is where our satellites, space shuttle, and the International Space Station travel. The design and testing of vehicle shielding is thus very critical, since collisions with these orbiting particles could catastrophically damage vehicles and hardware. Scientists have developed several computational models to aid in the design of these shields. The actual laboratory testing of shield designs can validate and improve models, or test final designs for flight worthiness. The NASA White Sands Test Facility (WSTF) Remote Hypervelocity Test Laboratory (RHTL) works in close partnership with the Johnson Space Center Hypervelocity Impact Technology Facility (HITF) to determine the risk posed by space debris, and to design spacecraft shields based on probability of impact and spacecraft geometry. HITF builds and sends target shields to WSTF for ballistic-limit verification testing, and the RHTL analyzes the results to improve the HITF models.

The RHTL uses a two-stage light-gas gun (figure 1) to propel projectiles to hypervelocity and simulate the impacts in a controlled environment. The first stage of the light-gas gun compresses hydrogen gas to extremely high pressure. This high-pressure hydrogen is released into the second stage – the gun barrel. The gun barrel is separated from the first stage by a high-pressure rupture disk. When the disk ruptures, hydrogen gas is released into the barrel and the sabot is accelerated down the barrel to hypervelocity. The sabot holds the projectile and protects the projectile from erosion as the sabot travels down the barrel. When the sabot exits the barrel, it separates from the projectile and impacts a "stripper" plate, thus allowing just the projectile to continue downrange and impact the test article. The test article, stripper plate, and barrel are contained in a chamber (flight range) so the test can be conducted in a vacuum, allowing for hypervelocity projectile flight.

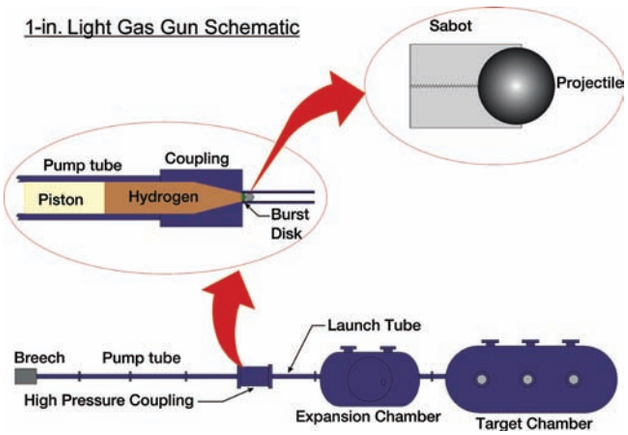

Fig. 1. *Two-stage light-gas gun.*

The WSTF RHTL is provided with a projectile, a test article, and the requested projectile velocity. This requires acquiring the projectile velocity during the test to ensure the test article was impacted with the prescribed velocity. The velocity of the projectile is captured by two laser stations set a specified distance apart from one another. These laser stations are comprised of a 690-nm visible wavelength, red laser source projected through the flight path of the projectile and terminating at a high-sensitivity, fast-acting photodiode. When the projectile or sabot intersect and break the beam, an event is triggered and recorded. Photodiodes used for this application have a response of 50 ns. While a photodiode receives uninterrupted light from the laser source, its resistance remains high and voltage across the detection circuit also remains high. When the beam is interrupted by the projectile or sabot, the resistance is lowered briefly, allowing current flow to lower the voltage across the detection circuit. The data acquisition system records voltage difference relative to time in microsecond resolution. The difference in time between the two recorded events and the known distance between the two laser stations allow projectile velocity to be calculated. Figure 2 shows a typical response from the photodiode captured by the data acquisition system. The laser velocity stations directly measure the sabot or projectile velocity.

Prior to the advent of the RHTL, primary laser stations were mounted external to the flight range and perpendicular to the flight path. The laser was projected through a view port in the flight range, across the path of the projectile, and terminated in a photodiode mounted externally in an opposing viewport. On smaller-caliber, two-stage light-gas guns, the projectile is often too small to register a detectable event or has drifted slightly out of plane. It is

impossible to predict the plane of separation of the sabot, and it is unlikely that it will coincide with that of a single-beam laser station. This results in a higher incident of tests where velocity cannot be provided by the single-beam laser station due to insufficient projectile size. The RHTL, by contrast, routinely shoots projectiles with an average size of 1.3 mm ranging down to single 0.05-mm projectiles.

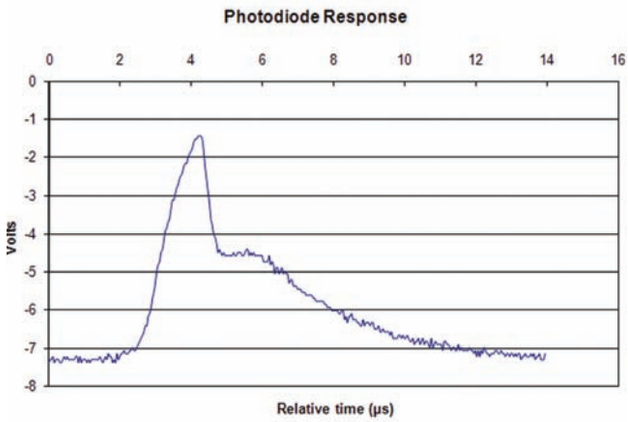

Fig. 2. *Response of photodiode from 2.5 km/s test.*

Increasing the density of laser beams traversing the projectile flight path increases the likelihood of the sabot or projectile being sensed by the laser station. Improvements made to the laser station do this by reflecting a single laser beam up to 10 times between two mirrors. Figure 3 illustrates a typical laser station and its parts. Items 7 and 4 are the laser source and photodiode, respectively. The gold-plated mirrors (items 5 and 6) reflect the beam to form multiple beam trajectories from one laser source, any of which, if interrupted, would be detected by the photodiode.

The gold-plated mirrors can be adjusted to increase or decrease the number of beam trajectories in line of the projectile flight path. The number of beam trajectories that can be created while maintaining a high resistance at the photodiode is restricted due to losses of incomplete reflection incurred at the mirror and limitations of the laser source power. Increasing the number of reflected beam trajectories can improve detection ability, but it would require a more powerful laser source – which would, in turn, produce a safety risk for personnel aligning and tuning the laser station assembly – to provide the optimal signal at the photodiode. Regular cleaning of the mirrors also reduces signal losses. In addition, the laser stations were moved inside the flight range as an assembly to avoid the losses and refraction caused by projecting through a glass viewport. The improved laser station design significantly increased successful detection of sabot velocity. On the 0.17-caliber light-gas gun range, where the laser stations capture the sabot, velocity has been successfully captured for every shot since installation of the improved laser stations.

Certain projectile sizes (e.g., smaller than 2 mm) require the sabot to be detected by the laser stations. The ability to acquire the velocity of small projectiles would be an added capability, useful in the analysis of impacts as it would be a direct measurement of projectile velocity. The WSTF RHTL team was recently approached to develop a new capability to launch single particles smaller than 0.05 mm. However, as this added capability presents an even greater challenge in acquiring direct projectile velocity without relying on the sabot, this may require an entirely new design of laser station or detection methods.

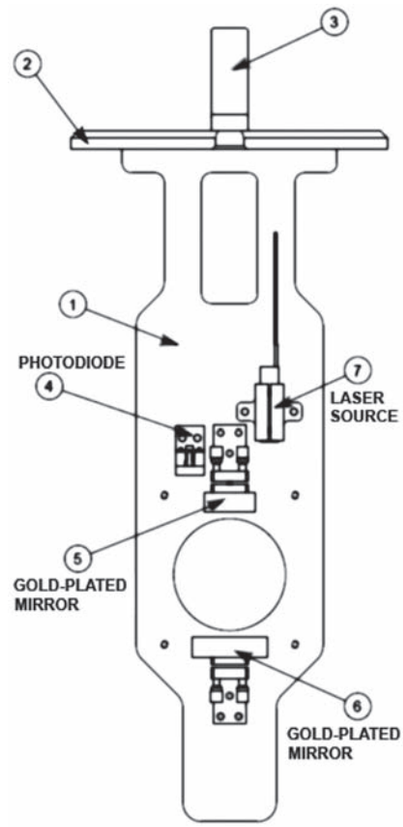

Fig. 3. *Improved laser station, sketch no. 33142.*

Lunar Dust and Lunar Dust Simulant Activation and Monitoring

William T. Wallace, *Johnson Space Center*

Antony S. Jeevarajan, *Johnson Space Center*

During the Apollo missions, many undesirable situations were encountered that must be mitigated prior to returning humans to the moon. Lunar dust (that part of the lunar regolith that is less than 20 µm in diameter) produced several problems with astronaut suits and helmets as well as with spacecraft mechanical seals and equipment, and could conceivably harm astronauts on future missions. Although efforts were made to exclude lunar dust from the cabin of the lunar module, a significant amount of material nonetheless found its way inside. During ascent of the lunar module from the lunar surface to rendezvous with the command module, major portions of the contaminating soil and dust began to float, irritating the astronauts' eyes even as they inhaled this particulate matter into their lungs. As our goal is to understand what properties might make lunar dust hazardous, we are studying methods to understand its dangerous chemical properties.

Lunar dust is likely in an "activated" state, particularly due to the 1/6g and the lack of significant atmosphere on the moon. The purpose of our research is to understand the reactive properties of active lunar dust. Lunar dust is probably the product of various sources, including pulverization by micrometeorite impacts, exposure to unmitigated ultraviolet (UV) radiation, and bombardment by galactic/cosmic and solar-wind particles. These activation methods may produce free radicals on the surface of the dust particles. Free radicals have long been monitored using electron paramagnetic resonance (EPR), but EPR technology is extremely costly and the instrumentation is bulky, making it unsuitable for use on the lunar surface. To overcome these limitations, we developed a novel fluorescent technique that is based on the conversion of nonfluorescent terephthalate to fluorescent 2-hydroxyterephthalate on exposure to hydroxyl radicals.

These hydroxyl radicals are produced when free radical species are exposed to aqueous solution. The response of this assay to hydroxyl radical concentration is linear, as can be seen in figure 1. The fluorescent product was synthesized using a method from the literature and purified until the fluorescence intensity was maximized. Using the spectra obtained from this product allows for the determination of hydroxyl radical concentration in a particular solution.

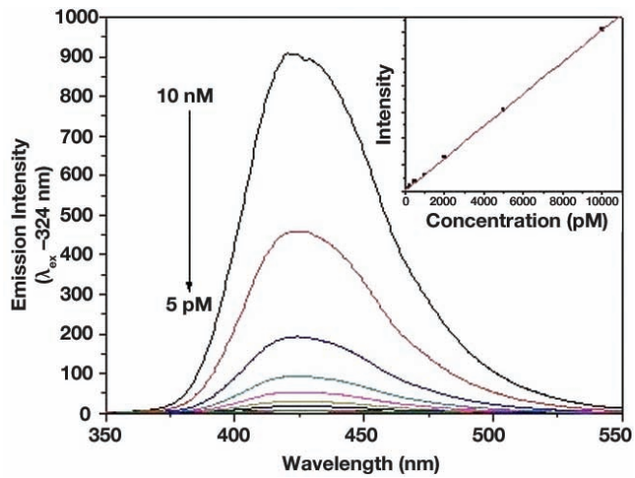

Fig. 1. *Fluorescence of synthetic z-hydroxyterephthalate.*

We used a mortar and pestle to hand-grind samples of quartz (Min-U-Sil 15), lunar dust simulant (JSC-1A-vf), and lunar soil that was returned by Apollo 16 (62241) to provide an initial activated mimic of conditions that will be found on the lunar surface. Quartz, which produces hydroxyl radicals after grinding, acted as a positive control. As expected, samples that were not activated (i.e., not hand-ground) did not produce a significant amount of radicals. Hand-grinding the different materials under identical conditions, however, leads to quite different emission intensities. As illustrated in figure 2, the level of activity increases in the following order: quartz < lunar dust simulant < lunar dust. Based on the calibration curve shown in figure 2, we can see that ground lunar dust produces two to three times the amount of hydroxyl radicals as lunar dust simulant and more than 10 times that of quartz under ambient conditions.

This work demonstrates a method of activating quartz, lunar dust simulant, and lunar soil and monitoring the various levels of activation. These results provide evidence of the need for further studies on these materials prior to returning humans to the lunar surface. We are also determining the mechanisms behind the activation of these materials (by grinding and UV exposure) as well as the time required to return activated samples to their passivated

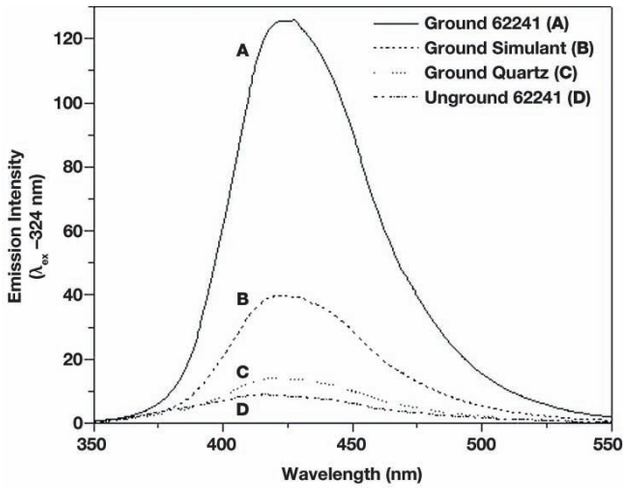

Fig. 2. *Emission spectra comparing ground and unground soil.*

state. These activation methods on lunar dust simulant and lunar dust in aqueous solution may have toxic effects on cellular systems. These studies will provide important information on the nature of lunar dust that will allow mitigation measures to be developed, ensuring the safety of astronauts and mechanical systems in lunar habitats.

Cleaning to Achieve Sterility: An Evaluation of State-of-the-art Cleaning Techniques to Remove Particles of Biological Origin

Rosella Sepulveda, *White Sands Test Facility*
Kenneth G. McLeod, *White Sands Test Facility*
Clifford D. Madrid, *White Sands Test Facility*

NASA planetary protection regulations stipulate that a surface may be considered "sterile" when a microbial burden of less than 300 aerobic bacterial spores per square meter can be treated to achieve a 10^4-fold reduction in viable endospores. In the cleaning process, single spores or small surface particles are immobilized by electrostatic charges, but can be removed only by extreme methods. If inexpensive cleaning processes exist that will produce a "sterile" surface without detrimentally affecting hardware, the process of readying spacecraft for final assembly and launch could be achieved simply and economically.

The NASA White Sands Test Facility (WSTF) was one of three participating facilities in a study to evaluate and refine existing cleaning techniques and identify cleaning methodologies that can achieve 4-log reduction levels on viable spore counts. Researchers evaluated the standard techniques used in the three facilities, and also explored variations in cleaning procedures and the chemistry of the cleaning solutions used.

Three cleaning procedures were evaluated at WSTF: (1) aqueous precision cleaning and verification without benefit of pre-cleaning; (2) pre-cleaning with a standard detergent called Simple Green® followed by aqueous precision cleaning and verification; and (3) pre-cleaning two groups of coupons in Simple Green® – the first with ultrasonics and flushing, and the second with ultrasonics, manual brushing, and flushing. Test results demonstrate that pre-cleaning with Simple Green® significantly improves cleaning efficiency, and the brushing method improves the efficiency of cleaning especially challenging surfaces. The WSTF cleaning procedure that included the brushing method was even more promising, averaging a 4.1-log reduction. However, due to limited sample size and variation between samples, statistical analysis indicates this method can reduce the bioburden by a 3.1 log with a 95% confidence level. Further studies with more replicates would determine whether this method will achieve a 4-log reduction level.

WSTF divides the cleaning and verification process into three distinct phases: pre-cleaning, precision cleaning, and verification. In pre-cleaning, we use chemicals, ultrasonic cleaning, steam cleaning, bead blasting, and other methods to remove grease, paint, and other contaminants, leaving the part visibly clean. For precision cleaning, we use solvents, ultrasonic cleaning, vapor degreasing, and other methods to clean parts to a specified level of particle and/or nonvolatile residue contamination. Finally, we use solvents to sample a part to verify the cleaning process, after which qualified technicians analyze the sample to accurately determine the cleanliness level of the part.

Pre-cleaning operations employ ultrasonic cleaning tanks, rinse tanks, and a nitrogen-purged drying oven. HEPA [high-efficiency particulate air] filtration alleviates the risk of contaminating already pre-cleaned components in the staging area. After inspection and staging work, these components go to the Class 100 clean room for precision cleaning and verification. The aqueous precision cleaning and verification equipment used in this study consist of a table-top ultrasonic tank, an ultrasonic probe and generator, clean sampling equipment, a deionized water source, and a low-pressure gaseous nitrogen source for blow-drying parts.

During early coupon testing, we were asked to use the aqueous precision cleaning and verification method without benefit of pre-cleaning the coupons. This method produced a 3-log reduction in viable spores, but did not meet the project objective of a 4-log reduction. Accordingly, we requested the opportunity to change the process to include pre-cleaning with Simple Green® followed by aqueous precision cleaning and verification. A new cleaning trial was arranged involving pre-cleaning two groups of coupons in Simple Green®: the first with ultrasonics and flushing, and the second with ultrasonics, manual brushing, and flushing. Both methods reduced the bioburden by more than 4-log. However, the coupons provided insufficient challenge to differentiate between the two pre-cleaning methods.

A simulated parts challenge used both cleaning methods (with brushing, without brushing) to pre-clean a mixture of 1/4- and 3/8-in. AN caps, elbows, and tees. WSTF received six batches of parts, all individually bagged to provide triplicate results for the two cleaning methods. Each batch consisted of five large (3/8-in.) AN caps, five small (1/4-in.) AN caps, five 1/4-in. AN tees, five 3/8-in. AN elbows, three contaminated stainless-steel coupons, and one clean, small (1/4-in.) AN cap, or 24 parts per batch.

Parts for each batch were debagged and placed in a basket before they were cleaned following the two prescribed methods. (AN refers to a manufacture's part identification).

The cleaned parts were bagged and returned to the NASA Jet Propulsion Laboratory (JPL) for biological analysis. Culturing at JPL determined spore counts and colony-forming units (CFUs), the results of which were transmitted to WSTF. We then tabulated detailed spore count and CFU/part data. Statistical analysis of these data sets suggests no batch-to-batch variation, so the data for each batch were pooled together. The CFUs before and after cleaning and the log reductions for each material are shown in Table 1 and figure 1.

Data indicate that fittings such as elbows and tees are more difficult to clean than caps or coupons. This is reflected in the higher spore counts, and is consistent with WSTF experience in previous cleaning studies. Based on earlier coupon cleaning studies, we anticipated that coupons would be cleaner than caps; this was not the case. Coupons were no cleaner than caps, and the coupons cleaned with brushing were not as clean as the brushed caps. We have been unable to explain this result based on the cleaning process. Analysis of this set of data indicates that these part-to-part variations are not statistically significant.

Early cleaning studies using coupons, together with coupon data from the multiple parts study, indicate that coupons do not provide a sufficient challenge to differentiate effective cleaning methods. Coupon studies appear to be limited to separating ineffective cleaning methods from those requiring additional evaluation. The data from this study suggest that, consistent with WSTF experience, a mixture of AN tube fittings provides a good cleaning challenge that will allow differentiation of different cleaning methods.

Based on data from this study, we conclude that normal pre-cleaning and precision cleaning using Simple Green® (with brushing) and deionized water, as conducted by our scientists, provides an average 4-log reduction in viable spore levels on parts of various materials and configurations. The data also suggest that manual brushing during pre-cleaning significantly improves the cleanliness level of a surface.

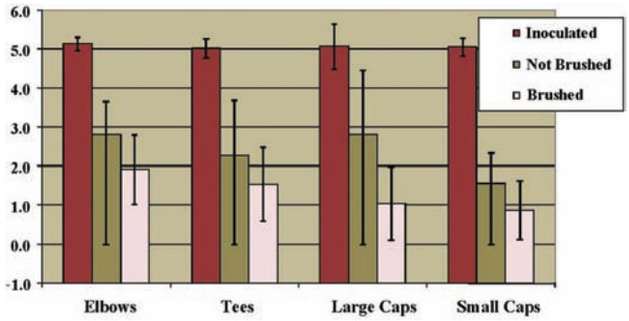

Fig. 1. *WSTF brushed and not brushed cleaning results.*

	Parts	No. of Replicates	Inoculation		After Cleaning		Log Reduction	
			CFUs	St. Dev.	CFUs	St. Dev.	Value	St. Dev.
No Brushing	Elbows	15	138,000	23,900	644.13	545.49	2.33	0.86
	Tees	15	104,000	26,100	189.50	266.58	2.74	1.43
	Large Caps	15	117,000	68,200	623.25	1030.24	2.27	1.75
	Small Caps	15	114,000	25,700	36.17	27.99	3.50	0.81
With Brushing	Elbows	15	138,000	23,900	82.25	73.17	3.22	0.91
	Tees	15	104,000	26,100	34.50	32.32	3.48	0.97
	Large Caps	15	117,000	68,200	11.00	10.29	4.03	1.10
	Small Caps	15	114,000	25,700	7.42	5.63	4.19	0.79

Table 1. *Comparison of cleaning efficiency for WSTF brushed and not brushed methods.*

Materials Development and Testing

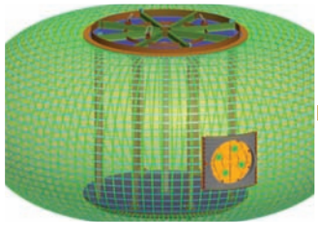

New Developments in Nondestructive Evaluation for Composite Pressure Vessel Testing

Regor L. Saulsberry, *White Sands Test Facility*
Nathanael J. Greene, *White Sands Test Facility*
Tommy B. Yoder, *White Sands Test Facility*

NASA White Sands Test Facility (WSTF) is supporting the recertification and life extension of aging Kevlar® and carbon composite overwrapped pressure vessels (COPVs). These vessels are directly associated with space shuttle orbiters and the International Space Station. WSTF is also helping to address the special issues associated with the application of carbon COPVs to Orion and future spacecraft. This task is challenging because the COPVs have varying criticalities, usage histories, damage and repair histories, times at pressure, and numbers of pressure cycles. The application of effective nondestructive evaluation (NDE) technologies is important to this effort and, in many cases, requires that techniques be refined and new standard processes be developed. Areas we are addressing include: the implementation of NDE into manufacturing to detect any defects and reduce variation; the development and application of effective impact detection methods; inspection for composite-to-liner interface issues; in-service structural health monitoring (or in-situ NDE); and evaluation of global material property changes as the vessels age and potentially progress toward a phenomenon known as "stress rupture." Stress rupture could result in a failure at operation pressure after an extended period of use.

One example of hardware development is a laser profilometer that maps variations in liner profile that could involve liner and composite interaction issues. Laser profilometry allows examination of areas not inspectable by other methods. When our engineers observed liner ripples with a videoscope (see the lower right image in figure 1), the amplitude and frequency could not be accurately measured to determine whether discrepant conditions exist. We developed laser profilometers to scan the inside of spherical vessels at 0.001 to 0.002 in. accuracy (depending on vessel diameter). Measurements provided from this technique allow analysis using modeling and analytical methods to quantify anomalies. The laser head, located at the center point of the vessel (indicated by the solid model in figure 1), fully maps the surface from near the lower port to near the upper port, allowing the entire surface to be viewed at once.

Profilometry is being used with other methods such as shearography to give a more complete characterization of vessel indications. Figure 2 illustrates a shearography image of multiple NDE indications taken from the outside of a vessel. These images are shown aligned with profilometry images taken from the inside. The profilometry data give the amplitude and frequency of the multiple ripples, as revealed in the plot. Shearography, on the other hand, images the resulting external "out-of-plane" deformations as the vessel is slightly pressurized. These deformations can also be measured using shearography analysis

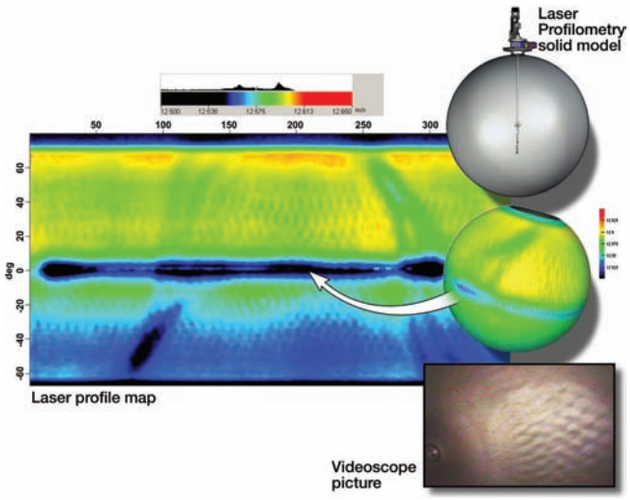

Fig. 1. *Laser profilometry of a COPV interior surface.*

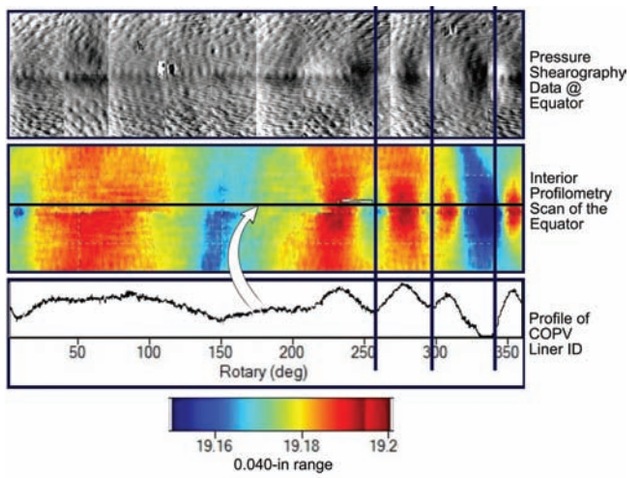

Fig. 2. *Laser profile map and measurements correlated to shearography images.*

software. Our next goal is to develop more complex laser profilometers to scan and map cylindrical vessels. The equipment will support several upcoming test programs and evaluation of flight vessels over the next few years.

Other projects include a correlation between impact damage, NDE response, and the associated reduction in burst pressure; development of NDE that can be implemented into manufacturing to reduce risk; in-situ NDE characterization of carbon composite micromechanics (for improved COPV health monitoring); and composite stress rupture NDE development. Composite stress rupture NDE involves extensive COPV testing to correlate NDE response to the various indicators of stress rupture progression. Further details on many of these projects can be found on our Website (http://nnwg.org/current/index.html) under "White Sands Test Facility." Although we manage these projects, other NDE specialists and experts from several NASA centers, industry, and academia are involved.

Among our new innovative endeavors is the Carbon Stress Rupture NDE Development Project. This project seeks to extend the success of a previous Kevlar® stress rupture NDE project by developing and demonstrating NDE techniques applicable to carbon COPVs. Testing will increase the data available for stress rupture characteristics of T1000 and IM7 carbon COPVs, and will provide NDE to help evaluate stress-rupture-related degradation. T1000 is a grade of carbon fiber produced by Toray Industries, N.Y., and IMF is a grade of carbon fiber produced by Hexcel, Stamford, Conn. T1000 is a premier fiber with fewer defects per unit length and currently being used on more performance-critical COPVs; IM7 is a somewhat older, weaker, and yet more economical grade used on lower-cost vessels and other structures where a lower cost and sometimes more available fiber are desirable.

For this project, 100 carbon-wrapped vessels will undergo stress rupture aging using an elevated stress technique at ambient temperature. To support this effort, a new stress rupture test facility is being built at WSTF that will house 20 vessels at a time in a Lexan®-covered blast enclosure (figure 3). The Lexan® enclosure will allow continuous, 360-deg visual inspection of the vessels to monitor for the onset of fiber failure.

The new system will hold the vessels at a constant elevated pressure while various NDE and specialized monitoring instrumentation record vessel stress rupture progression. We tracked the spools of carbon fiber used to wrap the vessels, and will evaluate representative carbon test specimens to set vessel stress levels for test. Techniques

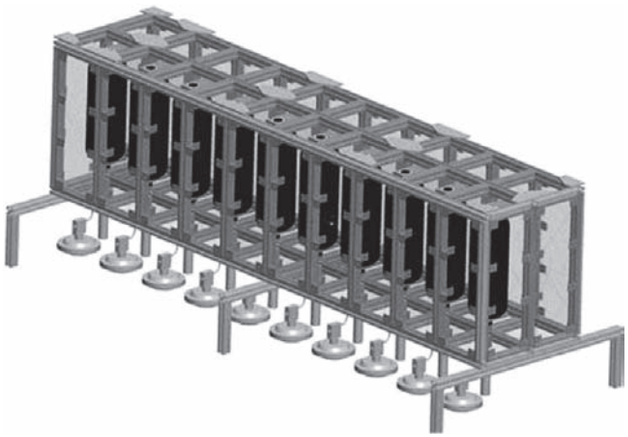

Fig. 3. *Enclosure design for carbon vessel aging, showing only one side populated with COPVs.*

such as visual inspection, acoustic emission, portable in-situ Raman spectroscopy, fiber Bragg gratings and conventional strain gauges, belly bands, and a wireless distributed impact detection system are to be applied. Following stress rupture aging to various levels, we will remove the vessels in lots and apply other methods (e.g., scanning Raman spectroscopy, laser-induced ultrasound testing (UT), other conventional scanning UT and UT-guided wave techniques, shearography, and thermography) to the test vessels.

Acoustic Emission and Microscopic Characterization for Improved Composite Overwrapped Pressure Vessel Health Monitoring

Jess M. Waller, *White Sands Test Facility*
Paul R. Spencer, *White Sands Test Facility*
Benjamin Gonzalez, *White Sands Test Facility*
J. Brooks Wolle, *White Sands Test Facility*
Regor L. Saulsberry, *White Sands Test Facility*

We are currently evaluating composite overwrapped pressure vessels (COPVs) to better quantify their reliability and likelihood of failure due to creep rupture, impact damage, and age-dependent issues. More specifically, NASA White Sands Test Facility (WSTF) is focusing attention on the Kevlar® fiber reinforced epoxy matrix (K/E) COPVs used on the space shuttle and on the carbon fiber reinforced epoxy matrix (C/E) COPVs used on the International Space Station. Together, these COPVs have varying criticality, time at pressure, number of pressure cycles, and damage and repair histories.

A group of nondestructive evaluation (NDE) experts is evaluating appropriate NDE methods for COPV health monitoring. One method showing particular promise in characterizing the failure of K/E and C/E composite materials is acoustic emission (AE). We have developed modal AE (mAE) techniques to correlate microscopic AE events such as matrix cracking and filament rupture with their corresponding mAE signatures. Of interest and reported here is the correlation of strain rate data with mAE data during progressive creep rupture degradation.

WSTF performed tensile creep rupture investigations on two COPV composite materials of construction: impregnated K/E strand (1140 denier Kevlar® 49), and impregnated C/E strand (12K T1000 and IM-7). As a control, the facility also performed investigations on unimpregnated carbon fiber tow (12K T1000). All tests were conducted under ambient conditions using two methods: an in-house accelerated stepped stress method (SSM), and ASTM [American Society for Testing and Materials] D 7337 *Standard Test Method for Tensile Creep Rupture of Fiber Reinforced Polymer Matrix Composite Bars*. We investigated the test results microscopically and by environmental scanning electron microscopy (ESEM) (figure 1).

A full description of the testing, including details of the test configuration and specimen preparation, is available on the NASA NDE Working Group Website, http://nnwg.org/current/, under White Sands Test Facility ("In-Situ NDE Characterization of Kevlar and Carbon Composite Micromechanics for Improved COPV Health Monitoring").

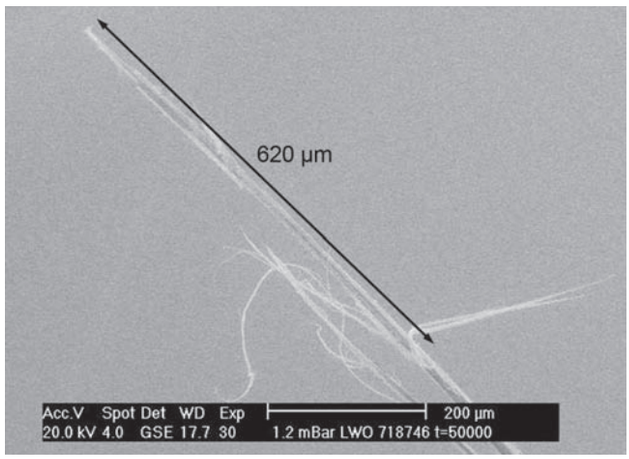

Fig. 1. *Post-creep rupture ESEM micrograph of a failed Kevlar® 49 filament.*

Determination of the ultimate tensile strength (UTS) allowed the load ratio (LR) to be calculated during SSM and ASTM D7337 creep tests. In the SSM case, the applied stress was stepped from LR = 0.6 to LR = 1.0 in 0.1-LR increments, each lasting 10,000 seconds. This allowed us to investigate the creep rupture behavior of the above materials of construction in an accelerated (overnight) test. In the ASTM D 7337 case, we subjected a representative specimen to a fixed LR of 0.8. Depending on the LR used, the expected creep rupture test duration could vary from 101 hours (high LR) to 104 hours (low LR). In both cases, we monitored strain and mAE activity simultaneously (ex.: figure 2). To elucidate microscopic and macroscopic changes, we also analyzed the specimens by optical microscopy, ESEM, and videography.

One of the interesting features observed for K/E strand specimens was that the strands did not always break in a single catastrophic event, but often in more than one partial rupture events. This may have important implications for the creep rupture behavior of K/E COPVs presently used in the shuttle fleet.

Creep data acquired for K/E using ASTM D 7337 (LR=0.8) demonstrated the feasibility of conducting 103- to 104-minute creep tests with AE sensors attached on creep specimens anchored by poured epoxy tabs, thus providing a straightforward way to estimate the creep rupture

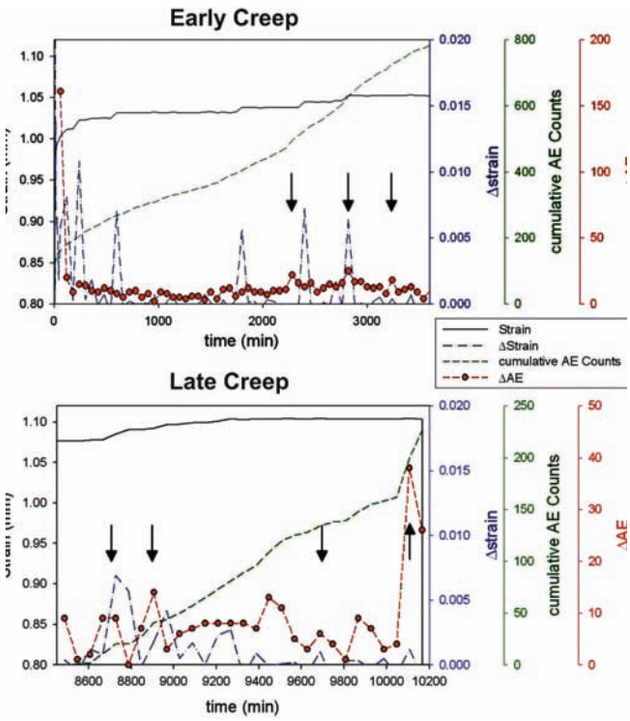

Fig. 2. *AE and strain data during early and late creep in a K/E fixed stress creep test.*

lifetime of COPV composite materials of construction. Due to time constraints, however, we performed most creep rupture tests using the quicker SSM approach.

ESEM images acquired at 20× magnification during SSM testing revealed very few changes aside from Poisson elongation and reduction of width, even at LR exceeding 0.9 relative to the UTS. ESEM at 500× revealed areas of higher electron contrast at LR = 0.92 that did not appear at lower LRs; however, more thorough ESEM analysis is needed to ensure these were not imaging artifacts.

Inspection after rupture during SSM testing of the K/E specimen clearly revealed a skin/core morphology in the Kevlar® filaments. Scientists observed fiber split lengths of 620 mm (about 50 times the 12-µm diameter (D) of a single Kevlar® filament) (figure 1). For a Kevlar 49 molecule, failure at chain ends within the core of a single filament would result in a fiber split length of approximately 150D; therefore, the 50D split lengths suggest chain scissioning is operative, which is expected for strands undergoing creep rupture at a LR > 0.7.

Optical microscopy at 60× magnification during testing of a K/E strand showed discernable macroscopic changes occurring during the SSM loading profile. Like the ESEM results, optical microscopy showed that creep damage is very subtle in terms of giving any indication of impending creep rupture, even during late creep.

Real-time mAE data acquired on a K/E strand during an ASTM D 7337 fixed-stress creep test revealed both an increase in the amplitude (energy) and in the number of events as we approached a critical creep rupture point (figure 2). Discrete creep events, as revealed by strain increases, often corresponded with increases in AE activity during early and late creep (see arrows in figure 2).

To date, WSTF has performed NDE on K/E strand, C/E strand, and carbon fiber tow. NDE measurements made so far include mAE, stress (load cell), strain (fiber Bragg grating and linear variable differential transformer), ESEM and optical microscopy, and low-magnification videography. An example of videography of an unimpregnated 12K T1000 carbon fiber tow appears in figure 3. The video frames show progression of creep rupture degradation from unloaded to post-rupture conditions. The explosive failure of the carbon tow was similar to the type of catastrophic and sudden failure observed in the K/E composite strand.

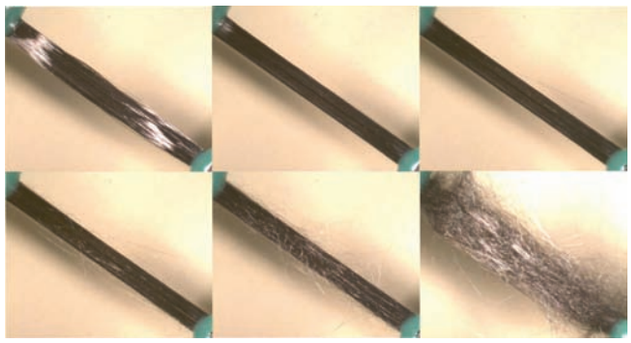

Fig. 3. *Creep rupture progression in an unimpregnated 12K T1000 carbon fiber tow.*

Orion Composite Overwrapped Pressure Vessel Safety Testing

Nathanael J. Greene, *White Sands Test Facility*
Regor L. Saulsberry, *White Sands Test Facility*
Ralph Lucero, *White Sands Test Facility*
Tommy B. Yoder, *White Sands Test Facility*

A joint test and analysis effort is under way at Johnson Space Center and NASA White Sands Test Facility (WSTF) to develop data and analysis to better understand the durability and reliability of composite overwrapped pressure vessels (COPVs). COPVs are used in virtually all launch vehicles and the International Space Station, and are planned for use on Constellation Program vehicles because of mass savings over all-metal pressure vessels. The mass savings come, however, with the added complexity of the anisotropic behavior of the carbon fiber-epoxy structure, sensitivity to mechanical damage, and the bond interface between overwrap and liner. In a study at WSTF, we are developing novel approaches to measure vessel health to understand pressure vessel durability with time, pressure, and temperature for the Orion Crew Exploration Vehicle.

Exploration of the moon, Mars, and other planets requires mass restrictions that drive these pressure vessels toward new technological limits. New applications for visual inspection and nondestructive evaluation (NDE) for verification of manufactured integrity include laser profilometry, laser shearography, heat soak or flash thermography, radiography, and videoscope. These applications have been applied to the vessels we are testing for Orion. We are also developing wired and wireless health-monitoring approaches for application during vessel lifetime, including strain measurement, acoustic emission, impact detection, audio signature, and video event mapping. The data collected are providing information for mass and factor-of-safety traits required for the optimization of Orion vehicle designs. Figure 1 shows an Orion test COPV instrumented in a recent test for measurement of strain, acoustic emission, internal volume, audio, and video health signatures to the point of burst failure.

Fig. 1. *Orion test COPV instrumented for multiple measurements during test to failure.*

We successfully used flash thermography and laser shearography to map manufacturing design features, including ply termination and wrap pattern bridges (figure 2). Laser profilometry has provided a full map of the interior of the vessel with precise measurement of liner ripple period and amplitude. Videoscope, laser imaging, and radiographic inspection have also been successful in identifying weld anomalies that may cause in-service premature leakage or rupture. As a result of this testing, three new American Society for Testing and Materials standards are being written for COPV inspection with multiple NDE methods. These are being broken down into composite, liner, and liner-to-composite interface standards.

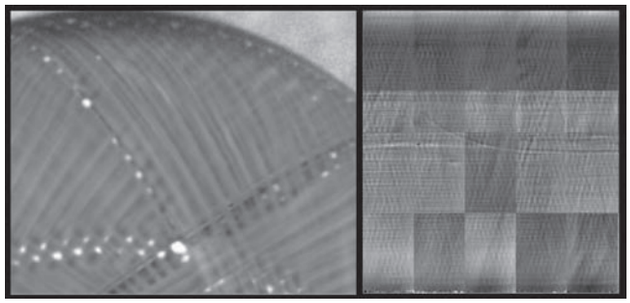

Fig. 2. *Heat soak thermography of ply layup (left); laser shearography of external surface (right).*

We correlated data collected during testing to provide a comprehensive assessment of vessel health over time. The analyzed data provide information useful for ranking health assessment techniques that can be applied for Constellation vehicle health monitoring. We also collected health data from an Orion test vessel during a burst test for instrument

Orion Composite Overwrapped Pressure Vessel Safety Testing

continued

sensitivity analysis (as shown in figure 1). Video and audio events during a typical test are shown in figure 3.

The new NDE and health monitoring techniques in development will open the door for safer space exploration tomorrow.

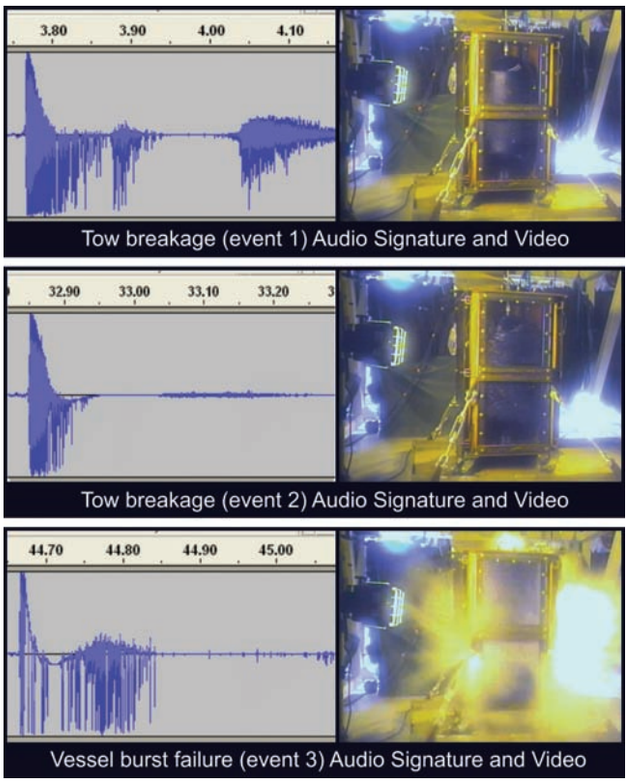

Fig. 3. *Example of data for vessel health during lifetime.*

Thermal Radiation Impacts Protection System

Pasha Nikolaev, *Engineering Research Consultants, Inc.*
Edward Sosa, *Engineering Research Consultants, Inc.*
Sivaram Arepalli, *Engineering Research Consultants, Inc.*
Scott Coughlin, *Johnson Space Center*
Padraig Moloney, *Johnson Space Center*
Peter Boul, *Engineering Research Consultants, Inc.*
Mike Fowler, *Johnson Space Center*
Leonard Yowell, *Johnson Space Center*
Eric Christiansen, *Johnson Space Center*
Bruce (Alan) Davis, *Johnson Space Center*
Jim Arnold, *Ames Research Center*
Mairead Stackpoole, *Ames Research Center*
Wendy Fan, *Ames Research Center*
Tane Boghozian, *Ames Research Center*
Jeremy Thornton, *Ames Research Center*
Sylvia Johnson, *Ames Research Center*
Jose Chavez, *Ames Research Center*
Mike Olson, *Ames Research Center*

All returning vehicles that enter the Earth's atmosphere have high heating rates that challenge designers. These high heating rates require vehicle heat shields that remain intact after long transit outside of the Earth's atmosphere. One of the Thermal Protection System materials under consideration for vehicle heat shields is phenolic impregnated carbon ablator (PICA), which was developed at the NASA Ames Research Center (ARC) in the mid-1990s for Discovery-class missions. Among these Discovery-class missions was Stardust – a capsule that completed a 7-year, 3-billion-mile journey to collect comet samples. This capsule's heat shield, composed of PICA, successfully executed the highest speed Earth entry to date on January 15, 2006.

PICA is a porous fibrous carbon insulation infiltrated with phenolic resin. While PICA is an excellent ablator, its desired thermal properties come at the expense of its mechanical strength. From an application standpoint, it is necessary to improve the mechanical properties of virgin PICA and, hence, its tolerance against micrometeoroid/orbital debris (MMOD) impact damage in space. Additionally, one of the protective mechanisms for PICA during entry heating is the formation of a char layer that both radiates heat away from the vehicle and insulates the vehicle, thereby preventing heat penetration. It is desirable to increase the yield and the strength of the char to ensure better performance. Lower-strength char can spall (chunks pop off, from internal pressure, deteriorating heat shield performance), so increasing the char strength will allow PICA to operate at higher pressures than those of the currently qualified ablator.

The Johnson Space Center (JSC) is collaborating with ARC scientists on the Thermal Radiation Impact Protection System (TRIPS) Team. The TRIPS Team is using carbon nanotubes as a reinforcement additive that will improve PICA properties by adding a supportive nanoscale fibrous structure that permeates the otherwise randomly oriented polymer. Successful incorporation of carbon nanotubes into PICA requires chemical modification of the nanotube surface to achieve desired chemical compatibility and dispersion of nanotubes. These are critical points, as only well-dispersed and compatible nanotubes can potentially create a supportive network of nanofibers within the PICA. Several types of nanotubes and several synthetic approaches were developed at JSC and ARC, followed by development of the corresponding processing techniques to manufacture nano-PICA. In addition, JSC scientists studied the properties of the nanotube – i.e., polymer interface and its influence on the load transfer mechanisms – as well as the mechanical properties of the composite.

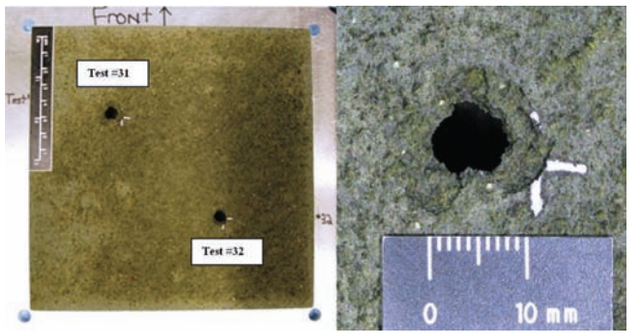

Fig. 1. *Nano-PICA following arc-jet testing to simulate atmospheric entry conditions. Thick char layer has formed outside.*

As a result of these studies, chemical functionalization and processing techniques were successfully scaled up to manufacture test articles for tensile testing, to perform arc-jet testing that simulates atmospheric entry conditions, and to complete MMOD testing that simulates hypervelocity micrometeoroid impact. Specifically, tensile tests demonstrated that a 46% increase in strength and a 76% increase in modulus can be achieved with certain combinations of nanotube type, concentration, and functionalization. Arc-jet tests demonstrated reduced

Thermal Radiation Impacts Protection System

continued

recession rates, reflecting on the higher char strength. Hypervelocity impact testing of nano-PICA is under way at the White Sands Test Facility (figures 1 and 2).

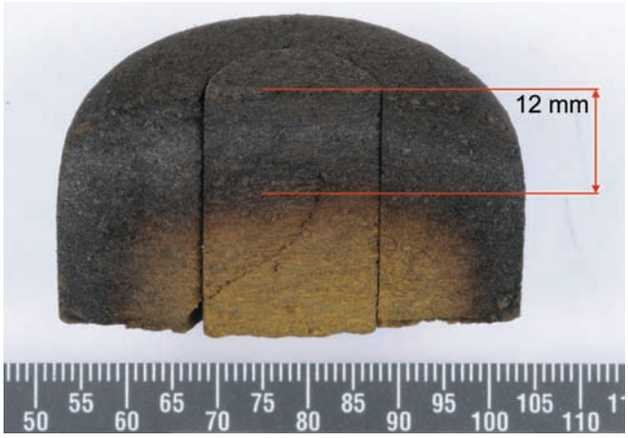

Fig. 2. *Nano-PICA following hypervelocity impact testing at the WSTF. The entry hole size is comparable to that in standard PICA. The internal damage dimensions will be determined by x-ray imaging.*

Type-specific Single-wall Carbon Nanotube Growth and Separation

Edward Sosa, *Engineering Research Consultants, Inc.*
Pasha Nikolaev, *Engineering Research Consultants, Inc.*
Peter Boul, *Engineering Research Consultants, Inc.*
William Holmes, *Engineering Research Consultants, Inc.*
Sivaram Arepalli, *Engineering Research Consultants, Inc.*
Leonard Yowell, *Johnson Space Center*

Single-wall carbon nanotubes (SWCNTs) have excellent electronic properties that, as in any nanomaterial, are strongly dependent on their molecular structure and size. Current SWCNT production methods yield polydispersed materials with various diameters and chiralities leading to distribution of types. This distribution of types, in turn, has limited the successful use of SWCNTs in applications in both the commercial sector and the aerospace industry. For many applications, the availability of exclusively metallic or semiconductive SWCNTs would be greatly beneficial. Such applications that would benefit from type-specific SWCNTs include: transistors, photovoltaic and optoelectronic devices, transparent conductive films, chemical and radiation sensors, and mechanically enhanced conductive nanocomposites. NASA scientists are particularly interested in using type-specific SWCNTs to provide electromagnetic interference shielding by transparent conductive films, conductive coatings for electrostatic discharge, radiation dosimeters, and quantum conducting wires (replacing copper). We focused on achieving metallic SWCNTs through both type-specific growth and type-selective separation.

One approach to acquire predominately metallic SWCNTs was to optimize the production parameters in the pulsed laser vaporization (PLV) technique to direct nanotube growth toward the metallic configuration. While this method may prove to be more difficult than the use of metallic tube separations, it is the more desirable method since higher yields and lower costs are to be expected. Even if the production of a single nanotube type is unattainable, the production of material with a narrow-type distribution would be favorable for subsequent separation efforts.

Cobalt/nickel and rhodium/palladium catalysts together with variations in the production temperature were used for SWNC synthesis. We monitored the nanotube-type populations through photoluminescence, ultraviolet-visible-near infrared (UV-Vis-NIR) absorption, and Raman spectroscopy. For both catalysts, lower production temperatures resulted in smaller nanotube diameters and exceptionally narrow type distributions (figure 1), with marked preference toward large chiral angles. The larger nanotube diameters tended to be associated with larger chiral angles. Although no drastic enrichment in metallic SWCNTs was observed, the results demonstrate that SWCNT growth can be directed toward a narrow distribution of particular nanotube types. Such material is highly favorable for separation attempts.

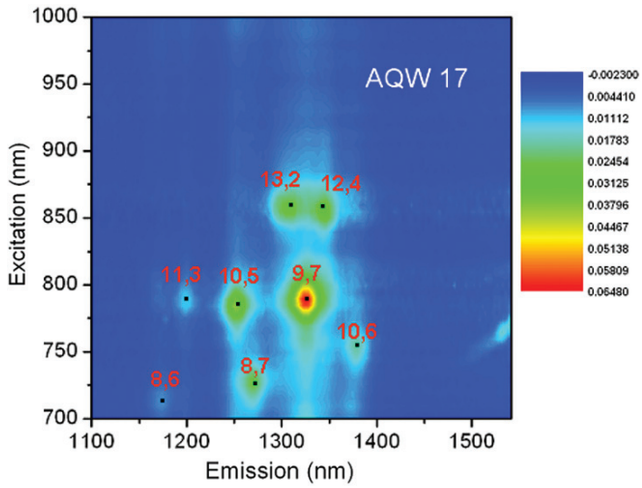

Fig. 1. *Photoluminescent spectral map of SWCNT sample produced at reduced temperature. Only eight semiconducting tubes are detectable, indicating exceptionally narrow type distribution. Regular SWCNT samples typically have 30 or more semiconducting nanotubes.*

The second approach to obtain metallic enriched SWCNTs is through separation techniques. Various separation methods, including electrophoresis, centrifugal density gradients, polymer and DNA [deoxyribonucleic acid] wrapping, and selective chemical functionalization, have been attempted. While these techniques have produced promising results, they still lack the ability to be scaled up toward large quantities. It is proposed that selective chemical functionalization is the most likely method to produce isolated nanotubes in greater than-microgram quantities.

Nanotube separations were performed on the nanotube samples with a narrow-type population produced at lowered temperature. Aryl diazonium salts are known to react preferentially with metallic nanotubes. Dodecyloxybenzenediazonium tetrafluoroborate, which is a special diazonium salt, was synthesized specifically for this task as it renders metallic SWCNTs soluble in tetrahydrofuran after reaction. Unreacted semiconducting tubes remained insoluble, and were separated from the

Type-specific Single-wall Carbon Nanotube Growth and Separation

continued

soluble metallic tubes by filtration. The metallic tubes were subsequently precipitated out by the addition of sodium chloride and methanol. Both materials were then heated in a furnace to remove the dodecyl functional groups and characterized by Raman and UV-Vis-NIR absorption spectroscopy. The suspended material showed increases in both the Raman and the absorption spectral features (figures 2(a) and 2(b)) associated with metallic nanotubes, indicating that the metallic types had been enriched. It is expected that further refinement of this technique will lead to more dramatic separations of types and diameters.

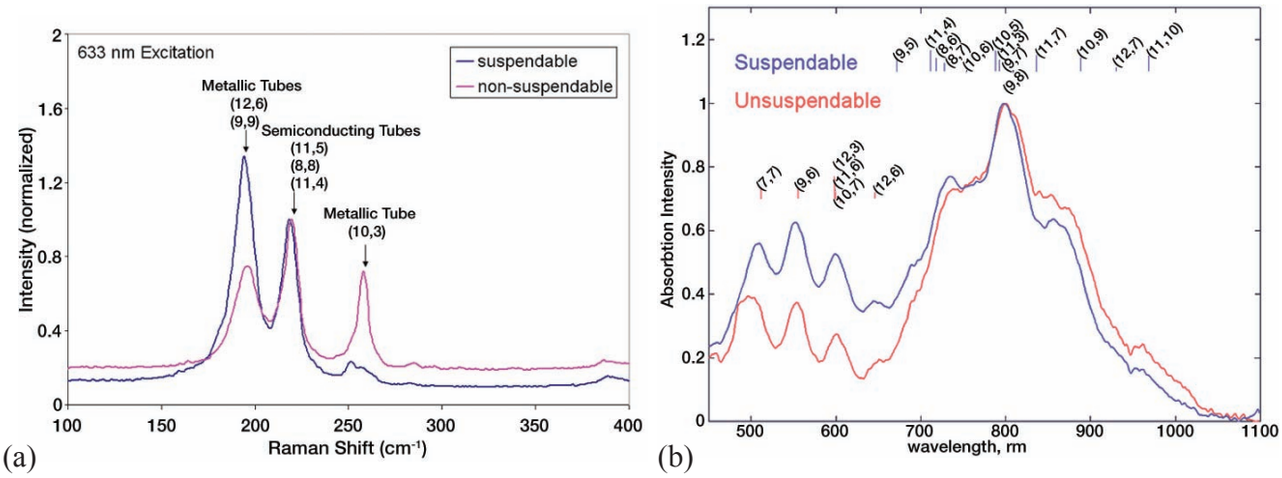

Fig. 2. *Raman (a) and absorption spectra (b) of SWCNT samples acquired after separation. Soluble (suspendable) sample shows increase in spectral features associated with metallic nanotubes, indicating enrichment in metallic types.*

Improving the Process: Assessing Reactivity of Nonmetals in Aerospace Fluids

Steven D. Hornung, *White Sands Test Facility*
Kurt A. Rathgeber, *White Sands Test Facility*
Miguel J. Maes, *White Sands Test Facility*

Reactivity tests generally expose a material to a test fluid under appropriate conditions and measure changes in pressure, temperature, and physical and chemical properties. NASA-STD-(I)-6001A Test 15, *Reactivity of Materials in Hydrazine, Monomethylhydrazine, Unsymmetrical Dimethylhydrazine, Aerozine 50, Nitrogen Tetroxide, and Ammonia*, is the standardized test for assessing aerospace fluid reactivity with a given material. The procedure requires a 2-hour screening test, often called a beaker test, in which a small sample is immersed in a beaker and observed for signs of gross reactivity. Factors that can affect material reactivity include, but are not limited to: exposure duration, surface conditions and geometry, surface area contacted, fluid phase(s) present, pressure, and temperature. If the material passes the screening test, a larger sample is immersed and maintained at 71°C (160°F) for 48 hours. Temperature and pressure are monitored, and both the fluid and the material are analyzed posttest. A test being developed at White Sands Test Facility takes compatibility testing one step further by exposing larger specimens and testing them for changes in mechanical properties while still wetted and/or permeated with the propellant for comparison with control samples. This type of testing is especially important for polymeric materials used in components as seals and valves seats. Very often propellants such as nitrogen tetroxide (NTO) and monomethylhydrazine (MMH) can produce significant changes in physical properties while wetted, making them unsuitable for the intended application.

Screening process

We use a stepwise screening process to ensure it is safe to condition larger material sample sets for use in physical property testing. The steps include

- Evaluating the sample material for known incompatibilities from available data and by similarity with other materials
- Verifying the material composition by using the certifications from the supplier and inspection by Fourier transform infrared spectroscopy
- Testing in accordance with NASA-STD-(I)-6001A Test 15

Specimen conditioning and testing

On completion of the screening process, we prepare two sets of material specimens for the desired physical property tests (e.g., tensile, hardness, flexure, compressive strength). We hold back one "control" set for baseline testing, and condition the other set in the test fluid at 71°C (160°F). After 48 hours, we turn the heater off and the system is allowed to cool to ambient temperature. The fluid is not drained from the conditioning vessel until conditions are right to transport the vessel from the test area to the chemistry lab.

Material specimens are distributed to each of the tests as soon as possible after the fluid is drained from the cooled conditioning vessel. We perform physical property testing without decontaminating specimens to test the material as close to a wetted use condition as possible. As appropriate, we also perform physical property tests in laboratory fume hoods or within local exhaust ventilation systems. Figure 1 shows an Instron® Universal Test Machine with a local exhaust ventilation system built around it to facilitate testing of contaminated specimens.

Fig. 1. *Instron® Universal Test Machine with local exhaust ventilation system.*

Example results with polychlorotrifluoroethylene

We performed the process for assessing reactivity of nonmetals in aerospace fluids on polychlorotrifluoroethylene (PCTFE) procured to the old Kel-F® 81 specification

Improving the Process: Assessing Reactivity of Nonmetals in Aerospace Fluids

continued

Aerospace Material Specification (AMS) 3650C, *Rods, Sheets, and Molded Shapes, Polychlorotrifluoroethylene (PCTFE) Unplasticized*. We compression-molded the material and slow-quenched it in an attempt to replicate Kel-F® 81 physical properties.

We screened the material for NTO service per the process described. We then performed property tests in accordance with the following ATSM methods:

ASTM D 638, *Tensile Properties of Plastics*

ASTM D 2240, *Rubber Property – Durometer Hardness*

ASTM D 695, *Compressive Properties of Rigid Plastics*

ASTM D 790, *Flexural Properties of Unreinforced and Reinforced Plastics and Electrical Insulating Materials*

One example of how a physical property can change on exposure and with the material still saturated with the propellant is illustrated in figures 2 and 3 for the tensile properties. The change from "control" to "conditioned" in each parameter, reported in Table 1 and shown in the two figures, is consistent with the material becoming softer and more pliable with the absorption of nitrogen dioxide. Tests of other physical properties have shown that physical properties for this material in NTO are similarly affected.

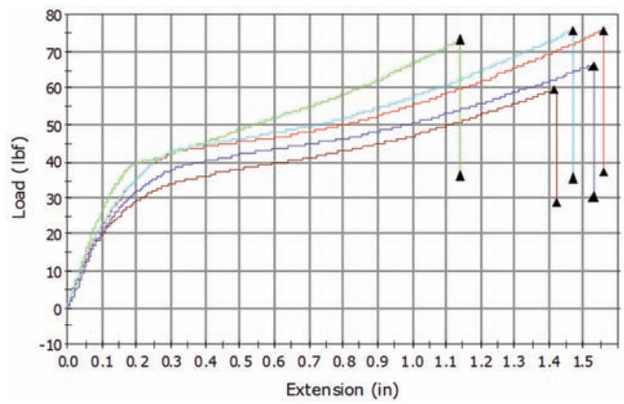

Fig. 2. *Extension-load curves for control samples.*

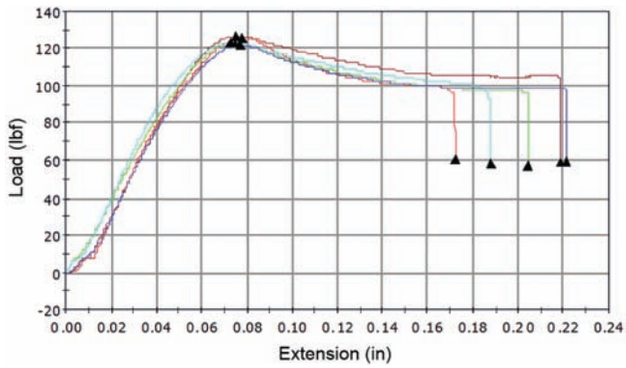

Fig. 3. *Extension-load curves for conditioned samples.*

	Percent Elongation at Yield (%)	Percent Elongation at Break (%)	Tensile Stress at Yield (psi)	Strain at Yield (in./in.)	Modulus (psi)
Control Specimens					
Replicate 1	121	146	6,400	0.18940	440
Replicate 2	120	158	6,400	0.18322	440
Replicate 3	120	154	6,300	0.17697	430
Replicate 4	119	150	6,300	0.17697	450
Replicate 5	120	159	6,200	0.18643	430
Mean	120	154	6,300	0.18227	440
Standard Deviation	0.6	5.6	84	0.00395	8.4
Conditioned Specimens					
Replicate 1	159	515	1,900	0.597	4,000
Replicate 2	293	478	2,000	1.930	3,400
Replicate 3	186	404	2,000	0.865	4,600
Replicate 4	154	492	1,700	0.545	3,800
Replicate 5	148	507	1,500	0.480	3,800
Mean	188	479	1,800	0.879	3,900
Standard Deviation	61	44	220	0.61	440

Table 1. *Tensile results for control and conditioned specimens.*

Conclusions

This example illustrates the importance of performing material tests in near-use situations, especially in the case of nonmetallic materials. Propellants such as NTO and MMH have been shown to affect the physical properties of materials in some cases by "plasticizing" the material. This effect can be missed if the physical testing is performed after decontamination.

The improvement comes from testing conditioned materials as close to a wetted use condition as possible to determine whether material properties are affected by the fluid. The data from the PCTFE physical property tests indicate that material properties can be dramatically affected by exposure to aerospace fluids; and, while exposed, materials may not retain the physical properties for which they were originally selected.

Lunar Inflatable Habitat Development

Gerard Valle, *Johnson Space Center*

Kriss J. Kennedy, *Johnson Space Center*

While surface habitats are necessary for planetary exploration missions, inflatable, lightweight habitats are critically needed. This is because inflatable habitats reduce the logistic issues of transporting a large volume to the surface of the moon as well as the launch weight. By including engineering development that directly feeds into the lunar surface system architecture, we are focusing on providing surface inflatable habitat concepts for delivery, emplacement/deployment, outfitting, and operations for lunar operations to make the missions more reliable, safe, and affordable. Before we can achieve this, many technical issues must be understood.

In January 2008, scientists jointly partnered through NASA, the National Science Foundation (NSF), and ILC Dover, Frederica, Del., to deploy an inflatable habitat in Antarctica (figure 1). Deployment took fewer than 50 minutes. Performance data (e.g., temperature, pressure, humidity, carbon dioxide concentration, power monitoring, and weather station) were subsequently measured, recorded, and monitored remotely by scientists at Johnson Space Center (JSC) throughout the 2008 Antarctic season. These scientists also investigated various operational scenarios, including packing efficiency, deployment, harsh environment performance (e.g., cold, ultraviolet, flex, crew interface), and integrated electronics. The NSF is currently working to extend deployment of the habitat as part of the Arctic Program.

Fig. 1. *(a) Inflatable habitat deployed in Antarctica. (b) Inflatable habitat during Antarctic winter.*

In August 2008, NASA White Sands Test Facility (WSTF) pressure-tested an 88-in.-diameter woven inflatable module to 45 psig (25% of ultimate burst pressure) and remotely severed a woven structural member using a linear-shaped charge (figure 2). Not only did the global inflatable module maintain its structural integrity during testing, but no measurable change in load was measured at the webbing-to-bulkhead interface, including at the interface of the severed webbing. This demonstrates that not only is the woven inflatable design

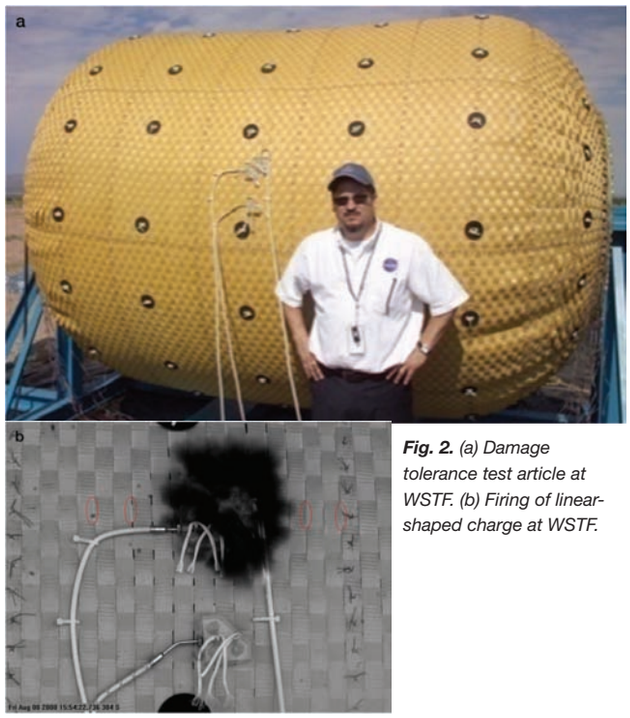

Fig. 2. *(a) Damage tolerance test article at WSTF. (b) Firing of linear-shaped charge at WSTF.*

tolerant to damage, but that the damage has a local effect that gets redistributed to adjacent members.

NASA is currently refurbishing the damage tolerance test article and integrating it with a 40-in. hatch that has a 48-in. frame. The integrated test article will be tested to lunar surface pressures times a 1.25 factor of safety (11.25 psig = 9.0 psig * 1.25). Various clevises, strain-gauged and calibrated to measure load during testing, will be used to verify analytical predictions. This integration will demonstrate the integration of a large penetration into an inflatable module. Boeing Phantom Works, Seal Beach, Calif., and NASA fabricated the hatch and frame. WSTF began Phase I pressure testing in the summer of 2009. This Phase I module (figure 3) will serve as a target during subsequent deployment and mating testing scheduled for fiscal year 2010 (FY10).

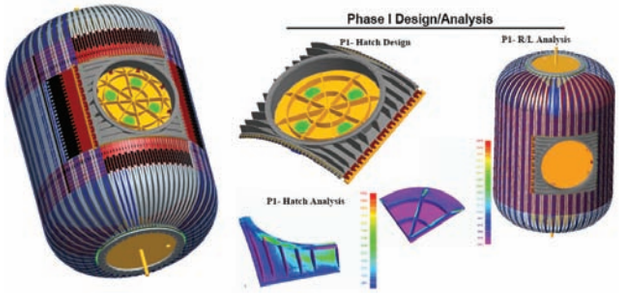

Fig. 3. *Inflatable structure: hatch integration Phase I.*

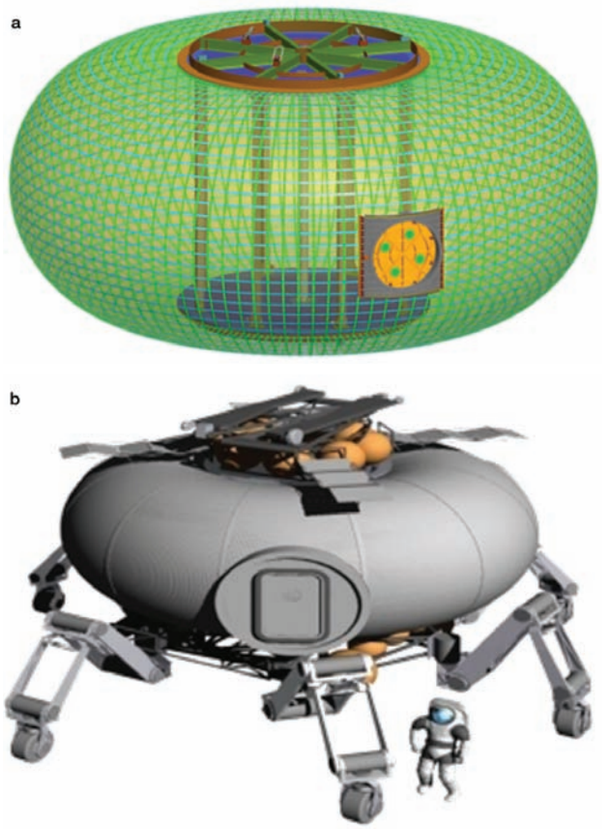

Fig. 4. *(a) Phase II test article. (b) Constellation trade set 1a torus habitat.*

For Phase II, NASA will design, analyze, fabricate, and test a full-scale, 28-ft-diameter Constellation Trade Set-1a torus habitat with integrated hatch penetration (figure 4). The product is a full-scale expandable structure with a 40-in.-diameter hatch. The objectives are: to design, fabricate, and integrate a hatch into the full-scale inflatable torus module; to scar the internal core longerons and hatch frame for a future addition of a hatch deployment system; to inflate in a 1g environment; to inflate the module to 11.25 psid (lunar and Mars surface pressures 9.0 psig * 1.25 Proof); and to compare the hatch frame and bulkhead clevis strain measurements with analytical predictions. Fabrication of the Phase II test article started in the summer of 2009 with pressurization testing at WSTF thereafter.

Phase III will use the Phase I and II modules for deployment and mating testing to ensure a Technical Readiness Level of 5-6. Phase III is currently scheduled for FY10 with funding forthcoming.

Computed Tomography Scanning and Analysis of the Stardust Heat Shield

Karen McNamara, *Johnson Space Center*
Dan Schneberk,
Lawrence Livermore National Laboratory
Ron Bastien, *Johnson Space Center*
Jack Warren, *Johnson Space Center*
Norman Ruffino, *Johnson Space Center*
Ovidio Oliveras, *Johnson Space Center*
Eddie Pompa, *Johnson Space Center*
Ajay Koshti, *Johnson Space Center*

When the Stardust sample return capsule returned to Earth at approximately 3:00 a.m. Mountain Standard Time on January 15, 2006, it made one of the most dramatic re-entries in NASA history (figure 1). The capsule, which was traveling at 12.4 km/s, is the fastest human-made object to re-enter the atmosphere of the Earth. To survive this fiery re-entry, the Stardust capsule was fitted with an ablative heat shield composed of phenolic impregnated carbon ablator (PICA). This material and its re-entry performance are of significant interest to NASA, most notably for the Mars Science Laboratory (MSL) mission and the Orion/Crew Exploration Vehicle (CEV) project. The MSL is currently scheduled to launch with a multi-segmented PICA heat shield in the year 2011. Engineers in the CEV program are also investigating the use of PICA for the forebody of the Orion capsule. Although we have used arc-jet testing to create models for PICA ablation, the Stardust sample return capsule heat shield provides the only actual ground truth with which to validate these models.

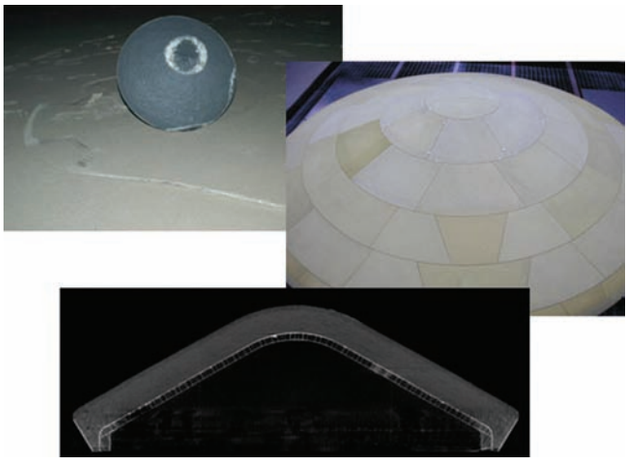

Fig. 1. *View of the landed Stardust heatshield on recovery in the field (top). Multi-segmented MSL PICA heat shield (middle). Cross-sectional (X-Y) computed tomography scan of the Stardust flight heat shield (bottom).*

PICA consists of a preformed, low-density, fibrous carbon structure infiltrated with a phenolic resin. The preform is cast to a proper shape and thickness, fired, impregnated with a phenolic resin, and hand-machined to meet specifications. It is then bonded to an aluminum honeycomb support structure to complete the heat shield. In the case of the Stardust sample return capsule, the steep re-entry angle and speed caused unprecedented peak heat loads that precluded the use of joined sections of PICA to form the outer ablative layer. The handcrafted PICA shell thus consisted of a single solid casting, the design of which was one of the greatest challenges for meeting Thermal Protection System requirements on the Stardust mission.

The Stardust capsule heat shield is the only PICA forebody that has flown a planetary re-entry to date. Its successful recovery on land makes it one of the most interesting re-entry bodies for engineering studies, as it was not exposed to the corrosive environment of the seas (as were the Apollo return capsules). Since the return to Earth of the Stardust sample return capsule in early 2006, the Johnson Space Center (JSC) Space Exposed Hardware (SEH) Group has supported a multitude of studies by NASA, industry, and academic partners. These studies are aimed at forming a better understanding of the performance of the Stardust capsule heat shield. Researchers made residual thickness estimates using at least three independent techniques: (1) mechanical surface height measurements; (2) high-resolution, three-dimensional (3D) laser surface scanning; and (3) thickness measurements based on core abstractions. We performed additional measurements at JSC to address the chemistry of ablation, microstructure, thermal, and mechanical performance.

For MSL, Orion, and other future missions, spatially resolved recession rates are the most critical data that can be amassed to understand heat shield performance. We could not determine the spatially resolved recession rate of the Stardust heat shield based on any of the analyses described above, however – in part because of the lack of pre-flight data for both the bonded and the unbonded PICA casting. Both castings are required to determine overall recession as well as variability, asymmetry, and peak recession. Due to budget, schedule, and scope constraints, we performed, for example, no pre-flight imaging of the heat shield or verification of the thickness, shape, and planarity of the

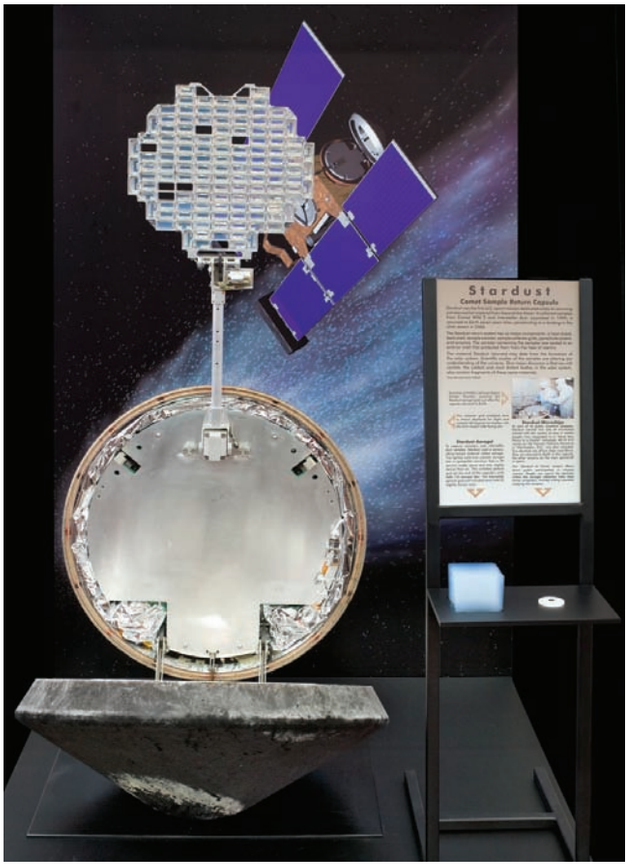

Fig. 2. *The Stardust sample return capsule on display in the National Air and Space Museum.*

surfaces or radii of curvature for the PICA shell. The same is true of the mated PICA form and the support structure.

We might have ended the quest for recession information from the Stardust heat shield there had it not been for a collaborative effort between the JSC SEH Group and the JSC Engineering Nondestructive Evaluation (NDE) Group. The SHE and NDE Groups, which worked with researchers from the Lawrence Livermore National Laboratory, Livermore, Calif., used a new state-of-the-art x-ray system to obtain a complete 3D computed tomography (CT) scan of the Stardust heat shield – one of largest objects ever scanned in a CT system.

Although absolute recession measurements could not be achieved without recourse to pre-flight data, the CT scans provided a 3D thickness map of the PICA layer at a 300-µm resolution that allowed a quantitative comparison of relative recession rates and a qualitative evaluation of arc-jet data and the resulting models. Bondline gaps between the PICA and the aluminum honeycomb substructure can also be clearly measured. These data are absolutely critical to both the MSL and the CEV, both of which will be using multi-segmented heat shield designs. For example, the Stardust heat shield shows extensive bondline separation along the curvature of nearly its entire circumference; this bondline separation could have major impacts on future manufacturing processes. The CT scan also provided values for the PICA density as a function of depth and spatial location. This gives insight into the depth of char and chemical alteration of the PICA, which is important to our understanding of the pyrolysis processes as well as the physical and mechanical performance of the material. Finally, CT scans allow spatial identification of the physical and chemical defects that can alter performance; we can use their results to develop and evaluate manufacturing processes.

Members of the Stardust CT scanning group are continuing to evaluate the data obtained from the flight heat shield. These group members are also planning to perform similar CT scans on the Stardust engineering model (EM) heat shield (figure 2). Although the EM heat shield is not identical to the pre-flight actual, it was manufactured under identical conditions and, thus, should provide insight into pre-flight characteristics and assist in differentiating manufacturing and flight defects.

Completing the NDE of the Stardust heat shield also allowed the JSC SEH Group to work with curators at the Smithsonian National Air and Space Museum in Washington, D.C. to place the reconstructed Stardust sample return capsule on permanent display in the premier “Milestones of Flight” gallery at the museum alongside the Apollo 11 capsule and the Viking lander model. This will be the first NASA artifact to be added to that collection in nearly 25 years.

Flammability and Explosives Technologies

Changing the Standards for Promoted Combustion Pass/Fail Criteria

Kyle M. Sparks, *White Sands Test Facility*

Joel M. Stoltzfus, *White Sands Test Facility*

A standard test for determining metals flammability in enriched oxygen is the American Society for Testing and Materials (ASTM) G124 *Standard Test Method for Determining the Combustion Behavior of Metallic Materials in Oxygen Enriched Atmospheres*. Promoted ignition testing determines the relative flammability of metals in oxygen-enriched atmospheres. The results of the tests are generally published as the threshold pressures or the lowest pressure in 100% oxygen that supports combustion of a metal test sample. Currently, the standard defines combustion as consumption of an entire 150-mm (5.9-in.)-long, 3.2-mm (0.13-in.)-diameter rod. However, the credibility of an entire rod burning to determine flammability has been questioned. Differences in interpretation of the burn criteria led to inconsistent ranking of materials at various test facilities. Therefore, NASA White Sands Test Facility (WSTF) initiated a study to help define the burn length criteria used for determining threshold pressures.

Promoted ignition testing determines the relative flammability of metals in oxygen-enriched atmospheres (ASTM G124). The burning promoter that ignites the metal rod has an incidental preheating effect on the test sample. WSTF performed experiments to determine the promoter heat affected zone (HAZ), which is the distance heated by the promoter just before its detachment or consumption. Based on the HAZ determined, 30 mm (1.18 in.) of rod must be consumed before the material should be considered flammable. This finding has modified historical views of metals flammability in the specific application of ASTM G124 and other tests. ASTM G124 is currently being revised and will incorporate these pass/fail criteria.

To determine the HAZ, test sample configurations replicated ASTM G124, except thermocouples were inserted along the sample at various depths and intervals. WSTF is equipped with a test chamber that is used primarily for ASTM G124 standard promoted combustion testing. One of the chamber viewports was modified to incorporate multi-thermocouple temperature readings at test pressures up to 34.5 MPa (5,000 psi). Temperature and pressure data were recorded at 100 Hz. High-speed video established the event duration, which was the time from ignition of the promoter to the first significant drop of molten metal or promoter detachment or consumption.

Test samples were 305-mm- (12 in.)-long and 3.2-mm- (0.125-in.)-diameter copper rods. Commercially pure copper was chosen for its high thermal conductivity and resistance to burning at elevated pressures and concentrations of oxygen. Magnesium and aluminum promoters were ignited using Pyrofuze® wire. The test matrix is shown in Table 1.

Promoter Material	Pressure		No. of Tests
	MPa	psi	
Magnesium	0.7	100	1
Pyrofuze®	3.5	500	1
Magnesium	3.5	500	4
Aluminum	3.5	500	4
Magnesium	6.9	1,000	3
Aluminum	6.9	1,000	3
Magnesium	34.5	5,000	4
Aluminum	34.5	5,000	3

Table 1. *Copper rod test sample configuration and test matrix.*

Figure 1 shows a typical temperature vs. time plot for copper samples with aluminum promoters; vertical lines denote the beginning and end of event duration.

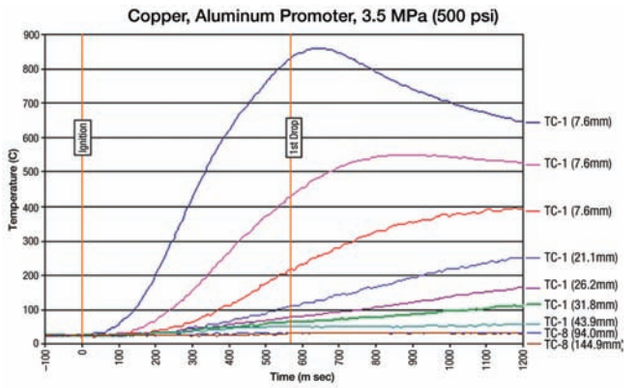

Fig. 1. *Typical time vs. temperature data, showing event duration.*

To determine the promoter HAZ, researchers must understand the amount of sample preheating, in terms

of temperature, necessary for the burning characteristics to be affected. Changes in flammability are noted by changes in either the *pressure* at which a metallic sample will support burning or the *rate* at which the sample melts while it is burning; both are indicators of metals flammability and are used historically to compare metals.

Temperatures at the end of the ignition events were used to determine the location, from the bottom of the rod, in which the samples reached 260°C (500°F). The data show that, including standard deviation (STDEV) error bars, the promoter HAZ did not extend beyond 17.8 mm (0.70 in.). This distance included the promoter engagement distance, which differs from ASTM G124 instructions.

The mean value and STDEV in the test pressure group with the largest promoter HAZ was found, and a 3-∑ distribution was applied using the Central Limit Theorem. Using the most severe condition (3.5 MPa (500 psi)) in heat generation/conduction, and combining both aluminum and magnesium promoter sample data, testing yielded a mean HAZ distance of 16 mm (0.63 in.) with an STDEV of 1 mm (0.041 in.). Applying three STDEVs resulted in a promoter HAZ of 19 mm (0.75 in.) from the bottom of the rod (figure 2).

Based on these data, which were also validated by thermal modeling, researchers discussed and decided that, within NASA, samples that burn more than 30 mm (1.18 in.) above the promoter (adding roughly 50% of the actual HAZ as a conservative buffer) will be considered a burn. Since most metals have a lower thermal conductivity than copper, this ensures that all metals that burn a distance > 30 mm (1.18 in.) are clearly burning independently of any promoter ignition effects. ASTM G124 is currently being revised and will incorporate these same pass/fail criteria.

The experimental observations and subsequent conclusion of the promoter HAZ study modifies the historical views of metals flammability in the specific application of ASTM G124 and other tests that often require that the test sample be consumed entirely or halfway to be considered flammable. This result is also specific to the igniter materials tested. Copper was chosen as the major test material based on several factors, most significantly its resistance to burning and high thermal conductivity. As the promoter in this experiment, HAZ is calculated using a 260°C (500°F) temperature bias. It should be noted that, with further research in respect to elevated temperature, the promoter HAZ may need to be modified accordingly.

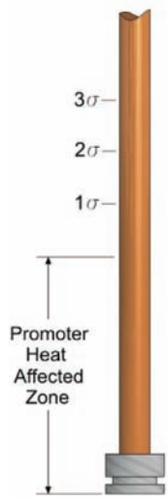

Three Sigma HAZ 260 °C / 3.5 MPa	
HAZ (mm)	16.1
Sigma (mm)	1.0
HAZ+3(Sigma) (mm)	19.2

Fig. 2. *HAZ produced from ignition promoter after applying the Central Limit Theorem using a 260°C (500°F) temperature.*

Long-term Testing of Oxygen Compressors

Michael S. Shoffstall, *White Sands Test Facility* ***Jon P. Haas,*** *White Sands Test Facility*

Since the inception of human space flight, NASA has dealt with the dilemma of pressurized oxygen systems aboard space vehicles. Oxygen is essential as an atmospheric gas for the crew and, by itself, is relatively benign. Unfortunately, it is also an effective oxidizer capable of rendering most materials flammable. Furthermore, as pressure and temperatures increase (a common occurrence on spacecraft), the flammability of materials in oxygen-enriched atmospheres increases.

To their credit, since Apollo 204, NASA personnel have successfully completed thousands of hours of human space flights without a fatal oxygen fire. Much of this can be attributed to the expensive lessons learned from Apollo 204, Apollo 13, and extravehicular mobility unit (EMU) fires and the resulting investigations. Figure 1 highlights some of this human space flight history including the Apollo launch, the Apollo 204 capsule and crew, an astronaut in an EMU, a fire-damaged EMU, the damaged Apollo 13 service module, and a shuttle launch. Through the investigation process, several test methodologies, reams of data, and methods for applying that data have been developed. NASA White Sands Test Facility (WSTF) personnel continue to add new information to yesterday's data to determine how to safely fly today and how to design safe spacecraft for tomorrow.

As NASA considers options for production and storage of oxygen for current and future spacecraft, it is apparent that the agency must develop a means to safely pressurize oxygen. Pressurized oxygen can be stored in smaller containers, reducing the weight and volume so critical in spacecraft. But, pressurizing oxygen increases the flammability of the materials involved and adds heat energy – a potential source of ignition. However, some of the concepts under consideration for future systems would pressurize the oxygen at a relatively slow rate, minimizing the rate of heating into the system and maximizing the system's ability to dissipate the heat generated. This approach, originally constrained by the rate of the oxygen production systems considered, could allow NASA to pressurize oxygen safely using less power – an added benefit on any spacecraft.

To determine the feasibility of this concept, WSTF personnel performed market research to determine whether commercial off-the-shelf units are available for the pressures and flow rates required to pressurize the airlock tanks on the International Space Station. Two units were acquired that met the operational envelope requirements; these were analyzed for suitability in oxygen systems. Our analysis determined that the materials and design were

Fig. 1. *Highlights of human space flight history.*

suitable, but we could not determine the service life or potential for failure. Furthermore, industry information indicates that when oxygen compressors fail mechanically, there is a good chance an oxygen fire will result.

Since either a mechanical failure or an oxygen fire would be unacceptable in space, WSTF personnel developed a test replicating what would be required on an extended mission by operating the compressors continuously in oxygen until failure (figure 2). The manufacturer's anticipated life is up to 5,000 hours, so the test was automated to prevent personnel having to staff a test console for 208 or more consecutive days.

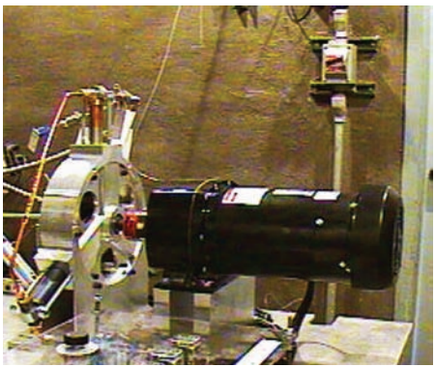

Fig. 2. *Oxygen compressor in test.*

Although automated testing is not new, testing an oxygen component to the point of failure or fire is usually performed with test personnel present. This allows these personnel to use the means necessary to limit the fire damage to the test article and protect the test facility. WSTF personnel determined it is possible to accomplish these goals through appropriate application of the oxygen system design tools that have been developed.

Most of the state-of-the-art oxygen system design tools are contained in *Safe Use of Oxygen and Oxygen Systems: Handbook for Design, Operation, and Maintenance* (previously *NASA Safety Standard for Oxygen and Oxygen Systems*, NSS 1740.15), a document maintained for NASA and the American Society for Testing and Materials by WSTF personnel. In the section "Design to Manage Fires," nine guidelines are offered to protect personnel and equipment in case of a fire. Table 1 lists the guidelines and how they applied to the design of this automated test system.

Since the inception of testing, both the test articles and test system have operated safely, continuously, and autonomously for over 1,600 hours. If and when an oxygen compressor fails during testing, WSTF personnel will review the data obtained from the test and use them to guide NASA in safely implementing oxygen compressors in current and future vehicles.

Guideline	System Design
1. Provide for accessible or remote shutoff	Four points of isolation (two valves, two regulators) are controlled from the remote test console. Manual valve is external to test cell.
2. Design for automatic source isolation	Data Acquisition and Control System (DACS) monitors: inlet and outlet pressure and flow, system temperatures, and pump motor current. In the event of an anomaly, the DACS isolates the oxygen source, vents the oxygen in the system, and alerts the test conductor.
3. Ensure easy escape for personnel	See item 4 – no personnel present.
4. Reduce personnel exposure	Test system contained within a concrete test cell; access to cell prohibited during operation.
5. Use remote operation for first use	Remote operation for all operations.
6. Design for fire containment	Concrete cell provides overall containment. Flexible hoses, used to connect test articles to the system, provide fire breaks between the two.
7. Ensure fire extinguishers are available	Remote operation fire deluge system in cell.
8. Minimize flammables near system	Test articles mounted on metal table in concrete cell.
9. Separate bulk storage from the system	Oxygen supplied to test cell via a distribution system with several points of isolation between the source and the test cell.

Table 1. *"Design to Manage Fires" guidelines and design applications.*

Design and Verification of a Robust Filter for Oxygen Service

Brian C. Anderson, *White Sands Test Facility*

John C. Anderson, *White Sands Test Facility*

An incident on September 8, 2007 in a 6,000-psi oxygen distribution system at NASA White Sands Test Facility (WSTF) resulted in the burn-through of a filter in this system (figure 1). The filter is the combination of both the filter housing and the filter element; both were evaluated. An investigation determined the filter was constructed of materials that are flammable in oxygen at the operating conditions. One resulting recommendation was to ensure that filters for oxygen service are constructed of burn-resistant materials and are of a robust design. This recommendation initiated the design of a burn-resistant and robust filter for oxygen service based on upgrading an older design.

Fig. 1. *Image of burned filter.*

Design process

When a new component is used, either out of necessity or in the interest of improvement, the component's function must be adequately understood. Considerations made in the design of this filter included: pressure rating, material compatibility, collapse pressure, flow capacity, metal-to-metal sealing, manufacturability, and resistance to plugging.

Engineers took great care in selecting materials for this filter so the materials were not only compatible in an oxygen environment but also mechanically compatible with each other. To achieve the necessary mechanical strength and compatibility, a different filter element was needed. Sintered nickel filter media, used with success in similar applications, were chosen for this filter element. This sintered element provided both excellent burn resistance and a greater tolerance for clogging due to the continuous flow path along its length (figure 2). We contacted several vendors, and as one was able to supply the required filter element, this vendor (Mott Corporation, Farmington, Conn.) was chosen as a supplier for the entire element assembly and was consulted regarding the flow capacity and collapse rating of this element.

We chose Monel 400® for the body of this filter because it has been proven as a burn-resistant material in oxygen systems. This housing material would serve not only to contain the pressure, but also to contain any combustion event if one were to occur. While Monel 400® proved a good choice for compatibility, concerns regarding the mechanical properties (specifically galling resistance) prompted careful material and lubricant choices in the mating materials.

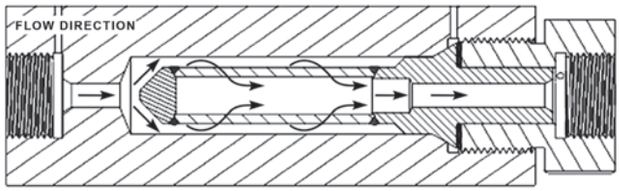

Fig. 2. *Cross section of filter.*

In high-pressure applications such as this component was designed for, polymeric seals create a vulnerability to oxygen fires. In this application, all seals within this component were metal-to-metal. The filter element itself also provided the seal between both the body and the outlet fitting. This feature resulted in the omission of a seal between the body and the outlet fitting, reducing the number of potential leak paths.

Particle impact is one of the primary ignition mechanisms in this type of component. Special care was taken in the design of this component to minimize the potential impact surfaces in the internal flow path.

Validation of design

In the development of a filter, validation of the design is as important as the design itself.

The filter design is based on several requirements, including the pressure rating, oxygen compatibility, and flow/filtering capability. The pressure rating is based on calculations per ASME [American Society of Mechanical Engineers] B31.3 code, and this code also requires each fabricated item to be pressure-tested. Generally this is a hydrostatic test to 150% of the design pressure. Oxygen compatibility is evaluated based on the configuration, pressure, and materials of construction. The flow/filtering capability is based on system requirements that are provided to the manufacturer.

A second, very important, design aspect of this component was the collapse rating of the filter element. Although the vendor provided an estimated collapse rating, we needed to establish this rating by testing. To collapse a filter element, the sintered media were coated with a high-quality household paint to fully plug the element. The element was then hydrostatically pressurized in the normal flow direction with the outlet of the filter open to ambient. A computer-controlled pressurization system was used to both control the pressurization rate and determine when the filter collapse occurred. Two filter elements were tested in this manner, and the lowest pressure at which collapse occurred was used to determine the collapse pressure rating for the filter. We used a factor of safety of 3 to determine the ratio between the pressure at which the element collapsed and the rated collapse pressure.

Oxygen compatibility was the final aspect of the design considered during validation. While significant test data demonstrate excellent oxygen compatibility for the Monel 400® alloys and Nickel 200 (commercially pure nickel), particularly in relation to burn resistance, little data are available for Nickel 200 in a sintered media form. The primary mechanism for igniting the sintered nickel element in this filter is by kindling chain. Kindling chain occurs when materials, such as debris trapped within the filter, combust and propagate to other materials in intimate contact with the combusting material.

We submitted samples of Nickel 200 sintered media for Promoted Combustion Testing to assess its propensity to sustain combustion in a kindling chain event. This testing

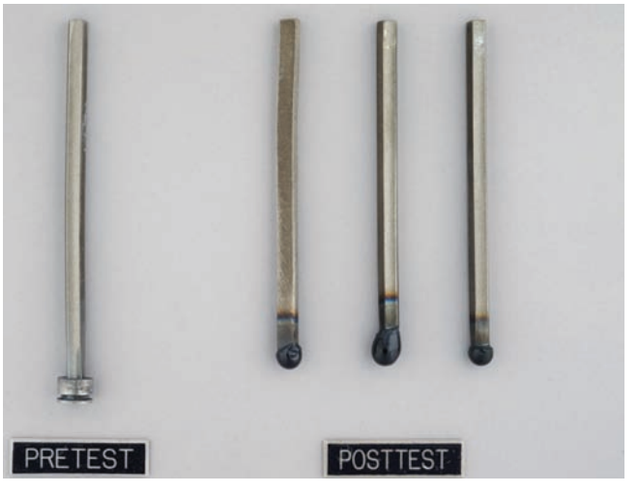

Fig. 3. *Tested samples pre- and posttest.*

is performed by initiating combustion of the test sample under pressure and monitoring its upward propagation. Increasing the test pressure helps us determine the threshold at which a given material will support combustion. Combustion in these Nickel 200 samples was not supported at pressures up to 10,000 psi, as seen in figure 3.

Other considerations

All filter elements must be cleaned at regular intervals. The length of these intervals, which is dependent on the use conditions, must be set short enough to avoid clogging and long enough to reduce maintenance costs. These intervals may also need to be adjusted over time based on the assessments performed at previous intervals. To better understand the maintenance requirements, we added a delta-pressure transducer to the pressure system to monitor the pressure drop across this component. In the event the delta-pressure exceeded pre-defined levels, this component would be removed and assessed. This transducer also provided a real-time assessment of the pressure system's health.

We also considered the specific process for cleaning these sintered elements. Unlike traditional mesh filter elements, sintered elements contain a high percent of entrapment areas due to the construction of the sintered media. These entrapment areas raise concerns for both entrapment of cleaning solutions and particulate. We therefore defined special procedures for cleaning these elements. Precautions such as the direction of flush, protection of the outlet side from contamination, and extend purges with elevated temperature bake-out were implemented to mitigate, or at a minimum reduce, concerns for entrapment.

Summary

Although it is often desirable to use commercial off-the-shelf hardware, there is occasion to design special components when system requirements eliminate off-the-shelf hardware from use. If designed correctly, these components can significantly improve the performance and/or robustness of a system. It is important in the design of these components to evaluate all issues relating to performance. In the case of this filter, we felt it was essential that a balance be found between mechanical function and oxygen compatibility.

Understanding Ignition of Oxygen System Components by Particle Impact

Joel M. Stoltzfus, *White Sands Test Facility*

Keisa R. Rosales, *White Sands Test Facility*

Fire hazards in oxygen-enriched environments have long been recognized as a significant threat to safe space flight and related ground support operations. NASA's history of fires in oxygen-enriched environments is significant and includes events such as the Apollo 204 command module fire (later renamed Apollo 1), in which astronauts Roger Chaffee, Gus Grissom, and Ed White lost their lives; and Apollo 13, in which the oxygen tanks were destroyed resulting in loss of the mission. In 1980, a fire in the 6,000-psi secondary oxygen pack plumbing destroyed a $3.4M extravehicular mobility unit intended for use in the Space Shuttle Program (figure 1).

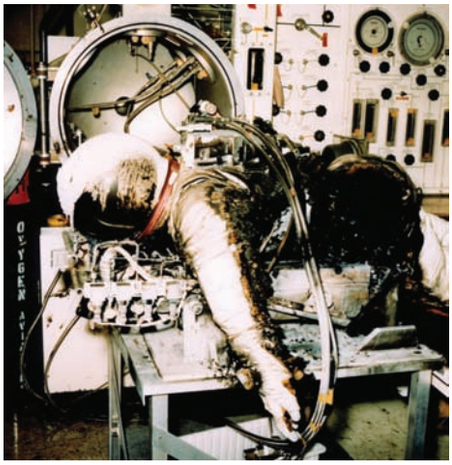

Fig. 1. *Extravehicular mobility unit destroyed in a fire.*

Because of these fire events, NASA has made a significant investment in understanding and controlling the fire hazards in oxygen-enriched environments. Test facilities developed at NASA White Sands Test Facility (WSTF) in the early 1970s perform hazardous tests using high-pressure oxygen. In the early 1980s, engineers at the NASA Lewis Research Center (later renamed NASA Glenn Research Center) became concerned that small, metal particulates borne in the 4,000-psi warm, gaseous oxygen in the shuttle Main Propulsion System (MPS) might cause a fire when they internally impinged the valve controlling oxygen flow to the external liquid oxygen tank. This particle impact ignition mechanism was reported in the open literature, but no specific tests or analysis had been performed on the shuttle MPS and the gaseous oxygen flow control valve (FCV). WSTF developed a particle impact test system and performed tests that produced a catastrophic fire in the shuttle MPS FCV (figure 2). As a result of this fire, the shuttle MPS gaseous oxygen FCV was redesigned using ignition and burn-resistant materials. The FCV in use today is not vulnerable to this ignition mechanism.

Fig. 2. *Fire in the space shuttle MPS flow control valve.*

Analysis of particle impact ignition mechanism

The particle impact ignition mechanism continues to be investigated at WSTF using analysis and testing techniques. WSTF has developed a protocol for analysis of valve components intended for use in oxygen systems: *Guide for Oxygen Compatibility Assessments on Oxygen Components and Systems* (NASA/TM-2007-213740). This guide for oxygen compatibility assessments describes the particle impact ignition mechanism as "heat generated when small particles strike a material with sufficient velocity to ignite the particle and/or the material." It further describes the characteristic elements necessary for ignition by particle impact as: particles that can be entrained in the flowing oxygen; gas velocities, typically greater than approximately 100 ft/s; and an impact point ranging from 45 deg to perpendicular to the path of the particle. It also indicates that test data show, in most cases, the particulate must be flammable to produce ignition of the target material.

Using this description of the particle impact ignition mechanism and the characteristic elements necessary for it to produce a fire event, an analysis can determine the likelihood of a particle impact fire. This analysis, of course, will make use of published WSTF particle impact test data.

To better understand the flow patterns inside oxygen system components, WSTF uses computational fluid dynamics computer software. This analysis technique enables engineers to visualize the velocity, temperature, and pressure fields inside components; to project the paths of particles carried along by the flowing oxygen; and, finally, to predict impact points within the component. This tool (figure 3) enhances WSTF's understanding of the particle impact ignition mechanism and enables WSTF engineers to design test programs to validate or nullify particle impact ignition hypotheses.

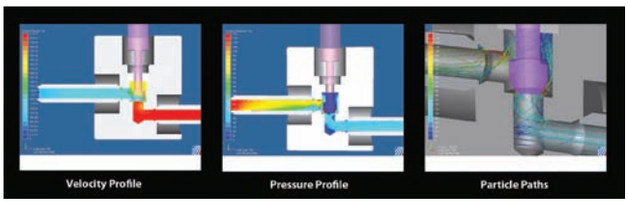

Fig. 3. *Outputs from a computational fluid dynamic calculation.*

Testing of particle impact ignition mechanism

Most recently, WSTF performed particle impact tests of the high-pressure oxygen valve shown in figure 4. This high-pressure, stainless-steel manual valve was impacted with a variety of particulate mixtures (Table 1) at temperatures ranging from 120°F to 150°F and at 4,000 psi inlet pressure. A pre- and posttest view of the valve is shown in figure 4.

Particulate Mixture	Material	Size and Configuration	Amount
A	316 SS	–60 mesh	100 mg
B	Iron	–60 mesh –50 + 100 mesh	100 mg (50 mg of each mesh)
C	Iron	–60 mesh –50 + 100 mesh	1,000 mg (500 mg of each mesh)

Table 1. *Particulate mixtures used for testing of a high-pressure, stainless-steel manual valve.*

We performed 300 tests using particulate mixtures A and B without igniting the valve. However, on the first test using particulate mixture C, a catastrophic fire resulted in destruction of the valve (figure 4).

A serious fire hazard related to particle impact ignition exists in oxygen-enriched atmospheres. WSTF engineers are actively studying this important ignition mechanism and making progress in understanding how to mitigate the hazards it poses. The state of the art is being advanced by WSTF's analysis and testing efforts. This information is continually being applied to NASA's current and future efforts to sustain safe space travel and ground support operations.

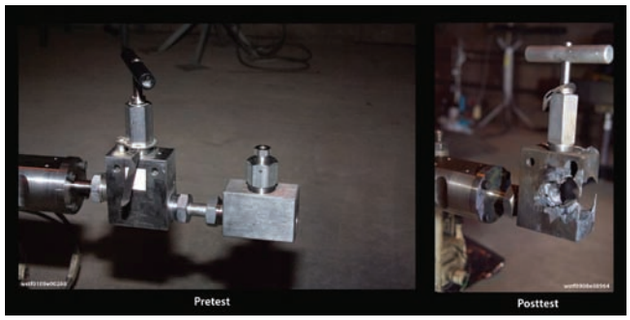

Fig. 4. *Pre- and posttest views of a high-pressure, hand-operated valve tested at 4,000 psi.*

Oxygen Compatibility Assessment Database Web Application

Stephen F. Peralta, *White Sands Test Facility*

Materials in human space systems are assessed for fire hazards as required by two NASA standards: NASA-STD-(I)-6001, *Flammability, Off Gassing, and Compatibility Requirements and Test Procedures*, and NASA-STD-6016, *Standard Materials and Processes Requirements for Spacecraft*. These standards reference a method for performing an oxygen compatibility assessment (NASA TM-2007-213740, *Guide for Oxygen Compatibility Assessments on Oxygen Components and Systems*). Hazards associated with the system and its components are identified and documented. Information needed to perform a compatibility assessment includes details on system components, configurations, and operating conditions. Material flammability, ignitability, and potential damage data are also used when assessing fire hazards. Currently, the Oxygen Compatibility Assessment Group at NASA White Sands Test Facility (WSTF) uses a database application to catalog and retrieve the wide variety of numerical data, explanatory text, pictures, and graphics that make up a properly documented assessment report.

Engineers at WSTF perform an increased number of oxygen compatibility assessments in conjunction with other NASA facilities. This collaboration reveals the need for engineers working at different NASA sites to have common access to the same compatibility information and assessment data. However, with the existing tools, only WSTF engineers can access report data for the assessment reports. To address this problem, WSTF developed the Oxygen Compatibility Assessment Database Web Application, a relational electronic database for performing oxygen compatibility assessments.

To make the WSTF Oxygen Compatibility Assessment Database Web Application a useful tool for engineers, one main requirement must be met: the report data for an assessment must be accessible by people at different locations. To solve this problem, we applied a two-layered, backend/frontend architecture (figure 1). Microsoft SQL Server® acts as the database management system to the backend of the application; it is responsible for storing the data and handling the different types of data requests. WSTF chose Microsoft SQL Server® because of its wide acceptance, availability, and robustness as a reputable and scalable database platform. The frontend of the application

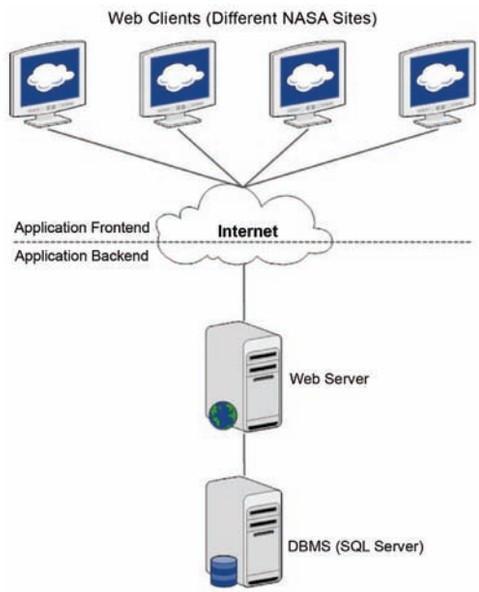

Fig. 1. *Backend/frontend architecture.*

is the user interface, where the user interacts with the data. In keeping with the goal of having an application accessible and usable by different engineers in different locations, the technology for the user interface should be readily and commonly available. The one piece of technology that meets these goals is a Web browser (client). A Web browser, regardless of operating system or computer manufacturer, is common to all computer platforms (figure 2). All clients (e.g., Internet Explorer, Firefox, etc.) use common "languages" to display and render information and data to the user. Any updates, bug fixes, or modifications to the application can be made without impact to the user – an advantage this model has over a stand-alone application. So a user would not be bothered with a request for updates or be concerned with backend compatibility issues. This is not the case if a stand-alone application model were used.

The backend uses a relational database with tables as the basis for modeling "real-world" data. In common database terminology, the columns and rows represent fields and records. Each table, or relation, represents a particular object or event (e.g., a compatibility assessment). However, any compatibility assessment is made up of many different parts, with some parts being related.

Having all of the information for many assessments in one table would make the database large and cumbersome, especially as the assessment database grows over time. Therefore, to model real-world data, a database must contain many different relations. By using relational database principals, a compatibility assessment is relatively easy to model and allows data to be queried and generated in various ways. The database provides a repository of all information used in hazards analyses, including drawings, materials data, and environmental information that can be used for future assessments. When performing a current compatibility assessment, users can quickly access all data and past assessments as a reference.

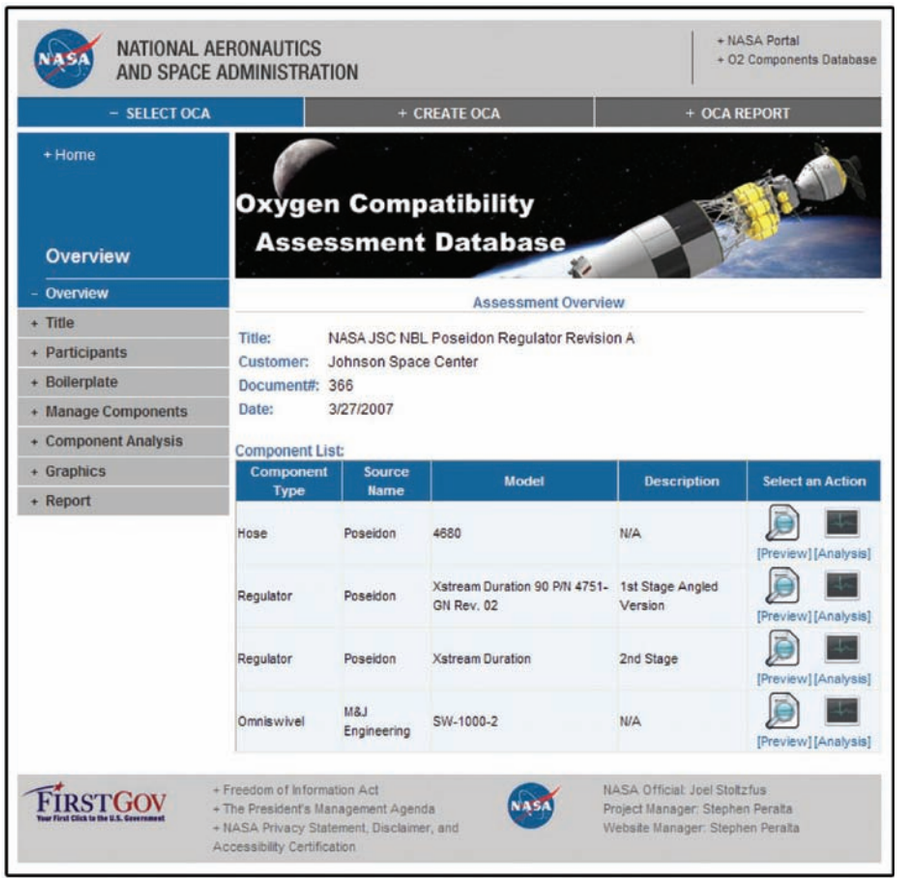

Fig. 2. *Oxygen Compatibility Assessment Database Website.*

The development and use of the relational Oxygen Compatibility Assessment Application makes performing oxygen compatibility assessments a very efficient process. Engineers executing analyses need only input the assessment data and information into the database, and the application provides a repository of information. The data-relational structure makes it easy to find answers to questions about the data by constructing and executing a simple query. New user interfaces can easily be constructed to handle greater amounts of data from a more complicated query, or to manipulate the data in other useful ways. Engineers can now quickly reference all data from past assessments as they meet requirements to develop new, accurately documented Oxygen Compatibility Assessments.

The following WSTF authors can provide access to the database: joel.m.stoltzfus@nasa.gov and stephen.f.peralta@nasa.gov.

New Methodology: Hazard Assessment Protocol for Aerospace Hydrogen Systems

Stephen S. Woods, *White Sands Test Facility*

Miguel J. Maes, *White Sands Test Facility*

The potentially hazardous environments associated with hydrogen use are controlled through fail-safe system design, operations reflecting best practices, and personnel training that instills a proper regard for safety given the physical, thermo-physical, and chemical properties of hydrogen. Hydrogen is useful in space flight because it is energetic; however, failure to manage it correctly may readily and rapidly produce hazardous conditions. One tool considered in the body of best practice is the use of hazard assessment to review systems and operations. Aerospace hydrogen systems follow hazard assessment practices consistent with standard industry, but must also consider a wide variety of hazards scenarios that arise in unusual or unfamiliar environments.

The NASA White Sands Test Facility developed a new and comprehensive approach to hydrogen hazard assessment. The Hydrogen Hazard Assessment Protocol (HHAP) contains a wealth of information about hydrogen, its qualities and properties, and associated elements for system controls including hardware, intrinsic design, and operational controls. Useful hazards information is provided with procedures to help with hazards considerations. The HHAP addresses hydrogen system design, system and safety engineering, and facility management as practiced in industry – including the aerospace industry – and accords with the requirements and guidelines in the ANSI/AIAA [American National Standards Institute/American Institute of Aeronautics and Astronautics] G-095-2004 *Guide to Safety of Hydrogen and Hydrogen Systems*. Eventually, the procedure will be published through the AIAA and managed as a voluntary consensus document.

HHAP is intended for application to any facility, system, equipment component, or process that involves hydrogen and to the hazards associated with the presence of hydrogen. It is intended to encompass, yet be flexible enough to accommodate, the wide range of applications that can be encountered in hydrogen use: from a large missile launch complex to a small experimental laboratory, and from a large liquid hydrogen production facility to a fuel-cell-powered vehicle in anyone's garage. It can be applied to government as well as to industrial facilities. The HHAP provides a simple procedure for an application that involves minimal hazards, yet is sufficiently complete to provide a critical examination of an application that involves significant hazards. Its purpose remains the same – to protect the workers, the public, equipment, facilities, investments, the mission, and the environment from injury or damage.

The HHAP provides a thorough background of hydrogen physical behavior, hazardous release scenarios, potential hazards without ignition, and combustion hazards. Unique aspects of aerospace hazards assessment are discussed in the HHAP. The assessment approach is adapted to the characteristics of hydrogen and includes the special challenges posed by its behavior. Evaluation for undesired release or entrainment of hydrogen addresses types of releases at ambient and cryogenic temperatures and sub-atmospheric environments, and includes a discussion of confinement geometry. Assessment of combustion considers the effects of flammability, ignition, confinement, and detonation. The HHAP is intended to be an integral tool for risk management.

In any application, hydrogen is controlled within a volume by a combination of elements that includes active engineering control devices, sensors, and passive engineering controls such as inherently safe design or exclusion zones, as well as by operations subject to administrative controls (figure 1). Central to the HHAP analysis approach is the concept that hazards are not intrinsic to hydrogen itself, but arise through the interaction of the elements of control with the hydrogen. Hence, analysis must consider the volume in which the hydrogen is controlled and all elements of control together. This concept is illustrated in the HHAP with diagrams and examples.

We present logically the methodology for hazards assessment protocol; and we provide charts, tables, and forms with useful examples. The HHAP guides the hydrogen user through assessment and documentation of the following major steps:

Identification of volumes for analysis

Assessment of factors/potential causes that might contribute to an unintended release

Evaluation of characteristics of the release within the volume

Determination of potential hydrogen behaviors arising from the release

Evaluation of consequences and associated risks

Recommendations for mitigation

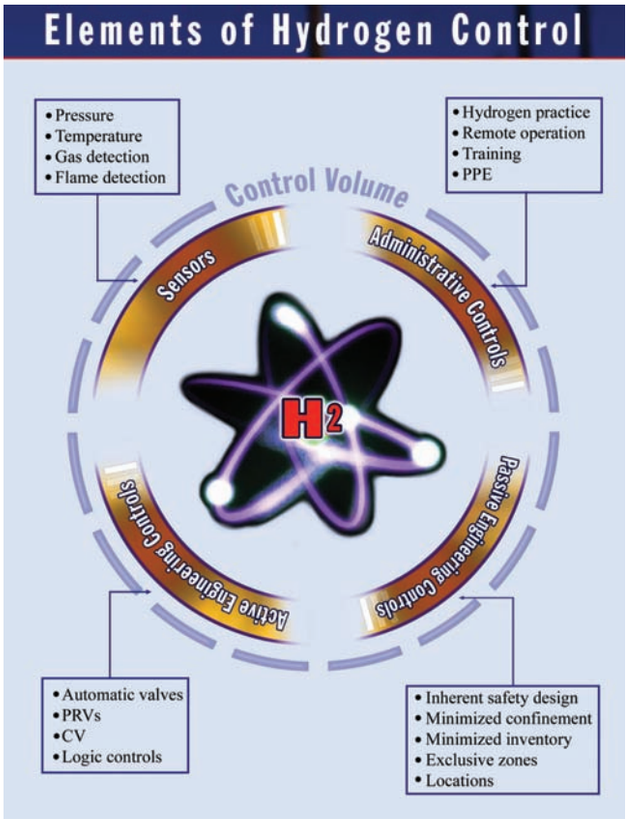

Fig. 1. *Operations subject to administrative controls.*

As an example, the volume analysis flowchart (figure 2) provides an overview of the relationship between analysis of hydrogen volumes and elements, and identification of causes. Analysis findings (Step 3, figure 2) are documented in a Hazard Control Table, an example of which is included in the HHAP. Incremental step-by-step analysis begins with the first volume prioritized for analysis. The first stage (Step 1) of the assessment process entails laying out a strategy for analysis. It is understood that the system may represent a material, a component, a multicomponent device, a facility, or whatever is appropriate for consideration. No one best strategy covers all systems; the HHAP incorporates several strategies in combination. A top-down approach identifies the largest volumes, greatest exposures, or other attributes that point to the worst case; analysis can then bore in to examine smaller volumes that may contribute to the hazard. Alternatively, a bottom-up approach sequentially considers all volumes from the point of hydrogen inventory through the system component by component, then examines volumes adjoining or surrounding the system components until the largest volume or exposure has been considered.

Resource requirements to conduct a hazards analysis using the HHAP depend on system complexity. Current experience suggests that a single component requires 1 day or less, but systems and facilities can take anywhere from 1 week to 1 month, depending on complexity. Complex systems require thorough advance preparation to keep the work group focused and working effectively.

This recommended practice conveys a flexible approach that can be applied to a variety of hydrogen systems at the component level (e.g., valves, instrumentation, connectors, and tanks); system level (e.g., fuel cells, electrolyzers, thrusters, storage systems, and transfer systems); and facility level (e.g., test, storage, and dispensing facilities and remote or auxiliary power systems).

Industry can directly apply the HHAP approach to aid in the development of commercial and transportation hydrogen technologies. Hazards analysis results can be used to help prove code compliance and ensure that liability issues have been addressed. The HHAP may eventually become accepted as state-of-the-art in liability cases. Through management by AIAA, a voluntary standards organization, HHAP may ultimately be used in the evaluation and certification of commercial hydrogen systems.

New Methodology: Hazard Assessment Protocol for Aerospace Hydrogen Systems

continued

The use of this approach to conduct hazard analyses of various hydrogen systems has shown the need for data that are not available, especially combustion and hydrogen embrittlement data. While basic data exist for ambient conditions, more information is needed for hydrogen mixtures at low and elevated pressures. A full evaluation of detonation initiation and some failure modes of electrolyzers requires more information. Finally, basic microgravity combustion data are needed for the aerospace community. When an analysis is challenged by incomplete information, the HHAP provides some examples for strategy to accomplish the hydrogen hazards assessment.

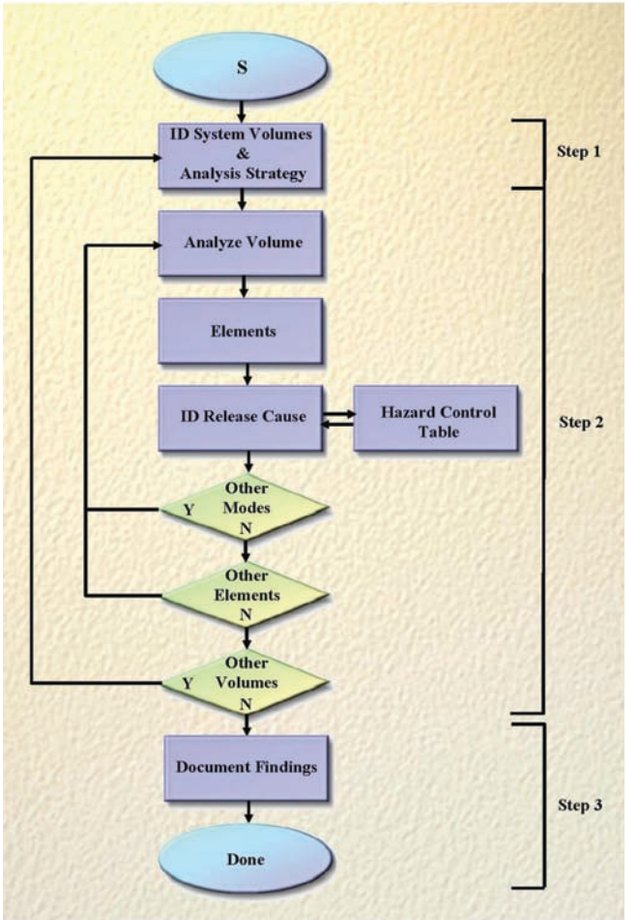

Fig. 2. *Volume analysis flowchart.*

Evaluation of Spacecraft Materials Flammability for the Constellation Program

David B. Hirsch, *White Sands Test Facility*

We must accurately predict spacecraft materials flammability because of the potentially steep penalties for incorrect assumptions. Correlation of ground 1g materials flammability test data with real-life spacecraft conditions rely on many assumptions. As we look to the future of long-duration space missions, those assumptions are challenged. On long space missions such as for the Constellation Program, fire safety design must take into account unexpected events and changes in environment conditions.

Some emergency events may result in pressure loss and ensuing oxygen enrichment. Examples include depressurization of the crew module (CM) caused by micrometeoroid impact, failed hatch or valve seal, or unforeseen leaks; nitrogen loss due to impact damage or leakage; emergency procedures to enable rescue of a distressed extravehicular activity; and venting the environment to control a spacecraft fire. Many other unexpected circumstances could challenge the space system fire safety design boundaries, such as Environmental Control and Life Support System malfunction or human error when using flammable materials.

A realistic evaluation of fire safety factors for space travel could be possible if rigorous correlations are established between 1g materials flammability qualification tests and data obtained in the ventilated microgravity environments of space systems. Most flammability testing, however, occurs on the ground. One disadvantage of ground testing, even in the anticipated "worst-case" environment per *Upward Flame Propagation Test Document* (NASA-STD-6001 Test 1), is that the qualitative nature of the pass/fail data does not correlate with microgravity data. However, evaluation of extinction boundaries does allow correlation with real-life spacecraft conditions.

NASA White Sands Test Facility (WSTF) proposed materials selection is based on extinction boundary, and is the focus of recent testing.

The Orion system design anticipates situations of varying pressures and oxygen concentrations. The present Orion Crew Exploration Vehicle CM plan is to operate in an atmosphere containing a maximum of 24.1% oxygen at 14.7 psia for missions to the International Space Station, and up to 30% oxygen at 10.2 psia for lunar missions. When the Orion CM returns to Earth, a snorkel device will be activated after splashdown to provide outside air to the crew; however, it is desirable to maximize the time the crew is able to breathe cabin air before the snorkel device is activated. To do so, scientists proposed to raise the oxygen concentration in the CM immediately before re-entry while maintaining the cabin pressure at 14.7 psia. Therefore, NASA needed to determine the oxygen concentration at 14.7 psia where the materials, found acceptable from a flammability point of view in 30% oxygen at 10.2 psia, would still be nonflammable.

WSTF established total pressure-oxygen concentration extinguishment limits to determine safe oxygen concentration levels at increased pressures that will result in extinguishment, even for materials that marginally pass the NASA Standard Test 1 certification requirements. Test results show that the effect of pressure on the oxygen concentration flammability threshold is strongly material dependent (figure 1). In the range of 7 to 17.3 psia, the

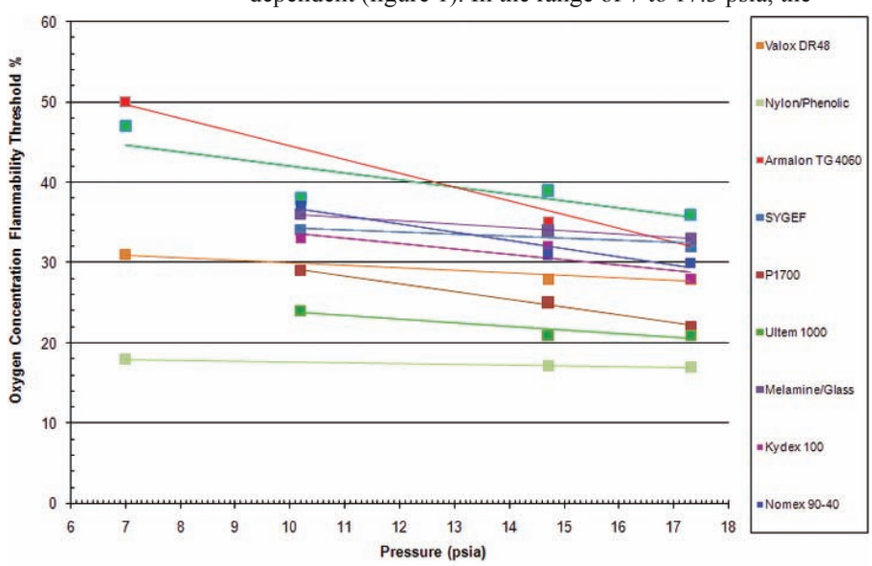

Fig. 1. *Maximum oxygen concentration flammability limits of materials at various total pressures.*

Evaluation of Spacecraft Materials Flammability for the Constellation Program

continued

oxygen concentration flammability threshold shows a near-linear dependence on total pressure, a finding that confirms previous data. Test results indicate that the oxygen concentration for the Orion CM at 14.7 psia cannot be set higher than 25.6% without invalidating the materials flammability certification for some materials established by NASA Standard Test 1. Data also indicate that materials certified in 30% oxygen at 10.2 psia would still be self-extinguishing in ambient air at 17.3 psia, the pressure intended to leak-check the CM.

To minimize the uncertainty of evaluating pressure-related effects on the oxygen concentration flammability threshold, we recommend that flammability threshold testing for Constellation materials be conducted at 14.7 psia, the highest operational space systems pressure. To determine the confidence intervals for the data, a study characterizing the precision of the proposed method would be advantageous.

WSTF's extinction boundary approach was followed by the NASA Glenn Research Center for tests performed in ventilated microgravity environments. Preliminary results on thermally thin fuels indicate that in certain ventilated environments, the fuels burned in microgravity at lower oxygen concentrations than they did using the NASA Standard Test 1 protocol. Further studies will be conducted to determine proper flammability safety factors for adequate selection of aerospace materials. Included on the horizon are plans at WSTF to conduct more studies of flammability thresholds at various pressures and in microgravity, lunar, and martian reduced-gravity environments under both stagnant and flowing conditions.

Evaluating the flammability threshold allows the option of selecting better, or best, aerospace materials as opposed to just "acceptable" aerospace materials from a flammability point of view. The net result will be an increase in space systems fire safety.

For more information and a fully referenced paper on this subject, see "Some Aspects Related to the Assessment of Space Systems Materials Flammability" by Hirsch et al., in *Proceedings of the 3nd IAASS Conference "Space Safety in a Global World,"* Rome, Italy, October 2008.

Determining the Time for Oxygen-exposed Materials to Return to Reduced Flammability

Susana Harper, *White Sands Test Facility*
David B. Hirsch, *White Sands Test Facility*
Sarah R. Smith, *White Sands Test Facility*

Catastrophic fires have occurred as a result of gaseous oxygen enrichment, even in low-pressure environments. Risk for localized oxygen-enriched areas can occur when textile and foam materials become saturated in enriched oxygen, making them more flammable and easier to ignite. Materials can also serve as barriers by trapping localized oxygen-enriched environments.

When materials are moved from a higher oxygen concentration environment to one with lower oxygen concentration, the corresponding flammability and ignitability risks are difficult to characterize. An industrial example of such a scenario would occur when a person performs liquid-oxygen-filling operations and is exposed to a high amount of oxygen vapor. An aerospace example would be when an astronaut completes an extravehicular activity performed in 100% oxygen and then moves into a spacecraft with a lower (e.g., 34%) oxygen concentration. In these scenarios, it is not known how long it takes for a person's garments to return to the normal flammability and ignitability expected in the lower oxygen concentration. Historically, the generally accepted rule of thumb has been to allow 30 minutes for diffusion to reduce oxygen concentrations. This rule of thumb is not based on data and could result in significant time lost, particularly in the case of an astronaut moving back and forth between different environments.

The NASA White Sands Test Facility developed a test methodology and conducted tests to relate oxygen permeation with the flammability of materials exposed to high levels of oxygen. This study examined two scenarios: (1) material *saturation* from exposure to oxygen-enriched environments, and (2) oxygen *entrapment* when materials function as a barrier to create localized high oxygen concentrations, particularly oxygen trapped between a material and a person's body.

NASA developed a list of realistic and applicable materials for testing. Thirteen materials were chosen and grouped into categories by function (extravehicular mobility unit materials, advanced crew escape suit equipment, cabin environment materials, and common/comparison fabrics). These materials were tested in their use thickness.

In both entrapment and saturation scenarios, when a material moves to a lower oxygen concentration environment, oxygen concentration decreases as a result of diffusion over time and flammability decreases correspondingly. The test methodology characterized flammability as a function of time, thereby relating flammability to the permeation of oxygen in entrapment and saturation scenarios. A two-phase approach consisted of permeability testing and flammability testing.

For the permeability phase, we used oxygen transmission rate data to perform calculations determining the time for materials to return to reduced oxygen concentrations. The permeation tests were performed per ASTM [American Society for Testing and Materials] F1927, *Standard Test Method for the Determination of Oxygen Gas Transmission Rate, Permeability and Permeance at Controlled Relative Humidity through Barrier Materials Using a Coulometric Detector*. This test method determines the transmission rate of oxygen gas at steady-state conditions at a given temperature and percent relative humidity. We conducted testing at conditions expected during use. The relationship between the oxygen transmission rate (absolute flux) and the concentration gradient is described by Fick's First Law of Diffusion when describing a steady-state stationary medium. Absolute flux can further be correlated with total amount of permeant.

The scenarios in question are not steady state due to their dependence on time for atoms to equilibrate from one region to another. Nonetheless, they can be evaluated at discrete time steps, each of which can be considered steady state. We used this method to determine the time needed for materials to return to reduced oxygen concentrations. For saturation scenarios, materials were assumed to be filled with oxygen. The extent to which a material can absorb a gas depends on the solubility of that gas in a solid. This relationship was used in conjunction with Fick's laws of diffusion in calculations of concentration decay.

The flammability phase of testing determined the maximum oxygen concentration (MOC) flammability limits for each material using NASA-STD-6001A Test 1 methodology. The test setup was a modified NASA-STD-6001A Test 1 configuration (figure 1) in which we performed non-edge ignition to better simulate a realistic ignition scenario. We conducted testing at a single worst-case pressure of 101 kPa (14.7 psia), while we varied the

oxygen concentration to determine the flammability MOC threshold. The MOC threshold established for each material is the desired oxygen concentration below which a material will have reduced flammability (i.e., safe for unrestricted use and continued operation).

Once MOCs were determined and environments defined, we performed permeation rate calculations to determine the time required for each material to reach the MOC. Because porous materials exhibit diffusion rather than permeation, we used natural oxygen diffusion coefficients in calculations for porous materials, and we did not generate permeability data.

Analysis and correlation

The two scenarios examined were oxygen entrapment (as found between clothing and a person's body) and saturation of the material (common for cabin insulation and other materials exposed to an oxygen-enriched environment). Note: The proposed scenarios are meant to model only typical real-life situations. Data should therefore be used as an order-of-magnitude approximation for time in similar situations with similar materials.

The entrapment scenario assumed 100% oxygen contained in 1-cm depth behind permeable material, and a well-mixed environment of 20.9% oxygen outside the barrier. Calculations ascertained how well each barrier material "trapped" oxygen and determined the oxygen-concentration decay in the confined area with time. Table1 shows the amount of time each material needed to reach the MOC threshold. We assumed diffusion through all porous materials to be the same; the only variation was thickness. The time to reach decreased flammability for the thinnest to thickest porous materials tested ranged from 0.026 to 1 second.

The saturation scenario concerned larger, bulkier materials, as such materials hold the largest quantity

Material	Thickness (m)	MOC (%)	Time (t) to MOC or ambient (hr:min:sec)
Entrapment Scenario			
Tiburon® surgical microfiber composite drape (to 20.9)	0.00022	20	05:10:01
Spandex-covered Viton® (Mosite) fluoroelastomer closed-cell foam (to 20.9)	0.00794	18	447:18:21
ACES O_2 hose (silicone, stainless steel, Nomex®)	0.00567	49	11:55:00
Minicel® polyethylene closed-cell foam (to 20.9)	0.05100	20	36:55:01
Minicel® polyethylene closed-cell foam with Nomex® covering	0.05169	28	13:34:59
Zotek® F-30 PVDF closed-cell foam	0.0254	36	04:49:00
Saturation Scenario			
Spandex-covered Viton® (Mosite) fluoroelastomer closed-cell foam (to 20.9)	0.50	18	10,000:00:00
Minicel® polyethylene closed-cell foam (to 20.9)	0.50	20	3,050:00:00
Minicel® polyethylene closed-cell foam with Nomex® covering	0.50	28	350:00:00
Zotek® F-30 PVDF closed-cell foam	0.50	36	121:00:00
Pyrell® polyurethane open-cell foam (to 20.9)	0.50	19	00:02:10

Table 1. *Permeable materials oxygen permeation to low-flammability conditions*

Fig. 1. *Modified NASA-STD-6001A Test 1 on ACES layup.*

of oxygen. We assumed that cubes of bulk materials 0.5-m long have solubility equal to that of oxygen in rubber at 298 K. Each material was initially saturated in 100% mole fraction of oxygen.

Conclusions and future work

Our two-phase methodology succeeded in correlating time required for exposed materials to return to reduced flammability, and is recommended for future use in examining flammability risks for localized, oxygen-enriched environments. Validation testing will consist of burning materials at time intervals after removal from 100% oxygen environments, and correlating burn lengths and burn rates to known concentration testing.

Data show that oxygen entrapment and saturation is a concern, especially when dealing with nonporous materials. For porous materials, the 30-minute rule of thumb is overly conservative: an entrapped oxygen concentration will equilibrate with the new environment in a matter of seconds, and even large, bulky saturated porous material will take only a few minutes. In contrast, nonporous materials can trap and retain oxygen for many hours. In these cases, the 30-minute rule of thumb may not be sufficient. The risks must be weighed to not overly restrict operations while not ignoring increased flammability. Localized, enriched-oxygen concentrations should be considered in operational planning, especially as more closed-cell foams are used (e.g., Mosite in the astronaut liquid-cooled ventilation garment). Although these foams exhibit superb properties for use, they provide formidable barriers for oxygen permeation and act as retainers of oxygen saturation.

Redesign of Promoted Combustion Test System: Inductance Canceling Feedthrough for Pressurized Systems

Kyle M. Sparks, *White Sands Test Facility*

Promoted combustion testing *Upward Flammability of Materials in GOX* (NASA-STD-6001, Test 17) is a standard test used to determine the flammability of metals in oxygen-enriched environments. In this testing, a metal rod of 0.318 cm (0.125 in.) diameter is forcefully ignited at varying test conditions and determined to be flammable or nonflammable. Traditionally, the test is performed with samples at ambient temperatures; however, elevated temperature testing has become of interest. We have proven that the temperature of a metal has an effect on its flammability, and elevated temperature testing is now being incorporated as a standard test parameter.

There are several approaches to heating test samples. A heating method developed by the NASA White Sands Test Facility (WSTF) in the early 1990s used an induction heater with a water-cooled coil fashioned from copper tubing; however, test pressures were limited due to the collapse pressures of the tubing. With advances in induction heater technology and with proper feedthrough and temperature control design, solid induction coils are now feasible to use, and test systems can be operated at pressures up to the maximum allowable chamber test pressures – in WSTF's case, 10,000 psi.

We overcame three major hurdles in the redesign of the heated promoted combustion test system: (1) designing an inductance-canceling induction coil feedthrough (ICF), (2) configuring an induction coil that uniformly heats a test sample rod, and (3) cooling the induction coil leads outside the test chamber. This report focuses on the design of the inductance-canceling feedthrough for pressurized systems.

When induction heater leads are oriented parallel to each other, a magnetic induction field is created. Metals within that induction field can potentially be heated. As parallel leads penetrate a pressure vessel, the metals surrounding nonmetallic seals and/or the induction leads themselves can heat to temperatures that can compromise the seals in contact with the metals, leading to pressure failures. We needed an ICF that would not heat surrounding metals, or "self-heat," to a large degree.

Using coaxial leads is one way to reduce the magnetic field energy around the outside of the leads. Theoretically, the field reduces to zero at this point; however, a field still exists within the coaxial feedthrough. Figure 1 shows the geometry and materials of construction of the coaxial feedthrough. Since induction heaters primarily heat metals, it was important to use fully nonmetallic seals.

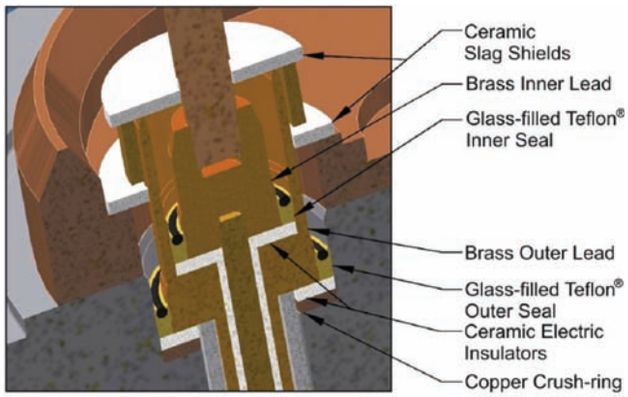

Fig. 1. *Coaxial feedthrough geometry and materials.*

We used glass-filled Teflon® pressure-activated seals with nonmetallic spring energizers for both the inner and the outer seals of the feedthrough. These seals have a working temperature up to 316°C (600°F). Ceramic slag shields keep any burning debris from contacting, and thereby failing, the seals during testing. Ceramic electric insulators must also be sized appropriately to ensure that an arc between the inner and the outer leads cannot occur.

We validated this design by testing. We placed thermocouples on various surfaces within the chamber (figure 2). The system was designed to heat a test sample via a closed-loop thermocouple attached to the upper end of the sample. We then set the desired sample temperature at the control console, based on sample temperature feedback, so the induction heater would power on and off to meet and maintain the temperature.

Technicians pressurized the test chamber to the desired test pressure using nitrogen, and the desired sample temperature was set to 704°C (1,300°F). When the sample reached its maximum temperature, we recorded data for all thermocouple channels at a 5-Hz rate for a minimum of 45 seconds. Scientists then analyzed the data and reported maximum values. Results of this can be seen in Table 1. Maximum sample

temperatures were slightly below the desired value of 704°C (1,300°F), as this was the initial testing on a redesigned system and small calibrations were needed.

The highest temperature around the seals was 81°C (177°F), far below the 316°C (600°F) maximum working temperature. These data show that the inductance-canceling feedthrough does a sufficient job of canceling any unwanted inductance that could lead to heating of the feedthrough and subsequent failure of the seals, while maintaining desired test sample temperatures. Applying the theory of coaxial cancellation proved to be a very successful method of introducing an induction heating coil into a high-pressure test system.

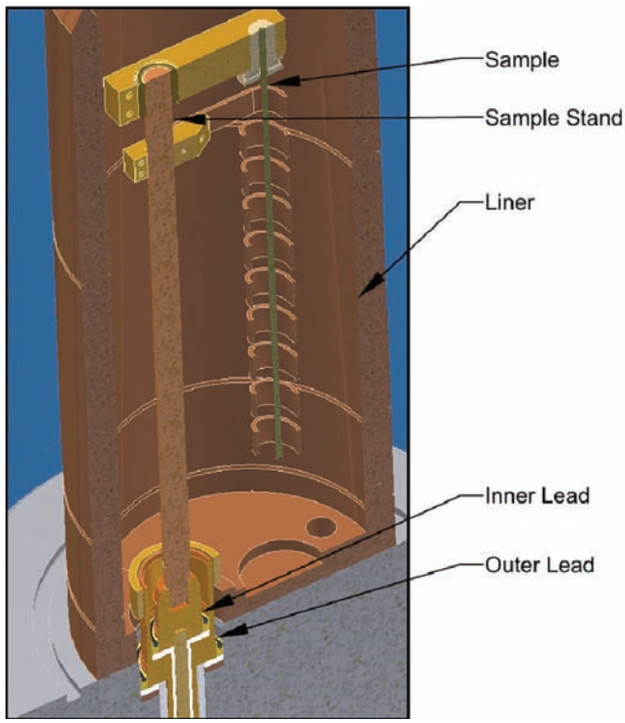

Fig. 2. *Placement of thermocouples within chamber.*

Pressure (psi)	Maximum Temperature (°F (°C))				
	Sample	Inner Lead	Outer Lead	Liner	Sample Stand
Ambient	1,228 (664)	139 (59)	112 (44)	91 (33)	139 (59)
250	1,215 (657)	137 (58)	96 (36)	92 (33)	146 (63)
1,000	1,205 (652)	154 (68)	98 (37)	102 (39)	174 (79)
5,000	1,184 (640)	154 (68)	101 (38)	104 (40)	152 (67)
10,000	1,167 (631)	177 (81)	106 (41)	109 (43)	143 (62)

Table 1. *Maximum temperatures within test chamber.*

Innovative Thermal Measurement Techniques for Y-shaped Primer Chamber Assembly Pyrotechnic Valves

Stephen H. McDougle, *White Sands Test Facility*

Several unique measurement techniques were developed at the NASA White Sands Test Facility in support of NASA's Conax® Pyrotechnic Valve Failures Investigation. This report discusses two techniques developed to measure the thermal environment at the pyrovalve booster interface: comparison of thermocouple (TC) and optical pyrometer thermal measurements, and use of an optical pyrometer method with a sapphire viewport.

The pyrovalve under investigation uses a Y-shaped primer chamber assembly (Y-PCA) design (figure 1). Two NASA standard initiators (NSIs), one on each branch of the Y, provide redundancy. Either one of the two NSIs is sufficient to ignite the booster, which then provides the force to drive the ram. The booster, essentially a small container made of 76-µm (0.003-in.)-thick stainless steel, contains a pyrotechnic charge that produces a relatively large amount of gas when ignited.

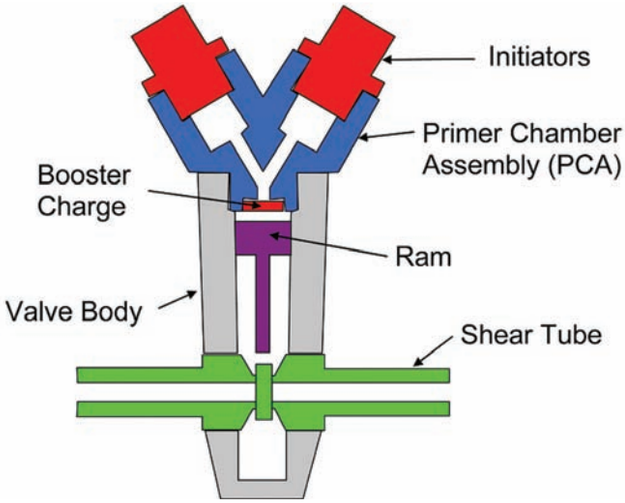

Fig. 1. *Conax® Y-PCA pyrovalve.*

We evaluated the two measurement techniques for characterizing the thermal environment in the booster area for both single and dual simultaneous NSI firing situations.

Comparison of thermocouples and infrared pyrometers

We selected fine-wire TCs and high-speed optical infrared (IR) pyrometers to measure temperatures on the underside of the booster's top cover. Both techniques were used previously, but this test compared temperature readings from the two methods at very high rates of temperature increase.

Technicians made inert boosters with thermal and mechanical properties to match the actual live boosters. The test articles consisted of a booster case with two fine-wire TCs welded onto the underside of the stainless-steel cover. To improve the structural stability of the booster top during the firings, an insulation disk filled the gap under the top of the booster case. An inert filler took the place of the pyrotechnic material inside the booster case. The TC leads were routed through this inert material and connected to the instrumentation system.

We installed the instrumented, inert boosters in a holding fixture such that a laser could be focused on the top cover. The laser provided the rapid heating necessary for the test. Two high-speed optical pyrometers were positioned to monitor the temperature from the front of the instrumented inert boosters.

Personnel encountered several difficulties with this test. One was ensuring that the TCs and the pyrometers were aligned with each other and with the laser-heated hot spot. The exact positions of the TCs could not be seen because of the filler in the booster case, so their positions had to be estimated when aligning the laser. Aiming the two optical pyrometers toward the exact spot illuminated by the laser was also difficult, and perfect alignment with the laser was hard to determine. Furthermore, any change in emissivity of the cover would affect the temperature indicated by the optical pyrometer, and any deflection of the cover could change the alignment slightly. The two pyrometers had different detection ranges, and neither would provide data below its lower limit. Despite the difficulties, we achieved fairly close agreement between the two methods. As shown in figure 2, an initial ramp-up rate of approximately 1,420°C (2,588°F) per second was reached. The maximum temperatures were approximately 370°C (698°F) for TC 1, 390°C (734°F) for both pyrometers, and 425°C (797°F) for TC 2.

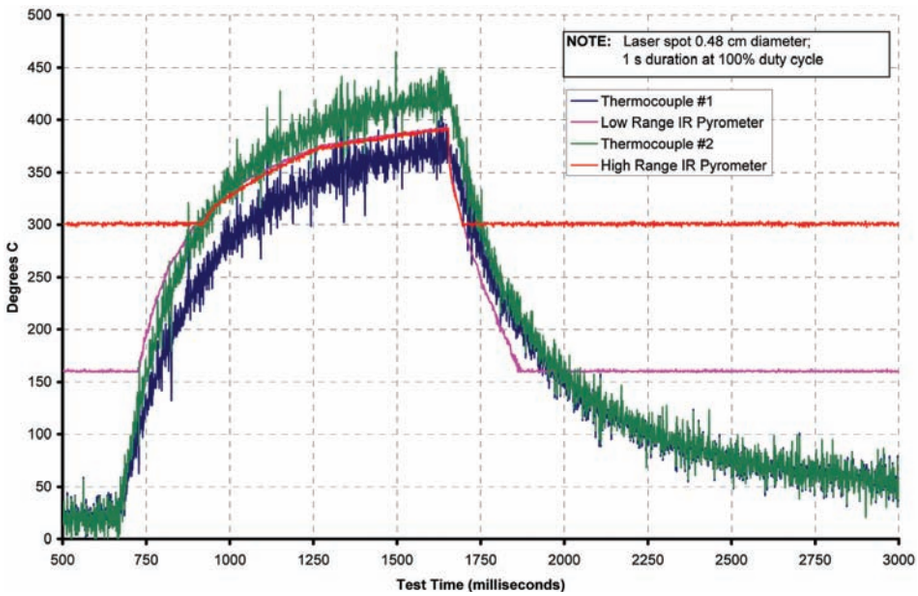

Fig. 2. *Response of TCs and IR pyrometers to rapid heating of an instrumented inert booster.*

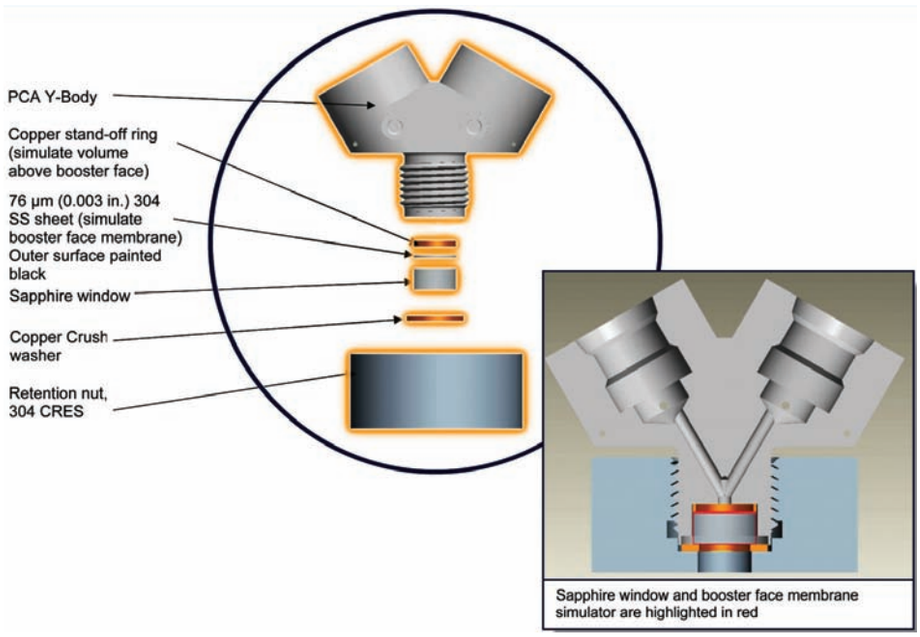

Fig. 3. *Exploded view of sapphire window assembly.*

Optical pyrometer method with sapphire viewport

This method used an optical pyrometer to measure the temperature in the booster cover. To apply the optical pyrometer method, we needed a new design for the Y-PCA test fixture (figure 3). This new design used a stainless-steel membrane to simulate the typical booster cover used in the Y-PCA pyrovalve application, similar to the one described in the previous technique. This cover was held in position and sealed with a copper standoff ring. A viewport, made from industrial sapphire, was installed underneath the sheet metal insert to provide viewing and necessary structural support and to allow the IR pyrometers to measure the temperature of the underside (propellant interface) of the simulated membrane. Sapphire is highly transparent to IR in the desired wavelength.

Through the sapphire viewport, a high-speed Phantom® video camera and a high-speed optical pyrometer recorded video and temperature on the back side of the simulated booster cover. The back side was painted black to provide a surface of known emissivity. Pressure transducers were installed in both Y-PCA NSI cavities.

We performed five dual- and three single-fire tests. It was important to maintain a seal around the stainless-steel membrane (booster cover simulator) and the sapphire window. The second dual-fire test was invalidated due to a leak (apparent from the video), which indicated much more flow and lower pressure in the NSI cavity on one side of the Y-PCA. However, this test did indicate that higher interface temperatures result from additional flow, agreeing with the overall test results. Booster interface temperatures for the dual fire series, excluding the second test due to the leakage, ranged from less than 150°C (300°F) to 383°C (721°F). Dual-fire test 5 resulted in a booster interface temperature of 603°C (1,117°F), but this appeared to be caused by burn-through that occurred very late in the event. Booster interface temperatures for the single-fire series ranged from 274°C (525°F) to 677°C (1,250°F). Posttest examination of the test articles revealed significantly more melted metal for the single NSI firings than for the dual simultaneous firings.

Analysis of a Pyrovalve Firing: Estimating Pyrotechnic Reactions

Stephen S. Woods, *White Sands Test Facility*
Christopher P. Keddy, *White Sands Test Facility*
Howard Julien, *White Sands Test Facility*
Regor L. Saulsberry, *White Sands Test Facility*

The NASA White Sands Test Facility has developed a computational modeling technique that uses a thermodynamic equilibrium code to assist in evaluating experimental data taken in the harsh environments created by combusting pyrotechnics. One such environment ensues when a NASA standard initiator (NSI) is fired into a narrow aluminum channel as part of the pyrotechnic chain in a pyrovalve.

To ensure pyrovalve discharge, a redundant pyrotechnic chain featuring two NSIs in parallel with a booster charge may be used. A common configuration takes the form of a "Y," where the fiery output from each NSI is directed through channels that lead to a chamber at the base of the "Y" into which a booster pyrotechnic charge is attached (figure 1). The pyrovalve design uses a Y-shaped primer chamber assembly, usually referred to as a Y-PCA. The booster, when ignited, generates gas that drives the cutting ram of the pyrovalve. Different firing sequences may be used so that one or both of the NSIs are ignited.

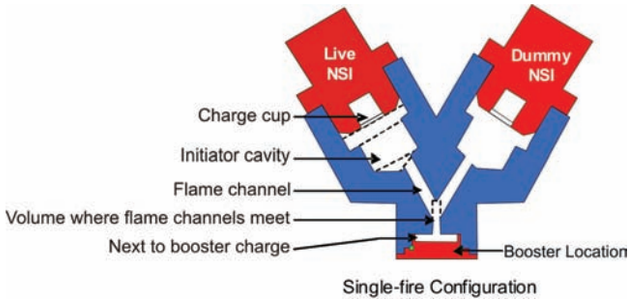

Fig. 1. *Cross section of the Y-PCA pyrovalve showing the various volumes.*

Study of system performance shows that the time to ignition of the booster is variable, the types and amounts of energies needed to ignite the booster propellant are not well understood, and it is unclear what system variables are responsible. In some instances, initiation of a single NSI has inadvertently caused the firing of the second NSI. We analyzed a pyrovalve firing to identify thermal and chemical processes leading to booster ignition to better understand this energy transfer process. Basic questions driving the investigation revolved around whether the booster propellant was directly ignited by penetration of driven materials or heated above the autoignition temperature. Physical observations, posttest metallurgical analyses, and in-situ temperature measurements were difficult to interpret. However, recessed pressure gauges showed reliable time-dependent behavior.

To develop an understanding of temperature behavior in the pyrovalve environment, we applied the notion that if the state of the pyrotechnic reaction products could be computed, knowledge of two state variables could allow determination of other state variables. The system of the reaction products is distinguished as separate from the fixture and booster, the environment into which energy from the reaction is lost. Pressure is the state variable that is measured; for each time a measurement is captured, the state of the reaction products, including the enthalpy, can be evaluated. The total energy of the pyrotechnic propellant and the volume into which it burns, or energy density, are also known at the start. From measurement to measurement, the loss of energy to the "environment" can be noted. For each new state, a temperature can be computed. We achieved this approach by using the NASA-developed chemical equilibrium with applications, a thermodynamic equilibrium code, and by keeping track of the energy lost to the environment.

Chemical equilibrium with applications calculations applied to propellant combustion

Combustion products interact with the cavity's internal surface. The reaction products partially pressurize the initiator cavity and rapidly flow through the flame channel to the booster cavity. This flow pressurizes the remainder of the Y-PCA. Depending on the test configuration (single- or dual-fire) and the amount of propellant, pressurization reaches different levels at different times. During the pressurization period, heat is also conducted to the surroundings. The release of energy by the chemical reaction occurs very rapidly: 10 to 20 µs (short compared to the 1 to 4 ms to heat and pressurize the entire Y-PCA system).

The amount of zirconium potassium perchlorate (ZPP) combusted for a specified Y-PCA volume represents a confined system that has a constant, common pair: internal energy and specific volume (density). This in turn determines the other states (e.g., temperature and

pressure) to maintain equilibrium. We subsequently used the parametric determinations of temperature and pressure to convert pressure-time states to temperature-time states. The chemical equilibrium with applications code does not account for energy losses; but in this analysis, the difference between code determinations of different states can be considered a measure of energy loss.

We performed chemical equilibrium with applications computations stipulating temperature-specific volume for the energy density in question and over a wide range of temperatures. Pressure-temperature state relationships for energy densities represent key charge loads (figure 2). Based on these data, we performed internal energy-specific volume calculations to determine the maximum pressure and temperature.

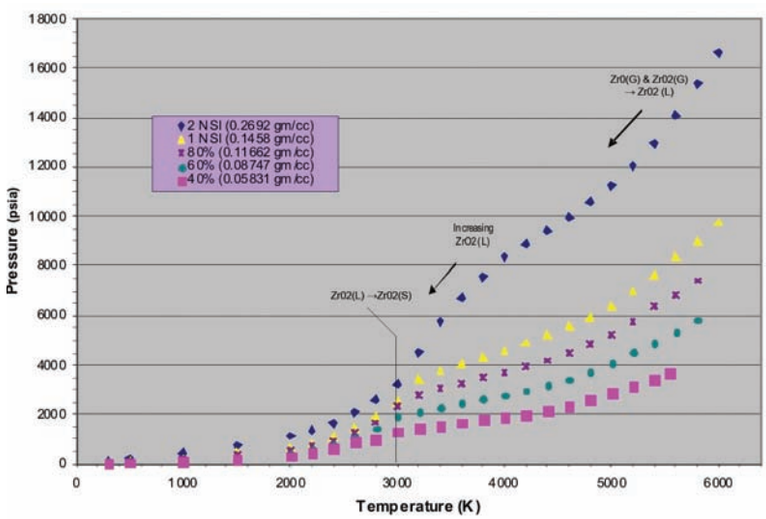

Fig. 2. *Pressure–temperature state curve.*

For a simple ideal gas, the relationship between pressure and temperature is linear. ZPP combustion creates a multicomponent hot gas and vapor at high pressure; within specific temperature ranges, the overall relationship is very roughly linear. Examination of product species predicted by chemical equilibrium with applications showed that several phase transitions and chemical reactions appear to contribute to the shifts in slope. Pressure-time data can be transformed using the pressure-temperature state relationship to develop a temperature-time relationship.

The pressure-temperature state curve shape is influenced by chemical recombination and phase-change processes occurring within the multicomponent mixture. At the elevated temperature of the reaction, the chemical equilibrium with applications code predicted more than 40 species in equilibrium, many of which are compounds related to the constituents of Viton®-B, a relatively minor constituent by weight. The primary species are related to the fuel, the oxidizer, and their combustion products.

System state determined by pressure vs. time data

Each unique pressure, as determined by the pressure-time data and combined with knowledge of the initial energy of the system, gives the state of the system, including losses to outside the system. For any given pressure, a corresponding temperature and amount of heat loss can be found to maintain equilibrium. We used the pressure-temperature state curve for a given energy density to transform selected points on the pressure-time curves to give a temperature-time curve. These curves are plotted in figure 3 for tests representing energy densities of interest.

On the scale shown, initial combustion of ZPP occurs during the first 20 µs (a fraction of the first tic mark in figure 3). The range of times over which single- and dual-fire booster ignitions happen as well as the solidification temperature for zirconium oxide (ZrO_2) are drawn in for comparison purposes. Interpretation of temperature vs. time results is not covered in this report, but we did propose several ignition modes based on the information developed and the observed behavior for booster ignition.

Conclusions

Heat transfer between the hot reactants and the Y-PCA body is greatly influenced by the phase change of ZrO_2 from liquid to solid and by the chemical equilibrium with applications-predicted property that increased liquid ZrO_2 formation is favored by higher Y-PCA system pressures

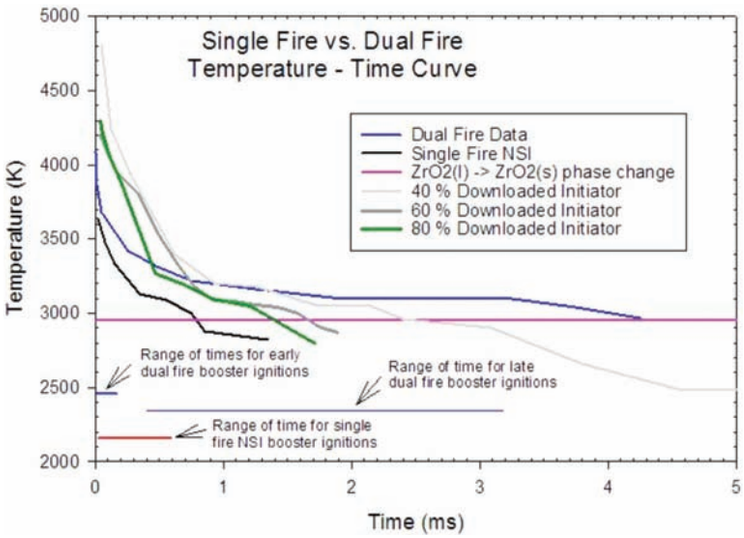

Fig. 3. *Temperature-time representations.*

at lower reaction system temperatures. As a consequence, for the range of charges examined (40%, 60%, and 80% downloaded, NSI, and dual-fire), the lower ZPP charge densities produce higher temperatures but less liquid ZrO_2. This contributes to the difference in heat transfer behavior between the single- and dual-fire events (two 100% NSIs) within the geometry of the Y-PCA fixture.

In the single-fire case, reaction products flow over the top of the booster cover into the unfired leg of the Y-PCA. The difference in flow for dual-fire events favors solidification of greater amounts of liquid ZrO_2 upstream. The liquid ZrO_2 transfers most of its heat content to whatever surface on which it solidifies. By contrast, the single-fire event, with only half the reactants, flows proportionally more reactants over the top of the booster, and more rapidly. Single-fire booster ignition events correlate with the period of greatest heat transfer.

Heat transfer in dual-fire events occurs more slowly as a "heat soak" process, probably driven by heat exchange of gaseous potassium chloride (KCl). Interpretation of chemical equilibrium with applications results suggests that KCl, the lighter reaction product that persists as a gas until it condenses (at much lower temperatures than the ZrO_2), is more effective than ZrO_2 at carrying energy to the booster at times when flow has stopped. The Y-PCA fixture requires reaction products to traverse the narrow flame channels, which join at a short channel (the leg of the "Y") before passing into the larger booster cavity. Hot KCl gas more readily penetrates through the channels. Posttest analysis of deposited reactants shows the presence of relatively more KCl in the booster region. This correlates with the later range of times for dual-fire booster ignition events.

The violent environment created when an NSI combusts inside a pyrovalve is difficult to characterize using experimental measurement techniques. This overview shows that by using the chemical equilibrium with applications as well as knowledge of ZPP reactants and physical volume and time-dependent pressure measurements, other state parameters for the reaction can be estimated. We determined computed values for reactant temperature vs. time, species, enthalpy, and internal energy.

Power, Batteries, and Propulsion

NASA Engineering and Safety Center-supported Battery Study

Judith A. Jeevarajan, *Johnson Space Center*

In the past 2 years, we performed extensive studies to understand the limitations of the protective devices internal to 18650 lithium-ion (Li-ion) cells. Cylindrical 18650 Li-ion cells, especially those with the cobaltate cathode, are equipped with a positive temperature coefficient (PTC) and a current interrupt device (CID). Testing of multi-cell battery configurations indicates that these devices do not always provide protection when cells are in series and/or parallel configurations. A comprehensive test program carried out by the NASA team showed that the PTCs have voltage limitations and spontaneously ignite when activated under high-voltage conditions. Although the CID devices do not cause this failure, they do not protect against it when the internal reaction is too rapid, especially when it involves the evolution of oxygen (at high voltages) and activation of the PTC at the same time.

Introduction

Lithium-ion commercial off-the-shelf (COTS) cells have been tested at Johnson Space Center to determine state-of-the-art characteristics with respect to both performance and safety. We tested these cells as a subset of the flight battery certification processes as well as stand-alone cells obtained from cell manufacturers. The COTS Li-ion cells of the cylindrical type (e.g., the 18650s) have internal protective devices such as the PTC and the CID.

These internal protective devices have been extremely reliable at a single-cell level, preventing the cell from reaching a hazardous condition 100% of the time. However, test programs in the past 5 years have indicated that batteries built with cylindrical COTS cells in multi-cell configurations (i.e., series and/or parallel) have experienced thermal runaway under various test conditions. Analysis of test data indicated the two major causes for thermal runaway are overvoltage and external short conditions. Further investigation on series cell strings confirmed the existence of this problem. We observed that the internal protective devices were either not protecting as expected or were themselves causing the hazards that we encountered. Confirmed evidence exists of PTC ignition above its withstanding (i.e., threshold) voltage, but overcharge catastrophes are not well understood. Hence, we initiated this study to understand the causes for thermal runaway in high-voltage and high-capacity battery modules, and to determine the limitations of the cell internal protective devices.

Experimental

Tests carried out on single cells, four-cell series strings, four-cell parallel banks, 14-cell series strings, and 16-cell parallel banks included: single-cell PTC-withstanding voltage tests, CID tests on cell header assemblies and single cells, research for a suitable diode, and tests on various lengths and sizes of cell strings and banks. A last set of tests included testing cells in parallel configurations under external short-circuit and overcharge conditions. We performed these tests with Sony® 18650 cells of 1.5 Ah capacity. A summary of the tests is provided in Table 1. The cells were, at first, removed from the Canon camcorder batteries. Initial tests indicated that the cells had been compromised during their removal from the packs, however, and that the results were more catastrophic in nature. After these observations, we used fresh single cells for the tests. For the cell combinations, we varied the limits to determine the tolerance and limitations of the protective devices. All string and bank configurations had the cells arranged in a single-row (i.e., fence-post) type and laid flat. The tests were all off-nominal to determine the limitations of these internal devices, and the Sony cells removed from the Canon camcorder batteries were purely used as a test vehicle.

Description	Volts	Amps	Load (Ohm)
Single-cell overcharge	12	1.5	
4P overcharge, 48V, 6A	48	6	
4P overcharge, 12V, 6A	12	6	
4P overcharge, 12V, 4A	12	4	
16P overcharge, 48V, 24A	48	24	
16P overcharge, 12V, 24A	12	24	
16P overcharge, 12V, 12A	12	12	
Single-cell external shorts			50
16P external short			2

Table 1. *Summary of tests.*

NASA Engineering and Safety Center-supported Battery Study

continued

Summary of results and conclusions

The test program provided valuable results on the limitations of both the PTCs and the CIDs that are internal to small cylindrical Li-ion cells. Tripping cell PTCs irreversibly increases their electrical resistance by as much as a factor of 2. Compromised or high-resistance PTCs cause catastrophic failures under overcharge conditions. The CID either did not protect or underwent incomplete opening and reset under overcharge conditions when the current and/or voltage limit values (i.e., 48V and 6A for a bank of four cells, or 48V and 24A for a bank of 16 cells) caused uncontrollable heating or PTC ignition (figures 1 and 2).

Fig. 2. *Cell 4 after the 4P overcharge test with 6A and 48V limit.*

We are making the following recommendations to provide guidance in designing the battery modules that use these cells in high-voltage and high-capacity configurations: (a) The PTC that is withstanding the voltage and trip current should be determined for the cell to be used in the battery design, by testing, as cells from different manufacturers will have different PTC ratings and this information is not provided in a cell specification. (b) Cell screening for the battery build for engineering, qualification, and flight-testing should not cause inadvertent activation of the PTC. (c) The CID activation and protection from overcharge catastrophes should be confirmed by test in the actual flight battery configuration, if the CID is used as a level-of-safety control. (d) These tests should be run at the module size for which the CID is being used as a safety control.

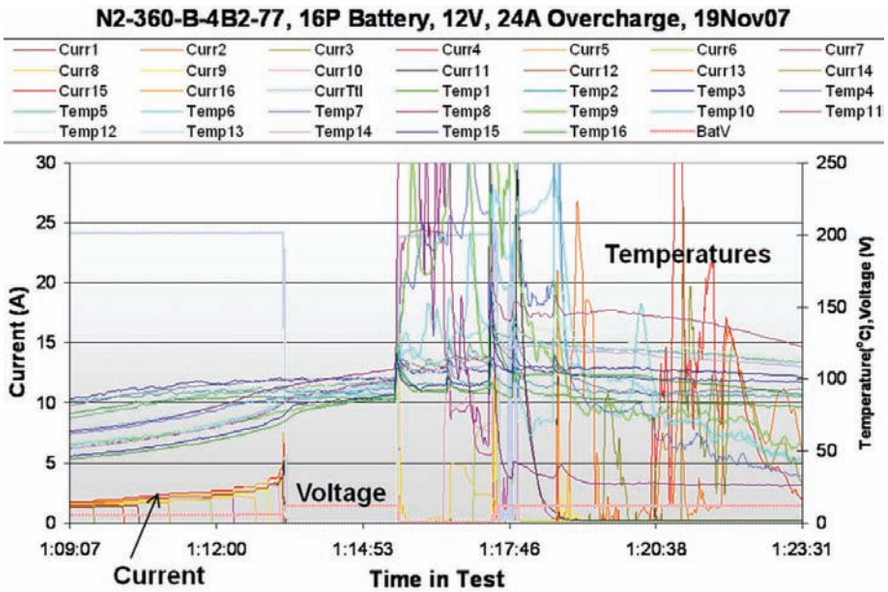

Fig. 1. *Overcharge test on 4P bank of Sony® Li-ion cells using 6A current with a 48V limit.*

Advanced Battery Technology Programs

Judith A. Jeevarajan, *Johnson Space Center*

Advanced battery technology programs focus on selection and procurement of state-of-the-art commercial off-the-shelf (COTS) and custom-made cells – delivered by Small Business Innovative Research (SBIR) program companies – for testing and inclusion in the existing Johnson Space Center cell database. COTS procurement allows for ease of selection, and the use of custom-made cells allows for quick-turnaround projects requiring power for government-furnished equipment (GFE) and payload hardware. This article describes the results of a few cell studies.

In the early stages of the exploration technology development program (ETDP), we studied primarily lithium polycarbonmonofluoride ($Li(CF)_x$) cells to improve their rate capability. As part of this effort, our laboratory characterized COTS $Li(CF)_x$ coin cells under different discharge rates and temperatures. These data formed a baseline for comparison with cells made with material improvements. We found that these state-of-the-art cells provided excellent performance at room temperature at very low discharge rates of capacity C/100 to C/200 (C refers to the current-equivalent rate based on capacity; for example, 1C rate for a 1 Ah cell is 1A). The voltage delay (observed as an initial drop) that occurs with this chemistry was negligible at room temperature (figure 1). However, at temperatures of –40°C, the performance drops significantly and the voltage delay is also pronounced (figure 2).

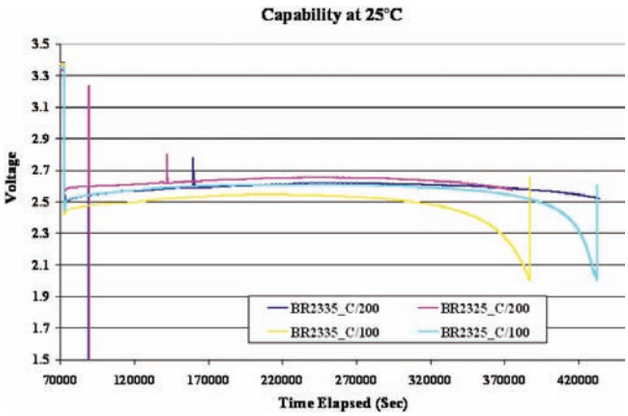

Fig. 1. *$Li(CF)_x$ COTS coin cell discharge at room temperature.*

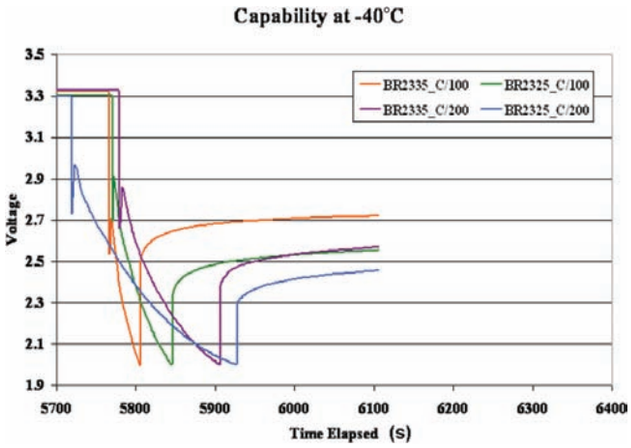

Fig. 2. *$Li(CF)_x$ COTS coin cell discharge at –40°C.*

In parallel with this study, an SBIR program involved the development of novel electrolytes for low-temperature performance of $Li(CF)_x$ cells. Covalent Associates, Inc., Corvallis, Ore., synthesized the low-temperature ionic liquid electrolytes and Quallion, LLC, Sylmar, Calif., manufactured the cells containing this electrolyte. We tested cells of different sizes (from coin to AA-size cells) at different temperatures. Laboratory cells performed at temperatures as low as –98°C (figure 3) and AA-size cells at temperatures as low as –70°C.

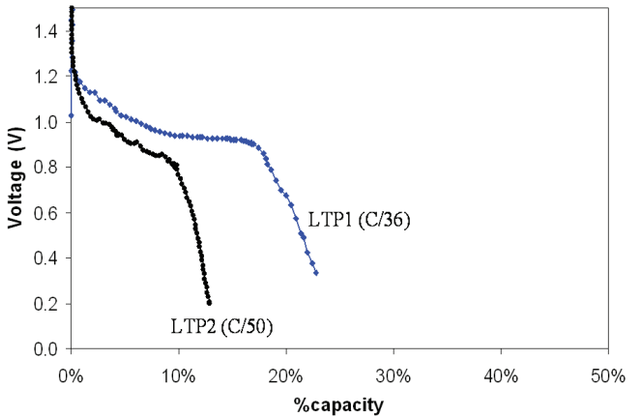

Fig. 3. *Performance at –98°C and at different rates of $Li(CF)_x$ coin cells with low-temperature electrolyte.*

Cell studies conducted under the GFE advanced technology program include performance and safety testing of the Altairnano lithium-ion 11-Ah high-rate polymer cell. The Altairnano (Reno, Nev.) cell has a traditional lithium cobalt oxide cathode and a nanotitanate anode. Due to the nature of the anode, the overall operating voltage of the cell falls to about 2.3V instead of the standard 3.6V obtained with a carbon-based anode. Although the cell can discharge under a continuous current load of 20 C (220A), only discharge rates up to 5 C (~50A) were carried out due to a lack of test equipment capability. The Altairnano cell provided excellent performance under these conditions with as many as 500 cycles.

A set of Altairnano cells underwent abuse testing under conditions of overcharge, overdischarge, external short circuit, and heat-to-vent. When single cells were overcharged at a 1-C rate with a 12V limit, they swelled up and, in some cases, caused the cell seals to open (figure 4). When we overcharged eight cells in a series configuration at a 1-C rate to 48V, one cell was charred externally (figure 5) by the burning of expelled electrolyte liquid and vapors. Charring was also observed when the cells were exposed to high temperatures under the heat-to-vent test. When the Altairnano cells were subjected to an overdischarge test, no catastrophic events occurred. The maximum temperature observed was 70°C.

NASA scientists also determined the characteristics of COTS cylindrical lithium-ion cells under a vacuum condition. Tests included overcharge and external short circuit in multicell configurations. These scientists determined that the overcharge test was benign due to a lack of rapid propagation of heat between the failed cell and the other cells, but the external short-circuit test proved catastrophic (figures 6 and 7) as the heat failed to dissipate fast enough either to the neighboring cells or to the environment.

Fig. 4. *Overcharge of a single Altairnano cell.*

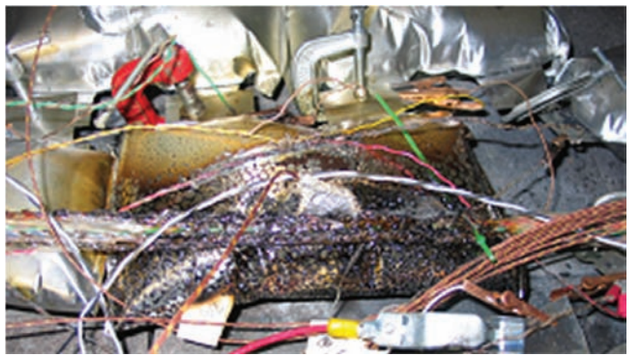

Fig. 5. *Overcharge of 8-series-connected Altairnano cells.*

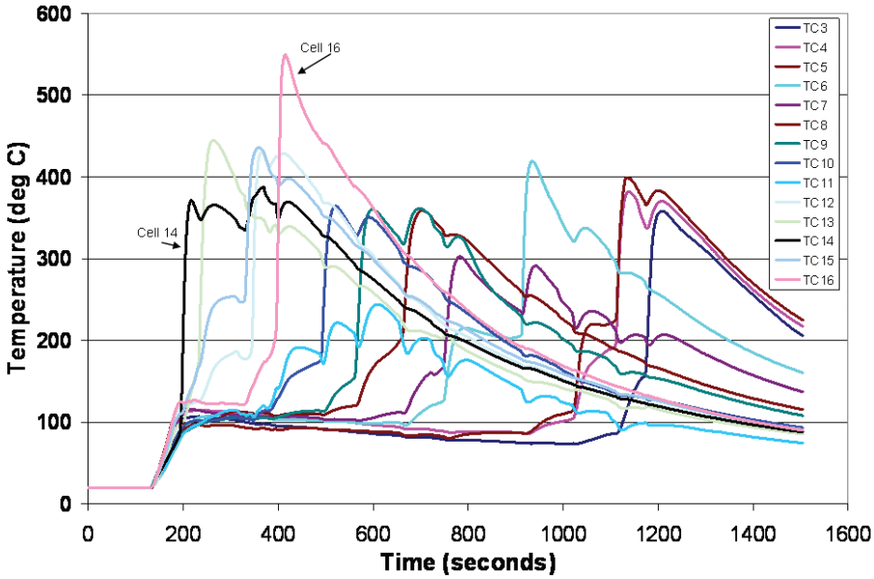

Fig. 6. *Temperatures observed during an overcharge test on a 14-series string in vacuum.*

Fig. 7. *Cells from the overcharge test on the 14-series string in vacuum conditions showing expulsion of cell contents and melted metal.*

Our laboratory evaluated an advanced cell chemistry – lithium-sulfur (Li-S). We compared baseline state-of-the-art cells provided by Sion™ Power Corporation, Tucson, Ariz., to cells (also provided by Sion™ Power Corporation) with an improved cathode and anode that increased the cycle life stability. We cycled these cells under three different rates as well as under vacuum conditions and safety tests that included overcharge, overdischarge, and external short. The excellent performance of the improved cells under vacuum conditions for the 25 cycles studied (figure 8) was comparable to that of the cells under ambient environmental conditions. The baseline cells fell in capacity to 1.7 Ah at about 45 cycles, whereas the improved cells provided as many as 65 cycles before the capacity fell to the earlier value. If the cycle life of the Li-S chemistry is improved further, it will produce a rechargeable battery with the highest energy density available in the market today.

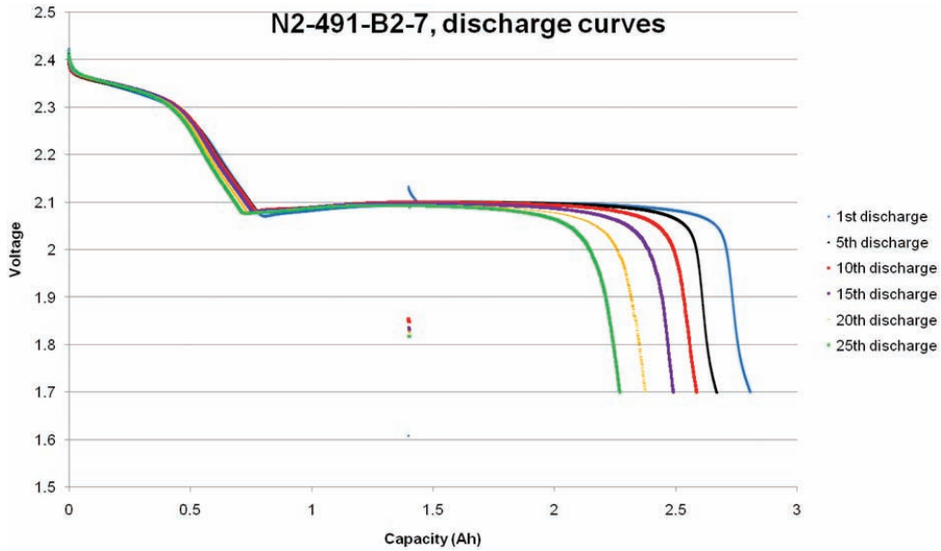

Fig. 8. *Discharge curves for the Li-S cells in a vacuum condition (315 mA charge and 250 mA discharge currents).*

Advanced Fuel Cells for Space Exploration Applications

Arturo Vasquez, *Johnson Space Center*

Scientists at NASA Glenn Research Center (GRC) are responsible for increasing technology readiness on fuel cell power systems. We are collaborating with them to develop passive components that have no or few moving parts, as high-speed components operating in pure oxygen (O_2) and hydrogen (H_2) environments are hazardous. Concepts and devices continue to be developed both within NASA (in-house) and at outside entities via contracts and grants.

NASA developed a proton exchange membrane fuel cell (PEMFC) test system under this effort. This test system – which incorporates an 8-kW, 72-cell PEMFC stack, two reactant pressure regulators with internal ejector reactant pumps, and a two-stage O_2/product water separator – provides a method to operationally verify these components while the components are used in an operating fuel cell power plant. All of these components were developed and evaluated at the component level in earlier phases of this effort. NASA envisions that fuel cell systems/subsystems such as these will enhance reliable and safe operation in the variable-gravity environments of future space exploration activities.

Fuel cell background

A fuel cell is an electrochemical device that can produce electricity from a catalyzed, low-temperature reaction between H_2 (a fuel) and O_2 (an oxidant). Unlike a battery, a fuel cell operates as long as fuel and oxidant are supplied to it. The by-product of this operation is water, which can be used for human consumption, vehicle cooling, or other purposes.

The PEMFC uses a thin, tough sheet of polymer plastic (an ion-exchange membrane) as the electrolyte. Platinum catalyst electrodes bonded to each side of the polymer membrane form a rugged and simple structure. Hydrogen reacts at the anode to give up electrons to an external circuit while simultaneously releasing H_2 ions into the electrolyte. The H_2 ions conduct through the electrolyte membrane to the cathode. At the cathode, H_2 ions from the anode combine with O_2 and electrons from the external circuit to produce water. Once this occurs, waste heat must be eliminated to maintain stable performance. Water can be removed from the cell cathode either by a wicking material (non-flow-through water removal) or by being entrained and swept out by a circulating extra-oxidant gas (flow-through water removal).

Integrated pressure regulator and ejector

The appreciable mass, volume, and complexity of the typical motor-driven compressor and its control and drive electronics can be eliminated in fuel cell water management through use of an ejector integrated into a pressure regulator. Such an ejector requires supply pressures ranging from 250 to 500 psig. However, these pressures are typically available with the use of supercritical cryogenic reactant storage systems, such as those currently used on the space shuttle. To provide an ejector-reactant-gas-circulation-pump internal to the regulator, TESCOM, Elk River, Minn., developed a custom regulator designed to accommodate a precision-orifice jet nozzle and a custom ejector mixer section. We completed a series of inert gas test runs with this component – covering a range of purposefully selected geometries (ejector jet nozzle and mixer diameters), pressures, and flows – to provide useful performance data for ejector configurations that could provide beneficial flow characteristics for reactant circulation pumping in spacecraft fuel cell systems with a power range of 0.7 to 20 kW. In the geometry, pressure, and flow ranges tested, approximately 10-to-1 mixer-to-jet diameter ratios for ejectors matched the presumed closed fuel cell circulation requirements of total-to-motive-flow flow ratios of 2.5 to 4.5 at the higher consumption flow ranges while providing maximum pressure differences in the range of 1.5 to 2.5 psid.

Water separator

NASA is also developing a two-stage water separator concept with inter-stage fluid pumps that use Liqui-Cel® membrane contractors (Charlotte, N.C.). The first stage is a bulk liquid and gas separator that receives two-phase flow from the fuel cell stack and passes only steam and reactant gas to the reactant pump suction flow inlet port; liquid product water accumulates in the first stage. An inter-stage pump will be used to transfer fluid accumulating in the first stage to the second stage de-bubbling membrane-contactor, and O_2 gas removed from the de-bubbled water stream will recycle to the first stage. Discussions, beginning in April 2007, took place with Liqui-Cel® representatives concerning the long-term compatibility of

Fig. 1. Polypropylene (left) and PVDF (right) membrane contactors.

the polypropylene used in their commercially available membrane contactor with high-temperature O_2 gas in a fuel cell system. These discussions led to the suggestion made by Liqui-Cel® representatives that polyvinylidene-fluoride (PVDF) could provide an alternative material to offer increased O_2 compatibility. One noncommercial PVDF membrane contactor and one noncommercial PVDF de-bubbler were procured from Liqui-Cel® in 2008. Both the polypropylene and the PVDF membrane contactors are shown in figure 1.

In NASA's advanced flow-through fuel cell system design, the first stage of the water separator must be compatible with the reactant pumping characteristics of the integrated pressure regulator and ejector. We worked in collaboration with Texas A&M University (TAMU) on a vortex/centrifugal separation section to augment inventory management of product water in the first stage and the subsequent transfer of product water to the second stage (which, again, is currently planned to be a membrane contactor de-bubbler) in multi-acceleration environments. The TAMU Center for Space Power, funded through a NASA grant, has specific expertise in the area of two-phase vortex separation systems, and has delivered both a gas-driven separator to GRC and a liquid-driven vortex separator to the Johnson Space Center (JSC) for evaluation; several technical reports, including a doctoral dissertation, also resulted from this effort.

Fuel cell operational verification testbed

Fuel cell systems incorporating ejector reactant pumps warrant investigation of operability at the low-power, low-flow operating range. (Note that the ejector circulation flow rates are lowest at the low-power operating range.) We developed a fuel cell operational verification testbed (FCOVTB) using two of the integrated reactant pressure regulator and ejector packages as well as a basic set of component housings for the multistage water separator design concept. This FCOVTB also incorporates a 72-cell PEMFC stack procured from Teledyne Energy Systems, Inc. (Hunt Valley, Md.) as the electric-power-producing component of the testbed as well as coolant, instrumentation, and control subsystems. The testbed is shown in figure 2.

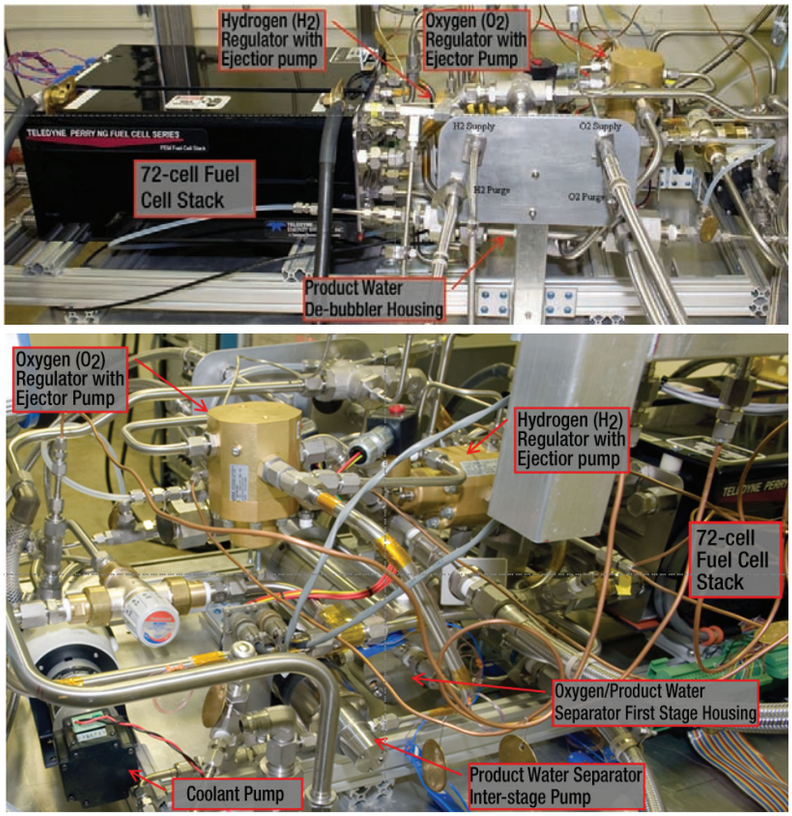

Fig. 2. Fuel cell operational verification testbed overall side view (top) and detail back view (bottom).

Advanced Fuel Cells for Space Exploration Applications

continued

Scientists completed a major upgrade of the electrical control system of the Reactant Supply System at the JSC Energy Systems Test Area to support fuel cell testing in general. This upgrade provided an electrical control system with: (1) the potential for greater overall reliability; (2) significant improvements in remote control capability and user interface; and (3) maintenance of required safety controls.

Forward work

At least three configurations of multistage water separators are currently planned for investigation. The first configuration, which employs a gravity-dependent first stage, is intended to verify basic operation of the overall testbed and to acquire baseline performance data from the fuel cell power plant. The second configuration will incorporate the PVDF membrane contactor in the first stage of the water separator. Finally, the third configuration will add a liquid-driven centrifugal separator section to the first-stage housing.

Orbiter Auxiliary Power Unit Hydrazine Fuel Line Vacuum Test

Michelle H. Barragan, *White Sands Test Facility*

Darren M. Cone, *White Sands Test Facility*

We have uncovered, through investigations into orbiter in-flight anomalies during STS-121 and STS-123, the critical need to thoroughly understand the physical behavior of a hydrazine (N_2H_4) leak in a space vacuum, as well as the resulting impacts to vehicle system integrity and exposure risk to crew members.

Although post-flight inspections revealed neither the STS-121 nor the STS-123 anomaly resulted from an N_2H_4 leak, in-flight data revealed a pressure decay corresponding to an equivalent N_2H_4 leak of approximately 2.0 lb_m/day. Except for a case in which the orbiter auxiliary propulsion unit (APU) fuel tank was nearly depleted, in-flight pressure and temperature data are not sufficient to distinguish between a gaseous nitrogen (GN_2) tank leak and an N_2H_4 tank leak. Therefore, the most conservative approach during flight is to assume an N_2H_4 leak occurred, resulting in potentially significant risk and mission impact implications.

The objective of the orbiter APU hydrazine fuel line vacuum test is to characterize the physical behavior of an N_2H_4 leak in a simulated space vacuum using a representative segment of orbiter APU fuel feed-line containing a laser-machined, 20-µm orifice sized specifically to allow for a media leakage rate that approximates the pressure decay noted during in-flight anomalies. The test line is roughly 2 ft in length and is made of 304L corrosion-resistant steel with a 0.50-in. outside diameter and a 0.025-in. wall thickness. This test also investigates the effects provided by the associated APU line heater and thermal insulation on the behavior of the fuel leak, and any deviation in the performance of the heater controller feedback circuit. We performed initial testing with water, as water is the most suitable physical analog for propellant-grade N_2H_4 and allows preliminary experimentation in the absence of toxic media.

Pressurization of the test media is provided by GN_2 at pressures up to 250 psia, representative of typical orbiter APU fuel tank on-orbit pressure. We used a modified vacuum test chamber capable of maintaining 10^{-1} Torr minimum through use of mechanical pumps and an in-line cryogenic trap to provide the vacuum surrounding the test article. Our team then positioned eight thermocouples axially along the tubing at specific interval distances from the leak orifice, and monitored and recorded vacuum chamber and test media pressure together with the thermocouple data at a 1-Hz sampling rate. The vacuum test chamber includes accommodations for the installation and control of an electrical feed-line heater, with and without thermal insulation, in configurations representing the actual orbiter APU feed-line system as installed. Nominal test media temperature is 65°F.

Results from preliminary tests, with water as the test media, reveal the development of ice structures at the orifice leak site, in either complex crystalline or continuous "ribbon" forms (figure 1).

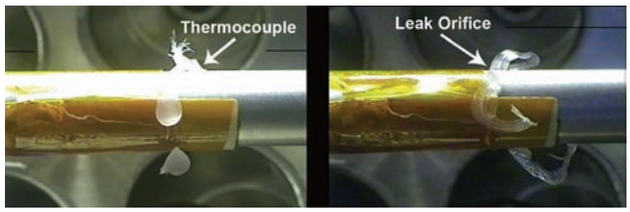

Fig. 1. *Typical ice structure formations.*

Figure 2 shows leak-site behavior typical to this series of tests in the formation of an ice "plug" structure blocking the media leak path and maintaining stability over varying amounts of time. Specific to this test, however, as the test media pressure was increased to 250 psi, a fine, nearly vertical stream of water was ejected from the orifice and through the "plug" structure. After several minutes, the ice formation shown in figure 2 was observed from the

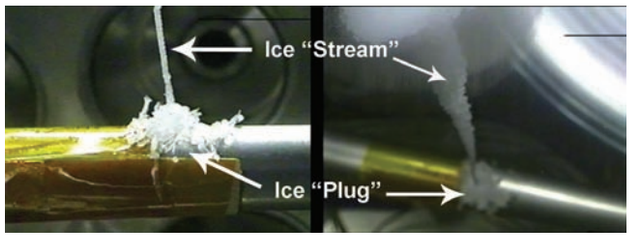

Fig. 2. *Ice plug and stream structures in front (left) and top (right) views.*

top port of the vacuum chamber. Fluid began freezing at the chamber wall and proceeded back to the orifice site, creating an ice stream that momentarily stopped the leakage. This behavior and physical structure

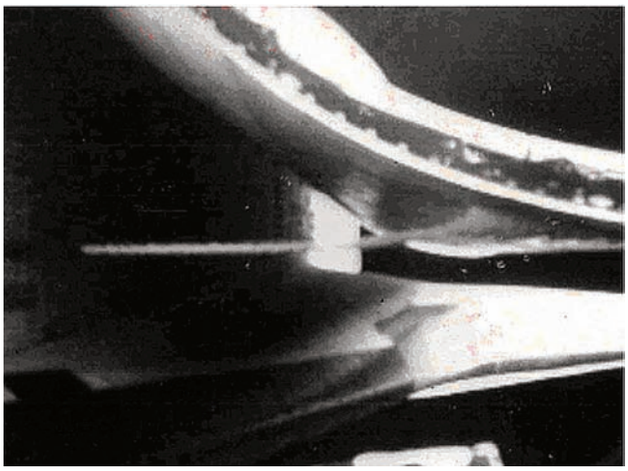

Fig. 3. *Space shuttle orbiter during on-orbit water dumps.*

matches very well with that observed in the space shuttle orbiter during on-orbit water dumps (figure 3).

We performed additional tests, approximating typical on-orbit usage of the APU fuel line heaters, using an actual APU line heater with representative wrap factor and a heater duty cycle of 17%. Test results with the line heater installed and energized (figure 4) show an ice structure formation that characteristically differs from those observed during previous tests without the line heater. For this test, we pressurized the test article to 250 psia, and placed the heater control thermocouple immediately adjacent to the leak orifice with the heater set point maintained at 65°F. Once this particular ice structure formed, it persisted with only slight alteration for the remainder of the test (~2 hours). This contrasts with the previous test's supplemental heating in which the ice structures detached after varying amounts of time, allowing subsequent formation of new, partially stable ice structures with different configurations.

Fig. 4. *Stabilized ice structure with electrical line heater installed.*

Conclusion

Preliminary testing with water allowed us to characterize several unique physical behaviors at the leak site simulating on-orbit space shuttle orbiter APU fuel leakage. As a function of test article pressure and application of supplemental heating, ice structure formations exhibit varying structural configurations and levels of stability. These results match very well with the ice formations observed in the orbiter during on-orbit water dumps. For tests including the flight configuration line heater, the heater controller response reflects the local thermal variation of the feed line near the leak orifice during vacuum solidification of leaking test media, physical detachment, and subsequent solidification of another structure. Based on the test expertise we have developed thus far, and with insights into the nature of the physical behavior of water leaking into the simulated space vacuum, the test team will move forward to perform identical test sequences with N_2H_4 as the test media to best represent the orbiter flight configurations. The new data will help characterize APU system performance and impacts to crew safety should an N_2H_4 fuel leak occur while the orbiter is in orbit.

Improved Method: Short-term Determination of Low Corrosion Rates in Hydrazines

Anna De Armond, *White Sands Test Facility*
Dion Mast, *White Sands Test Facility*
Miguel J. Maes, *White Sands Test Facility*

The NASA White Sands Test Facility (WSTF) must frequently assess the corrosion rates of materials proposed for the fabrication of aerospace systems wetted by fuels such as monopropellant hydrazine (MPH) and monomethylhydrazine (MMH). Corrosion rates describe the deterioration of a material caused by general corrosion, sometimes referred to as uniform corrosion, and can be used to predict the stability of metal/fluid systems over long periods of time. These rates can be determined by many methods, but only a few of them are suitable for use with hydrazine (N_2H_4) fuels; historically, they require months of immersion. Chemical characteristics such as toxicity, reactivity, low conductivity, and sensitivity to contamination by atmospheric carbon dioxide (CO_2) and moisture must be considered when working with N_2H_4 fuels. WSTF has addressed these issues using a method that combines relatively short immersion times with the high sensitivity afforded by inductively coupled plasma-mass spectrometry (ICP-MS).

Proposed materials, in coupon form with known surface areas, are immersed in the fluid of interest for several days. Immersion occurs in sealed vessels under a nitrogen pad to preclude atmospheric contamination. After 6 days, we remove the coupons and the fluid is evaporated. The immersion vessel is then rinsed with hot 5% nitric acid (HNO_3) to solvate corrosion residue. The HNO_3 rinsates are then analyzed by ICP-MS for elements specific to the coupon alloy. ICP-MS can detect elements in concentrations as low as parts per trillion. The ICP is depicted in figure 1.

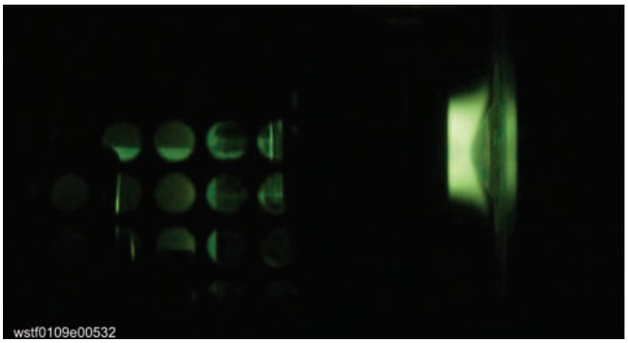

Fig. 1. *The ICP-MS.*

While other techniques require months to complete, this method allows for the determination of very low corrosion rates – on the order of 10^{-3} mil per year – in a matter of days. In addition, we have used this method to study the effects of fluid contaminants such as CO_2, water, and oxygen on corrosion rates by introducing known quantities of them into the immersion vessel. Finally, this method is not limited to MPH and MMH, but can be used for a variety fluids.

High-sensitivity Measurement for Hypergol Permeation of Personal Protective Equipment Materials

Mark B. McClure, *White Sands Test Facility*
Dion Mast, *White Sands Test Facility*
Miguel J. Maes, *White Sands Test Facility*

Scientists evaluated personal protective equipment (PPE) materials at the NASA White Sands Test Facility (WSTF) for breakthrough times from hypergol permeation using a new test cell design and methods compatible with ASTM [American Society for Testing and Materials] F 739-07 *Standard Test Method for Permeation of Liquids and Gases through Protective Clothing Materials under Conditions of Continuous Contact*.

The challenge fluids used in testing were hydrazine (N_2H_4), monomethylhydrazine (MMH), and nitrogen tetroxide (NTO). The toxicity of the N_2H_4 and NTO propellants has driven studies of alternative and less-toxic propellants in recent years, but no suitable alternatives have been identified for many applications, including aerospace. Therefore, the evaluation of PPE materials for compatibility and breakthrough time remains a concern for many groups working with these chemicals. Historically many commercial materials were tested, but some of these products are no longer marketed and several new products (e.g., laminated construction gloves and Viton® blends) have since come on the market. The ASTM F-739 method has also changed slightly, specifying a 2.5-cm (1-in.) cell rather than a 5-cm (2-in.) cell, which allows the use of a commercial off-the-shelf passive electrochemical detector monitor without modification.

We performed detection and data acquisition using a Draeger PAC III® monitor and data logging system. Integrating the detector sensor directly into the permeation cell minimized the collection chamber volume. That, in combination with a closed-loop configuration, maximized the sensitivity of the test system.

The PPE materials tested were obtained from gloves and Level A suits selected from those in common use at WSTF and Vandenberg Air Force Base, Lompoc, Calif. We also evaluated with this test system some PPE materials previously tested, and tested other PPE materials not previously reported.

We constructed three test cells, one for each challenge chemical, out of 300 series stainless steel. The cylindrical test cells were machined to a 2.5-cm (1-in.) inside diameter and a 2.5-cm (1-in.) depth. On the challenge side, we installed two female 0.3-cm (0.125-in.) national pipe thread (NPT) ports and one 0.635-cm (0.25-in.) NPT port for challenge chemical addition and posttest nitrogen purging to remove the challenge vapors. On the collection chamber side of the apparatus, we reamed the open end to 2.63 cm (1.04 in.) to be a slip fit on the hydrazine sensor cover of the Draeger PAC III® monitor (figure 1). The PAC III® monitor uses a different sensor cover for NTO, so we swapped it for an N_2H_4-style sensor cover to enable it to also slip-fit on the apparatus.

Fig. 1. *Test apparatus.*

We cut test samples with a 5-cm (2-in.) die punch for uniform sizing. Thickness and weight were recorded for each sample, and were tested as received with no preconditioning. The thin, non-elastomeric samples required polytetrafluoroethylene gaskets with an inside diameter of 2.54 cm (1 in.). These gaskets were die-cut from 0.159-cm (0.0625-in.)-thick sheet stock.

Tests were initiated by acquiring a clean air baseline on the monitor, then starting the data logging mode as the hypergol propellant was added. We terminated the tests by pulling the detector monitor out of the challenge chamber if the alarm went off or after 2 hours, whichever occurred first. Breakthrough times were determined in triplicate for the PPE materials tested.

The test cells have an internal exposed area of 5.1 cm^2 (2 in^2) for the sample area, as described in ASTM F-739. With the Draeger PAC III® installed, the collection chamber volume is 13 cm^3 (5 in^3) (0.013 L). At WSTF ambient conditions, the lower sensitivity of the Draeger detector is 0.011 µg/L for N_2H_4, 0.016 µg/L for MMH, and 0.16 µg/L for NTO. We set the sampling frequency on the Draeger detector to one data point every 10 seconds. Using the 10-second data collection frequency for time, the ASTM-calculated breakthrough sensitivities are quite low, as shown in Table 1.

Test Fluid	Breakthrough sensitivity.
N_2H_4	1.6×10^{-4} µg/cm^2/min
MMH	2.4×10^{-4} µg/cm^2/min
NTO	2.4×10^{-3} µg/cm^2/min

Table 1. *Breakthrough sensitivity.*

The ease of integrating a commercially available electrochemical detector with the new 2.54-cm (1-in.) test cell, now prescribed by ASTM F 739, facilitates hypergol permeation testing and maximizes the sensitivity of the test system.

Robotics, Autonomous Systems, and Software

Robonaut/Centaur

M. A. Diftler, *Johnson Space Center*
Robert Ambrose, *Johnson Space Center*
Bill Bluethmann, *Johnson Space Center*
Lucien Junkin, *Johnson Space Center*
Scott Askew, *Johnson Space Center*
Lyndon Bridgwater, *Johnson Space Center*
Rob Platt, *Johnson Space Center*
Phil Strawser, *Johnson Space Center*
Josh Mehling, *Johnson Space Center*
Ivan Spain, *Johnson Space Center*
Mars Chu, *TRAClabs, Inc.*
Rob Burridge, *TRAClabs, Inc.*
Eric Huber, *TRAClabs, Inc.*

Advancing robotic mobility and manipulation technology is an important step in preparing for NASA's planned lunar and martian missions. To address this challenge, engineers in the Robotic Systems Technology Branch at the Johnson Space Center (JSC) have combined the highly dexterous Robonaut upper body with a rugged and versatile four-wheeled base to yield the Centaur. Centaur's anatomy allows the robot to perform human-scale tasks away from the laboratory, in unstructured environments that simulate the lunar or martian surfaces where the robot would eventually work. Centaur, under both teleoperated and supervised autonomous control, completed testing with other NASA robots and suited crew members in recent field trials, demonstrating its utility as part of a lunar human/robot team.

Robonaut's most important feature is its ability to help astronauts perform tasks that currently only humans can perform. These tasks range from working with tools designed specifically for space-suited hands to assisting with the assembly and maintenance of habitats with human interfaces. These capabilities are realized through the human-scaled anatomy of Robonaut's upper body. With both dexterous arms and hands and a wide range of sensing capabilities, Robonaut is an excellent astronaut assistant that can work both alongside a suited crew person or be remotely supervised to perform tasks while the crew is attending to more important scientific and exploration activities.

Robonaut has multiple control modes. Teleoperation is the simplest. It allows a human operator in close proximity to control the robot's arms, hands, and neck directly using a collection of virtual-reality gear. The human's motions are picked up by the position sensors embedded in the virtual-reality gear and drive the robot's limbs and fingers to match the human's positions. Video screens in the virtual-reality helmet display the views from the robot's head-mounted cameras, allowing for very intuitive control. A second control mode, Shared Control, reduces operator workload by handing off certain motions to the robot. For example, the robot uses internal sensors to correct for lateral misalignments while the operator directs the robot's hand to insert a utility box into a receptacle. The final mode is Supervised Autonomy. In this mode, a remote operator sends high-level commands and then verifies that the robot has completed a subtask before going on to the next step in the sequence.

Robonaut has demonstrated its capability to assist crews under all three control modes over several years. As shown in figures 1 through 7, multiple teleoperated Robonauts have worked as direct helpers, providing parts to a suited crew person as that crew person assembled a prototype

Fig. 1. *Centaur with human/robot teammates, Meteor Crater, Ariz.*

Space Truss Structure in the Dexterous Robotics Laboratory at JSC. Later, Robonaut, in one of its early mobile configurations, graduated to the level where it could mate the truss couplers using its own hands while under shared control by a human operator. Working at the NASA Ames Research Center, Robonaut acted as part of a larger human/robot team, autonomously performing simulated welds on habitat panels handled by humans. Mostly recently, in its Centaur configuration, Robonaut moved outdoors to assist in higher-fidelity planetary exploration scenarios.

Robonaut/Centaur

continued

In the Centaur configuration, Robonaut has impressive body mobility. Not only can the entire unit traverse moderate to rough terrain, the built-in waist degrees of freedom allow the upper body to interact directly with the ground and the rear-mounted utility tray. During testing at Meteor Crater, Ariz., Centaur, under teleoperated control, bent close to the ground, scooped soil, and examined rocks. Under Supervised Autonomy, Centaur approached the back of a Crew Rover testbed; used machine vision, force, and position sensors to acquire a geological sample box; and then rotated 180 deg around to place this box on its utility tray for transport to an analysis station. A local

Fig. 2. *Two Robonauts assisting a suited astronaut.*

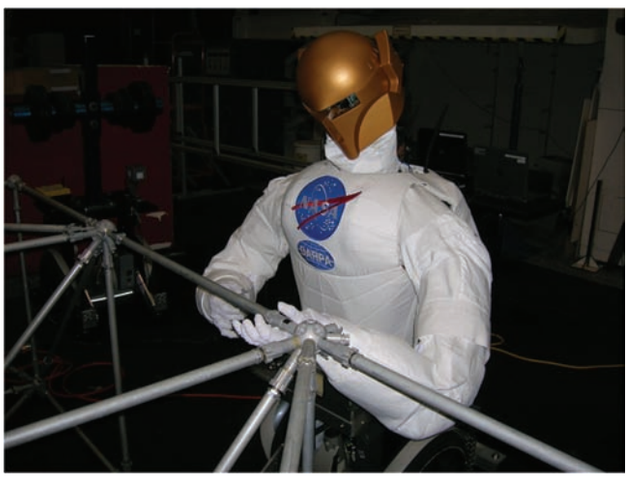

Fig. 3. *Robonaut manipulating truss couplers.*

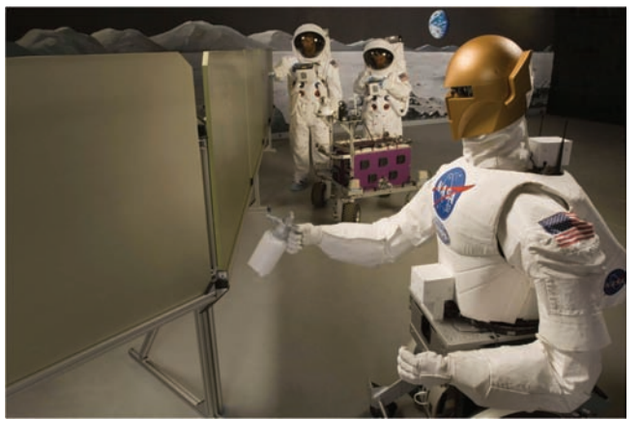

Fig. 4. *Robonaut preparing to weld.*

Fig. 5. *Centaur acquiring sample box from crew rover testbed.*

Fig. 6. *Centaur stowing sample box.*

operator and an operator located in Houston supervised this task, providing the same commands over a time delay that simulated Earth-to-moon communication.

Fig. 7. *Centaur bending over and acquiring a sample.*

Lunar Rover Development

Bill Bluethmann, *Johnson Space Center*
Lucien Junkin, *Johnson Space Center*
Mike Gernhardt, *Johnson Space Center*
Rob Ambrose, *Johnson Space Center*
Nathan Howard, *Johnson Space Center*
Barbara Romig, *Johnson Space Center*
Bruce Webber, *Ames Research Center*
Steve Cavanaugh, *Langley Research Center*
Rob Mueller, *Kennedy Space Center*

NASA's planned return to the moon requires a crew mobility beyond the limits of footed extravehicular activity (EVA). Crew mobility systems, such as lunar vehicles, can improve human safety while expanding EVA duration, range, and payload capacity. These benefits impact both outpost construction efforts and scientific endeavors. NASA studies analyzed various crew mobility options, including unpressurized rovers that must be driven by crew wearing spacesuits (EVA) as well as pressurized rovers that surface crew can drive from inside their vehicle (intravehicular (IV)). The lunar studies have modeled various scales of rovers and many unique chassis kinematic options. The trade studies included analysis of rover mass and power, system interfaces with numerous lunar-lander/cargo manifest scenarios using crew safety, mission duration, and exploration range as figures of merit. These studies identified one rover configuration, the Lunar Electric Rover (LER), as having an ideal combination of performance, mass, and range specifications. Two key features envisioned in the LER are a suit-port interface that enables fast EVA egress, and a shielded cabin wall that can provide radiation protection from solar proton events. While this performance fits the architecture well, such a vehicle does not exist today; therefore the development and testing of several new technologies is required. The Exploration Systems Mission Directorate has funded the development of the LER chassis and cabin prototypes to study this configuration and buy down development risk. Early tests show promising results.

Description of the cabin design

The prototype of the LER cabin, shown in figures 1 through 4, was built during fiscal year (FY)08 for field tests in FY09. The LER cabin is designed to house two crew members for operations over 3 days, or up to 2 weeks, with logistical and power resupply. The cabin can house four crew members in a contingency mode, allowing excursions with two LERs to be redundant and extend beyond the EVA walkback distance now estimated to be on the order of 10 km. The cabin has two identical hatches for docking with other LERs or pressurized modules such as an outpost's habitat chambers. These hatches, on either side of the cabin, serve primarily as IV transfer corridors

Fig. 1. *Chariot during field testing at Moses Lake, Wash., June 2008.*

for the crew, but they can also be used as emergency EVA entrances or exits. Additionally, the cabin has two rear suit ports that can be used to provide fast EVA egress. The suit port design includes two hatches: an outer hatch on the rear entry spacesuit, and an inner hatch on the LER cabin. When both hatches are open, crew members can climb from the cabin into the suit. Closing the two hatches allows the suit to separate and provides a path to EVA in 10 to 15 minutes. EVA crew members can return to the LER cabin through the suit port by backing their suit into the port, then opening the two internal hatches in reverse order. The cabin interior features two captain's chairs in the front of the cabin, connected to a center aisle with sleeping bunks on either side in the cabin's rear. Storage under the bunks and in the floor holds food, equipment, and clothing. The cabin exterior includes windows, radiators, lights, cameras, and tool boxes.

Description of the chassis design

The prototype of the Chariot chassis was built in FY07 and field-tested in FY08 as an unpressurized rover. The LER cabin prototype was mounted on Chariot for field tests in FY09. NASA provided the Chariot design requirements for payload, range, speed, and interfaces. Design challenges included a reconfigurable payload deck, a high ground clearance, an adaptive suspension, crab-steering, redundant drive avionics, high-energy density batteries, and a steep-

slope climbing ability. The prototype can be configured either with crew accommodations (turrets) or rear-mounted decks (contingency crew accommodations). Other modular interfaces include the ability to receive a bulldozer blade called LANCE and various sensor modules for navigation. Future work packages now in development include logistics pallets, excavators, and manipulators. The vehicle's kinematics provide a zero turning radius, and enable the vehicle to drive sideways for docking cabin hatches or other payload interfaces. The chassis suspension allows Chariot to level its frame or align with a lander or another surface element that is at a general angle. The redundant drive trains have two-speed transmissions, providing up to 5 kilometers per hour (KPH) in low and 20 KPH in high. We have tested the Chariot prototype on slopes over 35 deg, on soft soils (<1 psi), and in rocky (>30-cm) terrain. Engineering tests at the Johnson Space Center Rockyard include studies of drive train motor power, steering power, and suspension dynamics. New technologies being tested on the vehicle include cryogenic tires, drive trains, active suspension, composite materials, batteries, crew interfaces, dark navigation, and intelligent control modes.

Fig. 2. *The LER during testing at the Black Point Lava Flow, Ariz., October 2008.*

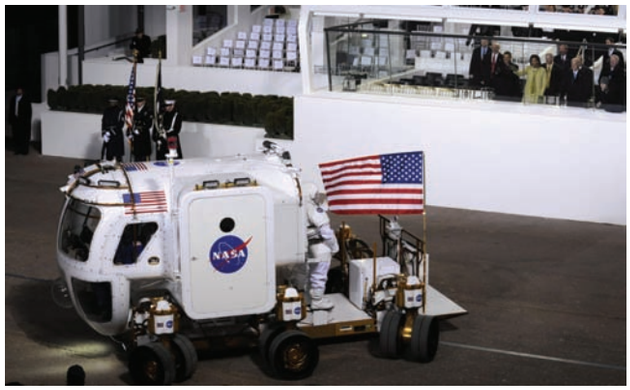

Fig. 3. *The LER during the Presidential Inaugural Parade, Washington, D.C., January 2009.*

Fig. 4. *The LER during the FIRST Robotics Competition, Houston, March 2009.*

Improving Robotic Operator Performance Using Augmented Reality

James C. Maida, *Johnson Space Center*
Charles K. Bowen, *Johnson Space Center*
John Pace, *Johnson Space Center*

Robotic operations performed in Earth orbit face unique challenges. In the case of the special-purpose dexterous manipulator (SPDM), a two-armed robotic device, operations can last multiple orbital days (figure 1). Because of the dynamic sunlit days and very dark nights on orbit, direct and indirect visibility can be difficult; we therefore developed and tested the use of augmented reality (AR) technology with a ground-based trainer (figure 2) to reduce the negative effects of these conditions.

The most difficult operator task is the alignment of an orbital replacement unit (ORU) attached to the end effector of the SPDM with the point of insertion into the ORU destination location. Alignments are accomplished based on the intrinsic physical features of the tool, payload, and surroundings as viewed through video cameras. On orbit it can take 8 to 10 hours, encompassing multiple days and nights, to complete a planned ORU replacement or maintenance operation. Multiple alignment tasks are interspersed within the same time period.

The purpose of these experiments was to determine whether overlays improve performance in maneuvering an ORU. The experiment was a classic "mixed"-factors design that had one factor (order of presentation of treatments) between subjects and one factor (treatment type – overlay or no overlay) repeated within subjects. Each subject performed a total of eight trials divided into two sets of four trials each. One set was performed without overlays, and the other set was performed with AR graphical overlays. Half of the subjects experienced a set of four trials with overlays followed by a set of four trials without overlays. The balance of the subjects experienced the same sets in reverse order. The need to use certified operators of comparable skill limited the number of subjects to 12. The remaining operators were used for pilot testing to optimize the design of the augmentation, the number of trials, and the design of the dynamic lighting conditions.

All trials involved maneuvering the ORU from a predetermined starting position toward the same receptacle. The same set of four different starting positions was used in the same order for the trial groups under the two treatments. Starting positions for the trials were selected to produce the same minimum time for completion (as determined by the mechanical characteristics of the dexterous manipulator trainer). Objective-dependent measures for this study are related to the ORU position/orientation at the pre-insertion position above the destination receptacle. These four measures included: (1) roll alignment error (deg) about the X axis; (2) composite pitch/yaw alignment error (deg); (3) translation alignment error in the YZ plane (in.); and (4) elapsed time to trial completion (seconds). In addition to the objective data collected, subjective evaluations of experimental treatments and methods were gathered by means of a written questionnaire provided to each subject following completion of the trials. We

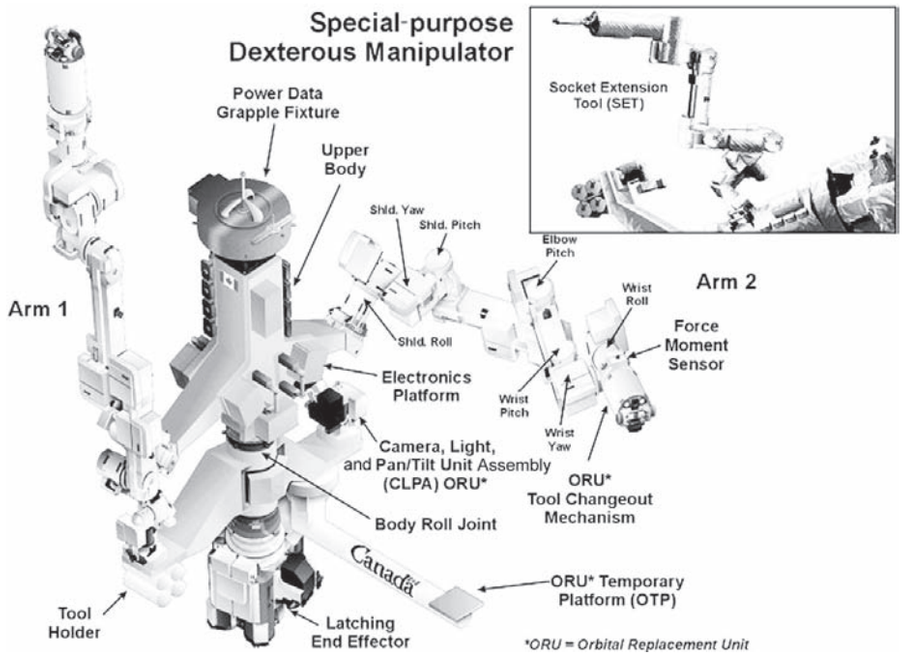

Fig. 1. *Special-purpose dexterous manipulator.*

encouraged these subjects to record any comments regarding the experiment on the questionnaire.

Data analysis included analysis of variance (ANOVA) and post-hoc testing of means with all of the significant dependent variables. Means comparisons were performed using contrasts to circumvent assumptions of homogeneity of variances among sample populations when necessary.

We designed the overlay symbol system to provide the following advantages: (1) alignment of ORU and receptacle within insertion tolerances using a single camera view, even under adverse lighting conditions; (2) "rubber-band" features that prompt appropriate control command motions, even when the destination receptacle is outside the field of view of the camera; and (3) separation of needed translation and rotation control inputs.

Performance on the alignment tasks described above was examined using ANOVA and post-hoc means tests. In comparing errors produced during the trials, large differences in variances were noted between the no-overlay-then-overlay and the overlay-then-no-overlay orders of trial presentations. This was the case in all but the YZ alignment error trials. For this reason, contrast test techniques that are not sensitive to nonhomogenous variances were used for the means comparisons.

Immediately after the subjects finished the trials, they completed a survey of questions about the test. The outcome of the survey clearly indicates that the overlays were helpful. All 12 subjects completely agreed that the overlay information was helpful or useful in performing the ORU alignment operation, and that it did not hinder completion of the ORU alignment.

The results of this experiment indicate that overlays improve performance in maneuvering an ORU in preparation for inserting it into a receptacle. Despite the small number of subjects who were available to participate in the test, three of the four performance metrics show statistically significant improvements in pre-positioning accuracy using overlays. Trial completion time results are slightly less clear-cut, but variability in performance was reduced for all metrics during trials using overlays.

This study illustrates some potential for the application of AR overlays in robotic control systems. With appropriate simulation software, the overlays might provide an advantage in training for robotic applications. A simulation that has the appropriate fidelity and AR overlays to prompt correct actions might provide valuable "refresher" training among infrequent actual robotic tasks during extended Exploration missions.

Fig. 2. *Dexterous manipulator trainer.*

The Performance of the Orbiter Wing Leading Edge Impact Detection System During Space Shuttle Ascent

Tammy Gafka, *Johnson Space Center*

As part of the shuttle return-to-flight effort following the *Columbia* accident, NASA developed an on-board instrumentation system to improve awareness of ascent debris impacts to the orbiter wing leading edge (WLE). The Wing Leading Edge Impact Detection System (WLEIDS) consists of an array of 66 accelerometers per wing together with associated electronic components that acquire and transmit measured data to the ground during flight. Accelerometers are located behind the orbiter wing spar at the four attach locations of each WLE panel (figure 1).

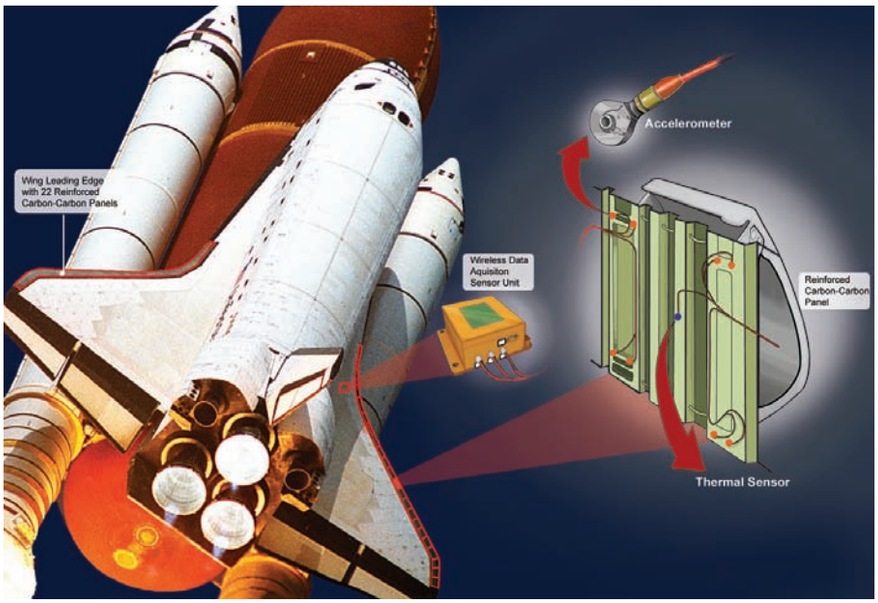

Fig. 1. *WLEIDS accelerometers and wireless data acquisition sensor units.*

During shuttle ascent, WLEIDS accelerometer data are collected by wireless data acquisition sensor units mounted in wing cavities near the fuselage, downloaded through wireless relay units to the astronauts' on-board laptops, and accessed by ground teams for engineering analysis in the Mission Control Center at Johnson Space Center.

Shuttle ascent is a highly dynamic period that includes main engine ignition, solid rocket booster (SRB) ignition, roll maneuvers, maximum dynamic pressure, SRB separation, and other significant loading events, all of which are captured in WLEIDS accelerometer data. The challenge for the WLEIDS engineering team is to discern from these dynamic data whether an impact has occurred to the WLE and, if so, when and where it occurred (for potential corroboration with ground imagery) and how much energy was associated with it (for damage severity assessments).

The Southwest Research Institute in San Antonio, Texas, developed WLEIDS data analysis methods and impact response prediction models anchored by more than 100 ascent debris impact tests. Test projectiles included various sizes and velocities of shuttle external tank (ET) foam and ablator, ice, and metal impacting three different, full-scale WLE test articles representing the various designs and regions of the shuttle wing structure. The "T-35" test article, representing the wing section around WLE panels 16R and 17R, is shown in figure 2.

Once the impact response prediction model was correlated by testing, we performed a statistical analysis on the results to define the damage probabilities associated with the WLEIDS impact indications measured at specific orbiter WLE panel locations. During flight, by mission elapsed time (MET) 18 hours, a full report of WLEIDS ascent impact indications is provided to the WLE hardware engineers, including structural dynamic characteristics and damage probabilities of each ascent impact. The hardware team considers WLEIDS results in a review of on-orbit WLE inspection imagery and, prior to orbiter re-entry, ultimately includes these results in an integrated assessment of WLE structural integrity.

In a typical shuttle flight, WLEIDS detects about 100 low-energy, non-damaging ascent debris impact indications. These indications are believed to be associated with small foam ("popcorn" foam) releases that occur due to aeroheating of the ET, causing internal pressure to build up and small divots in the tank foam insulation to separate. In figure 3, a typical ET aeroheating curve is

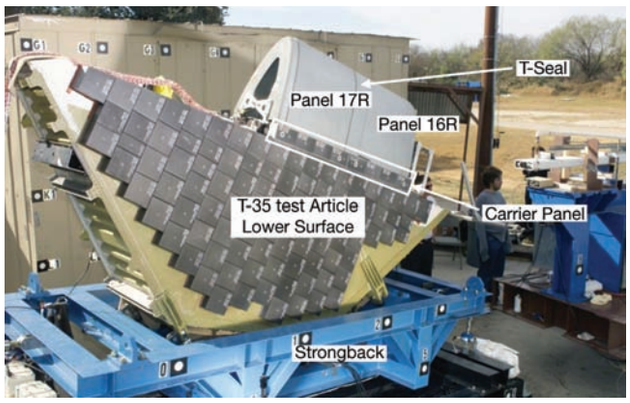

Fig. 2. *T-35 orbiter WLE test article.*

overlaid on a cumulative tally of WLEIDS ascent debris impact indications and their associated root-mean-square peak accelerations [gravity, root mean square (Grms)] for 10 flights, flights STS-114 through STS-124. Note that while the aeroheating curve exhibits a clear "double-hump" characteristic, the second WLEIDS data "hump" is much less pronounced. This is thought to be because, after an MET of approximately 165 seconds, little atmosphere remains to create notable drag forces on the foam and cause a significant velocity differential between a released piece of foam and the ascending orbiter. So, although the number of popcorn foam releases increases during this second hump, the foam does not have enough impact energy to register on the WLEIDS.

In summary, analysis methods for, and ascent damage predictions from, WLEIDS are grounded in an extensive test and model development program. WLEIDS data were also successfully used to confirm a known, in-flight phenomenon: "popcorn" foam release. As a result, we are highly confident that WLEIDS can detect both a large foam impact as well as smaller, damaging and non-damaging ascent debris impacts to the WLE such as the one that critically damaged the Space Shuttle *Columbia* orbiter.

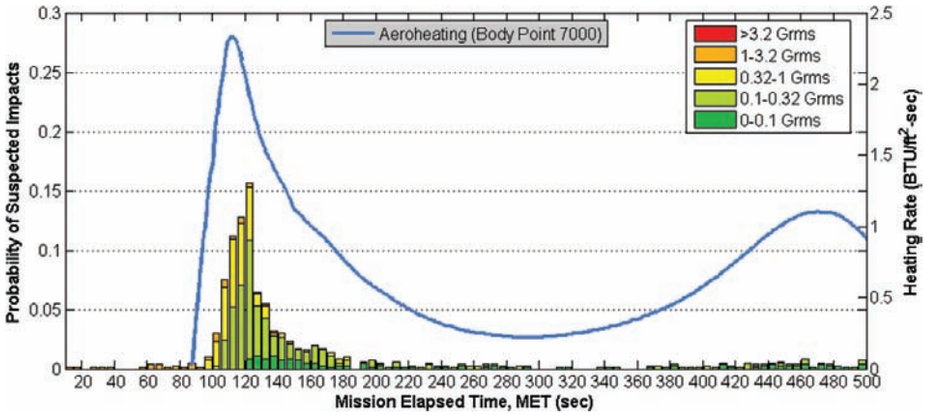

Fig. 3. *WLEIDS ascent debris impact indications (STS-114 to STS-124) overlaid with ET aeroheating.*

Anomaly Monitoring Inductive Software System

Ann Esbeck, *Johnson Space Center*
Andrew Hillin, *Johnson Space Center*
David Iverson, *Ames Research Center*
William Taylor, *Ames Research Center*

Johnson Space Center is collaborating with the NASA Ames Research Center (ARC) to develop, adapt, and deploy the Anomaly Monitoring Inductive Software System (AMISS) in support of International Space Station (ISS) flight operations. AMISS, which is based on the Inductive Monitoring System (IMS) software developed at ARC, complements current mission control practices by augmenting the health-monitoring capabilities in the Flight Control Room for real-time ISS systems. AMISS also allows for off-line analysis of archived data to detect unusual events in previous system behavior (figure 1).

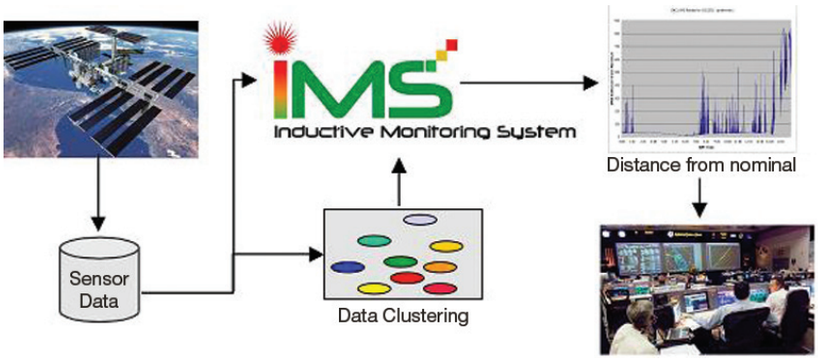

Fig. 1. *During off-line training, AMISS/IMS analyzes archived system data to model how a system normally behaves. In real time, AMISS/IMS alerts the operator if the monitored system behaves differently than expected.*

The AMISS software uses techniques derived from model-based reasoning, machine learning, and data mining to build system monitoring knowledge bases from archived sensor telemetry data. Unlike many other machine learning techniques, AMISS does not require examples of anomalous or failure behavior, which are often scarce or unavailable. It automatically analyzes archived nominal system data to form general classes of expected system sensor values, relationships, and interactions. This process enables the software to inductively learn and model nominal system behavior. The generated data classes are then used to build a monitoring knowledge base, or nominal system model, that is deployed on the flight control console. AMISS employs this knowledge base to perform real-time telemetry monitoring on the console. It compares concurrent vectors of incoming telemetry values to the model, determines the degree of deviation from historic nominal performance, and publishes the result for display or analysis by other software tools. Significant deviations or trends in AMISS monitoring results indicate out-of-family system behavior, which may be caused by system degradation or an incipient failure.

AMISS has been certified and deployed to monitor the control moment gyroscopes (CMGs) used to provide non-propulsive attitude control for the ISS. In off-line analysis of a previous CMG failure, AMISS detected early symptoms more than 15 hours before the CMG required deactivation due to excessive vibration (figure 2). We have also developed AMISS monitoring systems for the ISS thermal control, rotation rate laser gyro, and carbon dioxide removal systems. The thermal and rate gyroscope monitors are scheduled for certified mission control deployment in mid-2009.

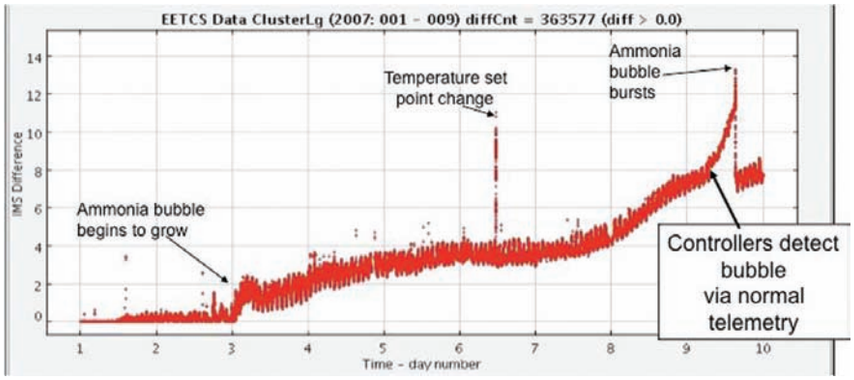

Fig. 2. *AMISS analysis indicated the formation of a gaseous bubble in the ISS Early External Thermal Control System liquid ammonia cooling loop nearly 6 days before mission controllers detected it via standard telemetry data.*

AMISS also supports the future ISS operations concept. Since new operators will not have the experience and insight that comes with many years of data observation, this tool will help them understand whether observed data trends are expected and nominal. If an unexpected data signature occurs, a concurrent, large AMISS degree of deviation will provide supporting evidence to the operator or specialist that something anomalous may be occurring and further investigation is warranted. For system specialists and engineering analysts, this tool provides an efficient method of reviewing a past day/week/month of system data vs. manually inspecting and comparing individual parameters.

The techniques used by AMISS are applicable to many instrumented systems with consistent behavior patterns. In addition to ISS system monitoring, AMISS techniques have been applied to space shuttle propulsion and impact detection systems, aircraft engine and flight control systems, and commercial electrical power systems. We have identified several additional ISS subsystems as candidates for AMISS monitoring, and ongoing AMISS research and development activity will provide additional system health monitoring and analysis capability.

Integrated Docking Simulation with Six-degree-of-freedom Dynamic Test System

Jennifer Mitchell, *Johnson Space Center*

The general purpose of the Six-DOF [degree-of-freedom] Dynamic Test System (SDTS) is to demonstrate and verify on-orbit tasks using berthing and docking/undocking such as assembly of space structures. The SDTS is a closed-loop dynamic testing system that combines high-fidelity test articles and software models to produce an integrated simulation of two-body berthing and docking in free space. Common uses of the SDTS include engineering evaluation of mechanical device operation, verification of in-space assembly procedures, development of crew training and operational procedures, and demonstration of advanced robotics technologies.

The SDTS provides a six-DOF motion base platform, a superstructure for mounting test articles and test sensors, an intercom network for voice communications, and a high-speed data acquisition system. It also provides multiple control bay workstations as well as three different dynamic and kinematic simulations to control the motion platform: a two-free-body docking simulation, a Space Shuttle Remote Manipulator System berthing simulation, and a Space Station Remote Manipulator System berthing simulation that includes Orbital Boom Sensor System dynamics. Truth data for the SDTS trajectories are obtained through an independent tracking system.

A task of the Sensor Technology Project (STP) was to develop a simulation and testing infrastructure in which to integrate and test relative navigation sensors at docking and undocking using the SDTS. This required integrating the Orion software simulation, also known as ANTARES, with the SDTS computer system for real-time, closed-loop testing with relative navigation sensors in the loop during docking and undocking scenarios.

ANTARES 7.2.0 is used to provide control inputs to the SDTS. It simulates the environmental and control forces exerted on the Orion spacecraft and the International Space Station (ISS). Low-, medium-, and high-fidelity guidance, navigation, and control (GN&C) functions, contained within the GN&C software, run independently on a PowerPC that is similar to the Orion vehicle management computer. ANTARES and the GN&C software together provide an array of docking capabilities for testing purposes. As the SDTS interface is also Trick-based, a module was integrated into ANTARES to transmit control parameters to the SDTS. Additional interfaces were developed between the GN&C software on the PowerPC and ANTARES and the relative navigation sensors. This multi-interface module enables data acquisition from the various sensors strapped to the platform and the test stand. This adds the capability to compare sensor data to truth data measured from the simulation. Sensor measurements from the platform are fed into the guidance and navigation software, which drives the test stand to the point of docking (figure 1).

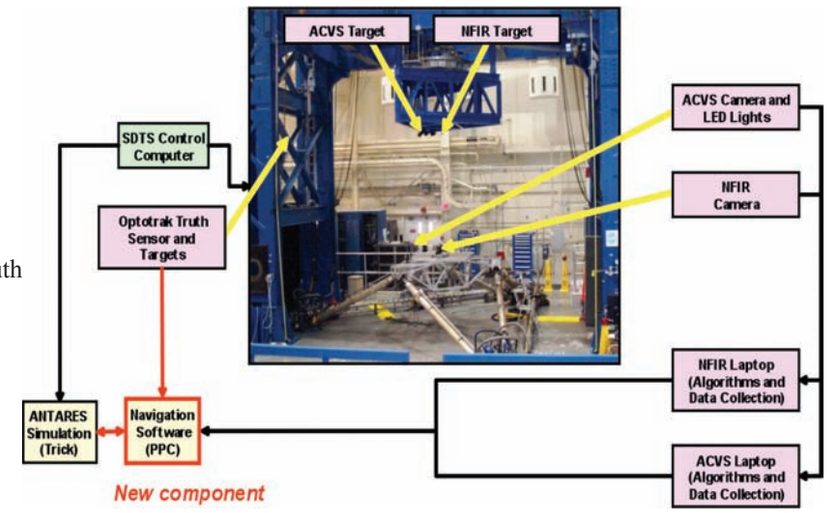

Fig. 1. *Six-DOF test stand equipment configuration.*

Currently, two test articles are available for testing at the SDTS: the AutoTRAC Computer Vision System (ACVS) and Natural Feature Image Recognition (NFIR). ACVS technology employs the "spot pose" technique, in which a sensor uses a cluster of retroreflectors in a known pattern to extract the six-DOF state, or "pose," of the sensor relative to the target vehicle. NFIR uses camera video to match image locations of the target vehicle features with a known

three-dimensional model to extract a pose. Math models for ACVS, NFIR, and a Flash LIDAR [light intensification detection and ranging] that is similar to the Orion visual navigation sensor (VNS) are also available for testing.

SDTS testing occurs at close range (from 3.04 me to contact distance) to mimic docking and undocking; therefore, the test stand is configured with docking targets. Due to the close range, NFIR uses only the docking target with a standoff cross rather than a full docking adapter mock-up. The docking target is nearly identical to the one that is used by shuttle when it docks to the ISS. The ACVS uses a target with a set of five retroreflectors (one of which is out of plane) with a mirror in the center.

Various trajectories have been developed for sensor testing. The trajectories that were selected are used to calibrate the sensors or mimic possible Orion docking trajectories. Three of the trajectories are calibration trajectories that are intended to ensure the sensors are performing consistently from day to day. The three check runs are as follows:

Radial Trajectory – Maneuvers the motion base from 0.914 to 0 m along the boresite of the docking cross. There is no lateral motion of the motion base and no relative rotation of the motion base with respect to the fixed test stand. The test objective is to ensure that the boresite of the sensor is in alignment.

Diamond Trajectory – Applies lateral motion to the motion base at a 0.457-m stand-off distance. The lateral motion is a ±0.305-m off-axis that forms a diamond in the X-Y axes. This trajectory tests the off-axis capabilities of the sensors.

Decaying Error Trajectory – Varies all translational and rotational components of the motion base relative to the fixed test stand. The lateral variations, which go up to a maximum of 0.914 m, vary sinusoidally to 0 m at docking. Likewise, the relative roll, pitch, and yaw offsets are a maximum of 5, 2, and 3 deg at the start of the trajectory and vary sinusoidally to 0 deg at docking. This trajectory is designed to provide distinctive signatures in all axes for sensor calibration and testing.

Four Orion docking trajectories are also on hand; these are designed to demonstrate the approach of the Orion to the ISS. The four test trajectories are as follows:

A nominal approach trajectory that has as its initial condition the Orion docking port, which is located 0.914 m along the boresite of the docking cross from the ISS docking adapter

A positional offset approach trajectory that has as its initial conditions the Orion 0.152-m offset in both lateral axes

A yaw offset approach trajectory that has as its initial conditions the Orion, which is located 0.914 m along the boresite of the docking cross from the ISS at a yaw angle of 5 deg

A retreat trajectory that begins the same as the positional offset approach trajectory and is commanded to a dock abort before it retreats back to a holding position

For the Orion guidance and navigation team, testing of the Orion guidance and navigation prototype software on a real-time processor with dynamic relative navigation sensors in the loop evaluates the accuracies and usefulness of the SDTS as an integrated testing capability. Test plans, procedures, scripts, processes, docking targets, and trajectories can be used as is or can be easily modified for future tests. The vehicles of the Constellation Program and all space flight vehicles require ground-test capabilities for testing, which encompass a broad scope of hardware and software-in-the-loop simulation and testing on real-time avionics. These elements have been combined at the SDTS, resulting in a six-DOF laboratory testing capability.

Autonomous Landing and Hazard Avoidance Technology

Chirold D. Epp, *Johnson Space Center*
Edward A. Robertson, *Johnson Space Center*

NASA plans to develop an integrated autonomous guidance, navigation, and control (AGNC) hardware and software system capable of detecting and avoiding surface hazards. This system will also be capable of guiding a crewed or robotic lunar lander to a safe touchdown at designated lunar landing sites.

To address both crewed and robotic missions, the AGNC system must be capable of operating in several modes from fully automatic to supervisory crew control to an advisory/standby mode. For crewed landers, the system must effectively communicate landing site hazard data to operators in a manner that facilitates timely integration with situational awareness information gathered from other sources.

The proposed global lunar lander will be used for sortie and outpost lunar exploration missions. To support global access, the lunar lander must be able to operate over a wider range of terrain and natural lighting conditions than was typical for the Apollo Program lander. For instance, NASA identified permanently shadowed craters near the lunar poles as attractive scientific targets. However, these locations are associated with more challenging surface hazard distributions, steeper local slopes, and more limited natural lighting conditions that produce long shadows. In contrast to the Apollo Program use of near-dawn (i.e., 7- to 20-deg) optimal lighting conditions to highlight surface hazards to provide visual identification, the solar incidence angle near the rim of Shackleton Crater will briefly peak at only approximately 1.5 deg. As a result, illumination of a landing site in that region of the moon will be very sensitive to local slopes and roughness. When these considerations are combined with the requirement for automatic operation and an ability to function autonomously, the result is a need for a highly capable, on-board, active sensor system that can perform both hazard detection and avoidance (HDA) and hazard relative navigation (HRN).

The flexibility and extensibility of the lander AGNC system are important considerations. The evolution of the Exploration program may lead to emplacement of navigation assets in lunar orbit and on the lunar surface. The AGNC system is designed to incorporate such inputs into the navigation filter, when one is available, but is not dependent on external navigation sources for mission success.

Multiple missions to a given area will result in more detailed and accurate knowledge of the terrain, knowledge that can be used to designate safe landing sites for future Exploration missions. However, reliance on assets specific to a local landing site may not support off-nominal mission scenarios in which a lander cannot reach its designated landing target.

We established five phases of the lunar descent trajectory, as shown in figure 1. The lander starts in a 100-km circular orbit. The deorbit burn sends the lander into a 100×15-km transfer orbit. The powered descent burn is initiated near perilune, and the lander then enters the braking phase during which the lander bleeds off most of its orbital velocity. The autonomous landing and hazard avoidance technology (ALHAT) system, during the braking phase, performs the terrain relative navigation (TRN) function that significantly improves the map tie between the lander

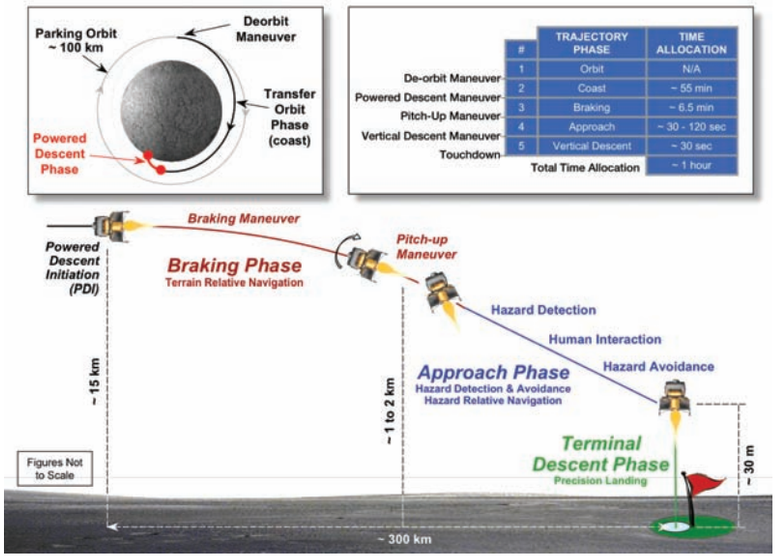

#	TRAJECTORY PHASE	TIME ALLOCATION
1	Orbit	N/A
2	Coast	~ 55 min
3	Braking	~ 6.5 min
4	Approach	~ 30 - 120 sec
5	Vertical Descent	~ 30 sec
	Total Time Allocation	~ 1 hour

Fig. 1. *Lunar descent trajectory.*

inertial state and the lunar surface. A map tie error is the uncertainty between the actual position of a feature on the lunar surface and the position shown on a lunar map due to measurement errors in the mapping process. This knowledge enables the lander to efficiently steer out the majority of the map tie error prior to the approach phase.

The lander pitches up to a more vertical orientation to begin the approach phase. The initial slant range from the lander to the landing target is expected to be in the range of 500 to 2,000 m. The duration of the approach phase depends on the initial slant range and the lander acceleration (throttle setting), which defines the lander velocity profile. Longer approach phase durations can be achieved at the expense of increased lander propellant (i.e., delta-V). A wide range of flight path angles is being investigated from a vertical descent (90 deg) down to an Apollo-type surface-skimming approach (~15 deg). Although higher flight path angles are more costly in terms of lander delta-V, they may provide a better view of the lunar surface for an HDA sensor. Moderate to low flight path angles are more efficient in terms of lander delta-V; they also provide greater opportunity for direct viewing of the landing site by the crew via a window. However, lower flight path angles also stretch the samples received by an HDA sensor, and can lead to overlooked hazards or false positives due to cracks/gaps in the high-resolution digital elevation map (DEM).

Note that high-resolution DEMs are generated "on-the-fly" by the ALHAT system to support the identification of safe landing sites and enable precision local relative navigation. These high-resolution DEMs are not the same as the lunar DEMs developed via lunar reconnaissance that are used for the pre-mission certification of a landing site and to support the TRN function.

During the approach phase, the ALHAT system uses these real-time-generated, on-board, high-resolution DEMs of the landing site to perform both the HDA and the HRN functions. The HDA algorithm evaluates the initial DEM and identifies safe landing areas based on lander hazard tolerance thresholds.

The HRN function enables precision local relative navigation using surface feature(s) tracked in successive DEMs to guide the lander to a spot directly above the landing target. The approach phase includes a "human interaction interval" to enable crew members to integrate safe landing site data from the ALHAT system with their own situational awareness information, and then decide whether to continue to the original landing target, divert to a new landing target, or abort the landing mission. The approach phase also includes the time/distance necessary to efficiently execute a short-range diversion to an alternate landing site.

The approach phase ends when the lander is precisely located 30 m above the landing target with a near-zero lateral velocity relative to the lunar surface. The low lateral velocity enables the lander to precisely descend the final 30 m using inertial navigation without additional HRN inputs. We conservatively selected this landing approach to avoid the complications associated with the potential impact of dust kicked up by the lander engine exhaust plume on the operation of the active sensor used for HRN. If the HRN function can be performed below 30 m, landing accuracy will improve.

The AGNC system must function in an integrated manner with the lander vehicle. Design factors such as lander hazard tolerance (slope, roughness), dimensions (footprint diameter), window location and field of view (visual piloting), and engine throttling range (acceleration profile for the approach trajectory and terminal descent) are critical to defining the sensor characteristics needed to perform HDA and HRN functions.

All lander designs necessarily represent a compromise between competing performance objectives. A large footprint provides increased landing stability at the expense of increased lander mass, but it also increases the required diameter for a safe landing site. Similarly, longer legs increase the hazard tolerance of the lander, but at the expense of decreased landing stability and increased mass.

We are investigating a wide range of sensor technologies (passive optical, radiometric, and light intensification detection and ranging (LIDAR)) with the objective of defining a sensor package that efficiently performs the TRN, HDA, and HRN functions in terms of mass, power, volume, cost, and complexity. Analysis and testing activities completed and planned are intended

Autonomous Landing and Hazard Avoidance Technology

continued

to characterize applicable sensor technologies and algorithms, and to identify key performance parameters and sensitivities, leading to a preliminary definition of the ALHAT reference architecture.

From a sensor and algorithm standpoint, the HDA function is more technically challenging than TRN, as it involves the collection and processing of a large quantity of digital elevation data in a short period of time. The slant range, flight path angle, and acceleration selected for the approach phase directly affect the design and performance requirements of the HDA sensor. Scanning and flash LIDARs are the only known sensors that can produce the required DEMs in real time during the short dynamic landing phase. Flash LIDAR technology is capable of gathering thousands of pixels of data in a single cycle, and ALHAT current research and analysis shows that it is the best choice for this sensor. The potential advantages of flash LIDAR make it an attractive candidate for a technology development project.

As previously stated, the ALHAT trajectory targets a highly precise location for the start of the terminal descent phase with a near-zero lateral velocity relative to the lunar surface. This low lateral velocity enables the lander to descend the final 30 m using inertial navigation without additional HRN inputs while still maintaining a high degree of landing accuracy. In addition to the TRN and HDA sensor(s) data, highly accurate velocimeter and altimeter information is needed to meet the ALHAT requirements for landing safety and precision. Lateral velocity errors, measured in the range of centimeters per second at the start of the terminal descent phase, can accumulate to several meters of additional landing error at touchdown. We are developing and testing a Doppler LIDAR velocimeter that is capable of determining the velocities required by the lander prior to terminal descent.

NASA is working with industry to develop state-of-the-art flash LIDARs that will meet the needs of the ALHAT HDA and HRN functions. These LIDARs, together with the Doppler LIDAR velocimeter and other sensors, have been and are being tested on helicopters and winged aircraft by the ALHAT Team. The final goal of this testing is to demonstrate an integrated AGNC lunar landing hardware and software system that can safely land a crewed or uncrewed landing vehicle on the moon.

Using the Orbiter Wing Leading Edge Impact Detection System for Micrometeoroid and Orbital Debris Impact Monitoring

Tammy L. Gafka, *Johnson Space Center*

Although the Wing Leading Edge Impact Detection System (WLEIDS) was originally developed to detect damaging ascent debris impacts to the orbiter wing leading edge (WLE), it is also being used to sense micrometeoroid/orbital debris (MMOD) impacts to the WLE. The risk of critical penetration due to MMOD impact remains one of the highest catastrophic risks to the shuttle at approximately 1 in 300 per mission. Monitoring with WLEIDS while on orbit can offer near-real-time knowledge of damaging MMOD impacts. A damaging MMOD impact to a WLE test article is shown in figure 1. The 6.1-mm hole shown in the figure was created by a 2.0-mm aluminum sphere projectile traveling at 6.93 km/s.

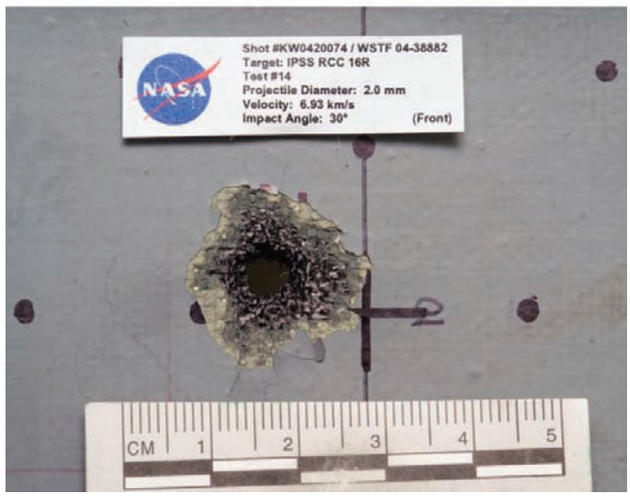

Fig. 1. *MMOD impact damage to WLE test article.*

The WLEIDS consists of an array of 63 accelerometers per wing together with the associated electronic components needed to acquire and transmit measured data to the ground during flight. Accelerometers are located behind the orbiter wing spar at the four attach locations of each WLE panel. WLEIDS accelerometer data are collected by wireless data acquisition sensor units (SUs) mounted in wing cavities near the fuselage; the data are downloaded through wireless relay units to the astronauts' on-board laptops and then are accessed by ground teams for engineering analysis in the Mission Control Center at the Johnson Space Center.

The most obvious limitation in using the WLEIDS, a system whose primary purpose is to monitor ascent (~a 10-minute event) for MMOD impact monitoring, is the limited battery life of the electronic components. Each SU records data for three accelerometers and has a battery life of about 21 hours. Based on testing, dynamic modeling, and flight experience, at least two corners of each WLE panel must be monitored to provide adequate detection and severity evaluation of MMOD impacts. The existing WLEIDS hardware therefore provides two accelerometer groups of sufficient resolution to detect damaging MMOD impacts. These groups are shown in figure 2; in this figure the blue dots represent accelerometers, the blue lines trace the accelerometers to the SUs that collect data for the accelerometers, and the numbered boxes represent WLE panels. MMOD impact monitoring of the WLE, using these two groups, can only be performed for a total of 42 flight hours – a small percentage of the total shuttle mission time of about 2 weeks.

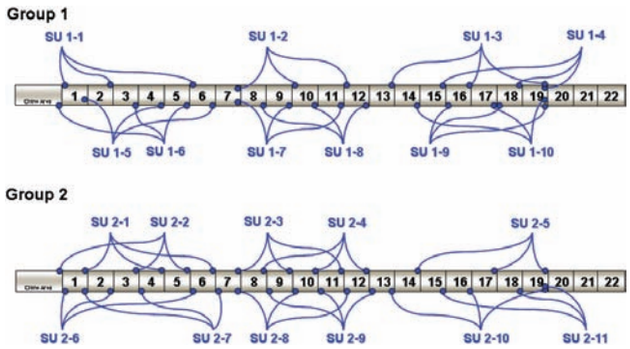

Fig. 2. *WLEIDS MMOD impact monitoring accelerometer groups.*

MMOD impact monitoring is performed during the highest critical MMOD impact risk periods. To best manage the 42-hour battery life of the two groups of accelerometers, the monitoring occurs when the orbiter attitude is such that the most vulnerable surfaces are oriented in the direction of the orbiter velocity vector. Monitoring can happen during orbiter docking and undocking with the International Space Station (ISS), on-orbit inspection of the orbiter Thermal Protection System, water dumps, and other mission activities. A typical WLEIDS MMOD monitoring plan for an ISS mission is shown in figure 3,

in which the normalized MMOD risk to the orbiter WLE is plotted against mission elapsed time (MET). WLE MMOD impact monitoring occurs during those times in which the area under the curve is shaded. Blue shading

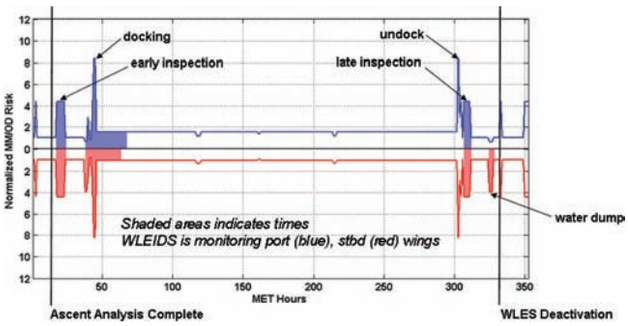

Fig. 3. *WLE MMOD risk vs. MET, indicating when the WLEIDS is monitoring.*

indicates port wing MMOD impact monitoring, and red shading indicates starboard wing monitoring.

Another limitation of using WLEIDS for MMOD impact monitoring is the sensitivity and sampling rate of the accelerometers. While damaging ascent debris impacts to the WLE cause significant localized accelerations at the wing spar, MMOD impact testing and analysis reveals that damaging MMOD impacts to the WLE can result in measured accelerations at the wing spar below the usable range of the accelerometer (i.e., ~0.3g). In addition, due to the extremely high velocities of MMOD vs. ascent debris, the effective sampling rate of WLEIDS (20,000 Hz raw data sampling rate with a 6,000-Hz anti-aliasing filter applied) likely results in clipping of peak accelerations and, thereby, significant uncertainty in the potential damage associated with a measured peak acceleration.

Extending the use of WLEIDS beyond its primary purpose of monitoring ascent debris impacts to the WLE to monitoring MMOD impacts offers both increased awareness of a critical orbiter risk and the opportunity to examine MMOD impact monitoring challenges for consideration in future human spacecraft programs. Due to the increased quantity of orbital debris with time, the MMOD environment continues to become more and more severe. Future programs should consider developing an adequate system with which to monitor and assess MMOD impacts to critical surfaces as part of a robust protect, detect, inspect, and repair approach to managing catastrophic MMOD impact risks.

Natural Feature Image Recognition Enables Docking

Jennifer Mitchell, *Johnson Space Center*

The Johnson Space Center (JSC) Natural Feature Image Recognition (NFIR) (figure 1) is a model-based approach to relative navigation that matches the image features of a target vehicle, as seen from a camera on a chase vehicle, to the corresponding features in a three-dimensional (3D) model. NFIR can use any high-contrast features on a target vehicle for which a 3D model exists; no special targets or reflectors are required. A computer running NFIR receives an image from a camera, searches that image for the target vehicle, locates the high-contrast image features of the target vehicle, and matches those features to the corresponding features of the 3D model. A pose (position and orientation of the target vehicle) (figure 2) is computed relative to the camera using the two-dimensional image to 3D model feature matches and the internal camera calibration. A Kalman filter is employed to determine the relative pose for the next image; this next image, in turn, is used to compute a search area in that image for each target vehicle feature being tracked.

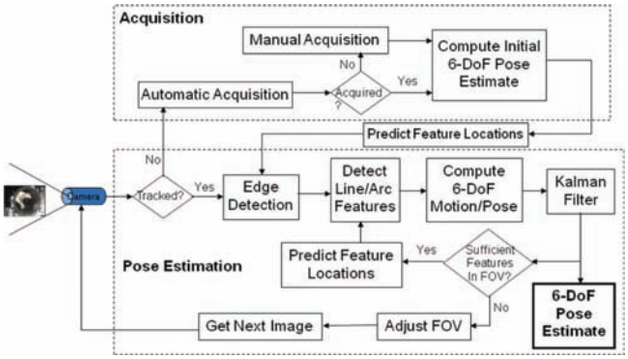

Fig. 1. *A high-level flow diagram shows how the NFIR tracker works.*

The development of NFIR began in 2003. In 2006, NASA selected NFIR as a pathfinder sensor to be characterized and tested as part of the automated rendezvous and docking (AR&D) Sensor Technology Project (STP). The NASA Marshall Space Flight Center (MSFC) flight robotics laboratory (FRL) completed an initial test that showed good performance in laboratory lighting using a full-scale pressurized module adapter mock-up that included the standard docking target. Using the planned Crew Exploration Vehicle (CEV) centerline camera and video processing unit (VPU), NFIR software could provide a software-only backup capability to the selected CEV visual navigation sensor and reduce the risk associated with relative navigation. In 2008, JSC integrated NFIR into the six-degree-of-freedom test system for use in the development of the docking closed-loop testing environment of a guidance, navigation, and control system. The major objective for NFIR in 2009 was to increase its technology readiness level (TRL) to TRL 6 and showcase its ability to use planned CEV hardware.

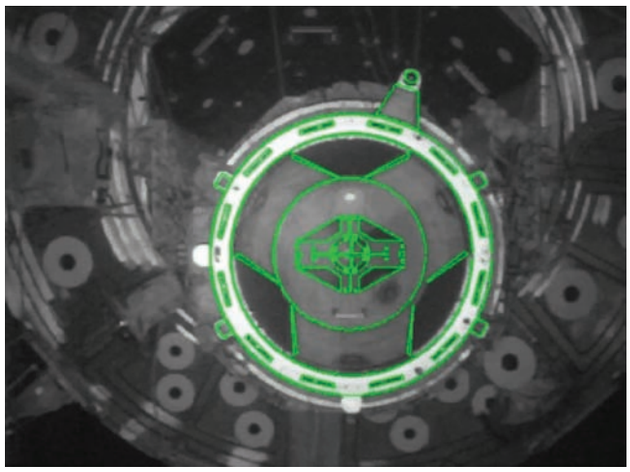

Fig. 2. *A projection of the NFIR pose estimate on a frame of the STS-118 docking camera.*

Recent upgrades to the NFIR include the following:

An automatic target vehicle acquisition/reacquisition capability

This allows NFIR to initiate tracking and pose estimates of the target vehicle automatically, and to reacquire the target vehicle if tracking is lost. Reference images of the target vehicle from the MSFC/FRL test were used to train the classifier to recognize high-contrast vehicle features. Points from the real-time image are matched to those extracted from training images.

An improved robustness to illumination variability

On-orbit lighting conditions are hard to mimic in a laboratory setting, and we are concerned with how well NFIR would work under these conditions. NFIR became

more adaptable to the dynamic lighting conditions seen on orbit when we added a contrast enhancement step at the front end of the process. This increased its capability to track and provide pose estimates of the target vehicle. Performance was improved with measures such as the overweighting premium features, the stand-off cross on the docking target, and dynamic computation of thresholds for feature detection. We tested the software modification using recorded video from the shuttle Orbiter Docking System camera during the final approach to docking with the International Space Station (ISS) on STS-116 and STS-118.

Robustness to image motion

Evaluation of the NFIR tracker using laboratory test videos showed that loss of track during nominal approach to ISS-type trajectories was minimal, and that when this loss occurred the target vehicle was successfully reacquired. This relaxes the NFIR constraints on relative motion between chase and target vehicles.

A port NFIR to an embedded processor with a clear path to flight

We developed a modular architecture for NFIR that can be compiled for embedded computers as well as for standard laptops. The existing NFIR tracking algorithm, the acquisition module, and lighting robustness improvements were implemented in the modular architecture.

Results from MSFC/FRL tests indicate that the NFIR performed well using video recordings in laboratory lighting. In general, root-mean-square pose estimation errors are less than 1% in depth and 0.75 deg in attitude (with smaller errors at closer ranges). After removal of the bias (probably due to errors in calibration of the pose of the camera relative to the truth sensor), the error standard deviations were less than 1% in depth and 0.5 deg in attitude.

The goal of the AR&D STP is to produce an NFIR brassboard for direct insertion into the mainline Orion (CEV) Project by the Orion critical design review. During 2009, we adapted NFIR to use cameras and computers similar to those selected for Orion, and to evaluate its functionality and performance for a new target vehicle. Future goals include

Converting the NFIR code to field programmable gate array architecture in preparation for porting to the CEV VPU.

Upgrading the NFIR to handle video from the Orion planned docking camera – a 2K×2K camera with a 512×512 region of interest in the center of the image that allows switching the field of view between 40 to 10 deg.

Expanding the automatic acquisition/reacquisition module to work with on-orbit video.

Developing a 3D feature model of the CEV docking adapter on the ISS for NFIR testing using simulated video of this model for a range of approach trajectories and lighting.

Testing of the NFIR with the above upgrades on real video acquired in the laboratory, and on video recorded during orbiter to ISS approach to docking.

This approach to relative navigation could be adapted to other target vehicles given a boresighted docking camera and an image processor on the chase vehicle plus high contrast features and a 3D model for the chase vehicle.

Fiber-optic Micrometeoroid Impact Sensor for Future Lunar Exploration Missions

Jer-Chyi Liou, *Johnson Space Center*
Mark Burchell, *University of Kent*
Robert Corsaro, *U.S. Naval Research Laboratory*
Frank Giovane,
Virginia Polytechnic Institute and State University
Nick Lagakos, *U.S. Naval Research Laboratory*
Eugene Stansbery, *Johnson Space Center*

The NASA Orbital Debris Program Office has been developing several particle impact sensors since 2002. The main objective of this development is to eventually conduct in-situ measurements to better characterize the small (millimeter or smaller) micrometeoroid/orbital debris populations in the near-Earth environment. The Program Office also supports instrument development to define the micrometeoroid and lunar secondary ejecta (MMSE) environment for future lunar exploration activities. Data returned from future lunar MMSE in-situ measurements will benefit: (1) fundamental lunar science by providing key data to improve our understanding of lunar cratering processes and the growth, mixing, and transport of the lunar regolith; (2) lunar exploration applied science by providing an accurate MMSE environment definition of reliable impact risk assessments for human lunar exploration activities, designing cost-effective shielding for habitats, and developing mitigation measures to address dust contamination issues for critical instruments and robotic components; and (3) planetary science by providing accurate flux and size distribution of micrometeoroids to place constraints on theories of collisions among asteroids and evolution of comets in the inner solar system. A well-established link between micrometeoroid impacts and lunar regolith is also key to understanding other regolith-covered solar system bodies from remote-sensing data.

One of the MMSE instruments under project development is the fiber-optic micrometeoroid impact sensor (FOMIS). The project objective is to design and build prototype FOMIS units that can be assembled into a large-area (tens of square meters or more), low-cost, low-mass, and low-power-consumption MMSE impact sensor on the lunar surface. The basic components of FOMIS are a thin film, under tension, and multiple fiber optic displacement (FOD) sensors mounted near the surface. The FOD sensor (originally developed at the U.S. Naval Research Laboratory, Washington, D.C.) consists of seven optical fibers with the central fiber serving as a light-emitting diode transmitter and the other six fibers functioning as receivers. When a particle impacts or penetrates the thin film, it causes the film to vibrate like a drum. This vibration, which is a function of particle size and impact speed, is measured via the variation in intensity of the reflected light (figure 1). Due to the high sensitivity of the optical fibers, the measurable vibration amplitude is up to 1 cm with better than 1 Å resolution.

Successful hypervelocity impact tests on a prototype FOMIS unit demonstrated in early 2008 the feasibility of the system by using the two-stage light gas gun at the University of Kent (Canterbury, U.K.). Figure 2 shows the front and back of the 17-cm-diameter prototype unit and the setup inside the test chamber. The thin surface is a 25-µm-thick aluminized Mylar® film under tension; three FOD sensors are mounted on the back of the unit. Additional large prototype units, up to 78 cm across, with different shapes are being constructed and will be subjected to both low-velocity and hypervelocity impact tests in 2009.

The FOMIS project is funded by the Focused Investment Group of the Johnson Space Center Mission Enabling Science Program and the NASA Orbital Debris Program Office. Additional collaborators in the project include the U.S. Naval Research Laboratory, Virginia Polytechnic Institute and State University, and University of Kent (Blacksburg, Va.). The near-term goal of the project is to advance the maturity of the system to a technical readiness level of 6 by 2012, and identify any possible future lunar deployment opportunities.

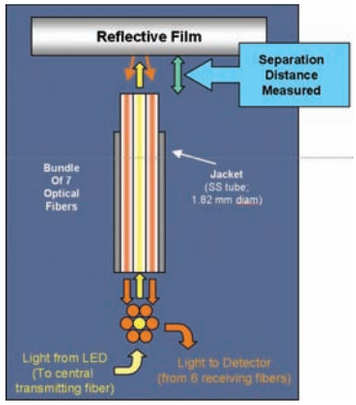

Fig. 1. *The concept used in FOMIS impact measurements.*

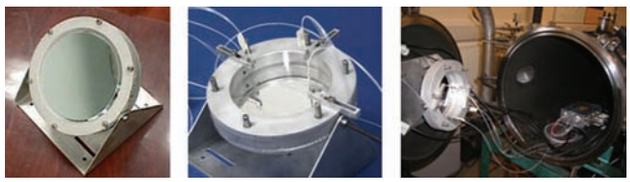

Fig. 2. *The front (left) and back (middle) views of a prototype FOMIS unit. The right image shows the unit and the electronics inside the two-stage light gas gun test chamber. Right before the closing of the chamber, the unit was turned 180 deg to allow the front side to face the incoming projectile.*

Technologies for Extravehicular Activity and Protection from Harsh Environments

Extravehicular Activity Technology Development – Thermal Subsystem

Luis Trevino, *Johnson Space Center*

Grant Bue, *Johnson Space Center*

The thermal subsystem provides temperature control for an astronaut. In current Constellation Program (CxP) Portable Life Support System (PLSS) concepts, the thermal subsystem consists of a single-phase water loop that contains a pump, an evaporative cooling device, an avionics cold plate, a water bladder that serves as an accumulator, and the liquid cooling and ventilation garment that the astronaut wears. The extravehicular activity (EVA) technology development team is developing critical thermal subsystem components to support the CxP lunar spacesuit. Development of suit water membrane evaporators (SWMEs) addresses PLSS heat rejection, and an advanced pump development addresses heat transport.

Sheet membrane suit water membrane evaporator

The sheet membrane SWME (figures 1 and 2) provides cooling to the spacesuit water loop by evaporating some of the water across a membrane into the vacuum of space. As the water turns to vapor, it takes the energy needed to cause the phase change with it as the vapor is vented into space. The sheet membrane SWME uses six concentric cylindrical membranes to create water passages separated by a vented space. A back pressure control valve is used to control the pressure within the evaporator assembly, which controls the amount of water that is evaporated; it therefore controls the amount of cooling the crew member experiences.

Fig. 1. *Sheet membrane SWME.*

A critical aspect of the SWME is its ability to maintain acceptable performance throughout the entire 6-month mission of a spacesuit on the lunar surface. Another critical aspect of this membrane-based device is its sensitivity to contamination. In addition to performance testing, the sheet membrane SWME will be subjected to life testing and challenge testing in which different contaminants are present in the water.

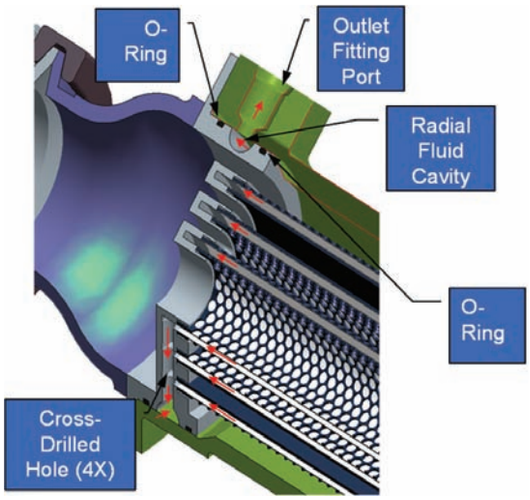

Fig. 2. *Detail of sheet membrane SWME.*

Hollow-fiber suit water membrane evaporator

The hollow-fiber SWME operates on the same principles as the sheet membrane SWME. Instead of using sheet membranes arranged in concentric cylinders, the hollow-fiber SWME uses a bundle of hollow tubes made from a hydrophobic material. Scientists compared three commercial off-the-shelf (COTS) hollow-fiber units through an accelerated life test (figure 3). A Membrana (Wuppertal, Germany)-made unit was the clear winner because it showed no performance degradation over a series of tests that simulated 100 EVAs. Once this specific technology was selected, additional tests provided sizing data to demonstrate the controllability of the unit by using a back pressure control valve. Other evaluations showed how the unit would handle bubbles in the water. Data taken from these tests were used to design a full-

sized engineering unit that will be submitted to the same series of tests as the sheet membrane SWME (figure 4).

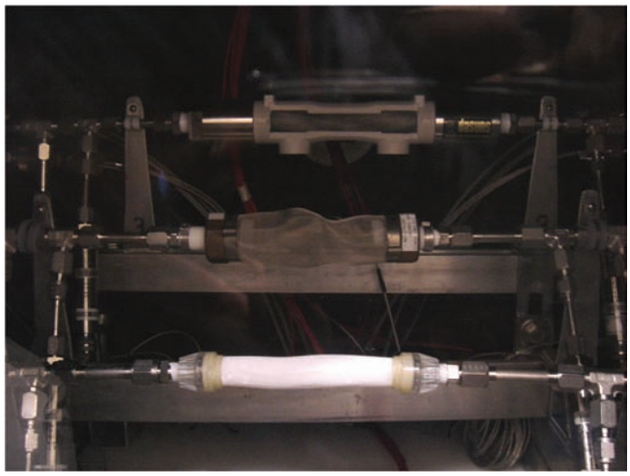

Fig. 3. *COTS hollow-fiber evaluations.*

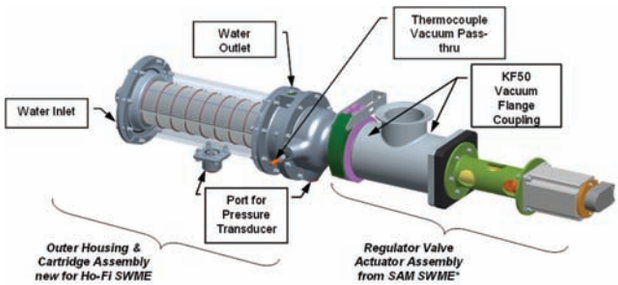

Fig. 4. *Hollow-fiber SWME design.*

Water pump

The shuttle spacesuit water pump had two on-orbit failures caused by water-quality issues. Due to the long duration of Constellation (Cx) missions and a drive to increase the robustness of the spacesuit, missions designers pursed water pump development. In addition to increasing robustness, the Cx spacesuit water pump must be able to deliver a wider range of pressure head than the shuttle unit. This led to the evaluation of several COTS positive displacement pumps, an aerospace heritage gear pump, and a custom gerotor pump (figure 5). Not only did we compare the performance of these pumps, we also subjected the pumps to a series of life tests and water quality challenge tests to evaluate their robustness.

Fig. 5. *Gerotor pump head.*

Extravehicular Activity Technology Development – Oxygen Subsystem

Colin Campbell, *Johnson Space Center*
Grant Bue, *Johnson Space Center*

The extravehicular activity (EVA) technology development team is devising critical oxygen (O_2) subsystem components to support the development of the Constellation Program (CxP) lunar spacesuit. The O_2 subsystem of a spacesuit Portable Life Support System provides the crew member with gaseous oxygen for metabolic consumption, a pressurized environment, and the ability to supply open-loop purge flows for carbon dioxide washout or supplemental cooling. The primary components of the O_2 subsystem are tanks and regulators. Additional components include quick disconnects, purge valves, and relief valves.

Primary variable regulator

The shuttle and International Space Station environmental mobility units have O_2 regulators with only two mechanically fixed set points. In contrast, the CxP requires a variable-pressure regulator. This regulator must perform the function of decreasing the pressure from 3,000 psia in the O_2 tank to a nominal suit pressure of approximately 4.8 psia (figure 1). Making the regulator capable of varying the pressure setting provides added functionality because it can be used to regulate the suit pressure to (1) match different vehicle pressures, (2) perform procedures to prevent or treat decompression sickness, or (3) minimize pre-breathe durations prior to going EVA. This project will develop an electronically driven regulator with a minimum of five set points and a goal of making the regulator continuously variable. Currently, this regulator (built by Carleton Technologies Inc., Orchard Park, N.Y.) has a stepper motor to adjust the compression of a spring that then mechanically sets the regulator. The current development not only includes the mechanical operations of the regulator, but also the electronics that drive the regulator and the control logic. The Johnson Space Center designed and built a test stand to evaluate candidate regulators for future spacesuit development (figure 2).

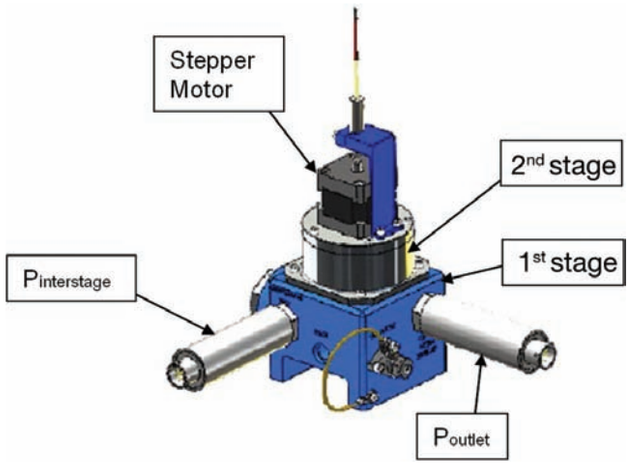

Fig. 1. *Primary variable regulator.*

Fig. 2. *Regulator test stand.*

Variable electronic regulator

The variable electronic regulator (VER) (figure 3) is an alternative to a variable pressure regulator. Instead of using a stepper motor and a spring to mechanically set the pressure of the regulator, the VER uses a variable orifice control valve and a feedback control scheme to actuate the valve. A pressure transducer within the VER measures the pressure and changes the valve position to control to the desired set point.

Oxygen subsystem component performance in dusty or dirty environments

Components such as quick disconnects, relief valves, and purge valves are all key components of the O_2 system. These precision fluid systems components are expected to be very sensitive to contamination by lunar regolith. A dust box, the lunar regolith environment simulator (LRES) (figure 4), tests these components. The LRES can deposit regolith and dust onto O_2 system components through direct spray, indirect spray, electrostatic deposition, and immersion, and by simply pouring the regolith on the components. Oxygen system components are exposed to contaminants in this facility, and their performance is then evaluated to quantitatively determine whether any degradation has occurred. The typical performance degradation for these types of components is an increased leakage rate.

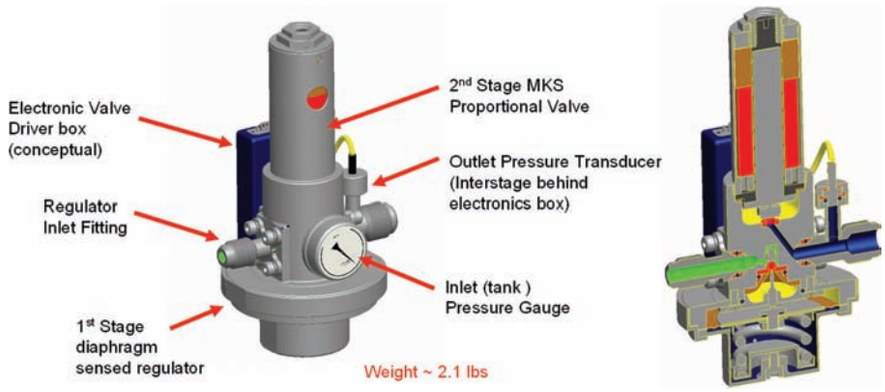

Fig. 3. *Variable electronic regulator.*

Fig. 4. *Lunar regolith environment simulator.*

Extravehicular Activity Technology Development – Ventilation Subsystem

Heather Paul, *Johnson Space Center*

The ventilation subsystem performs the functions of providing oxygen circulation, carbon dioxide (CO_2) removal, trace contaminant removal, and humidity control. The extravehicular activity (EVA) technology development team is devising critical ventilation subsystem components to support the development of the Constellation Program (CxP) lunar spacesuit.

Rapid cycle amine swing-bed

A rapid cycle amine swing-bed is the CxP baseline for spacesuit CO_2 and humidity control. This swing-bed operates by flowing gas in the ventilation loop through beds of aluminum foam packed with small polymer beads. The beads are coated with an amine that adsorbs both CO_2 and water vapor. Once the beds are saturated, a valve is actuated to expose the bed to the vacuum of space and desorb the CO_2 and water vapor. The swing-bed contains two sets of beds, one set of which is always adsorbing while the other set is always desorbing, thus allowing continuous regeneration during EVA (figure 1). The beds are thermally coupled so that a minimal net thermal load exists on the ventilation subsystem heat exchangers. Recent technology development efforts focused on packaging this swing-bed into a low-mass, cylindrical housing that rotates back and forth against a faceplate to cycle the beds. We built and tested several subscale test articles, including a flow visualization test article (figure 2), a test article to evaluate the rotating seal on the faceplate (figure 3), and a four-bed unit. A full-sized, 10-bed unit was designed.

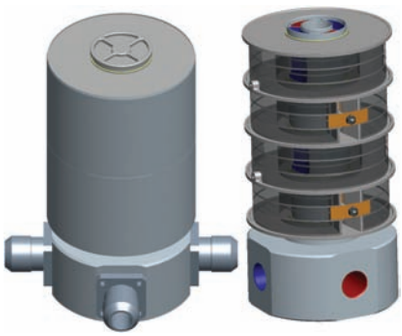

Fig. 1. *Rapid cycle engine conceptual design.*

Fig. 2. *Flow visualization testing.*

Fig. 3. *Face seal test article.*

Ventilation fan

Fan development for the ventilation subsystem focused on minimizing mass and power while providing adequate flow over a wider range of flow rates and pressure drops. After comparing numerous commercial fans, compressors, and blowers, we tested several units to generate reasonable power and determine whether the fans met mass and performance requirements. Hamilton Sundstrand (Hartford, Conn.) is designing and fabricating a fan for these tests (figure 4).

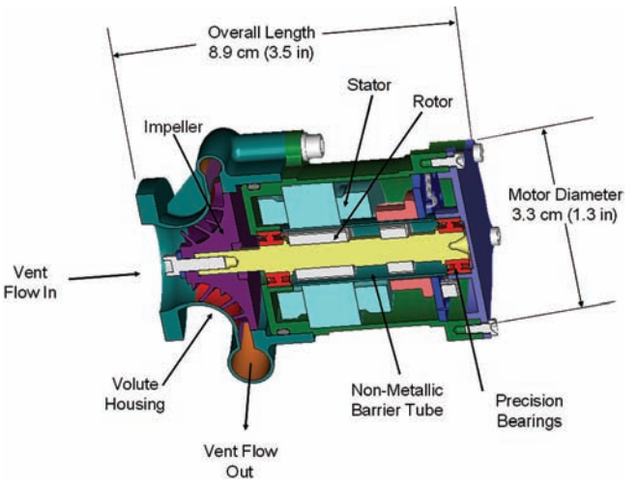

Fig. 4. *Fan cross section.*

Extravehicular Activity Technology Development – Ventilation Subsystem

continued

Humidifier

The humidifier in the ventilation loop needs to control the humidity level to within an acceptable range. We tested two commercial off-the-shelf (COTS) humidifiers units (figure 5) that operate by evaporating water across a membrane into the ventilation loop. We also tested a custom unit. Additional development efforts will optimize the size of the unit and develop a control scheme.

Fig. 5. *COTS humidifiers.*

Extravehicular Activity Technology Development – Portable Life Support System Packaging

Gretchen Thomas, *Johnson Space Center*

Evelyne Orndoff, *Johnson Space Center*

As NASA missions shift from microgravity extravehicular activities (EVAs) to EVAs performed on the lunar surface, the mass and center of gravity of spacesuits will become much more critical to mission success. Well-designed component packaging is crucial to hold, connect, and protect the hardware that ensures a spacesuit's life support functions. The current shuttle Portable Life Support System (PLSS) has a mass of 158 lbs., 79 lbs. of which are packaging. The EVA Technology Development Team, consisting of Johnson Space Center Crew and Thermal Systems Division personnel, is developing for the Constellation Program's lunar spacesuit an innovative foam packaging concept that will decrease the mass associated with packaging PLSS components.

Portable Life Support System packaging design and evaluation

The team has evaluated packaging arrangements to optimize the center of gravity of the suit as well as enable maintenance of PLSS components (figure 1). The components are held in place by compressible, open-celled foam that also helps protect the components in case a suited crew member falls on the lunar surface. A thin plastic cover is used to distribute the loads more uniformly across the foam, and multilayer insulation is placed on top of this cover to provide thermal control. Team members have performed the following: both analytical and experimental evaluations of this packaging concept; thermal analyses to define temperature requirements for the foam; and dynamic computer simulations to look at stresses seen by different components, optimize the shell design, and determine the amount of foam needed to protect the components. Several series of tests have correlated the dynamic models (figures 2 and 3). These include 1g drop tests using mass simulators, 1g drop tests of entire PLSS mockups in various

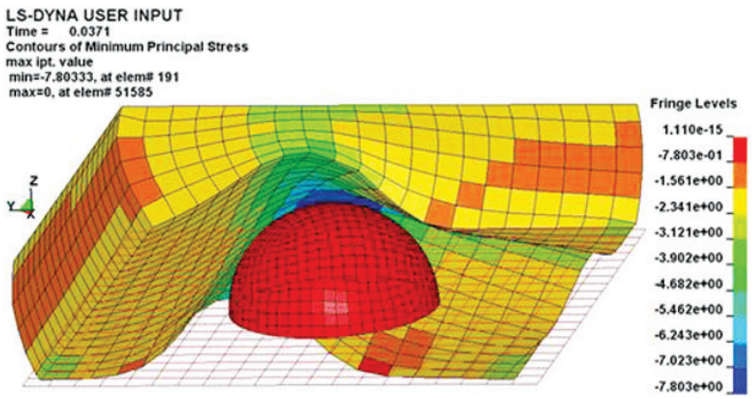

Fig. 2. *Stress analysis – falling on a rock.*

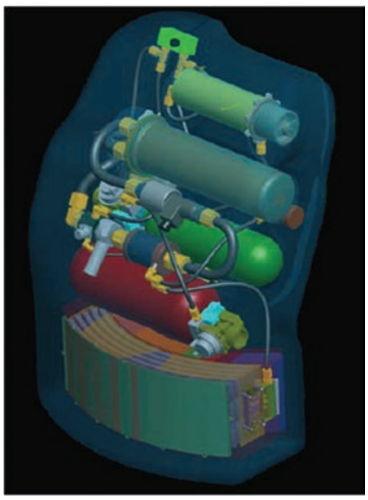

Fig. 1. *PLSS component layout.*

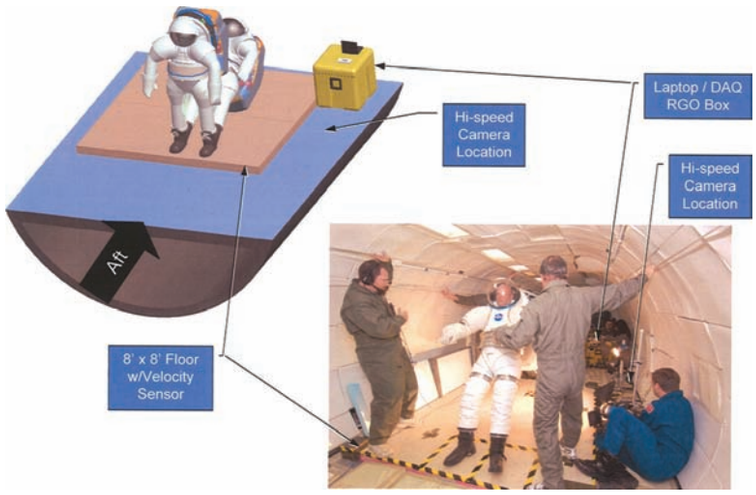

Fig. 3. *Reduced-gravity fall testing.*

orientations and using simulated rocks, and reduced-gravity fall tests with the PLSS mockup attached to a Mark III spacesuit.

Foam selection and development

The EVA Technology Development Team performed extensive research of available foams (figure 4). The foams that held promise of meeting the PLSS requirements mechanical properties were tested in a variety of simulated environments. These environments included the full temperature range based on the thermal analysis described above and also vacuum conditions. Stress-strain curves were produced, and the foam's compression set was measured for this range of environments.

The next step in developing PLSS foam packaging is under way. Contracts with Zotefoams plc (Croydon, England) and the Rochester Institute of Technology (Rochester, N.Y.) were awarded. These contractors are focusing on the development of new foams that improve performance at temperatures in the lower end of the PLSS requirements.

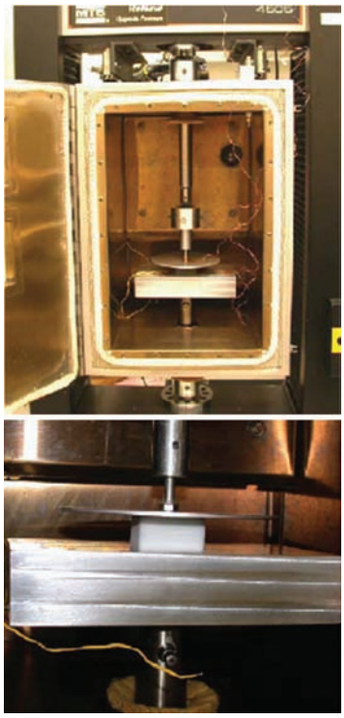

Fig. 4. *Foam properties testing.*

First-generation Suit Port Development and Testing

Barbara Romig, *Johnson Space Center*

Charles Allton, *Johnson Space Center*

Introduction

The Lunar Electric Rover (LER), formerly called the Small Pressurized Rover, is an integral part of the current lunar surface architectures under consideration in the Constellation Program. The LER is intended to optimize human safety and performance in planetary exploration by combining a comfortable shirtsleeve, sensor-augmented environment for gross translations and geological observations with the ability to rapidly place suited astronauts on a planetary surface via the suit port. Each LER incorporates two suit ports that enable rapid egress to a planetary surface to take full advantage of human perception, judgment, and dexterity in an extravehicular activity (EVA) suit and rapid ingress to the shelter of the LER in response to solar particle events, suit malfunctions, or medical emergencies. The suit ports also enable single-person EVA operations. Figure 1 shows the 1g LER mockup.

Fig. 1. *The 1g LER mockup.*

NASA developed a two suit port deliverables in fiscal year (FY) 2008: an aft bulkhead mockup for functional integrated testing with the 1g LER mockup, and a functional and pressurizable engineering unit (EU). This included the development effort for both of the deliverables, with support from NASA Ames Research Center (ARC) for initial suit port concepts and fabrication and testing of the EU and from NASA Langley Research Center for fabrication of the aft bulkhead structure.

Aft bulkhead mockup

We integrated the suit port aft bulkhead mockup with the mockup of the LER cabin and chassis. This mockup, located on the aft bulkhead of the LER cabin structure, includes hatches, a locking (Marman) mechanism, seals, interior and exterior suit don/doff aids, and exterior platforms to accommodate different crew member heights. A lightweight mockup of the Mark III suit was tested with the suit port aft bulkhead mockup. As there are several limitations to the suit port and mockup suits, results of the suit port evaluation need to be interpreted within the context of the limitations. Figure 2 shows the aft bulkhead mockup with suits attached to the suit ports, and figure 3 shows the aft bulkhead mockup from inside the LER cabin.

Fig. 2. *Aft bulkhead mockup with Mark III mockup suits attached to suit ports.*

Fig. 3. *View of aft bulkhead mockup from inside LER cabin.*

First-generation Suit Port Development and Testing

continued

At the Desert Research and Technology Studies at Black Point Lava Flow, Ariz., we tested the 1g LER mockup in October 2008. Overall, the LER met all necessary objectives in terms of human performance and crew accommodations. It adequately supported EVA operations through the use of suit ports and operational support for the EVA crew member; however, redesign of the suit port mechanism controls and external alignment guides to be more easily operated could further increase performance and productivity. We found no issues with the internal cabin volume for suit donning and doffing, but minor improvements were suggested for internal access to the suit port and general operations. Test subjects showed that the suit port concept was practical, viable, and a highly efficient way to perform EVA operations from the LER.

Engineering unit

The EU is a fully functional and pressurizable unit for testing the sealing interface between the LER and the suit. It consists of a pressure vessel with an inner hatch to simulate the LER cabin at 8 psi, an interface plate representing the interface between the suit and suit port (but the suit pressure is not represented), the locking (Marman) mechanism clamping the interface plate to the pressure vessel, and the seals (inflatable seals that close up the gap between the interface plate and the pressure vessel; lip and O-ring seals that prevent leakage between the cabin volume and the interspace/exterior; and dynamic seals around the shafts of the actuators passing through holes in the walls of the pressure vessel). Suit don/doff aids are not included in the EU. Figure 4 illustrates the EU conceptual design.

The EU is being assembled at ARC for design verification and operation and functionality testing. Operation and functionality testing examines the locking and sealing interface between the suit port and the suit interface plate per the operational concept. For testing, the EU is reconfigured to simulate the different phases of suit port operations; its internal volumes are pressurized to create the pressure differences that would occur during real operations. However, testing will be at ambient, not in a vacuum chamber.

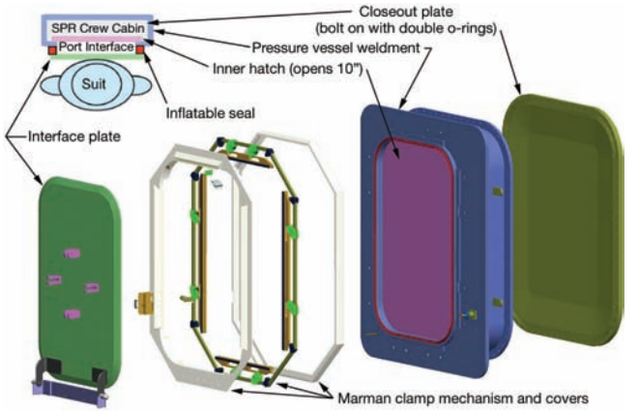

Fig. 4. *EU conceptual design.*

Figure 5 illustrates the four phases of suit port operations that will be tested. Configuration 1 represents the suit port configuration when the suit is ready for donning (cabin and interspace would be at 8 psi). Configuration 2 represents the case when the crew has donned the suit but has not depressurized the interspace or detached from the suit port (cabin and interspace would still be at 8 psi). Configuration 3 represents when the interspace has been depressurized to 0 psi, the pressure that would be achieved prior to operating the locking mechanism and detaching for an EVA. Configuration 4 represents the LER after the suit and interface plate are detached from the suit port. Pressure differentials and leak rates will be measured.

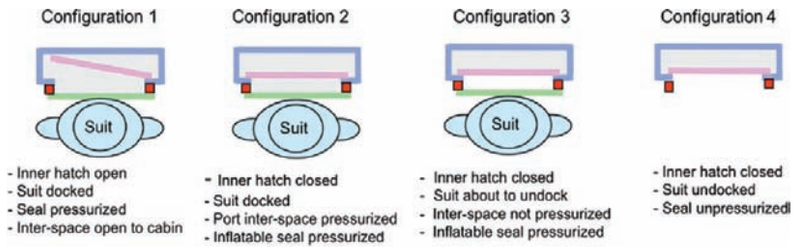

Fig. 5. *Suit port operational configurations.*

Conclusion

Testing of the suit port aft bulkhead mockup showed that with some minor modifications, the suit port concept is practical, viable, and a highly efficient way to perform EVA operations from the LER. The second-generation suit port will use electromechanical actuators to lock the suit to the suit port, thus being less fatiguing on the crew member. It will also incorporate an aft enclosure for the suits to protect them from the environment.

After operation and functionality testing is complete, the EU will undergo dust and vibration testing.

Electrical Shock Hazards during Extravehicular Activity on the International Space Station

Steve Koontz, *Johnson Space Center*
John Alred, *Johnson Space Center*
Leonard Kramer, *The Boeing Company*
Drew Hartman, *The Boeing Company*
Ron Mikatarian, *The Boeing Company*
Kendall Smith, *The Boeing Company*

The International Space Station (ISS) is the largest, most complex space vehicle flown. Natural and induced ISS spacecraft charging processes, common to this space vehicle, can lead to electrical safety concerns during extravehicular activities (EVAs).

While flying at high speeds through Earth's magnetic field, the ISS is operating in Earth's ionosphere – an electrically conducting medium. The ionospheric plasma environment interacts with the ISS structure and electrical power system components to produce electrical potential differences (floating potentials (FPs)) between the ISS and the surrounding plasma. Electric current flows in the plasma and through the ISS conducting structure between the vehicle's different parts. For example, electrons collect at positively charged surfaces, such as the arrays, while ions impinge on metal surfaces and remove electrons at other locations, notably the Russian modules.

Known ISS EVA hazards arise from both ISS and extravehicular mobility unit (EMU) spacecraft charging processes, in combination with the vulnerability of the human body to electric current and the fact that NASA's EVA spacesuits do not provide the wearer electric shock protection. In fact, the suit shell is penetrated at numerous points by electrically conducting, metallic materials that can contact the astronaut's body (figure 1). Providing an electrically safe EVA environment is the responsibility of the spacecraft on which the EVA is being performed.

ISS has two indentified shock hazard scenarios. In one case, charge collects on anodized parts of the suit when it is exposed to negative ISS FPs. This energy can discharge in an arc resulting from breakdown of the anodized layer on the EMU suit. Figure 2 illustrates arcing observed when an artificial plasma source was switched on and off at 5-minute intervals in a laboratory. The spike-like signatures occurring every few seconds are associated with high current that is potentially catastrophic to the human body.

A second shock hazard is associated with direct current passing through an astronaut's body when in contact with positively biased ISS environments. Although the ISS space flight environment is sometimes erroneously treated as an electrical insulator, in fact the ionospheric plasma brings the electrical ground into close proximity with the astronaut's suit and can provide substantial electric current to exposed metallic conductors. Plasma electrons collect easily on positively charged, bare metal surfaces, and current can move through the human body to the positively charged ISS structure or power system components.

Fig. 1. *Astronaut conducting EVA on the ISS.*

Generally, an EVA astronaut is exposed to a variety of positively and negatively charged environments, depending on the location of the ISS in its orbit and the EVA worksite on ISS. We currently manage these risks through active hazard monitoring and hazard mitigation hardware in combination with ISS flight procedures that control ISS FPs. Careful assessment and control of EVA procedures also contributes to making the chance of an astronaut sustaining an electric shock during EVA small.

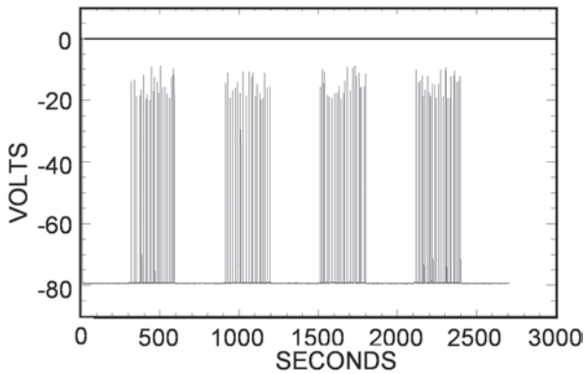

Fig. 2. *A laboratory test illustrating electrical arcing of anodized EMU suit materials.*

Water Egress and Survival

John Haas, *Johnson Space Center*

A requirement for the Orion crew module (CM) to splash down in the ocean brought back some old training requisites to the Johnson Space Center (JSC) Mission Operations Directorate (MOD). In typical training scenarios the crew and support personnel practice crew egress procedures under various configurations and conditions. In the past, we trained crews in full-scale trainers both in pool settings and in open water. When the new training requirement surfaced, we took a fresh look at how this might be accomplished.

Some things have changed in the past 40 years, and two notable changes are NASA's tighter budget constraints and the added availability of the JSC Neutral Buoyancy Laboratory (NBL) in which NASA astronauts train for extravehicular activities (figure 1). A study examining the cost of providing a ship that could routinely take the 18,000-lb. CM and a large test team out to sea portended significant budget challenges. Cost is clearly a big disadvantage in this scenario.

Fig. 1. *The JSC NBL.*

Another big disadvantage to training offshore is the unpredictability of the weather. Bad weather can lead to cancelled tests, and in flat water one may as well be in a pool. Astronaut's schedules are very tight in the year prior to launch, and changing them has a negative ripple effect. We thus proposed an alternative to open water testing in which a large mass located underneath the floor of the crew compartment would be manipulated to displace the center of gravity (c.g.) and generate motion in the controlled environment of the NBL. Being able to generate motion is critical in that it trains and prepares crews to perform tasks under very difficult conditions. Although the proposed concept will not produce the heave and surge found in nature, it could reliably provide very challenging conditions. The concept of an "active" trainer proved both financially appealing and practical from a training and scheduling vantage point.

NASA decided to pursue the active trainer concept by prototyping a one-quarter-scale model. The first obstacle to producing this one-quarter-scale model was a lack of data regarding how Orion would behave in the water environment. Up to this point a land landing had been nominal and was getting most of the program's attention. The one-quarter-scale model, the Water Egress and Survival Trainer-Prototype (WEST-P), was subsequently built by MOD and caught the attention of the Orion Program (figure 2).

Fig. 2. *The one-quarter-scale WEST-1.*

The Orion Program funded extensive testing of the WEST-P by the U.S. Navy at the Naval Sea Systems Command/ Carderock tow tank and by the U.S. Army at the Aberdeen Test Center large outdoor wave-generating site (figure 3). We used generated test data to make recommendations for flight vehicle sizing and placement of sea anchors, tow/ winch attach points, and flotation collars. We also assessed sea-keeping characteristics in rough waves up to 6 m high. Testing of the one-quarter-scale model showed that the WEST-P would make for a very uncomfortable ride. This suggests that rather than using a relatively large mass to manipulate the WEST-P c.g., we might use a small mass to excite motion at the resonant natural period (figure 4).

Fig. 3. *WEST-P at the U.S. Army's Aberdeen Test Center.*

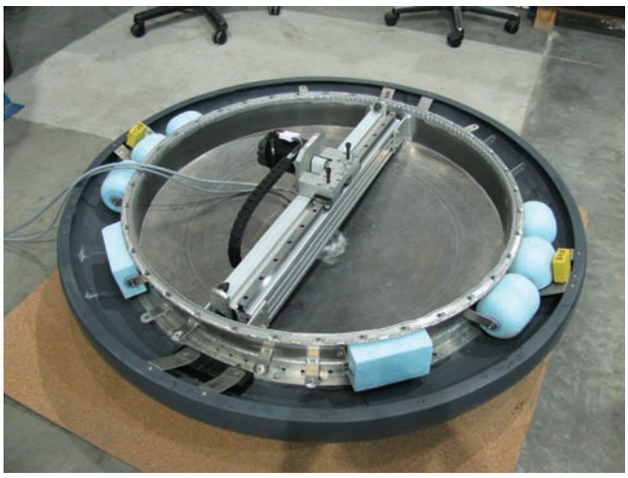

Fig. 4. *WEST-P with linear stage installed.*

The reduced component sizing and lower energy requirements of the resulting design provide benefits throughout the systems. Within the sealed, watertight test article are 24-Vdc lithium-ion batteries powering a brushless servomotor-driven linear stage controlled by a field-programmable gates arrays real-time controller using encoder slide position feedback and rotational velocity feedback from an inertial measurement unit. An ultra-mobile personal computer interfaces to the internal equipment and communicates via a wireless router to the outside world using Windows Remote Desktop.

Space and Ground Operations

The Mobile Information System: A Hands-free Procedures System

Harry L. Litaker, Jr., *Lockheed Martin*
Shelby G. Thompson, *Lockheed Martin*
Ronald D. Archer, *Lockheed Martin*
Richard L. Szabo, *Lockheed Martin*
Evan Twyford, *MEI Technologies*
Carl Conlee, *MEI Technologies*
Mihriban Whitmore, *Johnson Space Center*

NASA is investigating a "paperless" environment for new, 21st-century spacecraft-related procedures. A work environment with "hands-free" procedures/instructions promotes efficient operations. Giving an astronaut the ability to use both hands during a task will undoubtedly make that crew member's work easier; however, it could add complexity to the task and discomfort if the system is not properly designed.

We employed the Johnson Space Center Usability Testing and Analysis Facility to conduct a five-phased evaluation of a near-eye, head-mounted display (HMD) system – the Mobile Information System (MIST) – to examine its usability for future space and planetary exploration missions. With MIST, we then completed two pilot studies using simulated International Space Station maintenance procedures, two parabolic microgravity flights, and one long-duration study. This paper describes the last three phases of the program. The current components of the system include a miniature camera, a microphone, a tablet computer, a touchpad, batteries, and cables.

Two parabolic flight studies on board NASA's C-9 aircraft provided opportunities to evaluate MIST under simulated microgravity. Both test flights were part of a NASA Langley Research Center (LaRC) microgravity fabrication experiment that provided an opportunity to test MIST hardware and software in a real-world, operational environment using LaRC's experimental procedures displayed on the HMD. Researchers provided their observations on the MIST microphone. Our general objective in performing these evaluations was to assess the operability and functionality of MIST and its components. On the first microgravity flight study, two participants wore the MIST for half of the parabolic flight (figure 1, left). For the second microgravity flight study, we used the same experimental procedures with three LaRC flight members and the addition of voice recognition (figure 1, right).

We found that the mobility and compactness of the display were very desirable features to the LaRC flight team. MIST facilitated the tasks and enhanced the team dynamics, allowing the capture of more information than is typically captured under the same flight conditions

Fig. 1. *Usability Testing and Analysis Facility evaluator assisting LaRC crew member.*

without MIST. Furthermore, we discovered that using a touchpad rather than voice recognition was sometimes more efficient in the environment of the C-9 aircraft. Effects on the human voice, especially during 2g pullouts, led to an error chain in the voice recognition software; thus, further investigation is needed to understand and solve this issue.

These studies only tested MIST in short-duration settings ranging from 20 minutes to 1.5 hours. Most space and planetary exploration missions have procedures that can last up to 8 hours or longer. This prompted us to review literature on HMD usage lasting longer than 1.5 hours. A search of previous studies found that the average time the HMD technology was used was less than 30 minutes. Thus, a long-duration test of the MIST prototype was developed. We conducted this study to evaluate the comfort, usability, and impact of MIST during long periods of human performance. Two participants wore the system for approximately 4 hours each while performing task activities; e.g., assembling a second MIST, glovebox operations, and inventory data entry. Procedures were displayed on the HMD and controlled with voice recognition (figure 2).

Fig. 2. *Assembling MIST (left), glovebox (right).*

The Mobile Information System: A Hands-free Procedures System

continued

We collected several human factors measures, including: a modified Cooper-Harper Quality Performance Scale, measuring the level of compensation needed to meet performance objectives; a Discomfort Scale; the NASA Task Load Index to assess the physical and mental workload of the task; task time; and post-evaluation questionnaires for assessing system usability, user fatigue, and adaptability to the system. Cooper-Harper scores revealed controllability of the system to be acceptable, with minimal to no operator compensation needed to perform task goals. Participants wore and interacted with MIST for an average of 3 hours and 51 minutes each, with little to no physical discomforts being reported (figure 3). Usability and adaptability to the system were highly rated, with participants commenting they would recommend this type of system to assist in two-handed operations. Few issues of eye fatigue, headaches, or motion sickness were reported, indicating that a person could wear and interact with the near-eye display with no physical impairments. This study helps fill a gap in the literature concerning long-duration use of a near-eye display. Overall, the use of MIST to support procedures in microgravity and for long-duration operations was successful, with high acceptability from the user perspective. The study yielded valuable insights for development of guidelines for design revision and system enhancements.

While additional evaluations are necessary to further our understanding of the advantages and disadvantages of the system in various environments, these studies have shown that an HMD system such as MIST is a feasible technology for space operations. Future designs and enhancements will help increase system viability in terms of mobility and ease of use.

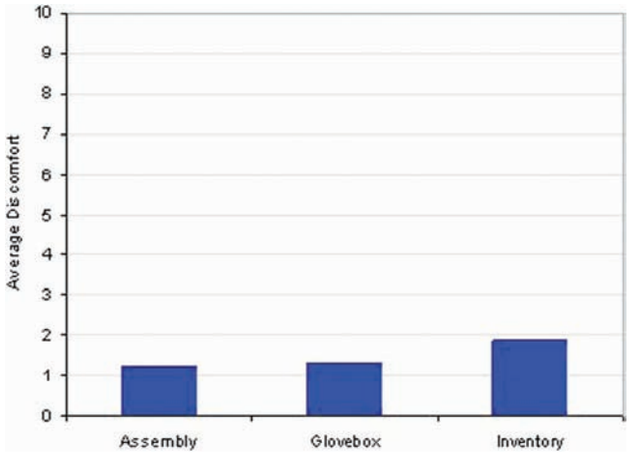

Fig. 3. *Average ratings of discomfort across tasks.*

Crew Exploration Vehicle Parachute Assembly System

Ricardo Machin, *Johnson Space Center*

The Crew Exploration Vehicle (CEV) Parachute Assembly System (CPAS) project is responsible for the design, development, fabrication, qualification, and delivery of the CEV parachute system to support the Orion pad/ascent flight tests and the first three orbital flight tests, including the first human mission. Project tasks include: (1) to conduct testing and analysis on the prototype (i.e., Generation 1 (Gen-1)); (2) to define system requirements and fabricate the flight engineering development unit; and (3) to support the Orion (CEV) vehicle flight testing (primarily Pad Abort 1 (PA-1)).

Generation 1 testing and analysis

The Gen-1 CPAS design is a scaled-up version of the Apollo Earth Landing System. In the CPAS design, two mortar-deployed drogue parachutes stabilize and decelerate the vehicle to conditions that allow for safe deployment of the main parachutes. On release of the drogues, three mortar-deployed pilot parachutes are fired, each of which individually deploys a main.

The CPAS test team conducted three tests: Main (Parachute) Development Test 3 (MDT-3), Cluster Development Test 3 (CDT-3), and Cluster Development Test 2 (CDT-2). For MDT-3, the team tested a single parachute to determine how it performed on its own; for CDT-3 and CDT-2, the team used a "cluster" of parachutes to determine how the parachutes functioned as a set. The team then analyzed and reviewed the data from these tests, as well as from cluster and drogue tests conducted in 2007 (figure 1).

Fig. 1. *Three inflated main parachutes during CDT-1.*

The MDT-3 test consisted of an overload test using a deployment dynamic pressure 30% higher than the design limit load for a single main parachute. This test condition, based on analysis from the prior two single-main parachute tests, takes advantage of the inflation characteristics of the main at the extremely low reefing ratio chosen for the first stage.

The canopy performed flawlessly, providing an opportunity to allow higher dynamic pressures and improve main parachute applicability for future CEV flight tests.

For the CDT-3, the cluster was deployed from a low-velocity air drop (LVAD) pallet, using two CPAS drogues as programmer parachutes to stabilize the pallet and static-line deploy the mains.

Posttest analysis indicates that while the average full-open performance met the pre-flight prediction, the variation in rate of descent exceeded expected dispersions, and the observed variation was greater than in the three-main parachute cluster test, CDT-1. The variation in payload attitude under full-open main parachutes also exceeded the desired ±5 deg. Lockheed Martin Space Systems Company (LM) (Bethesda, Md.) and the Landing and Recovery System team will use these data to simulate the performance for further analysis.

As part of the CDT-2 design activities, the team conducted a series of wind tunnel tests and computational fluid dynamics analysis to better understand the flow field and interaction between the parachute test vehicle (PTV) and the LVAD. CDT-2 was intended to be a full-up deployment of the CPAS from a PTV that accurately simulated the storage, rigging, and attachment of the CPAS to the CEV. In this test, the PTV, attached to the LVAD pallet, was extracted from a C-17 and released just after the assembled PTV/pallet cleared the aircraft (figures 2 and 3).

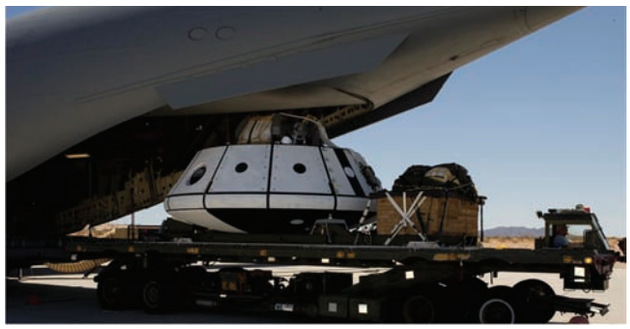

Fig. 2. *A PTV and its Critical Phase Software System (CPSS) are loaded onto a C-17 in preparation for a drop test.*

Crew Exploration Vehicle Parachute Assembly System

continued

The PTV separated from the pallet and the programmer parachutes deployed successfully; however, due to the attachment configuration of the programmers to the PTV, the wake deficit of the vehicle, and the close-coupled programmer parachutes, the primary programmer parachute failed to remain inflated.

As a result, the PTV and the two small programmer parachutes went into a large limit cycle that did not damp. The drogue parachutes deployed and inflated outside the intended attitude box, the drogue risers were severed, and the PTV eventually crashed. No one was hurt, but the PTV and associated on-board hardware were a total loss.

Analysis and model development

The team updated the design limit loads for the drogues and mains based on the Gen-1 flight and ground testing to facilitate implementation of the existing CPAS into the PA-1 test.

The team also extensively modified the decelerator system simulation to support the concept of operations development for the CDT-2. Based on the initial conditions from the CPSS vendor, a substantial risk existed that the PTV would tumble into an apex-forward orientation following separation from the CPAS. Based on modeling and analysis of this separation, the design team added an intermediate programmer parachute attach point to the PTV so the deployed programmer chute could reposition and maintain the PTV at the intended 180-deg angle of attack.

Flight requirements and engineering development unit

The CPAS team worked with LM to develop a vehicle-level architecture change that was approved as the baseline for CPAS integration into the CEV. Due to this change, the CEV forward bay cover (FBC) deploys all of the main parachutes, and the drogues attach to the crew module via the FBC using a multi-point attach harness. The team generated an independent estimate of the flight design CPAS reliability, derived from solid rocket booster experience and accounting for differences between the two architectures.

Based on Gen-2 (flight design) analysis, requirements for minimum-altitude deployment (pad-abort scenario), maximum allowable loads imparted to the CEV, and allowable system weight for the CPAS appeared to be an over-constrained problem with no unique solution.

Gen-2 system requirements were approved and baselined, and an Internal Design Review (IDR) was conducted for the design based on those approved requirements. The IDR indicated that the design failed to meet two major requirements: (1) loads imparted to the CEV were too high, and (2) the main parachute pack density exceeded the limit of 38 lb/ft^3.

Fig. 3. *CPAS team members route a pilot riser in the PTV.*

The team will continue to update requirements as the design process continues. Team members will also examine how long the CEV "rides the drogues" on a pad-abort deployment to optimize both the attitude at main chute deployment and the design limit load for the mains.

The team performed initial compatibility testing at NASA White Sands Test Facility (WSTF) to determine how CEV Reaction Control System exhaust products affect high-tenacity parachute materials.

The CEV preliminary design architecture publication included a parachute system to prevent the FBC rate of descent from exceeding that of the CEV under three full-open mains.

Project members worked with Rice University (Dr. Tayfun Tezduyar, Houston) to develop a modeling approach to help engineers understand the nature of the main parachute oscillations in full-open performance without modifying and testing the hardware.

Canopy joint efficiencies were reviewed in detail, including ground testing and redesigning joints that did not meet a minimum efficiency of 80%.

Orion vehicle flight testing

CPAS completed much work to support Orion flight testing, including CPAS to Flight Test Article integration fit checks for PA-1. Engineers supplied attach harnesses (or slings) to NASA Langley Research Center for proof-loading, and submitted detailed rigging and integration procedures for use at WSTF.

As a response to trajectory design issues, the deployment envelope boundaries were relaxed by (1) raising the limit dynamic pressure for the mains, (2) opening up the first stage of the drogues as far as possible, and (3) removing all margin from the drogue design limit load definition.

Ground testing for environments (primarily vibration) continues to address identified risks and determine whether the CPAS can be implemented without changes on PA-1.

International Space Station Operations

Elizabeth M. Taylor, *Johnson Space Center*
Jeanne S. Lynch, *Johnson Space Center*
Robert D. Banfield, *Johnson Space Center*

Those sustaining the International Space Station (ISS) from the Mission Control Center are known for their ability to monitor a tremendous amount of data; prioritize work; make important decisions quickly; communicate information clearly, concisely, and accurately; and, above all else, work together as a team in an environment requiring constant support. Behind the scenes are the instructors who train both flight controllers and astronauts in individual systems (e.g., power, thermal, communications, etc.); these also require in-depth knowledge of the system and an ability to communicate and convey that knowledge to others while integrating knowledge between systems (figure 1). All of this support is costly. Therefore, to reduce cost while maintaining quality and integrity, we developed a new operations concept for the ISS systems teams.

Fig. 1. *ISS instructor training an Increment flight crew.*

The traditional organization structure for the ISS systems divided flight controllers and instructors into separate groups. This generated separate training programs for the same technical content and introduced the potential for discrepancies in knowledge between groups. The traditional approach to supporting and training the core systems of ISS typically involves three positions: a backroom flight control position (Multipurpose Support Room (MPSR)), a front room flight control position (Flight Control Room (FCR)), and an instructor for each system. A new person in training would enter either the MPSR or the instructor training flows, spend years working towards a certification, and then begin gaining experience in his or her area. The MPSR would then begin additional training for the FCR position. Unfortunately, this method results in an inexperienced instructor training flight controllers to do a job the instructor has never done.

The new organization structure for ISS systems merges the flight controller and instructor groups by consolidating their training and taking the best of these personnel and assigning them to train the crew members and new flight controllers. This method ensures a common level of knowledge between positions and allows the most experienced personnel to become instructors. This creates a more defined career path and ensures a streamlined training process.

In addition to the reorganization of groups, we redefined the positions. A traditional FCR constantly supports console operations, with some positions using MPSR support for routine operations and all positions requiring MPSR support for complex operations (e.g., shuttle missions, extravehicular activities, and visiting vehicle activities). This design results in FCR flight controllers spending a significant amount of time on console during routine operations that do not require their in-depth level of knowledge (figure 2).

Operators, specialists, and instructors make up the new operations concept. An operator supports all routine and quiescent operations on board the vehicle and is trained to “safe” the vehicle in an emergency or off-nominal situation. A specialist is similar to the traditional FCR; this individual provides support during complex operations. If a specific complex operation requires more support than can be provided by a single specialist, the console is either staffed with a specialist in the front room and an operator in the backroom or with a specialist in the front room and a second specialist in the backroom. The complexity of the operations defines which configuration is used.

A specialist undergoes additional training, based on needs and the individual’s aptitude, to certify as an instructor. The specialist already possesses detailed knowledge of the vehicle systems, but requires training in advanced instructional techniques.

To consolidate operations further, we have redefined the division of the core systems. Traditional systems are divided into six disciplines: (1) command and data handling, (2) communications and tracking, (3) electrical power, (4) environmental control, (5) motion control, and (6) thermal control. These six "single" systems have been combined into four "dual" systems. We have therefore combined the command and data handling system with the communications and tracking system, the electrical power system with the external thermal control system, and the environmental control system with the internal thermal control system.

Fig. 2. *ISS specialist flight controller supporting real-time operations.*

Achieving this dual-system configuration requires many changes to the traditional way of doing business. A number of necessary tool improvements for both the operational and the training areas were made to enable this concept. The risk associated with increasing the amount of data being monitored by an individual during routine operations and decreasing that individual's depth of knowledge must be mitigated. This is being done with the development of smart tools that enhance the operator's awareness of his/her system.

Another challenge associated with reducing the cost of operations is reducing the time required to certify an individual in a particular position. We have addressed this by developing a structured training program for each of the dual-system positions. Rather than having individuals progress through a documented training flow at their own pace, this structured training program has a group of new hires train together in formal classes to participate in a shortened standardized training flow. This ensures a standard minimum level of knowledge, provides exposure to senior personnel and their knowledge, and promotes the team environment essential to working in operations.

This new operations concept not only reduces operational costs; it also better aligns with an employee's personal/family life. It allows our newest employees to certify as operators and support the majority of the constant console shifts. These operators are able to accumulate experience in the control center and gain real-time experience as soon as possible after being hired. As they progress, they gain more experience as operators, learn more about the vehicle and its operations, and then train and certify as specialists. The specialist is on a rotation that requires being on call 24 hours a day, 7 days a week, but he/she only supports console during complex operations, when called in for an anomaly, or to maintain console proficiency. As the specialist progresses to being an instructor, he/she is no longer routinely on call. However, the instructor can fill in as a specialist or an operator and will periodically work console to maintain proficiency. The majority of ISS operations are performed by recent college graduates, so the reduced amount of time spent on console as their careers progress fits well as their personal lives evolve to account for families and other changes.

In the end, this operations concept enables a reduction in training time and the number of people required to support operations while, hopefully, increasing morale.

Automating International Space Station File Management Using Agent-based Systems Integration

Timothy Hall, *Johnson Space Center*
William J. Clancey, *Ames Research Center*
Maarten Sierhuis, *Ames Research Center*
Deborah Hood, *Barrios Technology*
Tyson Tucker, *United Space Alliance*
Christopher Buckley, *United Space Alliance*

The crew of the International Space Station (ISS) receives around-the-clock support from a variety of specialists including flight controllers, physicians, planners, and engineers. Besides verbal communications and direct control of ISS systems, the most important means of communication between the crew and the ground team is through files, in over 30 types, including crew timeline updates, crew email, photographs, and exercise logs. A dedicated flight control position in the Mission Control Center (MCC) of Johnson Space Center (JSC) serves as the "switchboard operator" for transferring files between the space station computers (SSCs) and the ground support teams using folder drop boxes, email, and electronic flight notes to receive and forward files. Much of this work has become routine and can now be automated using intelligent software "agents" that integrate a variety of applications on different networks.

The Orbital Communications Adapter (OCA) Mirroring System (OCAMS) was deployed in MCC operations in July 2008 to assist the OCA Officer by automating the maintenance of a ground virtual copy (or "mirror") of the folders and files found on the SSCs. OCAMS reads the log of the OCA Officer's actions when transmitting files between the ISS and the MCC, including moving and deleting files. It then uses these data to mimic the OCA Officer's actions on the "Mirror local area network" computers. OCAMS agent rules define how file types are handled for privacy and practical reasons; e.g., medical files and photographs are not mirrored because they require special handling on the ground first (figure 1).

The "simulation-to-implementation" methodology for developing the OCAMS software is a novel demonstration of using simulation to design the system and quantitatively evaluate and test its performance on actual data prior to implementation (figure 2). This method (simulation-to-implementation) began with a partnership between the OCA Officer team and artificial intelligence experts in the Intelligent Systems Division of NASA Ames Research Center (ARC). ARC researchers observed OCA operations in the MCC backroom and then collaboratively simulated the manual mirroring operations in a tool called Brahms. Brahms models describe how people do their work, chronologically, including a model of the office environment, the workflow tools they use, and how they communicate (e.g., telephone, voice loop, email).

Using Brahms' "activity-based modeling," the joint JSC-ARC team quantified the "cost" or effort involved in the manual mirroring process. Subsequently, the team directly edited the "current operations" simulation to create a "future operations" simulation in which the model of what the OCA Officer did manually was converted into automated software agents. The future operations simulation included a prototype graphical interface, with which the OCA Officers could interact in the simulation,

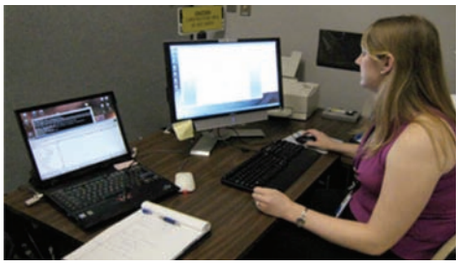

Fig. 1. *OCA Officer using OCAMS in MCC Multipurpose Support Room or "backroom."*

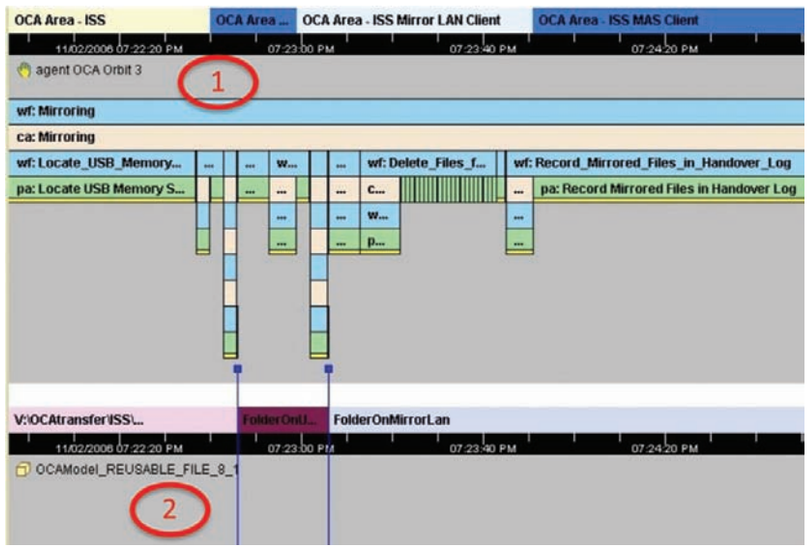

Fig. 2. *Simulation of OCA Officer's manual mirroring activity – using universal serial bus "sneaker net" method – during orbit 3.*

effectively controlling the prototype software. Another advantage was that the future operations simulation already integrated the software agents with actual systems to be used in the future tool (e.g., Microsoft® Excel and Word, email, and file transfer protocol programs). The team performed a validation of future operations simulation against historical logs of the OCA Officer file handling actions and produced metrics on the "cost" or effort savings to be expected. Team members then extracted the agents and graphical user interface from the simulation and converted them into a stand-alone software package called OCAMS. This agent implementation also integrated, for the first time in the MCC, new higher standards for security in communication across multiple networks of varying security levels.

By September 2008, OCAMS was used by all OCA Officers and estimated to save about 5% to 10% of each total shift time. This allowed the backroom flight controllers to focus on more complex priority tasks. The automated logging feature alone was especially welcome for eliminating a tedious process of recording the mirroring process, which itself already duplicated the work the OCA Officers had performed on the ISS computers (figure 3).

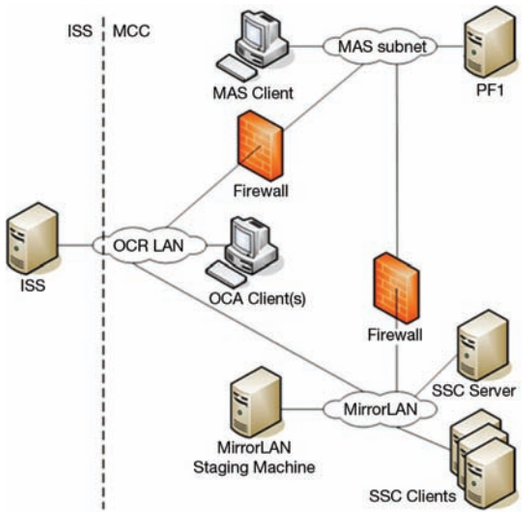

Fig. 3. *OCAMS initial implementation runs on the mirror local area network staging machine, transferring files between the OCA client computers and the SSC server that replicates a subset of the ISS file system.*

By early 2009, the OCAMS package included an editor for modifying file handling rules, enabling OCA Officers to modify OCAMS operations without engaging developers to reprogram the software agents (e.g., to change naming conventions or where files are stored). Archiving and delivering files (e.g., providing exercise logs to the Biomedical engineers) was also automated during 2009, further reducing the OCA Officer's workload by approximately 25% to 30%, thus enabling the position to be combined with another backroom flight control position. Following an OCA equipment upgrade scheduled for late 2009, OCAMS "Revision 3" agents were distributed, allowing for the file handling process to be monitored and controlled when necessary from remote console locations such as the OpsPlan flight controller position in the main MCC Flight Control Room, or "front room."

The final stage of automation planned for 2010 will automate most uplink and downlink operations to ISS, reducing the OCA Officers' workload by 90%, essentially eliminating the need for a dedicated OCA Officer position in the MCC. The remaining 10% OCA work will focus on special file transfer requests that require supervisory approval or manual overrides to the rules that will be managed with available bandwidth from other positions.

In summary, the OCAMS simulation-to-implementation development methodology combines ethnography, participatory design, multi-agent simulation, and agent-based systems integration to accurately model, simulate, and then automate tasks. OCAMS success can be used as leverage to reduce future costs of other NASA programs and operations. Models of existing operations and systems can be reused for designing extensions to OCAMS software. Agent components and application interfaces can also be reused for automating operations for other backroom and front room positions throughout the MCC for ISS as well as for future Constellation flight control positions. Time savings predicted by the work practice simulation can be validated by subsequent observation, improving our understanding of space flight operations. The methodology yielded a hybrid simulation that combined actual and simulated systems (e.g., mail) and objects (e.g., files) with simulated people. We used actual flight operations data to validate the simulations and the prototype workflow tool.

More generally, the project demonstrates a systems-integration architecture in which software agents are used to link arbitrary hardware and software systems to distributed teams of people on Earth and in space – a solution that will be needed throughout the future of human space flight.

OCAMS may thus be the first step in developing an interplanetary multi-agent system.

Planning and Monitoring International Space Station Solar Array Operations

Sudhakar Y. Reddy, *The Boeing Company*
Michael J. Iatauro, *Perot Systems*
Jeremy D. Frank, *Ames Research Center*
Matthew E. Boyce, *MCT, Inc.*
Jeffery P. Radigan, *Johnson Space Center*
Elif Kürklü, *SGT, Inc.*

International Space Station (ISS) solar arrays are designed to automatically track the sun to maximize power production as the station orbits the Earth. However, normal ISS operations such as water dumps, docking spacecraft, attitude changes through firing thrusters, and extravehicular activities (EVAs) can increase structural loads, environment contamination, and thermal stresses on the arrays, leading to the imposition of a variety of operational safety constraints known as Flight Rules. These rules not only prescribe the correct operation of the arrays, ensuring the safety of crew, vehicle, and mission; they also express preferences for vehicle longevity and mission effectiveness.

Managing the solar arrays on the ISS requires flight controllers to generate plans changing the orientations and modes of the arrays while balancing the complex constraints and preferences defined by the Flight Rules. These constraints include context-dependent constraints on legal configurations, temporal constraints limiting allowed transitions between configurations, as well as preferences for constraints. Satisfying all these constraints often limits power generation, and flight controllers need to balance the competing requirements of maximizing power availability and maintaining operational safety.

Over the past 3 years, researchers at NASA Ames Research Center (ARC), developed the Solar Array Constraint Engine (SACE) to assist the ISS flight controllers with planning and executing solar array operations safely and effectively. SACE provides automated solar array planning, what-if analysis, and real-time monitoring capabilities. It traditionally takes about 4 weeks to manually produce a solar array plan for a 4-week planning horizon. SACE has reduced this time to a few hours.

Problem

The ISS has eight solar arrays, each mounted on a rotary joint called the beta gimbal assembly (BGA). Sets of four BGAs on both the starboard and the port sides of the ISS are mounted on a truss attached to a solar alpha rotary joint (SARJ). Each solar array thus has 2 deg of rotational freedom, though some degrees of freedom are constrained by the shared SARJs.

Figure 1(a) shows the ISS solar array arrangement. Each SARJ and BGA has three modes: (1) Autotrack mode, where on-board software automatically rotates the solar arrays so the array surface is pointing directly at the sun; (2) Parked mode, where a drive motor is engaged to maintain the current array facing; and (3) Locked (for SARJ) or Latched (for BGA) modes, where a physical barrier is engaged to maintain current array facing.

The ISS impacts solar array safety by combining: an attitude reference frame; the yaw, pitch, and roll (YPR) of the station with respect to the attitude reference frame; the solar beta (angle between solar vector, pointing from the sun to the center of the Earth, and ISS orbital plane); which ground system is in control of ISS (U.S. or Russian); a list of events (e.g., docking, EVA, water dump); the port to be used for docking; the attitude control and reboost jet selects (configuration-specific combinations of thrusters fired, for attitude control and orbit maintenance, respectively); and the alternate jet selects used in case of thruster failure. This combination of information collectively defines the station's unique configuration. An operating plan for ISS consists of a sequence of configurations, such that the start time of one configuration equals the end time of the preceding configuration.

Four classes of constraints apply to pairs of SARJ and BGA angles: (1) power generation, (2) structural load, (3) environmental contamination due to particulate accumulation on array surfaces, and (4) longeron shadowing. These constraints are tables mapping an SARJ-BGA angle value pair to a color from the set red, yellow, and green. In most cases, red is infeasibility, e.g., insufficient power to run life support or forces strong enough to cause structural damage to the station; yellow values are acceptable but may reduce vehicle longevity or achievable mission objectives; and green is preferred. A representative table is shown in figure 1(b).

Figure 1(c) shows a sample solar array planning problem with two main events broken down into sub-events, each of which is associated with a time, a solar beta angle, an attitude type, a reference frame, and YPR. Events 5 and 6 have fixed start and end times, but other events have flexible end times. A thruster timeline (not shown) lists thrusters that are allowed to fire during various events, both during normal and contingency operations.

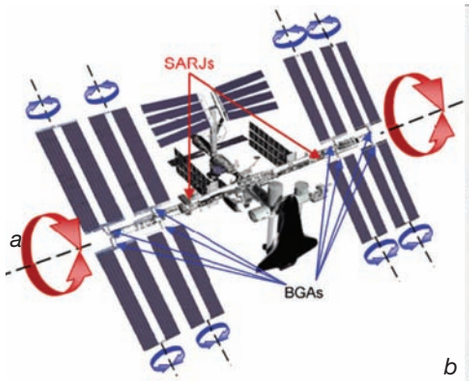

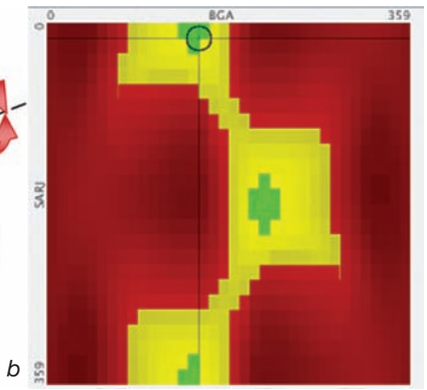

c

#	Start-Stop GMT	Beta Angle	Attitude Name	Ref Frame	YPR	Event
ATV_Propellant_Line_Purge (M08_170_A_04.UAF)						
1	170/08:30 --	-27	+XVV +ZLV TEA	LVLH	355.0 357.3 358.0	Handover US to RS for Prop Purge (SM)
3	170/10:00 --	-27	+XVV +ZLV TEA	LVLH	355.0 357.3 358.0	Handover RS to US Momentum Management
ATV_Reboost (M08_171_A_03.UAF)						
4	171/05:00 --	-28	+XVV +ZLV TEA	LVLH	355.0 357.3 358.0	Handover USS to RUS
5	171/05:05 171/05:10	-28	+XVV +ZLV	LVLH	5.1 357.2 0.0	Mnvr to Reboost Attitude (ATV on SM Aft)
6	171/06:56 171/07:01	-28	+XVV +ZLV TEA	LVLH	355.0 357.3 358.0	Mnvr to LVLH TEA
7	171/07:30 --	-28	+XVV +ZLV TEA	LVLH	355.0 357.3 358.0	Handover RUS to USS Momentum Management

Fig. 1. *(a) The ISS, showing the port and starboard assemblies of solar arrays and locations of the SARJs and BGAs. (b) A representative table indicating, for one SARJ and one BGA, the safety of setting the solar array orientations; the Y axis is the SARJ orientation and the X axis is the BGA orientation; green is preferred, yellow is acceptable, and red is (most of the time) infeasible. (c) A representative sequence of configurations for which a solar array plan must be generated. Each configuration has a start time or start time range, a solar beta angle, an attitude type, a reference frame, YPR, and events dictating which tables apply.*

Approach

SACE uses the extensible universal remote operations planning architecture (EUROPA) framework for automated planning (figure 2). EUROPA, a model-based artificial intelligence planning system, has been in continuing development at ARC over the past decade. It accepts a declarative description of a planning problem consisting of a list of timelines (concurrent threads of a plan), a list of states that may hold on each timeline over an interval, and compatibilities describing the relationships that must hold between timelines for a plan to be valid.

SACE represents the sequence of configurations and states for each array joint as EUROPA timelines. The configuration states are values of the configuration variables. For a given configuration of the ISS, SACE finds orientations and modes for different arrays that maximize the power availability while keeping them in a feasible space with respect to the various constraints. For a sequence of configurations, after each successive orientation and mode selection, SACE ensures the temporal constraints on mode changes and those imposed by the angular rotation rates are satisfied. The ideal solar array plan optimizes the orientations and modes in each configuration. However, there may be insufficient time to turn the arrays to a new orientation or command mode changes, especially from short configurations. Under these circumstances, SACE merges adjacent configurations and optimizes the new configuration.

Optimizing orientation for a single configuration is posed as an unconstrained optimization problem. Optimization problems for the starboard and the port sides of station are independent. The overall cost function is split into two independent functions, one for each SARJ. We calculate the cost of each orientation independently for each solar array. In designing the cost function, we ensure every infeasible orientation has worse cost than any feasible solution. An orientation is feasible if its power table entry is not red, its load entries (SARJ and BGA) are not red, and its longeron entry is not red.

The component cost functions refer to the color cost (due to different constraints being in the red, yellow, or green zones), mode cost (due to modes of the BGA and the SARJ), distance cost (due to the distance between orientations of arrays), direction change cost (due to change in direction of trajectory of arrays), and power cost (due to incremental differences in power within a constrained power zone). Weights on the different component cost functions are designed such that mode cost only matters when colors are equal, distance cost only matters when modes are equal, direction change cost only matters when distances are equal, and power output cost only matters when all other components are equal.

Planning and Monitoring International Space Station Solar Array Operations

continued

Summary

The SACE tool provides an end-to-end solution that starts with a timeline of ISS attitudes and events and automatically produces a solar array plan as well as a timeline of power availability. By using automated optimization and planning, SACE has dramatically reduced the time required for ISS solar array planning from several weeks to a few hours. It has a "telemetry view" for situational awareness, a "sandbox view" for what-if analysis and optimization, and a "plan view" for automated planning. The monitoring and optimization portion of SACE has been certified for flight operations, and the planning component is currently undergoing certification testing.

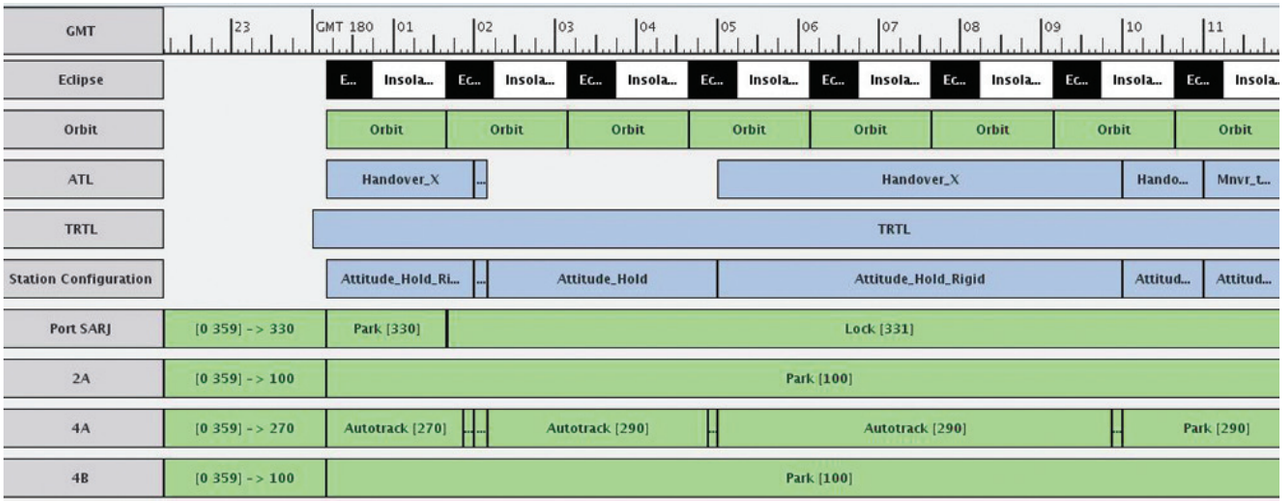

Fig. 2. *The SACE planning window shows timelines for attitude changes (ATL), thruster choices (TRTL), the configurations, and the different SARJs and BGAs, among other things.*

Search and Relationship-mining of Heterogeneous Flight Control Documents

Richard M. Keller, *Ames Research Center*
Brian J. Kelly, *Johnson Space Center*
Timothy A. Hall, *Johnson Space Center*
Christopher D. Knight, *Ames Research Center*
Daniel C. Berrios, *University of California, Santa Cruz*
Mohana M. Gurram, *SGT, Inc.*
Steven Lin, *Perot Systems Government Services*

Flight controllers for space shuttle and International Space Station (ISS) missions routinely locate specific operations documents and records from among tens of thousands stored on computers in the Mission Control Center (MCC). Relevant information – team notes, console logs, action requests, Flight Rules, anomaly reports, and flight procedures – is accumulated in a bewildering array of flight operations support systems, each of which must be accessed via a separate interface. Users must consult these different systems and manually integrate results to get a comprehensive view of the information relevant to tasks they are performing. This is a time-consuming and error-prone process.

To improve access to flight control information, we designed and built an application called XSearch that integrates data from disparate flight operations databases.

Through a common search interface, MCC personnel using XSearch can issue a single search query and simultaneously interrogate multiple mission operations data sources, including the ChitS system (used to store mission action requests), the Flight Notes system (used to store internal flight control team communications), the Anomaly Reporting System, the Polytron Version Control System change management system, and the Flight Rules repository. These systems store historical data back to 1995, and contain over 300,000 records. XSearch users can perform full-text searches across key text fields (e.g., title, problem description, action request, etc.) and view integrated results across these data sources.

The XSearch interface is displayed in figure 1. To use the interface, the flight controller types a search query (e.g., "EPS [Electrical Power System] load shed") in the

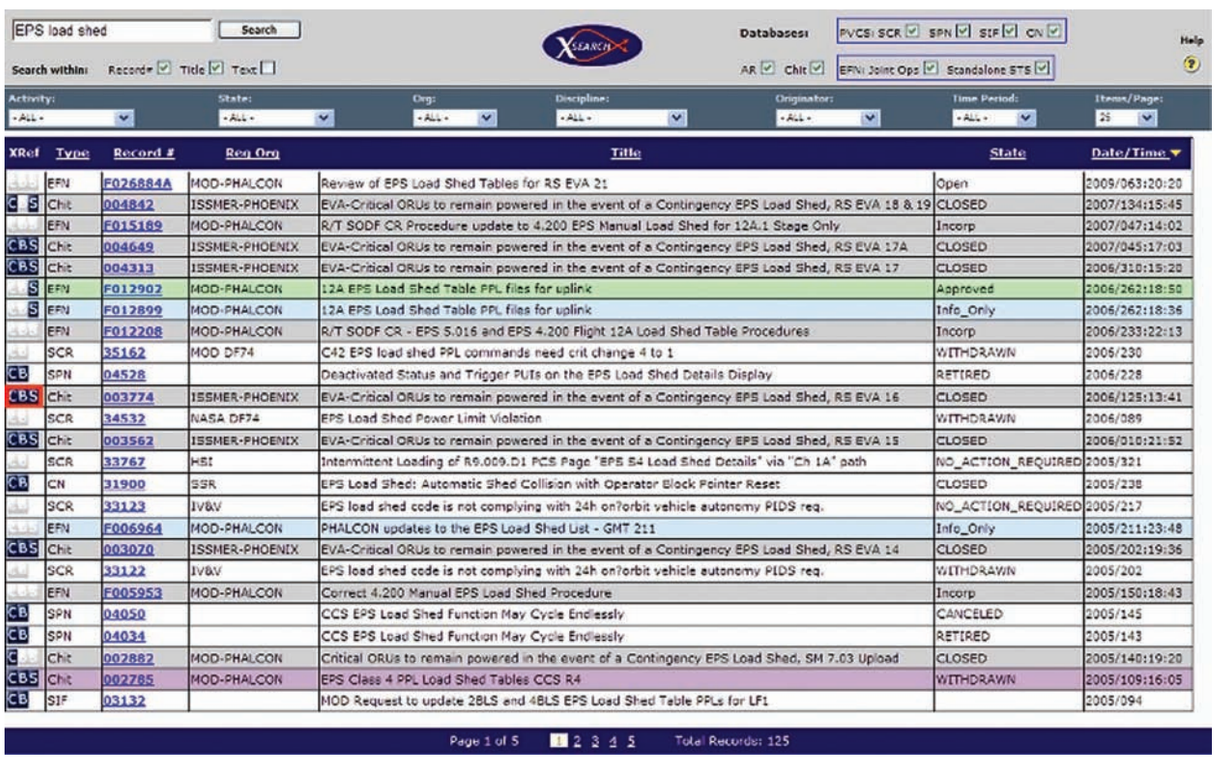

Fig. 1. *The XSearch interface display.*

box at the top of the screen and selects the databases to be searched. The controller can also select the fields to be searched, choosing one or more of the record number, title, and text fields. Search results are then retrieved from the specified databases and shown in a tabular display, with key information summarized in columns. Pull-down filters allow the user to narrow the results further.

In addition to conducting searches, the system provides two other important capabilities intended to contextualize search results: detection of cross-references and detection of textually similar records. Identifying records that are either cross-referenced by, or similar to, a given search result enables flight controllers to recover key information that may be necessary to properly interpret that result. This supplementary information provides the controller with important context intended to facilitate safer and more effective mission operations decision-making through enhanced situation awareness.

To detect embedded cross-references within results, XSearch parses text fields found in the results using a set of syntactic patterns that locates record citations (e.g., patterns that detect standardized document or record identifiers routinely used by authors). Using this technique, XSearch can identify both "outbound" and "inbound" references. Outbound ("Cites") references point "out" from a specific record to other records cited; "inbound" ("Cited-by") references point "in" to the specific record from other records that cite it.

To detect records that appear similar to a given search result, XSearch calculates and ranks the textual similarity between the result and all other records in the corpus. Those ranked highest are displayed to the flight controller. Similarity detection is computed using a standard vector space algorithm (term frequency inverse document frequency (TFIDF)) developed by researchers in the field of information retrieval. TFIDF identifies records that may be relevant to a given record based purely on textual similarity. It thus finds relationships that are different than those detected by the explicit citation-based, cross-reference detection approach.

Figure 2 illustrates the concept of cross-referenced and similar records. In the figure, we assume the flight controller has searched for the term "ALS [advanced life support] heater," which is found in the text of Chit 004361. Also within the text are citations to an anomaly report (AR 00447) and a flight note (EFN F0121902). These are Cites-type cross-references. Cited-by cross-references referring back to Chit 004361 can be found in subsequently written records (e.g., Chit 004374). EFN F013094 is found to be relatively "similar to" Chit 004361 based on the usage of similar words and phrases in their respective texts. For example, both records refer to "temperature instability" and "ALS heater failure."

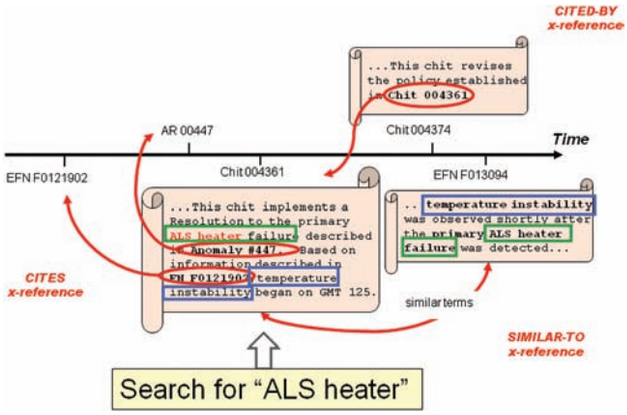

Fig. 2. *The concept of cross-referenced and similar records illustrated.*

Cross-references and similarities detected by XSearch are reflected in the user interface in figure 1. The leftmost column ('XRef') contains an indication of which types of cross-references are located for the search result: C for "Cites," B for "Cited-by," and S for "Similar-to." If a flight controller wishes to view these cross-references, he or she clicks the C, B, or S indicator and a cross-references display is presented (figure 3). This display contains a tab for each of the cross-reference types found. Clicking on the record number hyperlink brings up the record for viewing.

Our intention is to expand the scope of XSearch by adding more data sources into the integrated search, specifically the Inventory Management System, the flight controller Console Log Database, and the ISS problem reports database. The initial version of XSearch also provides a solid framework on which to develop more sophisticated and powerful relationship-mining capabilities. Our long-term strategy is to expand the information extraction methods we employ to recover many other types of cross-record linkages.

Back

Cross References for Chit # 003774

Help

Type	Record #	Req Org	Title	State	Date/Time
Chit	003774	ISSMER-PHOENIX	EVA-Critical ORUs to remain powered in the event of a Contingency EPS Load Shed, RS EVA 16	CLOSED	2006/125:13:41

Cites | Cited By | Similar

Type	Record #	Org / Serial #	Title	State	Date/Time	# Citations
Chit	003563	ISSMER-VI	Failure Scenarios and Time-to-limit for Transitioning to Contingency Maneuver for MT Thermal Protection	CLOSED	2006/011:15:49	1
Chit	003562	ISSMER-PHOENIX	EVA-Critical ORUs to remain powered in the event of a Contingency EPS Load Shed, RS EVA 15	CLOSED	2006/010:21:52	1
Chit	003533	ISSMER-PHOENIX	RPCM S03A-E RPC 18 Trip Troubleshooting Tasks	CLOSED	2005/350:21:04	2
Chit	003070	ISSMER-PHOENIX	EVA-Critical ORUs to remain powered in the event of a Contingency EPS Load Shed, RS EVA 14	CLOSED	2005/202:19:36	1
Chit	002685	ISSMER-PHOENIX	EVA-Critical ORUs to remain powered in the event of a Contingency EPS Load Shed, RS EVA 13	CLOSED	2005/069:15:39	1
Chit	002549	ISSMER-Manager	EVA-Critical ORUs to remain powered in the event of a Contingency EPS Load Shed, RS EVA 12	CLOSED	2005/018:23:45	1
Chit	002164	ISSMER-Manager	EVA-Critical ORUs to remain powered in the event of a Contingency EPS Load Shed, RS EVA 11	CLOSED	2004/232:16:13	1
Chit	002105	MOD-PHALCON	EVA 10 - Critical ORUs to be Inhibited for EPS Manual Load Shed	CLOSED	2004/210:01:47	1
Chit	001572	MOD-PHALCON	EVA-Critical ORUs to be Inhibited for EPS Load Shed	CLOSED	2004/035:20:45	1

1

Fig. 3. *A cross-reference display.*

Trajectory Guidance for Lunar Descent and Landing

Ronald R. Sostaric, *Johnson Space Center*

A lunar descent landing guidance concept, evolved from Apollo and shuttle heritage, is being developed to support the Autonomous Landing and Hazard Avoidance Technology Project. The primary function of a trajectory guidance system is to determine trajectory path and issue steering commands to guide a lander to touch down safely and accurately on the lunar surface. This system must perform adequately as part of an integrated autonomous guidance, navigation, and control (AGNC) subsystem by contributing to meeting the desired landing accuracy and achieving a soft landing. Guidance allows for dynamic retargeting to maneuver in such a way as to avoid surface hazards, such as rocks, craters, and slopes. The trajectory design takes into account constraints to allow sensors to "see" the landing area, as well as the time and altitude margin to adjust the trajectory based on information determined by the sensors. The trajectory shape may also be constrained to permit a direct crew view of the landing site via a window during descent.

The lunar descent trajectory is broken into phases, as shown in figure 1. The lander is assumed to begin in a 100-km circular orbit. The deorbit burn sends the lander into a 100×15-km transfer orbit. Following a coast of slightly under 1 hour to near perilune, the lander engine is ignited; at this time, powered descent initiation (PDI) occurs. The powered descent phase, shown in figure 2, begins at PDI and continues until touchdown on the lunar surface. The vehicle engine remains on throughout this phase. Powered descent consists of four subphases: braking, pitch-up, approach, and terminal descent. The braking maneuver removes most of the orbital velocity as efficiently as possible while targeting a certain altitude and range from the landing site. The timing of PDI is chosen so

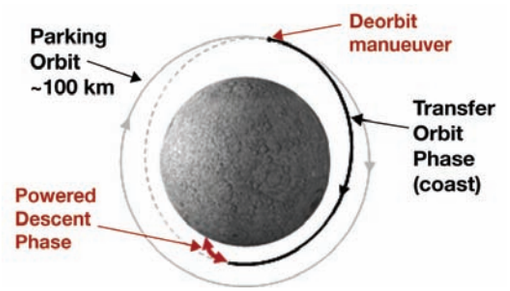

Fig. 1. *Lunar descent trajectory phases.*

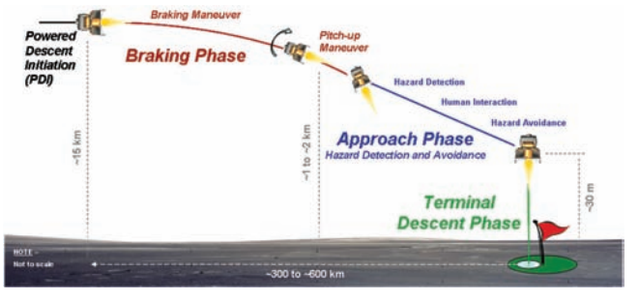

Fig. 2. *Lunar powered descent.*

that, given vehicle thrust constraints, the trajectory meets these target conditions efficiently. During braking, the engine is throttled to near the maximum available thrust, and the vehicle attitude is oriented roughly opposite to the velocity vector. During this maneuver, any trajectory dispersions due to burn execution errors or improved navigation state knowledge can be corrected. Errors in the along-track direction are mitigated by modulating the engine throttle, while cross-track errors are mitigated by directing the thrust out of plane to the trajectory.

The approach phase is designed to have a more vertical attitude and lower acceleration level than the braking phase. The vertical attitude provides better landing area visibility, while the lower acceleration level provides for both slower speeds and more observation time during target approach. The intermediate pitch-up maneuver phase provides a smooth transition in acceleration level and vehicle attitude from the high-thrust and near-horizontal attitude that affects these desired approach conditions during the braking phase.

The objective of the final terminal descent maneuver is to descend slowly to the landing site in a near-vertical orientation, staying above the landing target and nulling out any remaining horizontal velocity. At this point, the landing target will likely no longer be visible to the crew and/or sensors on board the vehicle. This is because the vehicle is descending from directly above the target (or nearly so) and lunar dust, scattered by the engine exhaust, is obscuring the terrain below. Based on the Apollo experience, the terminal descent maneuver begins at 30 m altitude.

During the approach phase, a series of critical functions necessary for safe landing is completed. These functions are collectively referred to as hazard detection and avoidance

(HDA). In the Apollo Program, the hazard detection function was completed by crew members who looked out the window at the landing area. Significant mission design and trajectory constraints were therefore placed on the Apollo missions to provide the best possible lighting conditions for viewing hazards during landing. One of the primary goals is to advance the state of the art in hazard detection technology by reducing the impact of mission design and landing location constraints and increasing safety and reliability for crewed, uncrewed, and robotic landings on the moon and other planetary bodies. NASA designers are pursuing the development of a flash light intensification detection and ranging (LIDAR) device; current research and analysis shows that this device is the best choice for performing hazard detection. The LIDAR generates a three-dimensional map of the landing area during the descent and is able to operate in virtually any lighting conditions. The sensor data provide the crew or an automated system information about potential landing sites, including a preferred target, at the time of the landing.

Hazard avoidance is the other major function completed during the approach phase. The trajectory guidance system provides an updated target based on any information obtained from the hazard detection scan. This target could come from an automated landing site prioritization algorithm or from crew input. The guidance system calculates the updated thrust vector command to steer the vehicle safely to the start of terminal descent directly above the updated landing site.

To effectively perform HDA, trajectory design must accommodate a set of constraints (figure 3). The slant range to the landing site during the scan must be such that the sensor can perform effectively. The hazard detection scan must then be completed with enough remaining time to choose a new landing location, if necessary, and perform an avoidance maneuver to achieve the new target. If a direct window view of the landing area is required, the trajectory must be designed accordingly. The exact limitation depends on the design of the window, but common sense and Apollo experience show us that there will be a limit on how steep the descent can be while still providing a direct window view (as there will be engine and vehicle structure below the crew). Conversely, there is a shallow limit at which the HDA sensor can perform effectively. Beyond this limit, hazard detection performance becomes degraded. Reasons for the loss of effective performance include stretching of the samples, which causes gaps in data, and obstruction of the smaller-size hazards behind the larger-size hazards due to the obliqueness of the angle.

NASA has ongoing work to assess the sensitivities to various trajectory constraints and sensor design parameters. At the same time, improvements in sensor technology are being made and tested on helicopters and aircraft. The end goal of the project is to demonstrate an integrated AGNC and sensor system, including hardware and software, that can safely land a crewed or an uncrewed vehicle on the lunar or other planetary surface.

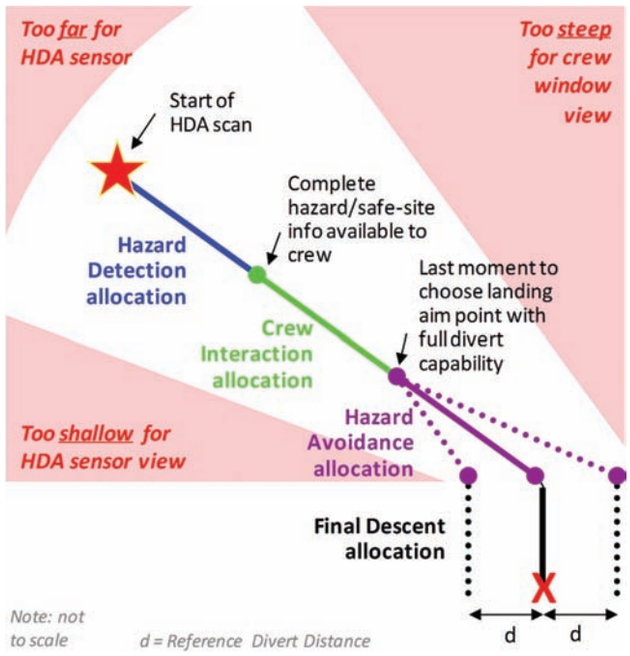

Fig. 3. *HDA functions and constraints.*

Targeting for Trans-Earth Injection Maneuvers

Ryan Whitley, *Johnson Space Center*

The Orion spacecraft guidance, navigation, and control (GNC), as part of the Exploration Architecture System, must meet a number of constraints. These are defined by the Crew Exploration Vehicle (CEV) Subsystem Requirements Specification document (CEV-T-031210). The requirements articulate a need for on-board computation of "translational maneuver targets" (GNC.0561) as well as for specific additional constraints on the mission relating to the timeline of various maneuver sequences. Translational maneuver targets include lunar orbit insertion, trans-Earth injection (TEI), plus any required trajectory correction maneuvers (TCMs). This on-board capability is generally assumed to be supplemental to any ground computation in nominal mission operations, and is primarily considered a viable alternative in loss-of-communications contingencies.

Of these maneuvers, the ability to accurately and consistently establish a flyable three-burn TEI target sequence is especially critical. The TEI is the sole means by which a crew can successfully return from a moon orbit to a narrowly banded Earth entry interface (EI) state that relies entirely on the TEI sequence plus any small TCMs to complete the transit. This ability is made even more critical by the desire for global access on the lunar surface. Currently, the designed propellant load is based on fully optimized TEI solutions for the worst-case geometries associated with the accepted range of epochs and landing sites. Thus, in addition to being feasible, the targets must not include burn sequences that exceed the anticipated propellant load. This is currently listed as a risk for the Operations Management Team GNC design.

It is well known that analytic solutions for transfers in the three-body problem are unknown. Thus, if a fully targeted solution is desired, a patched conic method must first be used to establish a so-called feasible initial guess. At this point, an iterative scheme that minimizes the discrepancy in the states is necessary. To address both of these needs (i.e., a reasonable initial guess and a robust iterative algorithm to converge on a flyable solution), we developed an adaptive targeting algorithm. This algorithm has flexible application to either ground-based targeting and/or on-board computation as it is designed to converge on fully optimized solutions quickly and efficiently.

The TEI three-burn maneuver sequence is uniquely tailored to minimize the ΔV cost for the full range of mission scenarios. While both single- and three-burn solutions can be obtained, the total cost of a three-burn sequence is almost always less expensive. This is especially true when the geometry requires a large plane change from the initial moon orbit to the Earth-moon transfer arc. Regardless of the date or orbit, the three-burn sequence has the same basic structure: (1) The first burn significantly raises the apolune of the 100-km circular orbit. This is generally the largest maneuver of the three conducted in the plane of the initial moon orbit. (2) The second burn occurs at or near to the apolune of this new large elliptical orbit and places the spacecraft in the departure plane. The cost to change the direction of the velocity vector is cheapest when the velocity magnitude is at a minimum. This is generally the least expensive maneuver. (3) The third and final burn occurs when the spacecraft sweeps back towards the moon near perilune. This final burn places the spacecraft on a very specific trajectory designed to hit a particular EI condition that can, depending on the landing site, have very tight constraints. Parameters involved in the selection of a viable EI state include altitude, flight path angle, azimuth, longitude, and latitude targets.

Figure 1 delineates the architecture for the three-burn sequence. In this particular example, the plane change (or relative declination to the Earth-moon plane) is large, near the maximum possible value.

Flexibility to accurately set up targets for the full range of epochs and orbits autonomously is an important attribute of the algorithm. To that end, we employed a vector-based approach that purposely avoids the use of complex trigonometric expressions due to their intrinsic singularities. As such, we derived vector equations to compute an associated v_∞ vector for an Earth return trajectory analytically. We determined this vector by the desired flight time and calculated from the resultant transfer arc between the current moon state and the associated antipode state at the Earth.

Targeting a v_∞ vector differs from successfully reaching a specific EI state. Over a multiple-day transfer, the impact of Earth and sun gravitational perturbations

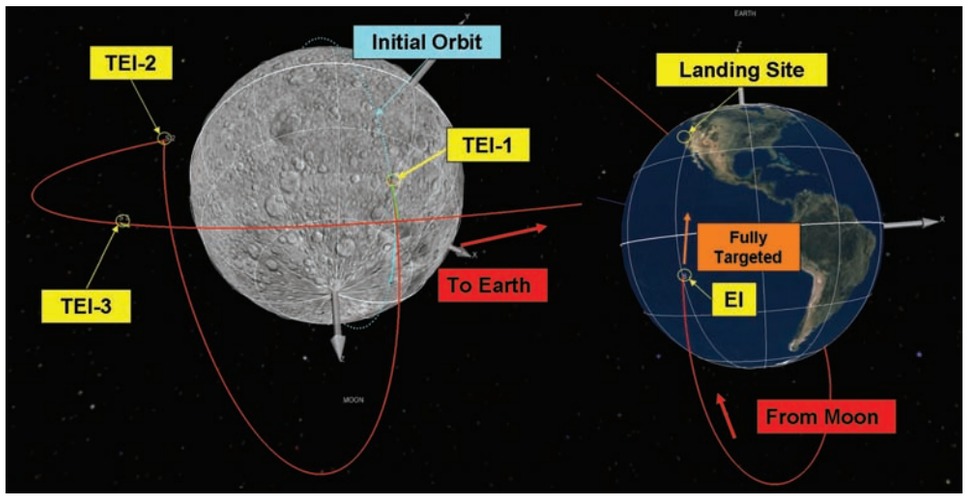

Fig. 1. *Burn TEI transfer design.*

can invoke large changes in the final state at the Earth, leading the spacecraft far from the desired EI targets. To correct these discrepancies, instead of propagating forward to EI, the optimization parameters associated with the target Earth state are propagated backwards in time. Setting a single point to match position and velocity for a continuous trajectory in the moon sphere of influence reduces the convergence difficulties associated with the large swings in EI parameters that correspond to small changes near the moon.

The desire for a flexible autonomous algorithm is naturally coupled with the need to minimize excessive iteration. Once the analytic guess is determined, it is vital that the targeter quickly converge to a feasible, flyable solution. Optimization-based algorithms take advantage of the assumption that the solution lies within the vicinity of the initial guess by designing search directions for variable optimization parameters that point towards the minimum feasible solution as efficiently as possible. We selected a sequential quadratic program due to its robust capability to solve nonlinear problems where the initial guess is in the vicinity of the solution.

Different modes of iteration are available depending on the requirements for expediency of obtaining a solution. The primary mode is full optimization, where the constraints and total fuel consumption objective function are simultaneously minimized. A feasible mode is available that does not attempt to minimize the solution but finds solutions within a few iterations and converges robustly. Another mode allows the targeter to conduct pre-optimization in a conics-only approach that minimizes the velocity increments tightly for the initial v_∞ vector. This can than be the initial guess for either the feasible or the optimal mode. Finally, a feasible constrained mode is available that simply adds a maximum ΔV magnitude constraint.

Our final goal is to have a stand-alone algorithm that always converges and does so efficiently. Testing is under way to assess the robustness of the algorithm and determine how to further expand its capability. We are currently investigating finite-burn modes that invoke steering laws similar to the anticipated closed-loop guidance that will fly out the targeted solutions.

Low-impact Docking System

By Tobie LaBauve, *Johnson Space Center*

Since 1996, NASA has been developing a docking system that will simplify operations and reduce risks associated with mating spacecraft. Our effort focused on developing and testing an original, reconfigurable, active, closed-loop, force-feedback, controlled docking system using modern technologies. The primary objective of this effort was to design a docking interface that is tunable to the unique performance requirements for all types of mating operations (i.e., docking and berthing, autonomous and piloted rendezvous, and in-space assembly of vehicles, modules, and structures). The docking system must also support the transfer of crew, cargo, power, fluid, and data. As a result of the past 10 years of docking system advancement, NASA developed the Low-impact Docking System (LIDS) (patent no. 6354540) (figure 1).

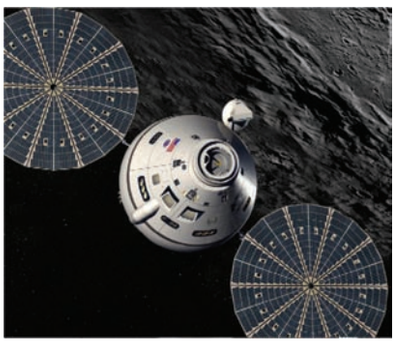

Fig. 1. *Head-on view of the new Orion vehicle showing crew module hatch surrounded by the LIDS.*

The current LIDS design incorporates the lessons learned and development experiences from both previous and existing docking systems (figure 2). After multiple iterations of prototype hardware development and testing, NASA established the feasibility of LIDS. The benefits of LIDS include: safe, low-impact mating operations; more effective and flexible mission implementation with an anytime/anywhere mating capability; system-level redundancy; and a more affordable and sustainable mission architecture with reduced mission and life cycle costs.

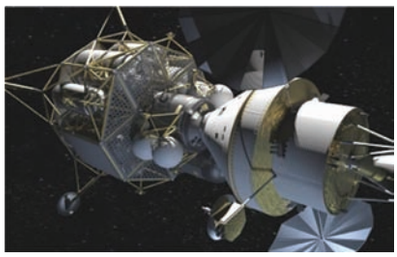

Fig. 2. *Orion is shown docking with Altair using the LIDS.*

In 1996, the LIDS project, known as the Advanced Docking Berthing System project, launched a 4-year developmental period. At the end of the 4 years, the team had built a prototype (figure 3) of the soft-capture hardware and verified the control system used to control the soft-capture system. In 2001, the LIDS team worked with the X-38 Crew Return Vehicle (CRV) Project and built its first engineering development unit (EDU) (figure 4). Due to budget cuts, the X-38 Project ended with the EDU only 60% complete. Over the next several years, our team worked to refine and develop the docking system design. In 2005, our team assessed LIDS applicability to meet the anticipated Orion vehicle docking scenarios.

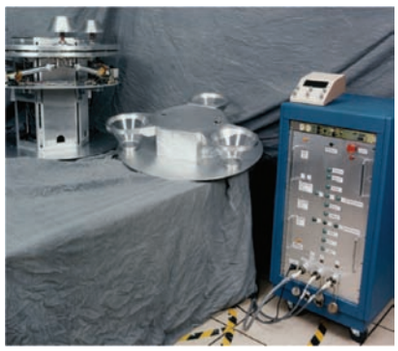

Fig. 3. *Prototype LIDS hardware and control system.*

Fig. 4. *X-38 EDU testing at the Bldg. 9 6DOF [six-degree-of-freedom] Facility.*

The following encapsulates the LIDS development history:

1996–2000

Prototype soft-capture system hardware and control system electronics built and test-verified

Dynamic tests of the soft-capture system completed successfully

Closed-loop, force-feedback, soft-capture control system design validated

Interface forces (i.e., docking and berthing operations) verified

2001–2002 (X-38/CRV)

Tasked with designing a 54-in. OD [outside diameter] EDU (figure 5)

Project halted at approximately 60% completion due to lack of funding

2002–2003 (SLI/OSP [Space Launch Initiative/orbital space plane])

Requirement developed and trade studies performed to support the LIDS concept

Prime contractor and program support

2004–2005 (ESMD/ESR&T [Exploration Systems Mission Directorate/Exploration Systems Research and Technology])

In-house technical maturation of the project commenced

Objective: LIDS to meet Technology Readiness Level 6 in 4 years

2006 (Constellation (Cx)/Crew Exploration Vehicle (CEV) and Hubble Space Telescope (HST))

Gradual phasing-in of additional Engineering and Science Contract Group resources to support EDU design

54-in. OD EDU soft-capture mechanism assembly complete

54-in. OD EDU hard-capture mechanism design complete

Decision made to use LIDS for Cx/CEV

Decision made to use LIDS as the vehicle interface for HST/Servicing Mission 4 (SM4)

2007–present (Cx/CEV and HST)

Complete build-up of the 54-in. OD EDU assembly

Deliver HST flight hardware to support 2009 shuttle mission

Successfully complete LIDS major project milestones (System Requirements Review and Preliminary Design Review)

Continue development of the 58-in. OD EDU LIDS design (figure 6)

The LIDS HST passive interface will function as the primary means of capture during future HST missions after the end of the Space Shuttle Program. These future missions include the HST end-of-life deorbit mission as well as potential future servicing missions. Historically, HST servicing was accomplished by Shuttle Remote Manipulator System grappling and berthing of the HST onto a soft capture mechanism (SCM) that is mounted on top of the Flight Support System in the orbiter payload bay (figure 7). During the HST SM4 shuttle mission, the SCM was left attached to the HST with the passive LIDS docking interface exposed on the HST aft bulkhead for future use.

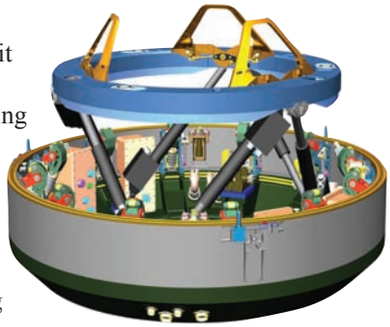

Fig. 5. *LIDS EDU-54 model.*

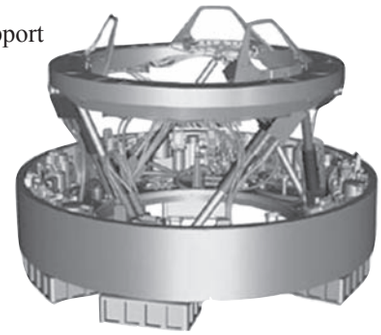

Fig. 6. *LIDS EDU-58 model.*

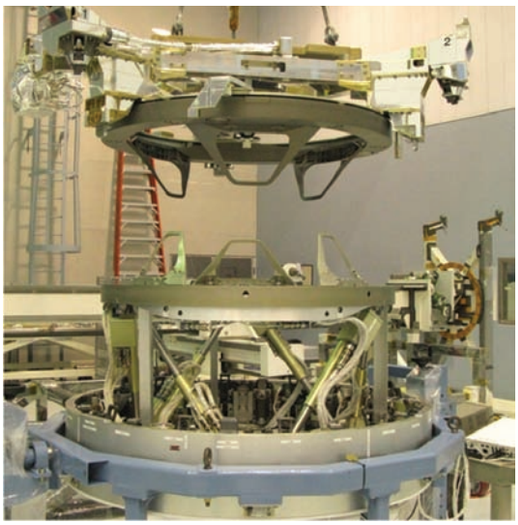

Fig. 7. *The EDU-54 unit undergoes latching test/fitcheck with the HST SCM at the NASA Goddard Space Flight Center.*

Planetary Sciences

Astromaterials Research and Exploration Science Overview

Eileen K. Stansbery, *Johnson Space Center*

The Astromaterials Research and Exploration Science (ARES) Directorate performs a unique role within NASA by leading the Orbital Debris Program and providing curatorial responsibility for all NASA-held extraterrestrial samples. ARES scientists and engineers also conduct research in basic and applied space and planetary science as well as provide support to the human and robotic space flight programs with expertise in science planning and operations, analysis of micrometeoroid/orbital debris (MMOD) risks to spacecraft, image analysis, and Earth observations. The ARES scientific staff – representing a broad diversity of expertise in physical sciences (physics, chemistry, geology, astronomy), mathematics, and engineering – is organized into three offices: Astromaterials Research, Astromaterials Acquisition and Curation, and Human Exploration Science.

Scientists within the Astromaterials Acquisition and Curation Office preserve, protect, document, and distribute samples of current astromaterials collections. This Johnson Space Center capability originated during the Apollo Program with scientists who were responsible for the science planning and training of astronauts for lunar surface activities. Since the return of the first lunar samples, ARES has been assigned curatorial responsibility for all NASA-held extraterrestrial materials (Apollo lunar samples, Antarctic meteorites – some of which originated on the moon and Mars – cosmic dust, solar wind samples, comet and interstellar dust particles, and space-exposed hardware). The responsibilities of curation encompass not only the long-term care of the samples, but also the support and planning for future sample collection missions as well as research and technology to enable new sample types. Research into the samples allows ARES scientists to provide a basic characterization of each sample and a fundamental understanding of the entire collection – all of which is shared with the external research community that relies on access to the samples. The Lunar Sample Facility and other curation cleanrooms, the data center, laboratories, and associated instrumentation are unique NASA resources.

Curation efforts are greatly enhanced by a group of planetary scientists that conducts peer-reviewed astromaterials research. Astromaterials Research scientists conduct peer-reviewed research in planetary science (e.g., cosmochemistry, origins of solar systems, planetary geology and geophysics) and participate as principal investigators or co-investigators in many of NASA's robotic planetary missions. Since the last report, ARES has achieved several noteworthy milestones. The discovery of a new mineral and the recognition from the International Mineralogical Society with naming privilege for Brownleeite prove the value of the extremely high-resolution instrumentation for precision analysis that was acquired and described in the previous Biennial Report. ARES scientists continue to identify grains of interstellar origin in cosmic dust and now also in Stardust samples. The landing and our real-time support to the Mars Phoenix mission was a logical extension of our other Mars mission support and data analysis, including the Mars exploration rovers Spirit and Opportunity. ARES scientists have unique expertise in "ground truth" relevant to the kind of rocks expected to be studied on Mars, making ARES a unique contributor to instrument development and calibration for the Mars Exploration Program. The Lunar and Planetary Institute (Houston) and ARES harnessed a long and successful history of collaborative research and exploration activities, beginning with the Apollo Program, to be selected as an integral part of the NASA Lunar Science Institute (managed by the NASA Ames Research Center). During this period, ARES scientists continued to modernize our analytical capability and acquired two new state-of-the-art instruments – a focused ion beam and an inductively coupled plasma mass spectrometer.

ARES is a world leader in orbital debris research, including modeling and monitoring the debris environment, designing debris shielding, and developing policy to control and mitigate the orbital debris population. We have aggressively pursued refinements in the knowledge of the debris environment and hazards that it represents to spacecraft. One of many recent activities included ARES researchers participating in the automated transfer vehicle (ATV)-1 Jules Verne re-entry observing campaign in collaboration with the European Space Agency by providing a low-light "intensified" video system to analyze fragmentation of the ATV breaking up as it enters the Earth's atmosphere and then using that information to verify computer models and enhance safety assessments of re-entries of spacecraft. The ARES Image Science and

Astromaterials Research and Exploration Science Overview

continued

Analysis Group has also been recognized as a world-class group as a result of the high quality of its near-real-time analysis of ascent and on-orbit inspection imagery to identify debris shedding, anomalies, and associated potential damage during space shuttle missions. ARES Earth scientists manage and continuously update the database of astronaut photography that is predominantly from shuttle and International Space Station missions, but includes the results of 40 years of human space flight. One of these photos, Atafu Atoll [ISS018-E-18129, acquired on January 6, 2009], was selected as third place in the Earth Observatory 10th Anniversary Favorite Image contest. The Crew Earth Observations Website (http://eol.jsc.nasa.gov/Education/ESS/crew.htm) continues to receive between 10 and 20 million hits per month. ARES scientists are influencing decisions in the development of the next generation of spacecraft and missions through laboratory tests on the optical qualities of materials for windows, MMOD shielding technology, and analog activities to assess surface science operations.

ARES hosts numerous students and visiting scientists as part of the services provided to the research community and conducts a robust education and outreach program. ARES scientists are recognized nationally and internationally by virtue of their success in publishing in peer-reviewed journals and winning competitive research proposals. Our scientists have won every major award presented by the Meteoritical Society, including the Leonard Medal, the most prestigious award in planetary science and cosmochemistry, the Barringer Medal, recognizing outstanding work in the field of impact cratering, and the Nier Prize, for outstanding research by a young scientist. Not only has ARES established numerous partnerships with other NASA centers, universities, and national laboratories, but our scientists also serve as society officers, journal editors, and members of advisory panels and review committees.

Discovery of a New Mineral from a Cometary Particle

Keiko Nakamura-Messenger, *Johnson Space Center*
Lindsay P. Keller, *Johnson Space Center*
Simon Clemett, *Johnson Space Center*
John Jones, *Johnson Space Center*
Michael E. Zolensky, *Johnson Space Center*
Scott Messenger, *Johnson Space Center*

The International Mineralogical Association (IMA) officially recognizes 4,324 minerals. Johnson Space Center Astromaterials Research and Exploration Science (ARES) scientists added one more mineral to the list, the first new mineral ever found in a cometary specimen. This new mineral, a manganese silicide (MnSi) named "Brownleeite," was discovered within a cosmic dust particle that likely originated from a comet – perhaps comet 26P/Grigg-Skjellerup. The Earth accretes about 30,000 tons of dust particles from space each year; these dust particles originate from the disintegration of comets and collisions among asteroids. This cosmic dust is a subject of intense interest because it is composed of the original building blocks of our solar system, the planets, and our own bodies. Since 1982, NASA has routinely used high-altitude research aircraft to collect cosmic dust. However, because of their complex histories in space, the sources of most cosmic dust particles are difficult to determine.

We had an opportunity to collect cosmic dust from a specific source. Comet 26P/Grigg-Skjellerup is a source of dust grains that could be collected in the Earth's stratosphere at a specific time of the year. NASA used a high-altitude aircraft to collect cosmic dust particles from this particular comet dust stream in April 2003. The particles collected at this time contained the new mineral, Brownleeite (figure 1).

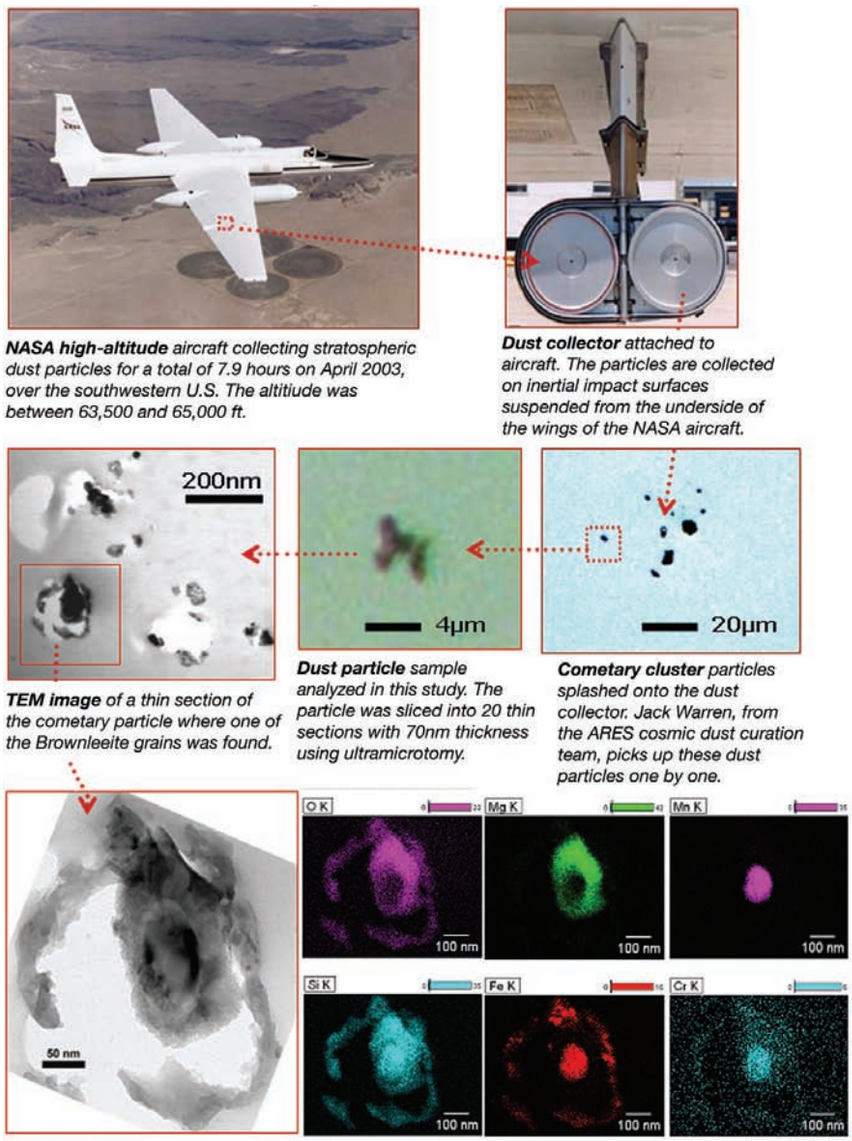

NASA high-altitude *aircraft collecting stratospheric dust particles for a total of 7.9 hours on April 2003, over the southwestern U.S. The altitiude was between 63,500 and 65,000 ft.*

Dust collector *attached to aircraft. The particles are collected on inertial impact surfaces suspended from the underside of the wings of the NASA aircraft.*

TEM image *of a thin section of the cometary particle where one of the Brownleeite grains was found.*

Dust particle *sample analyzed in this study. The particle was sliced into 20 thin sections with 70nm thickness using ultramicrotomy.*

Cometary cluster *particles splashed onto the dust collector. Jack Warren, from the ARES cosmic dust curation team, picks up these dust particles one by one.*

Brownleeite crystal *in the core Poikiolitically enclosed by LIME [low-Fe, Mn-enriched] olivine mantle.*

Nanoscale x-ray *elemental imaging by STEM2500SE EDX [energy-dispersive x-ray] system revealing that the Brownleeite grain (left) is free of O and Mg, but contains Mn, Si, Fe, and Cr.*

Fig. 1. *Brownleeite discovery flowchart.*

Discovery of a New Mineral from a Cometary Particle

continued

The ARES scientists installed, a powerful new transmission electron microscope (TEM), the JEOL [Japan Electron Optics Laboratory] STEM2500SE, at the ARES E-beam facility in 2005. Because of the exceedingly small size of the individual cometary dust components, we used state-of-the-art nano-analysis techniques in the TEM to measure the chemical composition and crystal structure of the Brownleeite. We discovered that one of the dust particles from the comet 26P/Grigg-Skjellerup collection contains three tiny grains (100, 250, and 600 nm in size) of an exotic phase that has never been found in nature before. In fact, no one predicted that this phase was either a cometary component or a phase formed by condensation in the solar nebula.

Recent analysis of material returned by the NASA Stardust mission comet Wild-2 demonstrates that cometary components originate in a wide range of astrophysical environments, including refractory minerals formed at high temperature in the inner solar system; low-temperature organic material from the outer reaches of the solar system or from interstellar molecular clouds; and dust grains from evolved stars whose origins predate the solar system. This new mineral (the Brownleeite) must have formed under rather reducing, oxygen-depleted conditions that were the average for our early solar system. Alternatively, MnSi may have condensed within the high-temperature and chemically heterogeneous ejecta of a supernova explosion. As previously found in meteorites and cosmic dust particles, mineral grains from supernovae can be identified on the basis of their exotic isotopic compositions. We may therefore be able to determine in future, using the ARES NanoSIMS 50L to produce silicon isotopic measurements, whether Brownleeite came from a supernova source.

The IMA-approved new mineral Brownleeite is named after Donald E. Brownlee, a professor of astronomy at the University of Washington, Seattle. Prof. Brownlee founded the field of cosmic dust research and is a principal investigator of the Stardust mission. Of all current sampling techniques developed by Prof. Brownlee, sampling in the Earth's stratosphere is the superior way to obtain the least-altered cosmic dust samples. Our current view and understanding of the early solar system established from cosmic dust studies would not exist without Prof. Brownlee's efforts.

Although Brownleeite has been synthesized and studied by materials scientists as a new-generation semiconductor, it has never been found in nature. There are places somewhere in the universe that are producing Brownleeite; and it is this mineral that is being supplied to the Earth, little by little, as cosmic dust enters our atmosphere.

Constraining Planetary Melting and Differentiation with Experimentation at High Pressure and Temperature

Kevin Righter, *Johnson Space Center*

Studies on the origin of volatiles and water in Earth as well as of the large amount of sulfur on the surface of Mars have a connection to deep planetary interiors. To simulate these conditions, we opened a High Pressure Laboratory in 2006. It houses two non-end-loaded piston cylinder apparatuses and two multi-anvil apparatuses. The combination of these four pieces of equipment enables us to attain pressures between 0.5 and 25 GPa. This pressure range also allows us to simulate the conditions that lie deep within planetary interiors such as the center of the moon (4.5 GPa), the core mantle boundary of Mars (~22 GPa), or the upper-lower mantle boundary in Earth (25 GPa). These facilities are used to explore a variety of research topics in Earth and planetary science, including: the conditions of planetary mantle melting; the origin of volatiles (hydrogen, carbon, oxygen, sulfur); the conditions during accretion; the origin of the Earth and the moon; and, finally, simply being able to synthesize high-pressure phases that do not exist at ambient laboratory conditions.

Pressure is generated in the piston cylinder apparatus by squeezing a pressure medium (sodium chloride or barium carbonate) into a cylindrical shape, with a sample and heater enclosed. In the smaller, multi-anvil assemblies, the shape is more equi-dimensional, with six steel wedges compressing eight triangular-faceted tungsten carbide cubes that are arranged in an octahedral shape (figure 1). The sample and a heater are then placed within the ceramic octahedral pressure medium, thus allowing the sample to be studied at pressure and temperature simultaneously. We use the synchrotron facility, which features a modified multi-anvil apparatus, to allow a strong and high-resolution x-ray beam to pass through the high-pressure assembly when a sample is being heated at pressure. We have also worked with the Argonne National Laboratory Advanced Photon Source (Argonne, Ill.) where we have simultaneously studied the compressibility and thermal expansion of metals and oxides, as well as the phase equilibria of planetary mantles (peridotite) and bulk compositions (chondrites) under extreme P-T [pressure and temperature] conditions.

Three models have been advanced to explain the origin of water on Earth (figure 2). The first of these is the traditional model in which the Earth's origin has been attributed to comets or another kind of volatile-bearing body that arrived late and well after accretion was complete. A second model proposes that water arrived just at the end of accretion, after the huge metallic core of the Earth had finished forming. The third model suggests that the Earth acquired its water early, during the accretion process.

The second hypothesis is linked to a class of elements called the highly siderophile elements; these elements are thought to reside mainly in the Earth's core. They are also present in the mantle at concentrations similar to those that would be expected if small amounts of chondritic material were added to the mantle after the core had formed. Because of this, the highly siderophile elements (HSEs) as well as the volatiles have commonly been linked in formation models for the Earth. This model was originally proposed in the 1970s, at a time at which relevant high P-T data were unavailable.

Fig. 1. *(from top): Sample is placed in white pressure medium between eight carbide cubes (four shown), placed between six steel wedges, and then placed in a hydraulic press. An Astromaterials Research and Exploration Science scientist is shown with the multi-anvil module and press at bottom.*

Fig. 2. *Did Earth have its water early, or did it acquire it later from comets? How did water survive a giant impact?*

Constraining Planetary Melting and Differentiation with Experimentation at High Pressure and Temperature

continued

To test this model more thoroughly, we studied the distribution of the HSE palladium (Pd) to test whether its abundance in the Earth's mantle requires the addition of later chondritic material, or whether its presence can be explained by simple metal-silicate equilibrium between the mantle and the core during accretion. The results, at pressures up to 15 GPa , have shown that the concentration of Pd in the Earth's mantle can be explained by high P-T distribution between the core and the mantle early in the history of the planet. The implications are that late additions of water- and HSE-bearing material are not necessary, and that water and HSE concentrations in the Earth's mantle were established very early during accretion. Other elements (e.g., gold, platinum, iridium, and rhodium) are being investigated to determine whether they are also compatible with this simple, and early, origin of water on Earth.

It has been known for some time that the surface of Mars contains sulfur, but the diversity and distribution of sulfates around the martian surface have been only more recently appreciated. The sulfur is thought to originate from interior degassing, but this hypothesis has not been rigorously tested with either experimental or more recent spacecraft data. If the sulfur comes from the martian interior, the main vehicle for transport would have to be magma, which is capable of dissolving significant amounts of sulfur. Although this process is well known for Earth basalts (e.g., mid-ocean ridges and Hawaii), it is relatively poorly understood for martian basalts such as the shergottites or those erupted from Olympus Mons (figure 3). Because magma generation in Mars likely takes place at pressures that are accessible in the Johnson Space Center High Pressure Laboratory, we have undertaken a study of sulfur solubility in martian magmas that includes the melting process in the mantle as well as later differentiation at shallower conditions at or near the surface. The results so far indicate that models based on terrestrial compositions and applied to martian systems are inadequate for predicting sulfur in magmas. The solubility of sulfur in martian magmas is perhaps two times higher than that predicted by Earth-based models. The results of this study will have fundamental implications for the total sulfur budget of Mars, as well as for our understanding of sulfur inputs into the martian atmosphere and the control of elements in the martian interior by sulfides.

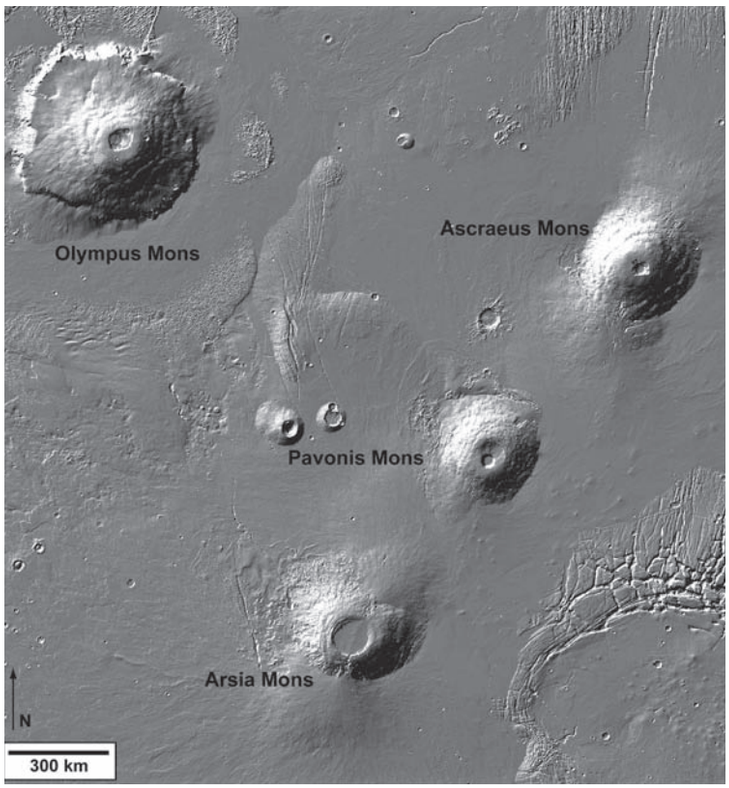

Fig. 3. *Did all the sulfur on the surface of Mars come from volcanic eruptions such as from Olympus Mons?*

Celebrating Thirty Seasons of Antarctic Meteorites: Johnson Space Center Antarctic Meteorite Laboratory

Kevin Righter, *Johnson Space Center*

In the winter of 1976, several scientists from the U.S. and Japan took part in a University of Pittsburgh expedition led by Dr. W. Cassidy that headed out from McMurdo Station Antarctica on the first Antarctic Search for Meteorites (ANSMET) to recover nine new meteorites. The U.S. team has returned every year (except for a cancelled season in 1990) to various locations within the Transantarctic Mountains (figure 1). These annual expeditions have resulted in a collection totaling approximately 17,000 meteorite samples. Three agencies – the Johnson Space Center (JSC), the National Science Foundation Office of Polar Programs (Arlington, Va.), and the Division of Mineral Sciences at the Smithsonian Institution (Washington, D.C.) – have been involved in this program since its initiation, each sharing different duties. Our role has been to serve as curators in the Antarctic meteorite group, a responsibility that entails receiving the samples, which are frozen on their return to the U.S.; keeping the samples in a controlled, stable, and contamination-free environment; performing initial characterization of new samples; announcing the arrival of new samples in a newsletter so the scientific community can make sample requests; and allocating samples to the scientific community after requests are peer-reviewed by a committee of experts assembled specifically for this process. Together with groups in our partner organizations, members of the JSC Antarctic meteorite group are celebrating 30 seasons of ANSMET meteorite samples. It is this 30-year milestone that has given the group time to reflect on how the collection of ANSMET meteorite samples has impacted the scientific community. Indeed, over the last 30 years the Antarctic meteorite group at JSC has published nearly 70 newsletters reporting new samples that are available for study by scientists, received more than 2,500 requests for samples, and prepared and sent out in excess of 14,000 individual samples in response to those requests.

Fig. 1. *Map of ANSMET collection sites in the Transantarctic Mountains (left). Image of Bill Cassidy (top right) and Ralph Harvey (bottom right) on ANSMET collections trips from the 1970s and 2000s, respectively.*

Highlights of the collection include: ALH A81005, which is the first recognized meteorite from the moon; EETA79001, which is a basaltic meteorite from Mars that contains trapped gases that match the martian atmospheric composition measured by the Viking spacecraft in 1976; and ALH 84001, which is a martian meteorite reported to contain evidence of fossil life. The U.S. Antarctic meteorite collection includes 19 lunar meteorites, nine martian meteorites, nearly 400 pieces of what scientists think are samples of the asteroid 4 Vesta (the howardite, eucrite, and diogenite meteorites), and hundreds of meteorites from asteroids and other small bodies. In addition to these well-characterized and well-understood samples,

the collection contains many examples of meteorites from unknown places that record conditions in the early solar system, illustrating the diversity of materials that were present in the early solar system (figure 2).

The U.S. Antarctic meteorite collection provides the link between some other NASA sample collections, including comets, solar wind, cosmic dust, and lunar samples. For example, ALH 85085 is a carbonaceous chondrite that contains similar and rare minerals (e.g., osbornite) that have also been found in the material returned by the Stardust mission. Chondrites and achondrites (figure 3) define oxygen isotopic variation in the solar system; this provided part of the impetus for the Genesis Discovery mission. Pre-solar grains, which are found in several ordinary, enstatite, and carbonaceous unequilibrated chondrites, record isotopic anomalies from stellar processes. Finally, as mentioned already, nearly 20 lunar meteorites enhance and complement our understanding of the moon provided by Apollo and lunar samples.

The future of this program is very bright, and is providing scientific support in several ways. First, research and curation of martian and chondritic meteorites continues to inform planning efforts for Mars and asteroid sample return. Second, instrumentation employed on many current and future missions can be tested and calibrated using these astromaterials (e.g., the Mars exploration rover, Dawn, which will study the 1 Ceres and 4 Vesta asteroids; and SMART-1 [Small Missions for Advanced Research in Technology-1], a European Space Agency project for the moon). Finally, we expect that the number of new meteorites will grow as collection efforts continue, and that the collection itself will grow with each new field season, thereby yielding interesting new astromaterials for study.

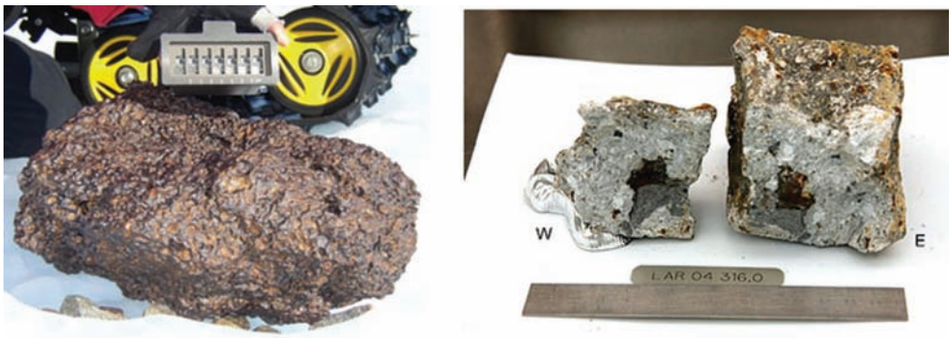

Fig. 2. *Photograph of pallasite (left) and aubrite (right) meteorites recovered in 2004-2005 ANSMET season.*

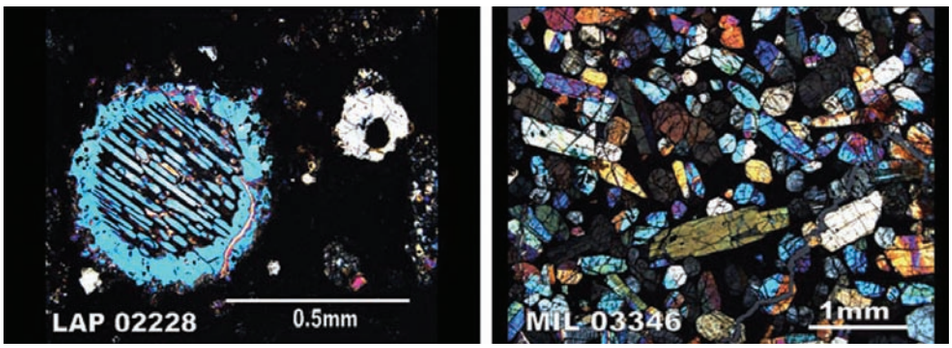

Fig. 3. *Photomicrographs of carbonaceous chondrite (left) and nakhlite (right) meteorites in cross-polarized light.*

New Perspectives on Geomorphic Processes: Megafans in Terrestrial and Planetary Environments

Justin Wilkinson, *Johnson Space Center*

The mesoscale sedimentary environment known as the megafan is a low-angle, partial cone of fluvial sediment generated where a river enters an unconfined basin and begins the process of avulsing over wide areas. The significance of megafans as a new feature was first revealed by astronaut handheld imagery. Our research, based on the first global study of megafans, has resulted in new perspectives in both terrestrial and planetary environments.

Planetary megafans: A new explanation for the martian landscapes of Sinus Meridiani

Explanations for the enigmatic geology of Sinus Meridiani, on which the NASA rover "Opportunity" still operates, are dominated by the common, but restricted, view that river channels only form in hilly country; i.e., channels are always confined within valley walls. The features of numerous megafans around the world closely parallel Meridiani landscapes, including: (1) networks of stream channels that (2) occupy vast plains, with (3) the channels forming more resistant elements in the landscape, thereby resulting in the classic sinuous "inverted" ridges of the terrestrial and martian landscapes. The Libyan landscapes on Earth even show a detail of sinuous ridges interacting with circular craters, which provides our most persuasive analog yet for the Meridiani Planum (figure 1).

Terrestrial megafans: A new explanation for the Kalahari Desert landscapes of south-central Africa

Maps of a series of megafans of the Kalahari basin provide a fundamental shift in our understanding of the landscape evolution, biological evolution, and water resources of the arid central Kalahari basin. A newly identified megafan shows that the large Okavango River once flowed alternately southward, into a basin in northern Namibia, and eastward, to the modern downstream megafan of the Okavango delta of northern Botswana. Paleontological data confirm that this alternative flow operated until approximately 6 Ma, at which point the Okavango River incised into the new fan, causing the drying up of the paleo-lake Etosha. This drying-up has been ascribed to climate change, but likely relates to activity on the faults of the Okavango Rift. Three geological publications have incorporated these new perspectives.

Tropical terrestrial megafans: A new explanation for the evolution of modern Amazon landscapes

We generated maps based on Mars topographic roughness algorithms for South America. These maps reveal that (1) the very widespread megafan plains of Argentina likely extended far to the north, explaining much of modern Amazonia in the later Neogene Period of the Cenozoic Era; and (2) megafans can act as species pumps for

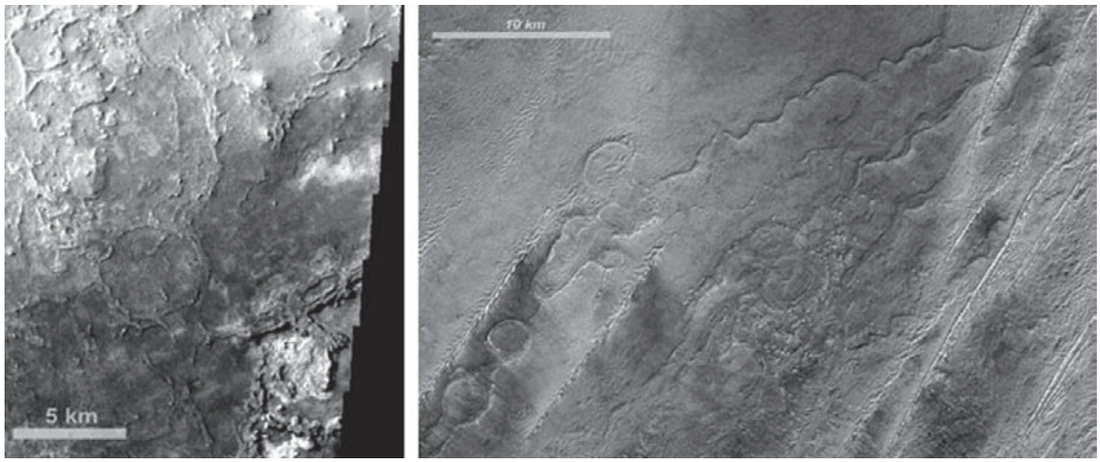

Fig. 1. *Sinuous and partly circular (crater) features, Sinus Meridiani (left). Craters with indurated rims and numerous stream channels (flow direction is NE, towards top right), Libyan Sahara (right).*

aquatic fauna, as argued by earlier work. Applying these arguments to Amazonia, we contend that paleo-megafans could well explain some of the fish biodiversity of the western Amazonia, where many species occupy the "megafan zone" against the Andes Mountains (figure 2).

Fig. 2. *Roughness map of South America. Darkest areas are lowest slope and smoothest landscapes, all dominated by megafans.*

Other new perspectives: A new biogeographic boundary coinciding with a tectonic plate boundary

This study portrays one of the few known Latin-American plate boundaries that coincides with the clear-cut distributional limits separating major biogeographic provinces. The Costa Rica Grande de Tárcoles River occupies the fault zone that defines the Costa Rica-Panama microplate boundary. The Tárcoles River also marks an unusually clear biogeographic frontier between the Pacific dry forest (the Mexican Pacific Coast Province) and the Pacific rain forest (the Western Panamanian Isthmus Province).

Species richness and endemicity maps for scarab beetles, which are probably representative of most insects, allow definition of four priority levels of conservation area. The single most critical zone of land use overlap is in the Central Valley of Costa Rica. This zone lies mostly outside of the protected zones, in which commercial agriculture land use is dominant. This analysis has significant policy implications for a country in which the protection of biodiversity is a key tourist attraction (figure 3).

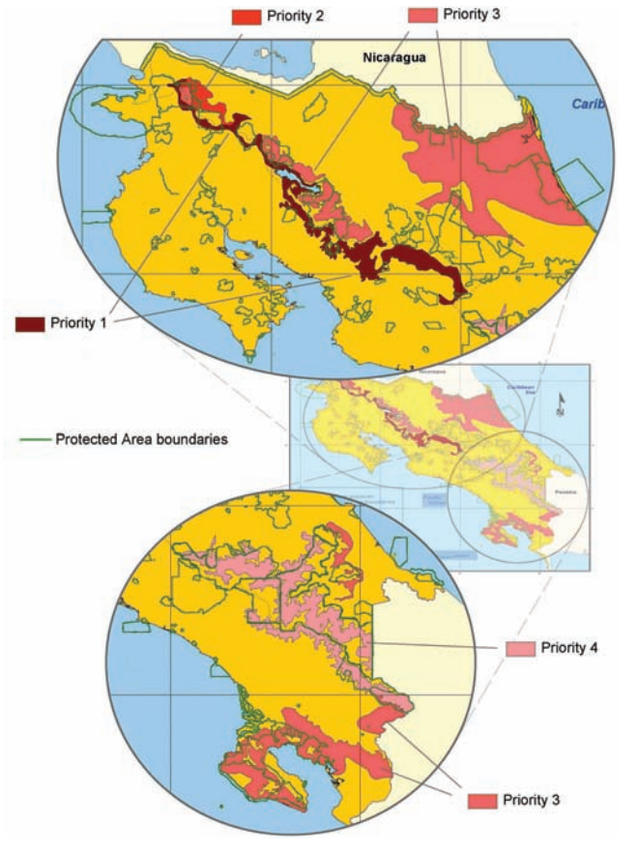

Fig. 3. *Central Valley of Costa Rica biodiversity zones.*

Searching for Antimatter and Dark Matter

Trent Martin, *Johnson Space Center*

Chris Tutt, *Johnson Space Center*

Johnson Space Center (JSC) is home to the Alpha Magnetic Spectrometer (AMS) Project Office. The AMS-02 experiment is a state-of-the-art particle physics detector being constructed, tested, and operated by an international team composed of 56 institutes from 16 countries and organized under U.S. Department of Energy (DOE) sponsorship. The JSC project office oversees and directs the overall payload integration activities and ensures that the payload is safe and ready for launch on the space shuttle and deployment onto the International Space Station (ISS). The AMS experiment will use the unique environment of space to advance knowledge of the universe and lead to the understanding of the universe's origin.

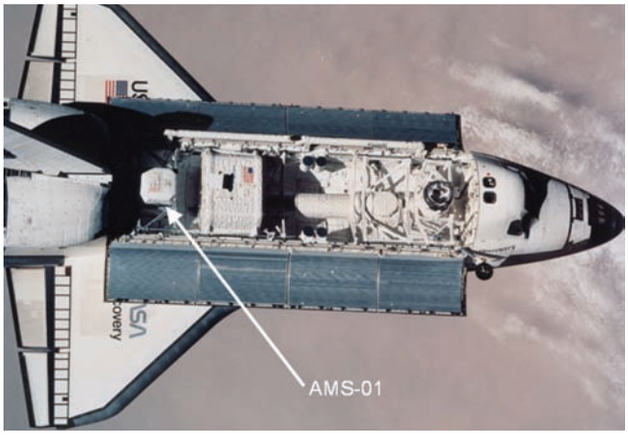

Fig. 1. *AMS-01 on STS-91.*

The AMS is a high-profile, space-based, particle physics experiment led by Nobel laureate Samuel Ting of the Massachusetts Institute of Technology (MIT). It flew in space in June 1998 aboard the Space Shuttle *Discovery* (figure 1), and is being integrated and tested to fly on the ISS. The AMS-02 will be transported in the cargo bay of the space shuttle for installation on the ISS. Once on the ISS S3 upper inboard payload attach site, the AMS will remain active for at least 3 years (figure 2).

Orbiting the Earth at an altitude of 200 nm, the AMS is pioneering a new frontier in particle physics research for the 21st century. This unique scientific mission of exploration seeks to understand fundamental issues shared by physics, astrophysics, and cosmology on the

Fig. 2. *AMS-02 on S3 truss of ISS.*

origin and structure of the universe. Although the AMS is specifically looking for antimatter and dark matter, as the first magnetic spectrometer in space AMS has, and will, collect information from cosmic sources emanating from stars and galaxies millions of light years beyond the Milky Way. The technical challenges to building such a detector for use in space have been surmounted through the close collaboration of AMS scientists and industries around the world, whose efforts have resulted in the development of new technologies and higher standards of precision.

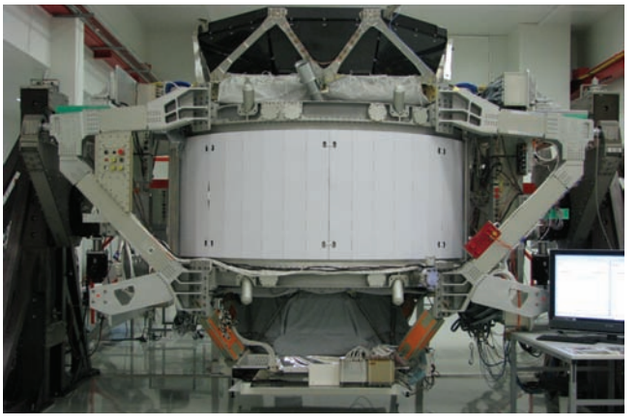

Fig. 3. *AMS-02 detector during integration in Geneva.*

The experiment (figure 3) uses a large, cryogenic superfluid helium (1.8 K) superconducting magnet to produce a strong, uniform magnetic field (~0.8 Tesla) over a large volume of approximately 1 m^3. The magnetic field is used to bend the path of charged cosmic particles as they

pass through five different types of detectors: (1) the transition radiation detector, which measures particles passing at speeds nearly that of the speed of light; (2) the time of flight detector, which measures the charge and velocity of passing particles; (3) the silicon tracker, which measures the coordinates of charged particles in the magnetic field; (4), the ring image Cerenkov counter, which measures both the velocity and the charge of the particles; and (5) the electromagnetic calorimeter, which measures the energy and coordinates of electrons, positrons, and gamma rays. Figure 3 shows the AMS detector and its response to different particles or nuclei. The AMS also employs two star trackers and a Global Positioning System. With over 300,000 data channels, the detector gathers an extremely large amount of data that is then processed and sent to Earth using the ISS power, communication, and data infrastructure.

AMS will provide the first operational experience with a superconducting cryogenic magnet in space and greatly extend the knowledge base regarding superfluid cryogenic systems operation in space. These are enabling technologies for the potential use of magnetic shielding as a method of radiation protection during extended human space flight, as well as for space power and propulsion systems.

Johnson Space Center involvement

The AMS Project Office, housed in the Engineering Directorate at JSC, is responsible for building all integration hardware and software to connect the collaboration-built science detector to the space shuttle and the ISS. This includes over 3,500 lbs. of flight integration hardware. The AMS Project Office liaises among the DOE-sponsored collaboration team and the Space Shuttle and ISS Program Offices, the Mission Operations Directorate, and other groups at JSC. The AMS Project Office is also responsible for certifying that the entire payload is safe and ready for flight and for acting as the prime integrator for the entire payload.

Search for antimatter

All evidence currently indicates that the universe is made of matter; however, the Big Bang Theory (figure 4) of the origin of the universe requires equal amounts of matter and antimatter. Theories explaining this apparent asymmetry violate other measurements. Whether there is significant antimatter is one of the fundamental questions of the origin and nature of the universe. Any observations of an antihelium nucleus would provide strong evidence for the existence of antimatter (figure 5). In 1999, AMS-01 established a new upper limit of 10^{-6} for the antihelium/helium flux ratio in the universe. AMS-02 will search with a sensitivity of 10^{-9}, an improvement of three

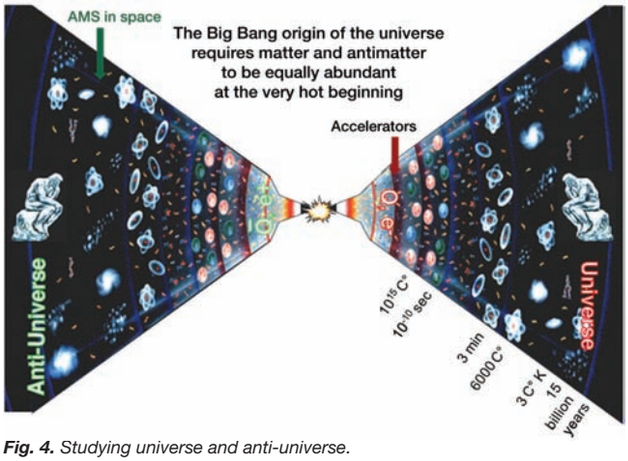

Fig. 4. *Studying universe and anti-universe.*

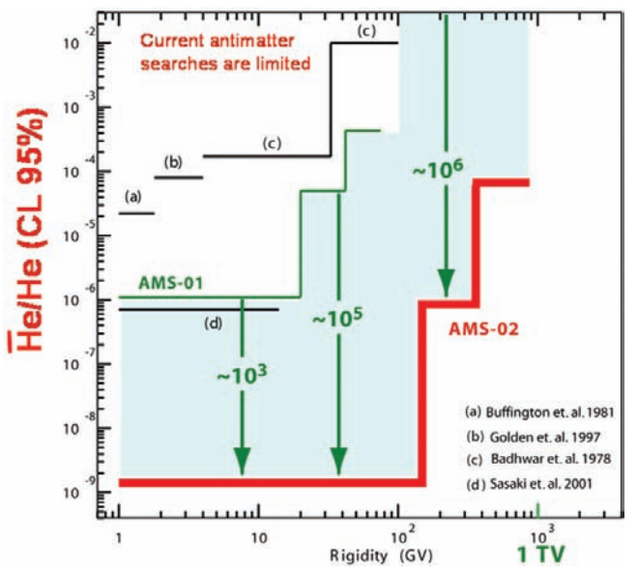

Fig. 5. *AMS-02 antihelium limits.*

orders of magnitude – sufficient to reach the edge of the expanding universe and resolve the issue definitively.

Search for dark matter

The visible matter in the universe (stars) adds up to less than 5% of the total mass known to exist from many other observations. The other 95% is dark – either dark matter (which is estimated at 20% of the universe by weight) or dark energy (which makes up the balance). The exact nature of both is still unknown. One of the leading candidates for dark matter is the neutralino. If neutralinos exist, they should be colliding with each other and giving off charged particles that can be detected by AMS-02. Any peaks in the background positron, antiproton, or gamma flux could signal the presence of neutralinos or other dark matter candidates. Preliminary data from the PAMELA [payload for antimatter exploration and light-nuclei astrophysics] and ATIC [advanced thin ionization calorimeter] missions appears to indicate the existence of such a peak at energy levels well within the range of AMS-02's capabilities

Cosmic ray measurement

Cosmic radiation is a significant obstacle to a human flight to Mars. Accurate measurements of the cosmic-ray environment are needed to plan appropriate countermeasures. Most cosmic ray studies are done by balloon-borne satellites with flight times measured in days; these studies have shown significant variations. AMS-02 will be operative on the ISS for a nominal mission of 3 years, gathering an immense amount of accurate data and allowing measurements of the long-term variation of the cosmic ray flux over a wide energy range for nuclei, from protons to iron (figures 6 and 7). After the nominal mission, AMS-02 can continue to provide cosmic-ray measurements. In addition to the understanding the radiation protection required for human interplanetary flight, these data will allow the interstellar propagation and origins of cosmic rays to be determined.

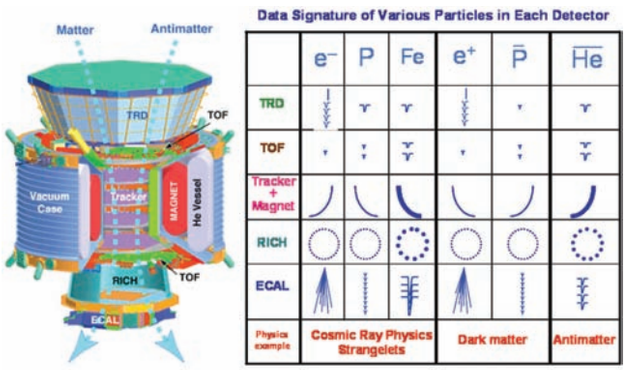

Fig 6. Cutaway view of the AMS detector (left). Response of the detectors layers to a charged particle of energy 0.3 TeV (data courtesy of MIT).

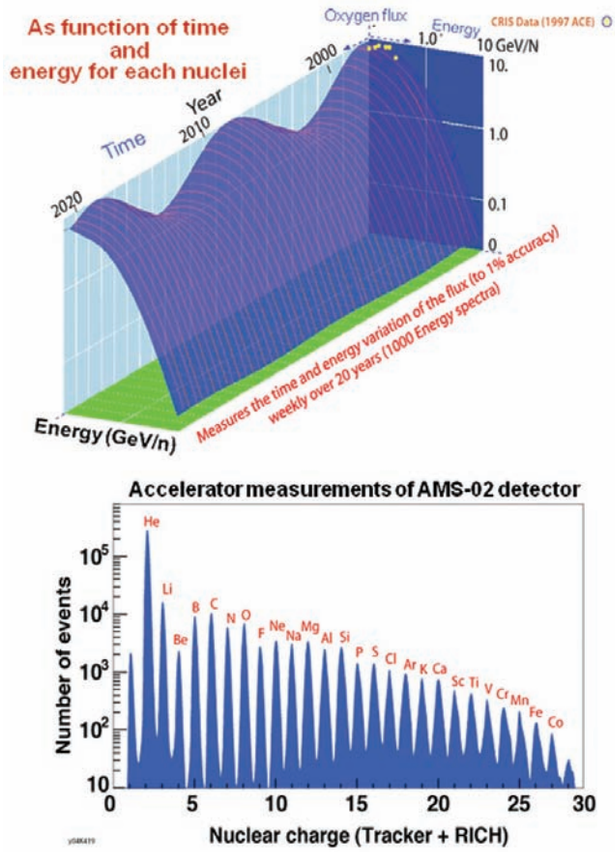

Fig.7. AMS-02 identification and measurement potential (data courtesy of MIT).

Image Science Support for Exploration Program

Tracy Calhoun, *Johnson Space Center*

The Constellation Program is using Johnson Space Center engineering imaging design as part of its design and testing for the new vehicle. This includes imaging concepts and requirements to analyze imagery acquired during laboratory and flight tests. This is especially notable as it is the first time that engineering imagery has been consistently factored for vehicle design. Traditionally, the Public Affairs Office was the key driver for vehicle imaging systems. While this type of imagery is vital for extending the space flight experience to the public, flight operations have evolved to depend heavily on engineering imagery as a data source.

Orion window photography testing

The Crew Exploration Vehicle (CEV) (Orion) underwent a review that focused on vehicle mass, resulting in a window redesign that changed the glass pressure pane to a polycarbonate pane. As part of the polycarbonate evaluation, we obtained and compared engineering photography through various Orion window configurations. Test photography using Orion and shuttle window mock-ups revealed that a polycarbonate pressure pane will not support engineering image analysis photography using long-focal-length (400 mm) lenses. The test did, however, reveal that window panes made of acrylic appear to have an optical quality comparable to the current shuttle windows and could support long-focal-length photography. These findings served as the basis for an Orion Project directive to change the pressure pane material from polycarbonate to acrylic, with further acrylic testing in 2009 (figure 1).

Imagery analysis in support of flight tests

Another task involved the CEV Parachute Assembly System Cluster Development Test-2, conducted at Yuma Proving Ground, Ariz., in July 2008. For the first parachute test, ground-tracking video of the test article, which experienced a failure of the programmer chute, was used to extract attitude and oscillation data as well as to build a failure event timeline.

We support other tests such as the test flights of Ares 1-X (new launch vehicle) and Pad Abort-1 (PA-1). All ground- and vehicle-based video acquired during Ares 1-X must undergo screening and analysis using the techniques and tools employed for each shuttle launch. In addition to extracting vehicle performance information, Ares 1-X will afford the agency an opportunity to assess how well the imagining laboratory for shuttle processes and laboratory facilities supports Ares. All PA-1 ground-tracking camera imagery are analyzed to compute attitude data and to assess system performance (figure 2).

Fig. 1. *Image Science and Analysis Group and Engineering Directorate personnel conduct Orion window photography tests.*

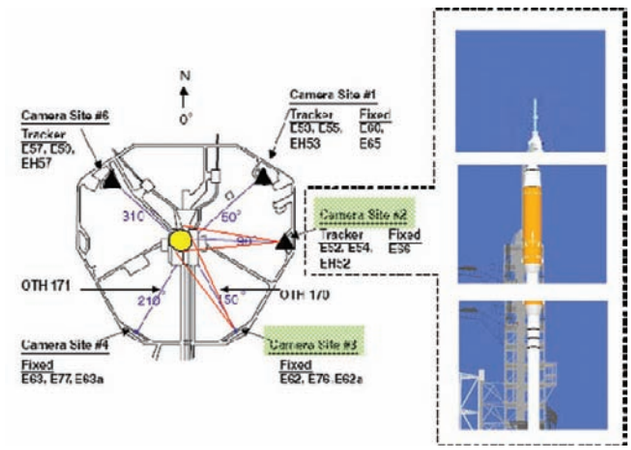

Fig. 2. *An example of launch site camera planning for Ares 1-X.*

Orion thermal protection system inspection capability studies

Our image group has extensive experience with on-orbit vehicle inspection that uses sensors and cameras to detect and measure structural damage from launch and on-orbit

debris, referred to as micrometeoroid/orbital debris (MMOD). The group's vehicle inspection skill set, which was developed and honed for shuttle, is now being applied to Orion. Block 1 missions to the International Space Station (ISS) will require that Orion be docked to the station for months, thereby exposing its Thermal Protection System (TPS) to potential MMOD damage. A verification of TPS integrity prior to re-entry will therefore be necessary.

A study revealed that existing ISS imaging resources are capable of detecting a surface feature that could indicate possible damage to the Orion TPS (assuming the currently predicted damage criteria). The group is now performing studies to identify an appropriate method of characterizing a tile cavity. Three-dimensional sensors from the shuttle are under evaluation for this purpose, as are new technologies that are currently in development. Photogrammetry techniques that extract depth data from the multiple images obtained with a conventional two-dimensional camera also continue to be refined and considered. While imaging tools and techniques can readily be implemented as Orion is docked to ISS, the team is also considering how TPS inspection can be performed on lunar missions that will not have the convenience of ISS resources (figure 3).

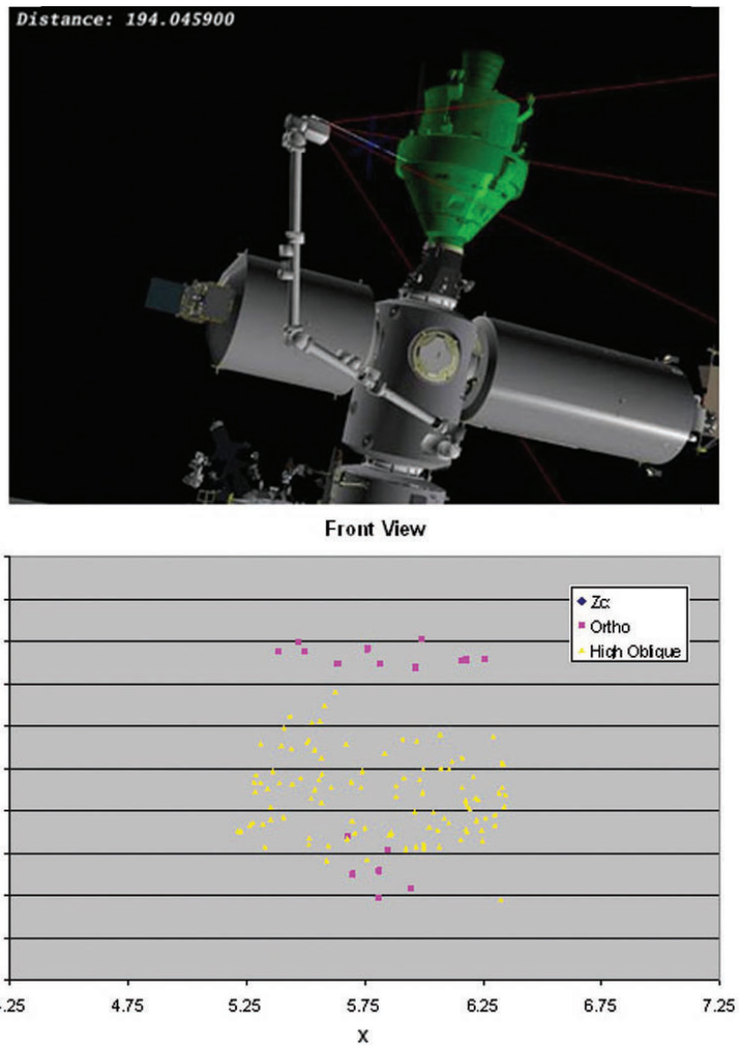

Fig. 3. *An illustration of Orion inspection for TPS damage while docked to ISS Node 2 (top). Three-dimensional Orion tile cavity characterization uses multiple images from a two-dimensional sensor. The pink points map the periphery of the entry hole and the bottom of the cavity. The yellow points map the lower extent of the sides of the cavity (bottom).*

Improving Access to Astronaut Photography through Google Earth

William L. Stefanov, *Johnson Space Center*

The Johnson Space Center (JSC) Crew Earth Observations Team directs the archiving and geolocational cataloging of Earth images acquired by International Space Station (ISS) astronauts. These images, together with descriptive and camera metadata for each image, are accessible at The Gateway to Astronaut Photography of Earth (http://eol.jsc.nasa.gov). This on-line searchable database is a highly valuable resource of historical and current imagery available to researchers, government, and nonprofit entities; planning and environmental professionals; educators; and the general public in both developed and developing countries. A group comprised of members from the NASA Ames Research Center, JSC, and the NASA Goddard Space Flight Center selects astronaut photographs and related descriptive content. These data provide a key component of the NASA layer in the free geographic browser Google Earth (http://earth.google.com). The astronaut photography comprises a distinct layer within the NASA-provided content in Google Earth. The site is periodically updated with new content. Users can view the cataloged imagery in The Gateway to Astronaut Photography of Earth within the Google Earth environment using on-the-fly .kml file generation, as shown in figure 1.

Geographic and map browsers such as Google Earth are powerful tools that can advance virtual geographic and geologic education. The ability of users to add geolocated placemarks and embed additional content, such as images and html links, greatly enhances the potential for interactive geoscience education. We have developed a Google-Earth-based series of geographic briefing modules for use in training ISS astronauts to recognize major terrestrial features and landforms from low-Earth orbit. The modules, which are designed to accommodate both instructor-driven presentation and automated flyover tour modes, include direct query links to the on-line digital database of astronaut photographs of the Earth.

This direct query functionality provides a wealth of seasonal and multi-resolution imagery of selected locations that augments the available Google Earth imagery. It is also a useful data resource for more detailed geomorphology, structural geology, oceanography, and ecology education.

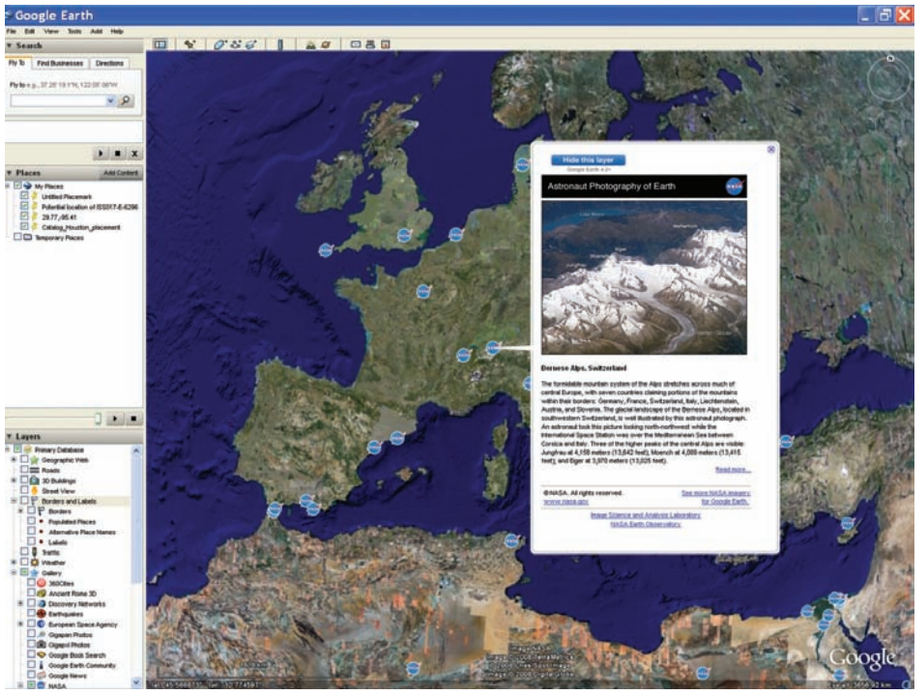

Fig. 1. *Screen capture of Europe in Google Earth with the astronaut photography layer selected. NASA logos indicate locations of image content. One such content item – an image of the Bernese Alps in Switzerland – has been opened.*

The training modules presented to astronauts host a wide range of geographic knowledge, simulating exposure to a broad range of class levels. All components of the modules (Google Earth, Wikipedia, and The Gateway to Astronaut Photography of Earth) are freely available on the Internet, making this a robust and attractive approach to improving terrestrial geographic literacy. In addition, the use of astronaut-acquired remotely sensed data for geoscience education – particularly K-12 – enhances interest in human space exploration and STEM [science, technology, engineering, and mathematics] career paths as shown in figure 2.

Fig. 2. *Google Earth and the astronaut photography database make an effective tool for teaching general geography. This example, from the Africa training module (top), illustrates the training entry for Mount Kilimanjaro (center) and a database entry page accessed through active links in Google Earth (bottom).*

Object-based Image Analysis of Astronaut Photography

William L. Stefanov, *Johnson Space Center*

Object-based image analysis is a subdiscipline of the geoinformation science devoted to partitioning remote-sensing imagery into meaningful image-objects, and assessing their characteristics through spatial, spectral, and temporal scale. This is particularly useful for analyzing high-resolution imagery.

A dataset comprised of high-resolution digital astronaut photography from the International Space Station is potentially useful for ecologic, geologic, and land use/cover studies. The entire public domain digital astronaut dataset, available from http://eol.jsc.nasa.gov, consists of imagery amassed from 1961 to the present and includes data for much of the Earth's surface (figure 1). We have a collaborative data collection and research agreement with the Long Term Ecological Research (LTER) Network of the National Science Foundation to assess the quantitative potential of digital astronaut photography. The LTER Network, which consists of 26 sites, represents a wide range of biomes, including temperate and tropical forest, deserts, grasslands, tundra, and urban, human-dominated ecosystems. We use this network to compare digital astronaut photography with remotely sensed data (i.e., Landsat) as well as field-based validation and measurement data.

In contrast to traditional, narrow-bandwidth, remote-sensing instruments, digital astronaut photography is acquired using off-the-shelf digital cameras that are sensitive to the visible red, green, and blue wavelengths; decisions to acquire imagery are made on-the-fly by astronauts. The wide bandpasses of the camera make traditional classification approaches difficult, as discrete spectral information is not typically obtained. We are thus using a multilevel, object-based image analysis approach to high-resolution digital astronaut photography of LTER Network sites that represent the range of continental and island biomes. This approach emphasizes the spatial relationships of similar pixels – through image segmentation – in addition to spectral information, and takes advantage of the high density of the spatial information captured in astronaut photographs. Digital astronaut photography, used with remotely sensed satellite and airborne data, can increase the temporal resolution of observed variables such as land cover, land use change, vegetation dynamics, and surface soil processes, as shown in figure 2.

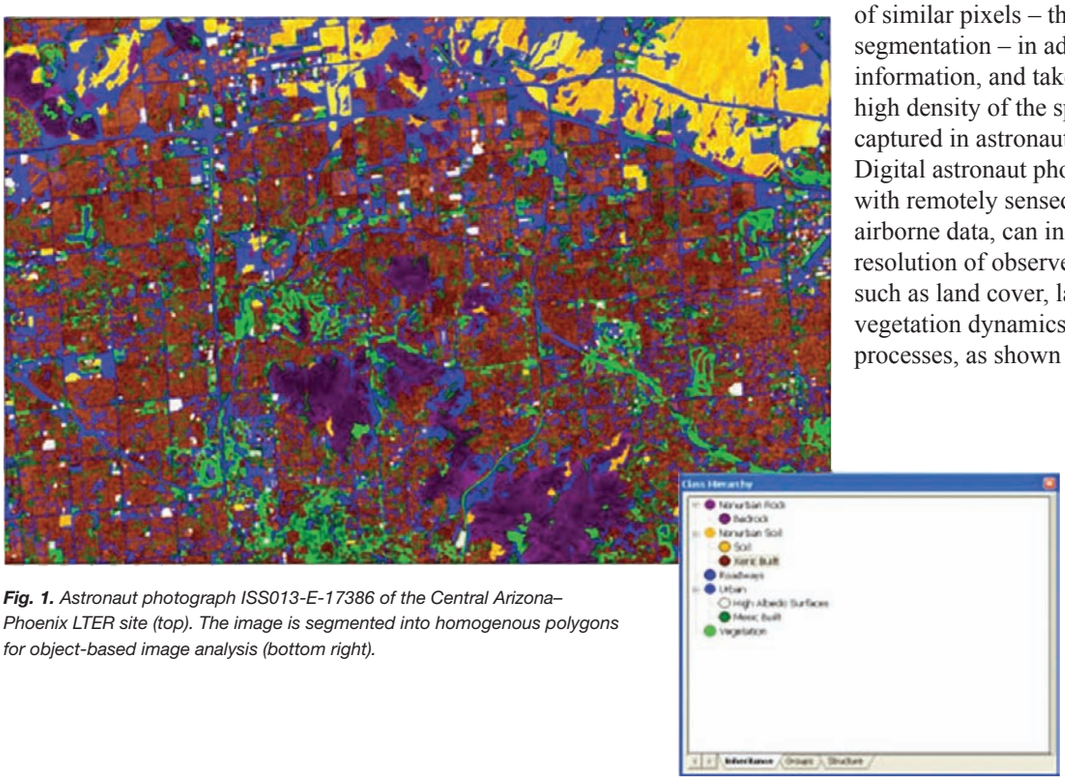

Fig. 1. *Astronaut photograph ISS013-E-17386 of the Central Arizona–Phoenix LTER site (top). The image is segmented into homogenous polygons for object-based image analysis (bottom right).*

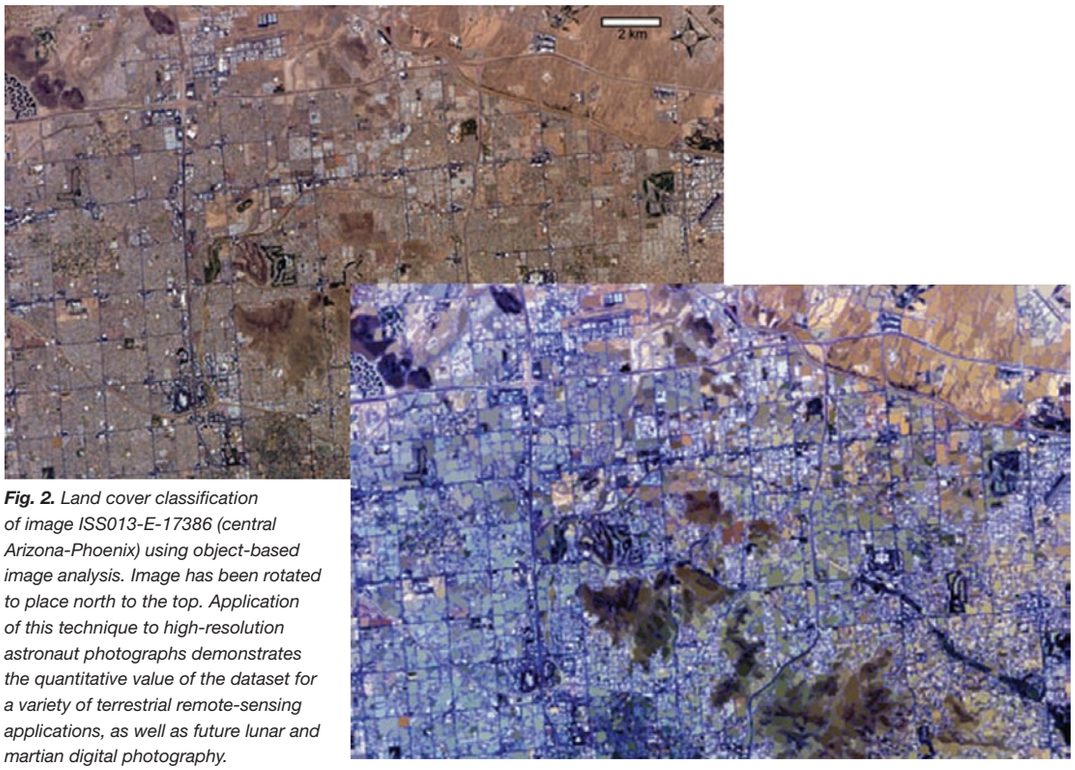

Fig. 2. *Land cover classification of image ISS013-E-17386 (central Arizona-Phoenix) using object-based image analysis. Image has been rotated to place north to the top. Application of this technique to high-resolution astronaut photographs demonstrates the quantitative value of the dataset for a variety of terrestrial remote-sensing applications, as well as future lunar and martian digital photography.*

REPORT DOCUMENTATION PAGE	Form Approved OMB No. 0704-0188

Public reporting burden for this collection of information is estimated to average 1 hour per response, including the time for reviewing instructions, searching existing data sources, gathering and maintaining the data needed, and completing and reviewing the collection of information. Send comments regarding this burden estimate or any other aspect of this collection of information, including suggestions for reducing this burden, to Washington Headquarters Services, Directorate for Information Operations and Reports, 1215 Jefferson Davis Highway, Suite 1204, Arlington, VA 22202-4302, and to the Office of Management and Budget, Paperwork Reduction Project (0704-0188), Washington, DC 20503.

1. AGENCY USE ONLY *(Leave Blank)*	2. REPORT DATE December 2009	3. REPORT TYPE AND DATES COVERED Technical Memorandum

4. TITLE AND SUBTITLE Biennial Research and Technology Development Report	5. FUNDING NUMBERS
6. AUTHOR(S) Helen Lane, Kamlesh Lulla	
7. PERFORMING ORGANIZATION NAME(S) AND ADDRESS(ES) NASA Johnson Space Center	8. PERFORMING ORGANIZATION REPORT NUMBERS S-1051
9. SPONSORING/MONITORING AGENCY NAME(S) AND ADDRESS(ES) National Aeronautics and Space Administration Washington, DC 20546-00011	10. SPONSORING/MONITORING AGENCY REPORT NUMBER TM-2009-214795
11. SUPPLEMENTARY NOTES *NASA Johnson Space Center	
12a. DISTRIBUTION/AVAILABILITY STATEMENT Unclassified/Unlimited Available from the NASA Center for AeroSpace Information (CASI) 7115 Standard Drive Hanover, MD 21076-1320 Category: 99	12b. DISTRIBUTION CODE

13. ABSTRACT *(Maximum 200 words)*

The Biennial Research and Technology Development Report highlights the diverse technical, scientific, and engineering research and technology development under way at the Johnson Space Center (JSC). The articles contained within this report further JSC's and NASA's historical tradition of working with colleges and universities, industry, federal laboratories, and other research and technology development organizations for the betterment of humankind. The report is organized into nine broad categories: (1) human health and medicine, including analog medical research (e.g., medical issues in Antarctica) as well as new, cutting-edge medical technologies; (2) environmental technology (e.g., recycling and recovery technologies, air quality monitoring, and radiation protection research); (3) materials development and testing (e.g., new developments in nondestructive evaluation tests, single-wall carbon nanotube growth); (4) flammability and explosion testing, including protection and testing standards; (5) power, battery, and propulsion technologies (e.g., NASA fuel cells and high-sensitivity measurements for permeation of hypergol); (6) robotics and automation technologies; (7) technologies for harsh environments, including extravehicular activity technologies; (8) space and ground operations (e.g., software developments for space station operations, data mining, and a low-impact docking system); and (9) planetary sciences (i.e., new discoveries of cometary particle, results from planetary and rover research, and educational and outreach initiatives).

14. SUBJECT TERMS	15. NUMBER OF PAGES	16. PRICE CODE
aerospace medicine; air quality; radiation protection; hypergolic rocket propellants; fuel cells; robotics; software development tools; test equipment; comets; nondestructive tests	246	

17. SECURITY CLASSIFICATION OF REPORT	18. SECURITY CLASSIFICATION OF THIS PAGE	19. SECURITY CLASSIFICATION OF ABSTRACT	20. LIMITATION OF ABSTRACT
Unclassified	Unclassified	Unclassified	Unlimited